UNIVERSITEIT VAN PRETORIA
UNIVERSITY OF PRETORIA
YUNIBESITHI YA PRETORIA

Exploring the potential of using unmanned aerial system imageries in managing the Miombo woodlands of Zambia

By

Hastings Shamaoma

© University of Pretoria

Submitted in partial fulfilment of the requirements for the degree of Doctor of Philosophy in Environmental Management

In the Faculty of Natural and Agricultural Sciences

University of Pretoria

Pretoria

Promoter: Prof. Abel Ramoelo
(University of Pretoria)

Co-promoters: Prof. Paxie WC Chirwa
(University of Pretoria)
Dr. Andrew Hudak
(US Forest Service)
Prof. Stephen Syampungani
(Copperbelt University/University of Pretoria)

© University of Pretoria

Declaration

I, Hastings Shamaoma, declare that the thesis/dissertation, which I hereby submit for the degree PhD Environmental management at the University of Pretoria, is my own work and has not previously been submitted by me for a degree at this or any other tertiary institution.

Signature:  Date: 5/12/2023

© University of Pretoria

Dedication

To the memory of my dad for the inspiration and support he gave me.

© University of Pretoria

Acknowledgement

My sincere gratitude goes to Prof. Abel Ramoelo, my main supervisor, for his advice, patience, and support. He offered me the flexibility, motivation, and support I needed to explore numerous study ideas. I am thankful to Prof. Stephen Syampungani for introducing me to the core ideas of forestry and for his guidance and critical remarks during my study. I will forever be thankful to Prof Paxie W.C. Chirwa and Dr. Andrew Hudak for providing insightful discussions, critical comments, and suggestions throughout my research. Indeed, the critical views and advice of Dr. Jules C. Zeken are greatly appreciated.

I gratefully acknowledge my debt to Dr. Ferdinand Handavu, for support and guidance during field work. The immense contribution of Mr. Enock Kilema, Geophat Qonda Mpatwa, Mr. Peter Malambo Shichoongo and Stephen Mwanza to my field data collection will forever be appreciated. Without the selfless efforts of these individuals, this thesis could not have seen light.

I express my sincere gratitude to The United States Agency for International Development through Partnerships for Enhanced Engagement in Research (PEER) program for funding most part of this research. I am also grateful to the Oliver R Tambo African Research Chair Initiative (ORTARChI) project, an initiative of Canada's International Development Research Centre (IDRC), South Africa's National Research Foundation (NRF) and the Department of Science and Innovation (DSI), in partnership with the Oliver & Adelaide Tambo Foundation (OATF) and National Science and Technology Council, Zambia for proving additional funding for this research.

I also thank the management at The Copperbelt University for giving me a study leave. Indeed, the support, understanding, and patience of the head of department, Ms. Idah Ethel Zulu, and colleagues: Prof. Roy A. Chileshe, Prof. K. Taylor, Dr. Chikondi Thole Banda, Mr. Alex Mumbala Simposya, Mr. Christopher Msipu Phiri, Mrs. Pricilla Kachapulula Mudenda, Mrs. Precious Moonga Mudenda, Mr. Gillie Cheelo, and Mr. Jervas Tembo at the Department of Urban and Regional Planning, School of the Built Environment, are greatly appreciated.

Above all, I owe a great debt of gratitude to my parents for their support, counsel, and for allowing me to make my own life choices. I would not have gotten this far without

© University of Pretoria

their help. Finally, but not least, I would want to thank my wife two sons Choolwe and Bukata for the support and understanding during my studies.

© University of Pretoria

Table of Contents

© University of Pretoria

© University of Pretoria

© University of Pretoria

© University of Pretoria

© University of Pretoria

List of Figures

© University of Pretoria

List of Tables

© University of Pretoria

© University of Pretoria

List of Appendices

© University of Pretoria

List of Acronyms

3D	Three Dimensional
ABA	Area Based Approach
AGB	Above-Ground Biomass
Adj-R^2	Adjusted Coefficient of determination
BA	Basal Area
CHM	Canopy Height Model
DAP	Digital Aerial Photography
DBH	Diameter at Breast Height
DEM	Digital Elevation Model
DRC	Democratic Republic of Congo
DSM	Digital Surface Model
DTM	Digital terrain model
EM	Electromagnetic Radiation
ExG	Excess Green Index
FSA	Forest Structural Attributes
FW	Fixed-Wing
GCC	Green Chromatic Coordinate
GCP	Ground Control Point
GCPs	Ground Control Points
GB	Gigabyte
GIOBIA	Geographic-Object-Based-Image-Analysis
GLCM	Grey Level Co-Occurrence Matrix
GLI	Green Leaf Index
GNSS	Global Navigation Satellite System
GPS	Global Positioning System
ha	Hectare
HS	Hyperspectral
IPCC	Intergovernmental Panel on Climate Change
ITD	Individual Tree Detection

© University of Pretoria

ITC	Individual Tree Crown
Km	Kilometre
lidar	Light Detection and Ranging
LULC	Land-Use, Land-Cover
m	Metre
MAE	Mean Absolute Error
ML	Machine Learning
MLA	Maximum Likelihood Algorithm
MPE (%)	Relative Mean Prediction Error
MR	Multi-Rotor
MRS	Multiresolution segmentation
MRV	Measurement, Reporting and Verification
NDI	Normalized Difference Index
NDVI	Normalized Difference Vegetation Index
NGRVI	New Green–Red Vegetation Index
NIR	Near Infrared
OBIA	Object Based Image Analysis
OLS	Ordinary Least Squares
Pred- R^2	Predicted Coefficient of determination
RCC	Red Chromatic Coordinate
RGB	Red Green Blue
RGR	Red–Green Ratio Index
RPAS	Remotely Piloted Aircraft Systems
RVI	Ratio Vegetation Index
R^2	Coefficient of determination
REDD+	Reducing Emissions from Deforestation and Forest Degradation
RMSE	Root Mean Square Error
rRMSE	Relative Root Mean Square Error
SfM	Structure from Motion

© University of Pretoria

SR	Simple Ratio Index
UAS	Unmanned Aerial System
UAS-SfM	Unmanned Aerial Systems and Structure from Motion approach
UAS-lidar	Unmanned Aerial System equipped with Light Detection and Ranging
UAV	Unmanned Aerial Vehicle
UHR	Ultra-High-Resolution
UNCCD	United nations convention on combating deforestation
UNFCCC	United nations framework convention on climate change
USA	United States of America
VI	Vegetation Indices

© University of Pretoria

Abstract

The efficient implementation of REDD+ programs and local sustainable forest management needs reliable data on species composition and distribution, forest biomass, and carbon storage, which are presently lacking in the majority of African vegetation formations. The study explored the use of unmanned aerial systems (UAS) imagery and associated processing tools in the management of the Miombo woodlands in Zambia. Four different studies were undertaken to meet the overall objective of this study. In order to have an overall understanding of the global application of UAS in forestry and the implications for its application to the Miombo woodlands, the first study was based on a review of the application of UAS in forest management and monitoring with a focus on challenges and opportunities for use in the Miombo woodlands. UAS technology, key attributes of the Miombo woodlands, and applications of UAS in forestry at the global and sub-Saharan African levels were reviewed, which enabled us to identify key prospects and challenges for UAS applications in the Miombo region.

As a demonstration of potential applications of UAS technology for managing the Miombo woodlands, the second study was focused on the use of multi-date and multi-spectral UAS imagery to classify dominant tree species in the wet Miombo woodlands in the Copperbelt Province of Zambia. Multi-date, multispectral UAS images taken at key phenological stages (leaf maturity, transition to senescence, and leaf flushing) and object-based image analysis (OBIA) with a random forest algorithm were utilized to classify the five dominant canopy species of the wet Miombo woodlands. The research found that combining multi-date raw band multi-spectral data with derived spectral indices produced better classification results (87.07% overall accuracy (OA), 0.83 Kappa) than using the best single-date multi-spectral data (80.12% OA, 0.68 kappa). The results from this study demonstrated the potential of using multispectral UAS imagery and phenology to map individual tree species in the Miombo woodlands of Zambia.

The third study was based on the application of UAS-Lidar to estimate forest structural attributes, which are critical to the management of the Miombo woodlands. UAS-Lidar data was used to estimate above-ground biomass, basal area, diameter at breast height, and volume, using multiple linear regression. The results indicate that the UAS-Lidar estimations provide the requisite degree of precision (relative root mean square error (RMSE): 3.40 - 20.89%) required for fulfilling international carbon reporting requirements

© University of Pretoria

and local forest management objectives. Furthermore, the use of unmanned aerial systems (UAS) equipped with Light Detection and Ranging (Lidar) technology offers a significant enhancement to the already utilized approaches for assessing Forest Structural Attributes (FSA) in the Miombo woodlands.

The fourth study was focused on bridging the spatial data gap that exists between detailed field inventory methods and satellite-based remote sensing methods that are required for wall- to-wall mapping of the Miombo woodlands. This study conducted a two-phase sampling design for wall-to-wall forest structural attributes estimation, where areas covered by a UAS-lidar were sampled by field plots and areas covered by wall-to-wall satellite imagery were sampled using a UAS-lidar. The results revealed that using UAS-lidar as reference data for predicting AGB using Sentinel-2 image metrics produced better results (Adj-R^2 = 0.70 Mg/ha, RMSE = 27.97 Mg/ha) than using direct field estimated AGB and Sentinel-2 image metrics (R^2 = 0.55 Mg/ha, RMSE = 38.10 Mg/ha). The results obtained demonstrated a practical solution to managing the Miombo woodlands using the available technology at multiple spatial scales.

The synthesis of these studies provides a holistic contribution for utilization of UAS technology and its accompanying processing tools in improving the acquisition of inventory data for the purpose of managing the Miombo woodlands in Zambia. This is a crucial necessity in effectively managing the diverse forested landscapes in the region.

© University of Pretoria

© University of Pretoria

Chapter 1 : General Introduction

1.1 Background

The Miombo woodland is the most extensive tropical woodland in Africa with an estimated coverage of 2.7 million km^2 mainly covering Angola, southern parts of the Democratic Republic of Congo, Malawi, Mozambique, Tanzania, Zambia, and Zimbabwe (Campbell, 1996). The Miombo woodlands are characterised by the dominance of three key deciduous genera (Brachystegia, Julbernadia and Isoberlinia) belonging to the family Fabaceae (Frost, 1996; Ryan et al., 2011a) The woodland offers a multiplicity of eco-services ranging from food (fruits, honey, edible insects, and bush meat), construction materials (poles, timber and fiber), fuel (charcoal, firewood), and medicine as well as large scale water management services (Syampungani et al., 2009; Chirwa et al., 2015; Kachamba et al., 2016a). However, the covered area is shrinking as a result of degradation and deforestation caused by competing requirements such as settlement and agricultural development, as well as unsustainable overexploitation of timber and fuel wood products (Luoga et al., 2002; Syampungani et al., 2009). Furthermore, climate change, invasive species, fire, and herbivory all have a detrimental effect on woodland coverage (Ribeiro et al., 2020a).

The rapid increase in CO_2 concentration in the atmosphere has attracted attention to preservation of carbon stocks in tropical ecosystems. The international community recognizes the importance of forests in the global carbon cycle evidenced by the establishment of Reducing Emissions from Deforestation and Forest Degradation, plus forest conservation, sustainable management of forest and enhancement of carbon stocks (REDD+) mechanism through the United Nations Framework Convention on Climate Change (UNFCCC) (Barquín et al., 2014). This mechanism provides a financial incentive to developing countries for forest conservation and implementation of sustainable forest management based on reported national level of carbon stocks to the UNFCC (Goetz et al., 2015). A credible forest monitoring system that provides a backbone for Monitoring, Reporting and Verification (MRV) is a prerequisite for implementation of the REDD+ programme, for each participating country (Day et al., 2014; Goetz et al., 2015). Consequently, countries are expected to establish a national baseline of carbon stock estimates to be used as a basis for reporting changes of carbon stocks over time (Goetz et al., 2015; UNFCCC, 2015)

© University of Pretoria

1.2 Motivation and philosophical argument

The effective execution of the REDD+ programs and local sustainable management of forests requires accurate data pertaining to species composition and distribution, forest biomass and carbon storage, which are currently deficient in the majority of African vegetation formations (Ribeiro et al., 2012; Goetz et al., 2015). Although ongoing efforts are being made to improve the field inventory designs in the Miombo ecoregion (Mugasha et al., 2013; Kachamba et al., 2016a; Handavu et al., 2021), it is important to note that field-based approaches still need a substantial investment of time, financial resources, and labour in order to gather an adequate quantity of data for effective forest management and international reporting requirements. Furthermore, woodlands are extensive and mostly situated in remote areas with limited accessibility for efficient field inventory plot installation and monitoring. Therefore, it is necessary to investigate technologies that may supplement field forest inventory methodologies in order to bridge data gaps and increase capacity for monitoring forest and carbon changes with accuracy that fulfills local forest management and international reporting criteria. The use of remote sensing technologies provides opportunities for accomplishing this task (Gizachew and Duguma, 2016).

1.2.1 Remote sensing for forest management in the Miombo woodlands

Remote sensing offers a comprehensive and integrated approach to obtaining spatially precise observations, facilitating the rapid and adaptive gathering of forest inventory data over large regions in a cost effective manner (Wulder et al., 2013; White et al., 2016; Liu et al., 2018b; Shen et al., 2019). Several studies (Kashindye et al., 2013; Halperin et al., 2016a; Macave et al., 2022) have effectively utilized medium-resolution imagery remote sensing, specifically Landsat and Sentinel-2, to estimate forest structural attributes (FSA) over large areas in the Miombo woodlands. However, these estimates do not meet the level of precision necessary for international reporting mechanisms and sustainable forest management at a local scale. Also, the medium-resolution satellite images that are normally used to make the National Forest Inventories (NFI) (Chamuya and Mgoo, 2014; GRZ, 2016; Government of Malawi, 2018) have problems such as: (i) inability to capture carbon stocks and carbon changes at appropriate resolutions for REDD+ (Gizachew and Duguma, 2016); (ii) inability to capture vertical structure of vegetation (Gibbs et al., 2007); (iii) failure to estimate biomass at dense leaf canopies due to saturation (Gizachew and Duguma, 2016); (iv) difficulty in capturing the spatial variability in the Miombo

© University of Pretoria

woodland, which alternates between open and dense vegetation (Ribeiro et al., 2012); and (v) failure to capture disturbances of minor spatial extent such as selective harvesting of trees for timber and fire wood (Day et al., 2014). Mauya et al. (2015) estimated above ground biomass (AGB) in the Miombo forests of Tanzania using airborne light detection and ranging (airborne-lidar) with acceptable precision for global reporting systems and sustainable local forest management. Although airborne lidar has the capability to capture 3D vegetation structure information that aligns with international reporting standards, it is not suitable for wall-to-wall coverage, and its acquisition cost is a significant barrier for the majority of forest managers operating within the Miombo ecoregion (Mitchell et al., 2017). For effective management of the Miombo woodlands, a wide range of forest data products from precise field inventories is required for comprehensive satellite remote sensing-based mapping. Therefore, there is a need for cost-effective tools that have possibilities for bridging the spatial data gap that exists between field inventory and satellite-based methods. Research on the other vegetation formations (Anderson and Gaston, 2013; Tang and Shao, 2015; Banu and Borlea, 2016; Iglhaut et al., 2019; Eugenio et al., 2020; Guimarães et al., 2020) provides sufficient evidence for us to postulate that unmanned aerial systems (UAS) can facilitate forest management objectives in the Miombo woodlands ecoregion.

1.2.2 UAS for forest management

Numerous forest applications have seen the use of UAS, including: estimation of forest structural attributes (FSA) (Kachamba et al., 2016b; Guo et al., 2017; Liu et al., 2018b; Cao et al., 2019a), identification of tree species (Gini et al., 2014, 2018; Feng et al., 2015; Lisein et al., 2015; Franklin and Ahmed, 2017), forest health assessment (Czapski et al., 2015; Dash et al., 2017), tree species phenology (Park et al., 2019), forest fire assessment (Smigaj et al., 2015; Hristov et al., 2018), and monitoring selective tree harvesting (Samiappan et al., 2017; Ota et al., 2019; Thiel et al., 2020). Despite the demonstrated applicability of UAS in forest management (Anderson and Gaston, 2013; Tang and Shao, 2015; Banu and Borlea, 2016; Iglhaut et al., 2019; Eugenio et al., 2020; Guimarães et al., 2020), the use of UAS technology in the Miombo woodlands has thus far been limited to estimating forest structural attributes using Structure-from-Motion (SfM) photogrammetry applied to photographs captured by unmanned aircraft systems (UAS) (referred to as UAS-SfM) at a single site in the dry Miombo woodlands of Malawi (Kachamba et al., 2016b, 2017; Domingo et al., 2019). In a groundbreaking study, Kachamba et al. (2016b) used UAS-

© University of Pretoria

SfM-derived point clouds to estimate AGB in the dry Miombo woodlands of Muyobe forest, Mzimba District, in northern Malawi, with enough accuracy for international reporting mechanisms and sustainable local forest management. However, UAS-SfM has been shown to underperform in denser forest settings (Mlambo et al., 2017), making it difficult to disseminate to denser regions of the Miombo woodlands. UAS-mounted lidar systems (UAS-lidar) has been reported to perform well even in denser forest environment (Guo et al., 2017; Liu et al., 2018b; Cao et al., 2019a).The availability of low-cost UAS-SfM technology and the largely open canopies of the Miombo woodlands (Ribeiro et al., 2020a), combined with the steadily declining cost of UAS-lidar sensors (Colomina and Molina, 2014), speak to the potential of using UAS technology for acquiring 3D vegetation structure information that is useful for FSA estimation and related applications, which need to be explored.

The other aspect of the Miombo woodland that is still neither well studied nor understood is the species distribution and abundance in the region. Species abundance and distribution are a key aspects of sustainable forest management as they enable forest managers to effectively suggest possible management practices that will enable efficient and sustainable use of the forest resources. However, species distribution maps needed to support sustainable forest management are still lacking in Zambia and the rest of the Miombo woodland ecoregion. Current forest inventories and other field-based data acquisition methods, such as field assessments, are not appropriate for mapping tree species due to the coverage extent and accessibility challenges of the forest areas involved. Therefore, there is need for new methods of mapping tree species composition and distribution in the Miombo ecoregion. The high spatial resolution of UAS images, together with the flexibility of temporal resolution (Colomina and Molina, 2014) and the evident phenological differences across Miombo woodland species from season to season (Frost, 1996), provide an opportunity for the use of UAS in tree species classification, species distribution mapping, and related applications.

1.3 Conceptual framework

Monitoring forests and implementation of mechanisms such as REDD+ and MRV for sustainable forest management requires adequate affordable data and tools to satisfy various forest applications (Figure 1.1). Forest data are collected at different scales to satisfy different applications and management levels. The freely available Landsat and

© University of Pretoria

Sentinel-2 imagery with moderate-spatial resolution, high temporal resolution and large area coverage are used to derive data products that are suitable for regional applications and decision making (e.g., early warning, hot spot identification). Moderate resolution (10 – 30 m) satellite imagery will require field data collections for georeferencing, ground truthing, model calibration, model validation and accuracy assessment. But the model results from moderate resolution satellite imagery are too coarse for application at a local level. The UAS imagery with ultra-high spatial resolution, flexible temporal resolution, and less area coverage are suitable for use at a local level to bridge the gap between coarse medium resolution products and ground methods. Miombo woodlands have characteristics that are amenable to most UAS forest applications, such as the suitability of applying UAS-SfM for estimating FSA due to the largely open canopies, and the interspecies phenological differences being easily captured by flexible temporal resolution UAS for tree species classification. The UAS can be used for generating detailed forest structure products that can be used for forest management and decision making at a local or stand level. However, UAS imagery also need filed data for georeferencing, ground truthing, model calibration, model validation and accuracy assessment. Furthermore, UAS imagery derived data products could also be used as reference data for moderate resolution satellite imagery data products.

© University of Pretoria

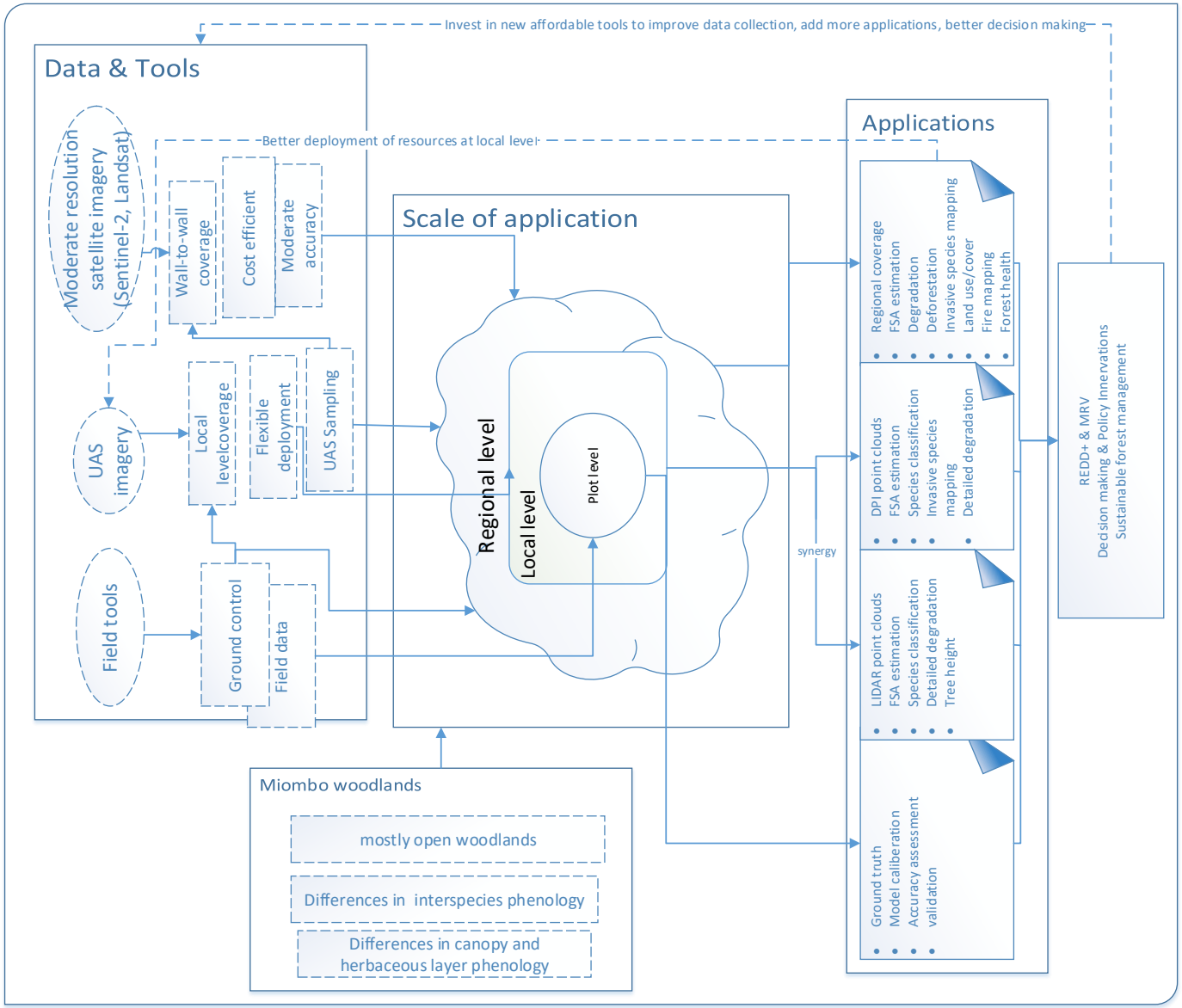

Figure 1.1. Conceptual framework for data generation and application

© University of Pretoria

1.4 Research aim and objectives

The aim of the thesis was to explore the application of UAS technology and associated processing tools in inventory data acquisition for use in management of the Miombo woodlands of Zambia.

1.4.1 Specific objectives

i. To review literature on the application of UAS in forest management and monitoring with a focus on challenges and opportunities for use in the Miombo woodlands

ii. Investigate the use of UAS imagery to classify tree species in the Miombo woodlands of Zambia following these research questions:

   (a). What is the optimal single season window for acquiring UAS imagery to discriminate tree species in the Miombo ecoregion?

   (b). Could multi-season imagery improve the discrimination of tree species in the Miombo ecoregion?

   (c). What other image features can improve Miombo species classification?

iii. Explore the potential of UAS-lidar for estimating forest structural attributes of the Miombo woodlands in Zambia

   (a). How can UAS-lidar be used to improve FSA estimations in the Miombo ecoregion region?

   (b). What are the suitable UAS-lidar metrics for estimating AGB in the Miombo woodlands of the Copperbelt province of Zambia?

   (c). How does the regression model developed using data from a single site compare with that developed using combined data from two sites?

   (d). Are the models developed on one site transferable to a different site where ground reference data are unavailable?

iv. Explore UAS-lidar as a sampling tool for satellite-based AGB estimations in the Miombo woodland of Zambia

   (a). What are the suitable UAS-lidar and Sentinel-2 metrics for estimating AGB in the Miombo woodlands of Zambia?

   (b). What are the optimal prediction models for mapping and estimating AGB using UAS-lidar and Sentinel-2 data?

   (c). (iii) Could UAS-lidar-estimated AGB replace field-estimated AGB as reference data?

© University of Pretoria

1.5 Thesis outline

There are six chapters in this thesis. Chapter 1 is an introduction, followed by four chapters (2, 3, 4, and 5) in the form of articles in the format prescribed by the target peer-reviewed journals, and Chapter 6 is a summary of all the results from the previous chapters. Among the set of four papers under consideration, Chapters 2 and 3 have been published. The other two chapters are in the manuscript stage and ready for publication. Each individual paper has been presented as its own chapter, establishing it as a discrete contribution to the main research objective. Because of this approach, certain overlaps in technique explanation, formulation, and illustration are unavoidable in the various chapters. Only a single reference was adopted to maintain consistency.

Chapter 1 introduces the research problem and outlines the aim and objectives of the thesis.

In Chapter 2, the use of UAS technology in the field of forestry is reviewed. The primary emphasis is placed on the various sensors utilized in this context, the methodology implemented for processing the collected data, as well as the challenges and limitations associated with this application. Furthermore, a review was conducted on the fundamental characteristics of the Miombo woodlands, including their structure, composition, and phenology, with the aim of determining the most effective methods for implementing this technology inside the Miombo woodlands. This chapter is based on:

Shamaoma, H.; Chirwa, P.W.; Ramoelo, A.; Hudak, A.T.; Syampungani, S. The Application of UASs in Forest Management and Monitoring: Challenges and Opportunities for Use in the Miombo Woodland. Forests 2022, 13, 1812. https://doi.org/10.3390/f13111812

Chapter 3 explores the use of Multi-Date and Multi-Spectral UAS imagery for classifying the dominant tree species in wet Miombo Woodlands of Zambia. The five dominant canopy species of the wet Miombo woodlands in the Copperbelt province of Zambia were classified using multi-date, multispectral UAS images acquired at important phenological phases (leaf maturity, transition to senescence, and leaf flushing) using object-based image analysis (OBIA) with a random forest algorithm. This chapter was based on:

© University of Pretoria

Shamaoma, H.; Chirwa, P.W.; Zekeng, J.C.; Ramoelo, A.; Hudak, A.T.; Handavu, F.; Syampungani, S. Use of Multi-Date and Multi-Spectral UAS Imagery to Classify Dominant Tree Species in the Wet Miombo Woodlands of Zambia. Sensors 2023, 23, 2241. https:// doi.org/10.3390/s23042241

Chapter 4 demonstrated the use of UAS-lidar to estimate four forest structural parameters above ground biomass, basal area, diameter at breast height, and volume at two locations 90 km apart in the wet Miombo woodlands using a multiple linear regression approach. In addition, the transferability of models produced from one location to another was evaluated. This chapter was based on:

Shamaoma, H.; Chirwa, P.W.; Zekeng, J.C.; Ramoelo, A.; Hudak, A.T.; Handavu, F.; Syampungani, S. Exploring the potential of UAS-lidar for estimating forest structural attributes of the Miombo woodlands in Zambia (Manuscript)

The emphasis of Chapter 5 was on bridging the spatial data gap that exists between accurate field inventory techniques and satellite-based remote sensing technologies necessary for wall-to-wall mapping of the Miombo woodlands. The study utilizes a two-phase sampling approach for estimating wall-to-wall AGB, with field plots sampling regions to be covered by a UAS-lidar and UAS-lidar sampling areas to be covered by wall-to-wall satellite imaging. This Chapter is based on:

Shamaoma, H.; Chirwa, P.W.; Zekeng, J.C.; Ramoelo, A.; Hudak, A.T.; Handavu, F.; Syampungani, S. Exploring UAS-lidar as a sampling tool for satellite-based AGB estimations in the Miombo woodland of Zambia (Manuscript)

Chapter 6 summarizes all of the study results from the preceding chapters. The contribution of the study results to society and forest management is discussed. General conclusions are offered, and additional efforts are recommended.

© University of Pretoria

Chapter 2 The application of UAS in forest management and monitoring: Challenges and opportunities for use in the Miombo woodland

This chapter is based on:

Shamaoma, H.; Chirwa, P.W.; Ramoelo, A.; Hudak, A.T.; Syampungani, S. The Application of UASs in Forest Management and Monitoring: Challenges and Opportunities for Use in the Miombo Woodland. Forests 2022, 13, 1812. https://doi.org/10.3390/f13111812

© University of Pretoria

Abstract

The Miombo woodland is the most extensive tropical woodland in south central Africa. However, field sample plot data about forest cover changes, species distribution and carbon stocks in the Miombo ecoregion is inadequate for effective forest management. Owing to logistical challenges that come with field-based inventory methods, remote sensing plays an important role in supplementing field methods to fill in data gaps. Traditional satellite and manned aircraft remote sensing platforms have their own advantages and limitations. The advent of Unmanned Aerial Systems (UAS) has made it possible to acquire forest data at unprecedented spatial and temporal scales. UAS are adaptable to various forest applications in terms of providing flexibility in data acquisition with different sensors (RGB, multispectral, hyperspectral, thermal, and light detection and ranging [lidar]) at a convenient time. To highlight possible applications in the Miombo woodlands, we first provide an overview of the Miombo woodlands and recent progress in remote sensing with small UAS. An overview of some potential forest applications was undertaken to identify keys prospects and challenges for UAS applications in the Miombo region, which will provide expertise and guidance upon which future applications in the Miombo woodlands should be based. While much of the potential of using UAS for forest data acquisition in the Miombo woodlands remains to be realised, it is likely that the next few years will see such systems being used to provide data for an ever-increasing range of forest applications.

Keywords: UAS; Miombo woodlands; Forest structure, Tree species, Forest degradation

© University of Pretoria

2.1 Introduction

The Miombo woodland covers 2.7 million km^2 in Africa, mainly Angola, the southern parts of the Democratic Republic of Congo, Malawi, Mozambique, Tanzania, Zambia, and Zimbabwe (Campbell, 1996). The Miombo woodlands are characterised by the dominance of three key deciduous genera belonging to the family Fabaceae, subfamily Caesalpinioideae in the genera *Brachystegia, Julbernadia and Isoberlinia* (Frost, 1996). They occur on areas with generally poor soil nutrients and characterised by distinct wet and dry seasons, with annual mean rainfall ranging from 650 mm to 1500 mm (Frost, 1996; Ribeiro et al., 2012).The Miombo woodlands are divided into dry and wet woodland types in line with rainfall in the zone of occurrence (White, 1983) as well as species composition and structure (see Table 2.1).

Table 2.1 Categorization of the Miombo Woodlands.

Category	dominant species	Average canopy height	occurrence	Annual Rainfall
Dry Miombo	*Brachystegia spiciformis, Brachystegia boehmii, and Julbernardia globiflora*	15 m, with less crown overlap	southern Malawi, Mozambique, and Zimbabwe	less than 1000 mm
Wet Miombo	*Brachystegia floribunda, Brachystegia glaberrima,* Brachystegia longifolia, *Brachystegia wangermeeana, Julbernardia paniculata, Isoberlinia angolensis and Marquesi macroura*	Trees greater than 15 m with some crown overlap	eastern Angola, northern Zambia, DRC, central Malawi and south western Tanzania	more than 1000 mm

The Miombo woodland is home to natural resource dependent communities and offers a multiplicity of eco-services ranging from food (fruits, honey, edible insects, and bush meat), construction materials (poles, timber and fiber), fuel (charcoal, firewood), medicine and water provisioning services (Syampungani et al., 2009; Ryan et al., 2011b; Chirwa et al., 2015; Kachamba et al., 2016a). However, rapid population growth coupled

© University of Pretoria

with increase in electricity tariffs and prices of petroleum products has led to increased demand for land for settlement and agriculture expansion as well as overexploitation of timber and fuel wood products (Luoga et al., 2002; Syampungani et al., 2009). Consequently, there is a rapid upsurge in deforestation and degradation of the woodlands across the ecoregion (Mayes et al., 2015; Halperin et al., 2016b).

However, current estimates of forest cover changes, species distribution and carbon stocks in the Miombo ecoregion are inadequate for effective forest management, and international reporting requirements such as for the Reducing Emissions from Deforestation and Forest Degradation plus (REDD+) necessary for forest conservation (Herold and Schiller, 2009; Ribeiro et al., 2012; Barquín et al., 2014; Mayes et al., 2015).

Many studies have been conducted on UAS applications in forestry in a number of continents with the goal of sharing knowledge on their utility, e.g. (Anderson and Gaston, 2013; Banu and Borlea, 2016; Eugenio et al., 2020; Guimarães et al., 2020). Nevertheless, a review focusing on UAS forestry applications in Miombo woodlands is still not available. A web-based search for articles on the following keywords: "Unmanned Aerial Systems", "Unmanned Aerial Vehicles", "Unoccupied Aerial vehicles", "Remotely Piloted Aircraft Systems", "Drones" and their acronyms "UAS", "UAV" and "RPAS" in combination with commonly use synonyms in forestry: "forest", "forestry" and "forests" from 1st January 2010 to 31st December 2020, in the Web of Science Database (WoS) based on Author affiliation revealed that Africa had the least number of publications compared to the other continents (Figure 2.1). Thirty-two articles were published with participation of African affiliated authors and only 9 of those articles were purely UAS forestry application related articles from sub-Saharan Africa. Furthermore, all these articles were published between the years 2016 and 2021. Table 2.2 shows that these studies were focused on biomass estimation and other forest structural attributes. Only three of these studies included other forest applications namely: (i)) height estimates of woody vegetation for monitoring disturbance from fire and grazing (Mayr et al., 2018), (ii) use of multi-spectral UAS imagery to estimate pre-fire AGB for the purpose of quantifying the fuel load (Eames et al., 2021), and (iii) extracted tree crowns morphology for predicting tree species (Bossoukpe et al., 2021a). With the continuous improvement of UAS platforms, sensors and processing technologies, the number of applications in sub-Saharan Africa are expected to increase, making it necessary to undertake a review of

© University of Pretoria

UAS applications in forestry to understand the associated opportunities and challenges in forest monitoring and management. Therefore, this paper is designed to summarize UAS applications in forestry and implications for management of Miombo woodland attributes.

2.2 UAS platforms, sensors and data processing

2.2.1 Classification of UAS

There are many classifications of UAS, which are based on different characteristics such as size, weight, endurance and range capabilities (Table 2.3: (Anderson and Gaston, 2013)). The majority of UAS used in forest application are in the 'Small, and 'Micro classes because of relatively low cost and ease of operation compared to other classes (Tang and Shao, 2015). This trend is expected to continue in the application of UAS in the Miombo woodlands e.g. (Kachamba et al., 2016b; Domingo et al., 2019) and therefore this study will be focused on these two classes. Typically, UAS are classified based on takeoff and landing technique: (i) horizontal take-off and landing - characteristic of fixed-wing (FW) aircraft (i.e., airplanes), and (ii) vertical take-off and landing characteristic of rotary-wing (RW) aircraft (i.e., helicopters, multi-rotor quadcopters, hexacopters, etc.). RW have capability for vertical take-off and landing, making them suitable for deployment and launching in areas with limited space such as built-up areas and forests. Compared to FW aircraft, RW aircraft are cheaper, more compact and portable, easier to use for both auto pilots and humans, and are more stable leading to superior image quality (Colomina and Molina, 2014; Tang and Shao, 2015). The major limitation of RW is that they have complex mechanical systems with many rotor blades which consumes a lot of power making them have low speed and less endurance resulting in less flight time and area coverage per flight compared to FW.

The FW have high speed, large payload capacity, longer endurance and are able to cover longer distances within one flight, which makes them more suitable for mapping large areas compared to RW. The disadvantage for the FW is inability for vertical take-off and landing which makes them less suitable for application in dense forest environments with limited space, and they are relatively more expensive than RW (Colomina and Molina, 2014). In addition, FW have lower stability especially in windy conditions, which can impact image quality (Tang and Shao, 2015). In terms of potential for application in the Miombo woodlands, which are characterised by generally open canopies, both FW and

© University of Pretoria

RW aircraft have high potential for application but the RW is likely to dominate in line with global trends as revealed in a study by Eugenio et al. (2020) who carried out a global review of the application of UAS in forestry from 2010 to 2019 and found that RW where more popular than FW platforms. A similar study by Guimarães et al. (2020) corroborated these findings. The RW ease of use, affordability, and compactness gives it an edge over the FW counterpart albeit the FW has an advantage of high endurance. Furthermore, most UAS study sites are small, and regulations in the Miombo ecoregion countries require maintaining the line of sight by the pilot, which are compatible with RW.

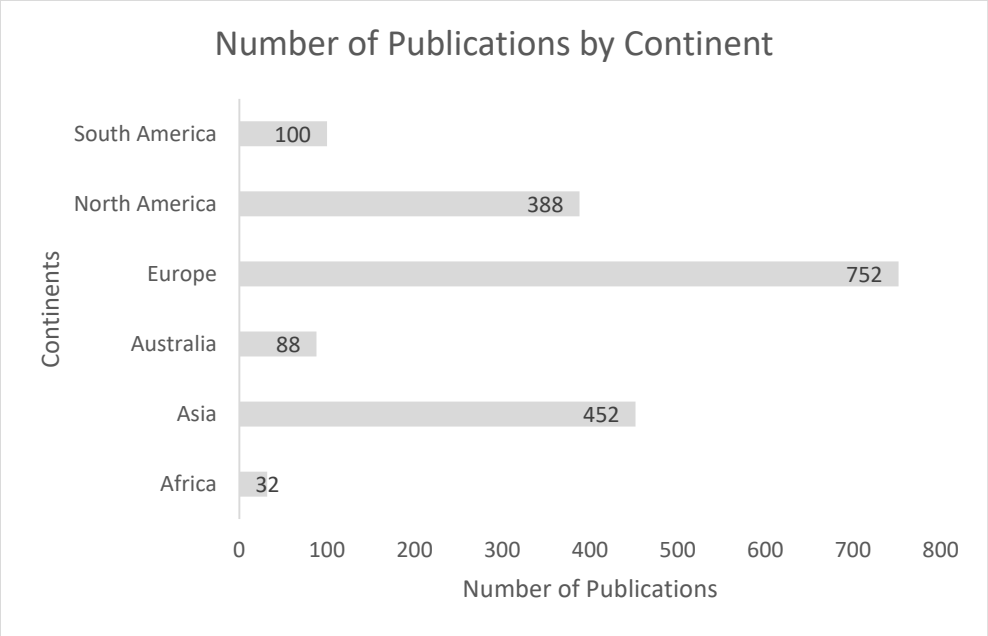

Figure 2.1. Showing number of forest-related UAS publications by continent

2.3 UAS Sensors

UAS are flexible platforms with capability to host a wide variety of sensors that can serve different types of forest applications including: forest inventory, conservation and monitoring of natural resources, fire monitoring, disease detection and mapping, and many others (Eugenio et al., 2020). In this section we present some of the sensors most commonly applied in forestry studies with great potential for application in the Miombo woodlands.

© University of Pretoria

Table 2.2 Summary of studies that applied UASs in forestry in sub-Saharan Africa.

UAS/Type	Sensor	Aim	Location	Product	Performance	Reference	Year
SenseFly eBee (FW)	RGB	Biomass estimation and impact of DTMs generated from different methods on AGB estimates	Malawi	AGB	R^2 = 0.58-0.67	(Kachamba et al., 2016b)	2016
SenseFly eBee (FW)	RGB	Assess influence of plot size on AGB estimation	Malawi	AGB	R^2 = 0.31-0.64	(Kachamba et al., 2017)	2017
Soleon Coanda x12 (RW)	RGB	Monitor disturbance of fire and grazing on woody vegetation	Namibia	Mean tree height metrics	R^2 = 0.7	(Mayr et al., 2018)	2017
SenseFly eBee (FW)	RGB, NIR	Assess UAS influence of image resolution, sensor type and image overlap on AGB estimation accuracy	Malawi	AGB	R^2 = 0.55-0.76	(Domingo et al., 2019)	2019
Unspecified DJI (RW)	RGB, and MS	Monitoring structural characteristics of vegetation	Botswana	Mean tree heights, crown area	N/A	(Kolarik et al., 2020)	2020

© University of Pretoria

Phantom 4 DJI (MR)	RGB	Derive tree heights and assess sensitivity of derived heights on AGB estimation	Ethiopia	AGB	R^2 = 0.99	(Hadush et al., 2022)	2021
Spark DJI (RW)	RGB	Assess woody and herbaceous phytomass	Senegal	AGB	R^2 = 0.59 and 0.71	(Bossoukpe et al., 2021b)	2021
Spark DJI (RW)	RGB	Estimate tree height and crown area	Senegal	Mean tree heights, crown area	R^2 = 0.84 and 0.93	(Bossoukpe et al., 2021a)	2021
Matrice 100 DJI (RW)	MS	Monitor pre-fire AGB	Botswana and Mozambique	AGB	R^2 = 0.91 and 0.77	(Eames et al., 2021)	2021

RW = rotary-wing, FW = Fixed wing, RGB = red, green, blue, MS = multi-spectral, AGB = above ground biomass.

Table 2.3 Classes of UAS platforms.

Size	**Large**	**Medium**	**Small**	**Micro**
Operating range.	Up to 500 km	Up to 500 km	< 10 km	< 10 km
Endurance	Up to 2 days	Up to 10 hours	< 2 hours	< 1 hour
Flying altitude	3 -20 km	< 4 km	< 1 km	< 250 m
Payload	50 kg	50 kg	5 - 30 kg	< 5 kg

© University of Pretoria

2.3.1 Visible light sensors (RGB)

The sensors that are sensitive to the portion of the electromagnetic spectrum (EM), about 0.4-0.7µm, that is also sensed by the human eye, are referred to as visible light or Red, Green and Blue (RGB) sensors (Lillesand et al., 2015). According to a review by Colomina and Molina, (2014), RGB sensors are the most commonly used sensors by UAS systems for forestry. A review by Eugenio et al. (2020) on the global development and application of UAS technology in forestry from the year 2010 -2019 revealed that 57% of UAS forest applications used RGB sensors. The major contributing factors to their popular use include: (i) low cost compared to the other sensors; (ii) less sophistication, easy to operate and light weight; (iii) low cost and readily available processing software; (iv) RGB images are easy to process compared to those from other sensors; and (v) most low cost UASs come with an RGB camera integrated on the system (Colomina and Molina, 2014; Eugenio et al., 2020). These attributes explain why the RGB sensor has been most applied in pioneering forestry applications in sub-Saharan Africa (Kachamba et al., 2016b, 2017; Mayr et al., 2018; Domingo et al., 2019; Kolarik et al., 2020; Bossoukpe et al., 2021a; b; Hadush et al., 2022).

Despite their wider application, the limited spectral range of RGB sensors makes them inadequate for analyzing many vegetation parameters that require spectral information beyond the narrow visible spectrum (Nebikera et al., 2008). For example, a study by Effiom et al. (2019), in nature reserves, Amtsvenn, Germany, demonstrated that a combination of UAS-RGB images with Multispectral Paleiades images significantly improved overall tree species classification from 62% to 84% compared to using UAS-RGB images alone. Similar observations were made by Franklin and Ahmed, (2017), who found that the addition of a near-infrared band to RGB improved the tree species classification by about 11%. In another study, Kolarik et al. (2020) assessed the effectiveness of UAS imagery for monitoring structural characteristics of vegetation in a semiarid savanna woodland, Chobe Enclave in northern Botswana, by comparing multiple approaches for extracting woody vegetation structure from UAS imagery. They assessed the efficacy of UAS imagery from RGB and multi-spectral sensors to extract vegetation structure parameters (crown area and fractional woody cover) and found that the NIR band in the multispectral sensor improved tree crown delineation and estimates of crown area, fractional woody cover, and herbaceous cover. However, despite the limitations of RGB sensors in the discrimination of tree species and studies of forest health, photogrammetric point clouds derived from RGB stereo images have been found to be comparable to and cost less than three dimensional (3D) lidar data (Iglhaut et al., 2019), which are currently lacking in the Miombo woodlands.

© University of Pretoria

2.3.2 Multispectral

Multispectral sensors are sensitive to visible part of the spectrum as well as wavelengths that fall beyond the visible spectrum, which may include: Near Infrared (0.7-1.3 μm), Middle Infrared (1.3 – 3 μm), and Thermal Infrared (3 – 14 μm) regions (Lillesand et al., 2015), and spectral bands are stored as separate images in monotone. This allows for flexibility in choice of spectral bands to form desired image composites for image analysis. However, separate spectral bands increase the sophistication, weight and cost of the sensor as well as the processing and storage requirements of the resulting imagery (Whitehead and Hugenholtz, 2014). Multispectral sensors that include the Near Infrared (NIR) part of the EM have significant advantages in vegetation applications because of the high vegetation reflectance in NIR compared to the visible part of the EM. Many studies have used UASs with multispectral sensors in forest management related applications. For example: (i) species identification (Franklin, 2017; Franklin and Ahmed, 2017; Gini et al., 2018; Xu et al., 2020), and (ii) exploiting the dissimilarities in reflectance properties between the visible and near infrared to calculate vegetation indices and monitor plant health (Czapski et al., 2015; Minarik and Langhammer, 2016; Dash et al., 2017, 2018). Advantages of these sensors compared to RGB sensors is that the addition of NIR increases the possibility for computing various vegetation indices (Bannari et al., 1995; Xue and Su, 2017) required for analyzing vegetation health and increases the possibilities for discriminating various tree species, e.g. (Gini et al., 2014; Franklin and Ahmed, 2017). For example, Ahmed et al. (2017) compared UAS RGB and multispectral imagery io classify different vegetation covers and found that multi-spectral based classification results were 10-15% higher compared to RGB image-based results. The disadvantages of the multispectral sensors compared to RGB sensors include higher cost and the requirement for more complex pre-processing methods in order to extract useful information from the captured images. As a result, less studies have employed UAS multi-spectral sensors compared to RGB sensors (Eugenio et al., 2020) and this also is reflected in the number of studies in sub-Saharan Africa under this review (Table 2.2). The Miombo woodland canopy is characterised by diverse tree species with similar appearance (Frost, 1996), and addition of NIR bands improves capability to discriminate tree species that might be difficult to discriminate by RGB sensors.

2.3.3 Hyperspectral Sensors

Hyperspectral sensors capture imagery in narrow spectral bands over a continuous spectral range, recording the spectra for all pixels in the scene. They capture more detailed information than multispectral sensors because an entire spectrum is acquired at each pixel. The major advantage of hyperspectral sensors is that they are able to discriminate small spectral details over narrow bands of the EM which could otherwise be generalized by multispectral

© University of Pretoria

broadband sensors (Adão et al., 2017). This is useful for detailed vegetation analysis for example discrimination of different vegetation species (Fung et al., 2008; Naidoo et al., 2012; Fassnacht et al., 2014b). According to the comparison of UAS sensors in a review by Colomina and Molina (2014), the disadvantages that limit its application with UAS include heavy payload, high cost of sensors, requirement for huge storage space due to the large number of bands, and complexity of data acquisition and analysis. Yao et al. (2019) added that most hyperspectral sensors are a linear-array and require specialized processing software, and users are expected to take care of data formats and geometric corrections. Due to these disadvantages, only a few studies have utilized this sensor type in other parts of the world (Eugenio et al., 2020; Guimarães et al., 2020), and none so far in sub-Saharan Africa. However, with continuous developments in both sensor and processing software technologies, some of the stated limitations are expected to be overcome, and the cost is expected to decrease which will open room for more applications (Colomina and Molina, 2014) including in sub-Saharan Africa.

2.3.4 Thermal sensors

Thermal infrared sensors capture information about the temperature of the heat emitted by objects, as opposed to reflected solar radiation, and images are produced based on temperature response of the emitting objects as opposed to their spectral reflectance properties. The application areas for UAS-Thermal sensors in forestry studies include: forest fire monitoring(Merino et al., 2012; Hristov et al., 2018), forest health monitoring (Smigaj et al., 2015), and detecting warm-blooded animals in the forests (Witczuk et al., 2017). The use of UAS thermal sensors in forestry studies is limited (see (Eugenio et al., 2020) for number of published articles compared to other sensors and (Guimarães et al., 2020) for summary of applications) and is yet to be applied in sub-Saharan Africa. This could be due to their low spatial resolution compared to RGB and multispectral sensors, which limits the number of applications that can use the data. Another challenge for active fire remote sensing is the huge dynamic range of the brightness temperatures, which presents much more of an engineering challenge to measure. As a result, most thermal IR images saturate where there are active flames, especially the sensors light enough to be a feasible payload on a UAS (Colomina and Molina, 2014). Thermal cameras are also more expensive than RGB, further limiting their application in the Miombo.

2.3.5 lidar Sensors

lidar is an active laser-based remote-sensing technology that measures distance based on the return time of emitted light (Pádua et al., 2017). The advantage of lidar in forest applications lies in its ability to characterize forest structure in 3D with high accuracy (Popescu and Hauglin,

© University of Pretoria

2014). For example studies in conifer stands by Naesset, (1997) in Norway and by Magnussen and Boudewyn, (1998) in British Columbia used airborne lidar to estimate stand height with (R^2 = 0.90) and volume with (R^2 = 0.45 to 0.89). The other important advantage is ability to penetrate the forest canopy, which makes it possible to capture understory vegetation as well as bare earth terrain in forested areas, although terrain accuracy is reportedly reduced with increasing canopy cover (Reutebuch et al., 2003). For example, an assessment of a lidar-generated DTM in a mountainous forested area of western Washington State, United States of America under varying vegetation conditions (Reutebuch et al., 2003), found a mean DTM error ranging from 0.16 m for bare ground to 0.31 m for dense canopy. Examples of applications of UAS mounted lidar (UAS-lidar) systems in forestry include: below canopy mapping (Chisholm et al., 2013), tree stem detection and diameter measurements (Kuželka et al., 2020), forest change detection (Wallace et al., 2014), and estimating forest structure parameters (Wallace et al., 2016; Cao et al., 2019a). Despite its advantages compared to other sensors, UAS-lidar applications are still less pronounced as evidenced by the number of articles published in a review by Eugenio et al. (2020) and so far, there is no example of its application in sub-Saharan Africa. The major drawback of a UAS-lidar is heavier payload which requires bigger and relatively more expensive drones, and the associated higher cost of lidar sensors. However, the ability of lidar to penetrate forest canopies and detect bare earth elevations in difficult forest environments (White et al., 2013b) compensates for some of the disadvantages; with expected reductions in cost and improvements in sensor technology, the number of studies employing this technology is expected to increase. A pioneering study by Lin et al. (2011) developed a UAS-mounted lidar system (UAS-lidar) and were able to estimate tree heights and detect utility poles. In a similar study, Wallace et al. (2012b) developed a low-cost UAS-lidar system with an accompanying workflow for producing 3D point clouds, and used it to measure tree location, height, and crown width.

2.4 Data processing

Typically, many UAS sensors will generate huge data volumes which need to be processed to give meaningful information to satisfy various forestry applications. There are several post-processing options for UAS imagery that can be pursued to satisfy intended forestry applications. Some common outputs from UAS imagery include: (i) mosaicking, that gives a seamless synoptic view of the area under study, (ii) 3D point clouds that are used in forest inventory and estimating forest structure parameters, (iii) vegetation indices for the monitoring forest health and discriminating different species, and (iv) classification and regression.

© University of Pretoria

2.4.1 Mosaicking

UAS use small format optical sensors that capture a series of overlapping photographs covering an area. Such single images cover an area of very limited spatial extent of a forest for meaningful analysis and need to be stitched together to form one composite image known as a mosaic. Most UAS optical imagery processing software use a scale invariant feature transform (SIFT) algorithm to mosaic UAS imagery. Jia et al. (2015) divides mosaicking process into three stages (i) image pre-processing (correction for image distortion); (ii) image registration (feature extraction, feature matching, model transformation, and parameter estimation); and (iii) image fusion (eliminating discontinuity of colour and achieve smooth transition from one photo to anther). Finally, the mosaic is georeferenced using ground control points or orthorectified using a DTM.

2.4.2 Three-dimensional point clouds

Three-dimensional (3D) point clouds are generated either directly using active lidar UAS sensors e.g. (Wallace et al., 2012a; Kuželka et al., 2020) or indirectly from passive optical UAS Digital Aerial Photography (DAP) using the Structure from Motion approach (SfM) (Dandois and Ellis, 2010; Kachamba et al., 2016b; Tomaštík et al., 2019; Xu and Ruan, 2020).

The SfM approach stems from computer vision automatic feature matching algorithms (Snavely et al., 2007), and the principle is well described in Westoby et al. (2012) and Iglhaut et al. (2019). According to Westoby et al. (2012), SfM involves the re-establishment of the camera pose and scene geometry simultaneously through matching features in multiple overlapping, offset images and generating 3D point clouds in the image space coordinate system. The image space 3D point cloud is transformed to the object space in real world coordinates by the use of Ground Control Points (GCPs) with known coordinates in both systems to generate a Digital Surface Model (DSM), orthomosaic or other point cloud statistics. The DSM is the key product from which a canopy height model (CHM) can be generated by subtracting a Digital Terrain Model (DTM) from a DSM (Kraus and Pfeifer, 1998).

Conversely, the UAS lidar sensor directly generates a 3D point cloud which undergoes three processes to produce a CHM: (i) de-noising to remove outliers (e.g., signals bouncing off from captured birds flying above the canopy) to generate a DSM; (ii) filtering or classifying, which entails separating ground from non-ground points to generate a DTM representing the ground terrain; and (iii) normalizing the DSM to generate a CHM by subtracting the DTM from the DSM.

© University of Pretoria

Two methods have been applied to extract forest attributes from point clouds: the area-based approach (ABA) and individual tree detection (ITD) (Yu et al., 2010; Chen, 2013). In ABA methods, forest characteristics, such as mean tree height, mean diameter, basal area, volume and biomass are estimated at stand or plot level using statistics calculated from point clouds resulting in canopy height and density metrics used in regression, discriminant analysis or nonparametric estimation techniques, e.g., as in (Means et al., 2000; Naesset et al., 2004; Hudak et al., 2008; Maltamo et al., 2014a; Cao et al., 2019c). In the ITD methods, individual trees are segmented from point clouds and tree level attributes such as tree height, crown width and crown base height can be derived either directly from point clouds or statistical metrics such as those used in area-based approaches using crown metrics derived from point cloud data within individual tree segments (Vastaranta et al., 2011; Mohan et al., 2017; Guerra-hernández et al., 2018)

The ABA approach can operate accurately with lower lidar pulse densities but requires more field measured plots for calibration. On the other hand, the ITD-based approach requires less field data for calibrating the individual tree measurements (Yu et al., 2010). However, the application of ITD approach is still limited compared to ABA due the lack of generic algorithms that can extract individual trees in varying complex forest environments especially broadleaf trees that have an inconsistent morphological structure, which is difficult to model using existing algorithms (Chen, 2013).

2.4.3 Image classification

Apart from extracting point clouds for estimating forest structure parameters, ultra-high resolution (UHR) optical UAS imagery can be classified to extract various forest characteristics that include (i) forest cover maps, (ii) forest burn severity, (ii) forest health (Dash et al., 2017) and forest tree species identification (Franklin, 2017; Feng and Li, 2019). Classification of UHR UAS imagery is either based on pixel-based classifiers, e.g., maximum likelihood algorithm (Gini et al., 2014), or Geographic Object Based Image analysis (GEOBIA), machine learning (ML) algorithms (Franklin and Ahmed, 2017), or a broad range of variants and hybrids of these methods (Singh et al., 2015). However, the UHR UAS imagery presents new challenges, which include intra-crown spectral variability (Gini et al., 2014; Franklin, 2017), illumination differences due to occlusion (Whitehead et al., 2014), and challenges in tree crown extraction (Gomes and Maillard, 2016). GEOBIA, in which the classification is based on image objects that correspond to targeted real world objects (e.g., individual tree crowns) instead of individual pixels (Blaschke, 2010) has been found to be effective in addressing some of these challenges (Franklin and Ahmed, 2017).

© University of Pretoria

GEOBIA has two main processing steps: (i) image segmentation, which is the process of dividing an image into homogeneous regions or objects that correspond to discernible features in remote sensing imagery, e.g., trees, buildings, grasslands, and water bodies (Pal and Pal, 1993; Costa et al., 2017); and (ii) classification of segmented image objects. Segmentation algorithms are categorized by the approach used to divide image objects: (i) pixel based (ii) edge based, (iii) region growing and (iv) hybrid method; a detailed discussion of these approaches can be found in (Pal and Pal, 1993; Hossain and Chen, 2019). In natural forest environments, segmented objects correspond to individual tree crowns. Therefore, GEOBIA entails first delineating individual tree crowns (ITCs), followed by classification of identified ITCs into appropriate species basing on the spectral characteristics of ITCs (Gomes and Maillard, 2016). Tree species classification based on ITCs has been found to yield better results compared to pixel based classification; for example, (Franklin, 2017) reported 60% and 80% for pixel based and GEOBIA, respectively. Segmentation techniques have been applied to delineate ITCs from different UAS products such as orthophoto mosaics, CHMs, point clouds or a combination of these. For example, Guerra-hernández et al. (2018) extracted ITCs from UAS-SfM and UAS-lidar generated point clouds in a Eucalyptus plantation in Valongo, Porto, Portugal with accuracies of 80% and 96%, respectively. In a study by Franklin and Ahmed (2017), they segmented multispectral UAV images acquired over a northern hardwood forest in eastern Ontario, Canada, then classified the generated image objects using a Machine Learning (ML) algorithm (Random Forests) to identify different tree species. A study by Mishra et al. (2018) used GEOBIA to identify different vegetation species in the Himalayan Langtang National Park, Nepal by segmentation, followed by multi-level image analysis and achieved 78% accuracy.

2.4.4 Vegetation indices

Vegetation indices (VI) are useful algorithms for quantitative and qualitative monitoring and evaluation of vegetation cover, vigor, health, and growth dynamics (Xue and Su, 2017). VIs are based on the reflection of EM radiation by vegetation, which makes it possible to distinguish vegetation from other ground elements. As a result, many VIs have been developed for various vegetation monitoring applications (Bannari et al., 1995; Xue and Su, 2017). There are two broad categories of VIs that are commonly extracted from optical UAS imagery for monitoring vegetation (see Table 2.4 for formulae used to calculate these indices): (i) those that are based on multispectral or hyperspectral imagery (e.g., Ratio Vegetation Index [RVI], Normalized Difference Vegetation Index [NDVI], Simple Ratio [SR] Vegetation Index, etc.) and (ii) those that are computed based on the visible spectrum (e.g., Excess Greenness Index [ExG], Normalized Difference Index [NDI]), Red Green Ratio Index [RGRI] etc.).

© University of Pretoria

NDVI has been the most widely used VI, which is calculated from multispectral images as the normalized ratio between the red and near-infrared bands and used to detect and monitor vegetation status (Xue and Su, 2017). However, with regards to UAS, as revealed above, the RGB sensors are the most used sensors, but they do not have the near-infrared band which facilitates vegetation detection. As a result, there are new efforts of establishing VIs based on RGB sensors as demonstrated in a study by Zhang et al. (2019), who introduced the new green-red vegetation index (NGRVI) to extract vegetation information in arid and semi-arid lake Ebinur basin of Xinjiang Uygur region of China with more than 90% accuracy. Another study by Agapiou, (2020) explored the use of various published VIs on openly licensed RGB UAS imagery from several case studies in different countries with different environments and found that green leaf index (GLI) yielded the best results for all case studies.

Table 2.4 Examples of visible-spectrum- and multispectral-based indices.

Examples of multispectral based indices.		
Index	**Abbreviation**	**Formula**
Normalized Difference Vegetation Index	NDVI	$\frac{NIR - R}{NIR + R}$
Ratio Vegetation Index	RVI	$\frac{R}{NIR}$
Simple Ratio Index	SR	$\frac{NIR}{R}$
Excess Greenness Index	ExG	$2G - R - B$
Normalized Difference Index	NDI	$\frac{G - R}{G + R}$
Red Green Ratio Index	RGRI	$\frac{R}{G}$
New Green-Red Vegetation Index	NGRVI	$\frac{G^2 - R^2}{G^2 + R^2}$
Green Leaf Index	GLI	$\frac{2G - R - B}{2G = R + B}$

2.5 Classification of Miombo tree species

The Miombo dominant canopy species have similar physiognomy resulting in similar appearance attributed to the fact that most of these species are of the family Caesalpiniodeae (Frost, 1996). This familial similarity in appearance presents challenges as there is high spectral similarity between co-occurring species, which may be difficult to discriminate by low spatial/spectral/temporal resolution remote sensing imagery. UAS platforms provide flexibility to accommodate multiple sensors (RGB, multispectral, hyperspectral, and lidar), which can be

© University of Pretoria

used to acquire ultra-high spatial resolution imagery at convenient frequent intervals for use in the identification of tree species (Colomina and Molina, 2014). UAS enables the acquisition of imagery at sub-metre resolution, making it usable for the identification of individual tree species. However, ultra-high spatial resolutions may lead to different spectral responses from parts of the same tree such as leaves, branches and trunks, which can make it difficult to identify trees at species level due to variation of textures and spectral signatures within the same tree. Other challenges in using high resolution optical data from UAS for classification of tree species that might affect the quality of results include: (i) variation in illumination conditions for images taken on different dates and at different times of day that will result in different spectral response for the same objects, (ii) intraspecies variation in phenological development, which is common in the Miombo woodlands, and (iii) similarities in leaves and morphology of different tree species in the Miombo woodlands, which will result in mixing of different species. As a result, object-based image analysis is preferred to conventional pixel-based classifiers for UAS imagery. For example, a study by Franklin and Ahmed (2017) showed an improvement in classification results for identifying tree species from 50-60% for pixel-based classification to 80% percent for object-based classification using the same UAS imagery in the same area.

2.5.1 Flexible temporal frequency

UAS provides a flexible temporal frequency (Tang and Shao, 2015) at which data can be acquired to coincide with important phenological events that can help discriminate different tree species. The proper timing of these events in the Miombo for example can help discriminate: (i) herbaceous layer from tree canopy using Normalized Difference Vegetation Index (NDVI) at the end of the rainy season in May, (ii) discriminate *Brachystegia* species from other species at leaf flushing using reddish colour, (iii) discriminate *Julbernardia* species using the late flowering event (Frost, 1996). For example, Lisein et al. (2015) used the Random Forest (RF) classification algorithm to classify 5 deciduous species groups on a 130 hectare broadleaved forest in Grand-Leez, Belgium, using single date, two-date and three-date multispectral UAS image combinations at critical phenological stages and found that three date combinations yielded superior results compared to the other combinations because of different phenological characteristics of different species.

2.6 Monitoring disturbances

UAS may be a useful tool in monitoring the disturbances and recovery of the Miombo woodland at landscape level. The disturbances in the Miombo arise from mainly the interaction of three factors namely (Frost, 1996); (i) anthropogenic, (ii) fire and (ii) herbivory

© University of Pretoria

2.6.1 Anthropogenic disturbances

Disturbances as a result of Miombo woodland utilization by people include complete clearing for cropping, shifting cultivation, selective harvesting of trees for timber, firewood, charcoal production, medicine and livestock grazing. While disturbances from huge clearings for cropping and charcoal production are detectable using freely available moderate resolution satellite imagery such as Landsat and Sentinel e.g. (Mayes et al., 2015; Sedano et al., 2020b), small scale disturbances from selective cutting and lopping of trees and understory grazing are difficult to detect from such imagery and occur at spatial and temporal scales that are difficult and costly to cover by field methods (Hosonuma et al., 2012; Romijn et al., 2012; Mitchell et al., 2017). Furthermore, for shifting cultivation agriculture, which is common in the Miombo woodlands, some clearings are too small (0.5 – 2 ha) to be resolved by moderate resolution imagery (Mayes et al., 2015). UAS can be used to capture ultra-high spatial resolution imagery with timing and frequency required to monitor disturbances and recovery from selective harvesting and lopping of trees and bridge the temporal and spatial gap between freely available satellite imagery and field methods. For example, a study by Thiel et al. (2020) used repeated UAS flights to monitor selective logging at the individual tree level in a pine-dominated forest in Germany; they were able to detect felled trees with a precision and recall of 97.5% and 91.7%, respectively. In a post-harvest assessment of charcoal and timber, Ota et al. (2019) used UAS imagery before and after a selective logging event in a tropical forest in Myanmar to quantify changes in above ground biomass (AGB). In addition, UAS methodologies proposed by Samiappan et al. (2017) and Puliti, (2018) in quantifying the harvested timber and detect illegal logging in protected areas may be useful in monitoring of such in Miombo woodlands. Further, UAS-SfM imagery can be used to monitor biomass changes due to grazing in open Miombo woodlands of less than 50% canopy cover, while in greater than 50% canopy cover UAS-lidar which can penetrate through the canopy and give a full vertical characterization of the forest can be used to monitor disturbances related to understory grazing (Mlambo et al., 2017).

2.6.2 Fire related disturbances

Fires are a major cause of changes in the structure and composition of Miombo woodlands (Frost, 1996). Therefore, pre-fire, during-fire, and post-fire forest management are important. UAS with ultra-high spatial resolution and flexibility of deployment are one of the emerging remote sensing tools for fire management (Fraser et al., 2017; Mckenna et al., 2017; Shin et al., 2019). Grass and woody plant leaf litter are the major fuel load for fires in the Miombo woodlands (Ribeiro et al., 2020a) that could be quantified using UAS to assess the risk and serve as an early warning indicator for the likelihood of a fire occurrence. In terms of fire prevention

© University of Pretoria

and early warning, Fernández-Álvarez et al. (2019) proposed a methodology based on high resolution UAS-lidar point clouds that can be used to characterize forest fuel load. Barber et al. (2021) used a UAS mounted with infrared and visible light sensors to capture imagery and employed reflectance in six wavelengths in the visible and infrared ranges to estimate fuel moisture in grasslands in western Washington, United States of America (USA). Another study by Shin et al. (2018) evaluated the feasibility of using UAS imagery for estimating forest canopy fuels in a ponderosa pine stand, in Flagstaff, Arizona, USA and accurately estimated canopy cover (R^2 = 0.82, RMSE = 8.9%). During a fire event, UAS with thermal infrared sensors can be used for active fire detection and monitoring. For example, Merino et al. (2012) deployed a fleet of three UAS mounted with infrared and thermal sensors to measure and monitor the evolution of fire and demonstrated that UAS can cover the gap between the spatial measurement scales of cameras deployed on satellites and on towers. Valero et al. (2017) used UAS thermal infrared imagery to track the development of an active wildfire in real time and generated valuable data for managing the wildfire emergency response. For assessment of post-fire damage and recovery, the potential of using indices derived from RGB sensors mounted on UAS was demonstrated in studies by Mckenna et al. (2017) and Fraser et al. (2017), who were able to assess the extent and severity of fires and subsequent recovery of the ecosystems at landscape scale. The above examples of application of UAS in fire studies speak to the potential that UAS has in bridging the data gap in fire studies in the Miombo woodlands.

2.6.3 Herbivores related disturbances

Herbivores have been associated with causing changes in plant biomass, forest structure and diversity across the African savannas (White, 1983). In the miombo woodlands, the largest share of herbivory related disturbances have been attributed to elephants (Frost, 1996; Hempson et al., 2015; Ribeiro et al., 2020b). For example; a study by Thomson, (1975) revealed that increased elephant numbers in Chizarira National Park, Zimbabwe, contributed to destruction of 67% of the 500 original mature *Brachystegia boehmii* trees. Another study by Guy, (1981), who monitored biomass changes over a four year period (1972 -1976) in the Sengwa wildlife Research Area in Zimbabwe, reported 46% decline in biomass of canopy trees, 42% decline in basal area and 23% decline in density, which was attributed to elephants. Other studies in similar environments have attributed the structure changes in vegetation cover to combined effect of elephants and fire (Dublin et al., 1990; Ribeiro et al., 2008). The impact of herbivory on vegetation is heterogenous and mainly species specific and occurs at different spatial scales (Thomson, 1975; Frost, 1996; Hempson et al., 2015). The interactions between herbivores and vegetation as well as their spatial heterogeneity are essential for understanding ecosystem structure and function of the Miombo woodlands (Frost, 1996). Though remote

© University of Pretoria

sensing has been identified as an essential tool for quantifying the impacts of herbivory on vegetation structure (Levick et al., 2009), it is still underutilised for this purpose in the Miombo woodlands (Ribeiro et al., 2012). The advent of UAS provides an opportunity to collect high spatial/temporal resolution imagery data that are suitable for quantifying herbivory (Anderson and Gaston, 2013). For instance; Siewert and Olofsson, (2021) used repeated UAS fights from 2018 and 2019 to quantify vegetation impacted by rodents at four complex landscapes of northern Sweden. They applied image raster math by subtracting 2019 NDVI imagery from 2018 NDVI imagery to estimate changes in NDVI values as indication of rodent impacts on vegetation. These methods and high resolution UAS imagery has potential for monitoring disturbances caused by herbivores in the Miombo which occur at smaller spatial scales that would otherwise be difficult to detect from medium resolution satellite imagery

2.7 Bridging the data gap

Miombo woodlands exhibit multifaceted vegetation patterns varying from sparse to dense vegetation emanating from edaphic factors and disturbances (anthropogenic, fires and herbivory) factors (Frost, 1996). If not well captured, small-scale spatial variation in vegetation cover can lead to inaccurate quantification of biophysical and ecological properties of vegetation (Aubry and Debouzie, 2001). Effective forest management and international reporting requirements such as REDD+ requires vegetation data products covering the whole spatial spectrum from detailed field inventories to satellite remote sensing based wall to wall mapping (Mitchell et al., 2017). On one hand, detailed field inventory methods have been used to estimate biophysical properties of vegetation within the Miombo eco-region (Mugasha et al., 2012; Chidumayo, 2013; Kachamba et al., 2016a; Handavu et al., 2021), though these studies were conducted on relatively small sites that are inadequate for regional wall-wall mapping. On the other hand, medium spatial resolution imagery (10- 250) has been used in mapping forest cover changes (Sedano et al., 2005; Cabral et al., 2010; Mayes et al., 2015; Halperin et al., 2016b) and estimating charcoal related degradation (Sedano et al., 2020a; b) in the Miombo woodlands and achieved promising results that can be used for wall-to-wall mapping. However, medium resolution satellite imagery are unable to detect forest changes that occur at a smaller spatial scale in the Miombo woodlands (GOFC-GOLD, 2016), for example: (i) selective tree harvesting for firewood, charcoal production, and timber (Chidumayo and Gumbo, 2013), (ii) shifting cultivation and small field clearings of less than two hectares (Mayes et al., 2015), and (iii) under canopy biomass removal due to grazing (Chidumayo, 2013). From this review, UAS technology has demonstrated potential to bridge the spatial data gap that exist between detailed field inventory methods and satellite-based remote sensing methods that are required

© University of Pretoria

for wall-to-wall mapping of the Miombo woodlands. This can be achieved through a two-phase sampling design where areas covered by UAS are sampled with field plots and areas covered by wall-to-wall satellite imagery are sampled using UAS

2.8 Current status of application of UAS in Miombo woodlands

Although there is great potential for application of UAS in the Miombo woodlands, the current status of application (Table 2.5) is still at a rudimentary level and all studies were done in one site in the dry Miombo (Kachamba et al., 2016b, 2017; Domingo et al., 2019). This shows that more studies need to be done in different environments of the Miombo woodlands to actualize the potential benefits of UAS technology.

Table 2.5 Overview of UAS application status in the Miombo woodlands.

Application	Sensors	No of studies	Country/Category
Estimation of forest structure (AGB, BA, CW, TD, CC, TH, TV)	RGB, NIR	3	Malawi., dry Miombo
Classification of tree species	-	-	-
Forest health	-	-	-
Forest fire	-	-	-

AGB = above ground biomass, BA = basal area, RGB = red, green, blue, CW = canopy width, TD = tree density, CC = canopy cover, TH = tree height, TV = tree volume.

2.9 Challenges for UAS implementation in the Miombo woodland

Although the advent of UAS technology has presented a lot of opportunities to improve management of forest resources in the Miombo woodland region, they come with challenges which need to be understood for successful implementation of the technology (Table 2.6). These challenges come from the limitations of the UAS technology as well as global operating guidelines and regulations.

© University of Pretoria

2.9.1 Regulation

Globally, UASs are subjected to aviation safety rules just like manned aircraft, and countries have developed legislation to regulate the use of UAS with the goal of minimizing the risks to other airspace users and also to both people and property on the ground (Stöcker et al., 2017). Therefore, it is important for any UAS operators to consult the legislation regulating UAS use in the country of intended use (Duffy et al., 2017). In the Miombo woodland ecoregion, Democratic Republic of Congo (DRC), Malawi, Tanzania, Zimbabwe and Zambia have legislation and Mozambique a directive guiding the operation of UAS, while in Angola there is no known legislation ("Global Drone Regulations Database," 2014).

Despite good intentions, the implementation of UAS regulations presents barriers to their successful application in forestry. The challenge comes in bureaucratic procedures and time taken to approve an application for flying permits (Rango and Laliberte, 2010), which might result in missing the timing of data collection for important forest related research events in the Miombo woodlands (e.g., vegetation phenological events) (Ribeiro et al., 2020a). The other challenge is the restriction that the UAS should be flown within the Visual Line of Sight (VLOS) of the pilot, which restricts the area that can be flown per flight. Furthermore, the restriction that UAS be flown up to a maximum height of 120 m above ground (and for Malawi 45 m above ground) results in increased resolution of the captured imagery and the number of captured photos, which increases computer processing demands. Where there are disparities in the laws and policies on the use of UAS among the Miombo ecoregion countries, cross frontier projects among practitioners and researchers, which are very important in forest management, may be negatively impacted.

2.9.2 Site environment challenges

A detailed understanding of the operational site potential hazards and distractions are a key requirement for successful mission planning and execution of UAS data collection (Cromwell et al., 2021). Some section of the Miombo woodlands is home to a variety of wildlife some of which are aggressive (e.g., lions, buffalos, and elephants among others) (Ribeiro et al., 2020a), and may distract the operators of UAS. Furthermore, flocks of Guinea fowls, large birds of prey such as eagles and other birds that inhabit Miombo woodlands might cause bird strikes on UAS. To mitigate such accidents from wildlife, UAS operators should be aware of their occurrence and behaviour beforehand.

Site topography has been found to have a big influence on the quality of 3D point clouds required for estimating forest structural parameters (Zahawi et al., 2015; Domingo et al., 2019).

© University of Pretoria

For example, a study by Domingo et al. (2019) conducted in the Miombo woodlands found that errors in tree height estimates increased with increase in steepness of the slope, with largest errors coming from slopes above a 35% incline. Another study by Alonzo et al. (2018), used UAS-SfM to quantify boreal forest structure and composition in interior Alaska, USA, and reported difficulties in acquiring data along the steep slopes due to problems in adjusting the UAS platform to sustain a constant flight altitude above the entire site terrain.

2.9.3 Weather Limitations

UAS operations are sensitive to weather conditions, such as high wind speed, precipitation and extreme temperatures which might impede UAS data collection at the optimal time of capturing relevant events (e.g., phenology, fire, insect infestations and many others) and sometimes may damage UAS components (ClimaCell, 2018). In addition, varying illumination conditions during image capture affect image quality, which may complicate image processing and lead to poor results (Cessna et al., 2021). Furthermore, wind-induced motion of leaves and branches during image capture can bring about complications in processing UAS imagery resulting in mismatch of features in overlapping images and poor quality orthophotos and 3D point clouds (Iglhaut et al., 2019). According to historical climate data (Weatheronline, 2022), in the Miombo ecoregion high wind speeds are experienced between June and October, a period when most Miombo tree species goes through dropping, flowering and leaf shooting, while rainfall occurs around November to April (Frost, 1996). Clouds are a prominent feature in the Miombo ecoregion especially from November to June (Weatheronline, 2022), and changes in cloud conditions during data collection can lead to changes in illumination conditions, which can cause biased estimation of measured spectral and structural variables (Dandois et al., 2015; Doughty and Cavanaugh, 2019). Adverse weather conditions may result in poorly timed UAS operations and an inaccurate assessment of forests or affect operations times resulting in project delays, discourage potential forest managers from using the technology. High overlap and side lap as well as restricting flight times to around noon has been proposed as some of the mitigating measures for unfavourable illumination conditions (Dandois et al., 2015; Iglhaut et al., 2019). Ultimately, observation of prevailing weather conditions in the area of interest is critical to proper flight timing to reduce the effects of wind, clouds and shadow within imagery in order to produce the best data possible for the intended application (Poley and McDermid, 2020).

© University of Pretoria

Table 2.6 Summary of opportunities and challenges for potential UAS application areas in the Miombo woodlands.

Application	Opportunity	Challenges
Estimation of forest structure (AGB, BA, CW, TD, CC, TH, TV)	Availability of affordable UAS-SfM in mostly open woodlands Availability and reducing cost of UAS-lidar for generating accurate DTMs Flexibility for multi-temporal deployment	Low accuracy DTM in dense forest environments Variation in illumination conditions Phenological differences Limited area coverage area coverage per flight Heavy payload and high cost Limited area coverage per flight
Classification of tree species	Availability and reducing cost of UAS multispectral, hyperspectral sensors Availability of OBIA and manchine learning algorithms Phenological differences in tree species Flexibility for multi-temporal deployment	Difficulties in separating differentspecies using RGB sensors with limited spectral resolution High cost of multispectral and hyperspectral sensors Steep learning curve for manchine learning algorithms Cost of specialized processing software Heavy payload demanding larger expensive UAS for hyperspectral sensors Interspecies homogeneity Intra species heterogeneity due to variation in illumination conditions Steep learning curve for processing hyperspectral imagery Limited area coverage per flight
Forest health	Availability of multi-spectral and hyperspectral sensors Availability of vegetation indices	Heavy payload demanding larger expensive UAS for hyperspectral sensors Vegetation phenology Steep learning curve for processing hyperspectral imagery Limited area coverage per flight
Forest fires	Availability of multi-spectral and thermal sensors	Heavy payload demanding larger expensive UAS for thermal sensors High cost of sensor and specialized software Steep learning curve for processing algorithms
Forest degradation	Availability of low-cost RGB sensors Availability and reducing cost of UAS multispectral, hyperspectral, thermal and lidar sensors Difficulties in characterizing small-scale degradation activities with freely available satellite imagery	High cost of multispectral, hyperspectral, thermal and lidar sensors Steep learning curve for processing hyperspectral and lidar data Limited area coverage per flight

AGB = Above Ground Biomass, BA = Basal Area, CW = Canopy Width, TD = Tree Density, CC = Canopy Cover, Tree Height, TV = Tree Volume, UAS = Unmanned Aerial System, SfM = Structure from Motion, DTM = Digital Terrain Model, lidar = Light Detection and Ranging, OBIA = object oriented image analysis.

© University of Pretoria

2.9.4 Limitation of UAS sensors

Most cameras that are used in UAS are not designed for remote sensing applications and as such spectral response curves for such cameras are poorly calibrated, making it difficult to convert brightness values into radiance (Whitehead and Hugenholtz, 2014), which is essential for comparative analyses. Moreover, most consumer grade cameras have limited spectral resolution and no infrared band, which limits their application for vegetation analysis. Another limitation of such cameras is that they are susceptible to vignette, where the centre of the image appears brighter than the edges (Kelcey and Lucieer, 2013), which is a result of differences in light paths between the centre and edges of the lens causing a radial shadowing effect at the edges of the image (Whitehead and Hugenholtz, 2014). Such negative effects have to be corrected in order to preserve spectral and structural attributes that are required for vegetation monitoring (Whitehead et al., 2014). In instances where information beyond the visible part of the EM is required (e.g., species discrimination and detailed vegetation analysis), multi-spectral or hyperspectral sensors can be used (Guimarães et al., 2020).

Furthermore, for optical sensors, single UAS photos are usually mosaiced before any analysis at landscape level (Jia et al., 2015), but the process of mosaicking presents challenges caused by vignetting, relief displacement, misregistration, as well as image artifacts created when image balancing algorithms fail (Whitehead and Hugenholtz, 2014). Poor quality mosaics cause errors in spectral analysis, which can lead to biased estimates of forest inventory attributes. Some of the mosaic artifacts can be mitigated by following the UAS data collection protocol proposed by Dandois et al., (2015).

2.9.5 Endurance challenge

The major limitation of most small UAS that are used in forest applications especially multi-rotors is low endurance, which means they can cover only a small area per flight (Colomina and Molina, 2014; Tang and Shao, 2015). Flight times for most UAS batteries ranges between 10 – 30 minutes (Hardin et al., 2018). However, this limitation is mitigated by mission planning software, which allows the pilot to pre-plan a photographic mission, set mission parameters (flying height, endlap, sidelap, camera shutter speed, aircraft speed, etc.), predetermine flight time and area to be covered, and fly the aircraft autonomously, with minimal intervention. When the battery power is nearly depleted the aircraft automatically comes back to land and the pilot can change the battery and re-launch the aircraft to continue the mission where it ended. Even with this capability of mission planning software, the limited area coverage per flight is still a challenge which may discourage some practitioners from embracing this technology in the Miombo ecoregion.

© University of Pretoria

2.9.6 Processing and storage challenges

Automatic interpretation of ultra-high (under 10 cm) resolution image collected by UAS for species mapping is challenging to achieve using per-pixel classifiers that are implemented in most commonly used commercial image processing software packages (Franklin, 2017). However, progress has been reported in the use of GEOBIA and machine learning techniques to classify tree species (Franklin and Ahmed, 2017; Liu et al., 2018a), though these solutions tend to be site specific and data dependent, and thus cannot be easily generalized. Furthermore, image interpretation using GEOBIA and machine learning requires expensive specialized commercial software or open-source software with a steep learning curve, which might be beyond the capacity of most forest managers in the Miombo ecoregion. Another challenge is that ultra-high-resolution data collected by UAS demand expensive computer hardware with high processing and storage capacity that might be unaffordable for many institutions in the Miombo ecoregion countries and therefore may impede their application. For example, Agisoft Metashape, a popular software for generating point clouds and building mosaics from UAS imagery, requires a minimum of 16 GB for processing UAS imagery (Agisoft LLC, 2019). Depending on the size of the project and available hardware, processing of UAS imagery to generate meaningful data products for various applications can take many hours, which can be discouraging for many professionals.

2.9.7 Vegetation cover challenges

Miombo woodlands are generally open with little overlap between tree crowns (Table 2.1), but the density of trees varies in response to climate, topography, disturbance and edaphic factors (Frost, 1996; Ribeiro et al., 2012). Vegetation cover has significant influence on the performance of data processing algorithms and quality of generated data products (Dandois and Ellis, 2010; Lisein et al., 2013). The quality of a CHM, which is a fundamental product in estimation of vegetation structural attributes (Maltamo et al., 2014b), is highly correlated to the quality of the DTM used in generating it (Kraus and Pfeifer, 1998). Mlambo et al. (2017) evaluated the performance of UAS-SfM in two United Kingdom sites: (i) Meshaw, Denvo, which has a relatively open canopy and (ii) Dryden, Scotland, which has a closed canopy. Comparison of the CHM generated by lidar and UAS-SfM 3D point clouds exhibited high correlation (R^2 = 0.75) at Meshaw. At Dryden, there was poor correlation between UAS-SfM estimated and ground measured tree heights (R^2 = 0.19), which was attributed to poor canopy penetration of UAS imagery. Their study recommended that the effect of poor canopy penetration can be mitigated by capturing UAS imagery during leaf-off season in deciduous forests. Their recommendations were corroborated by Aguilar et al. (2019), who used leaf-off UAS-SfM derived DTMs as ground reference for supporting teak plantations inventory in the dry forests

© University of Pretoria

of the coastal region of Ecuador. A study by Hentz and Strager, (2018) assessed tree damage in West Virginia Research Forest using leaf-on generated UAS-SfM DSM, which gave better definition of the top canopy definition and leaf-off DTM, which gave a better definition of the ground. From lessons learnt from (Mlambo et al., 2017; Hentz and Strager, 2018; Aguilar et al., 2019), we anticipate challenges in the quality of DTM that will be generated by UAS-SfM in the closed canopies environments that characterize some parts of the Miombo woodlands. However, the UAS-SfM DTM quality challenge can be mitigated by either using leaf off UAS imagery or UAS-lidar to generate one-off DTM that can be used repeatedly with multi-temporal UAS-SfM DSM to compute CHMs for monitoring forest structural attributes.

In terms of classification of individual tree species, the detection accuracy of ITCs tends to decrease with increases in the tree density, species diversity, and canopy structural complexity, which ultimately affects the quality of the final tree species classification results (Pu, 2014; Wang et al., 2018; Xu and Ruan, 2020). The Miombo woodlands are characterized by irregular tree crowns with a similar appearance (Frost, 1996). In wet Miombo there is typically overlapping of the crowns of neighboring trees. These attributes of the Miombo have been reported to cause challenges in identification of ITCs in similar forest environments (Lisein et al., 2015; Franklin, 2017; Xu et al., 2020). Some studies use fusion of structural and spectral information, and multi-temporal imagery (Lisein et al., 2015; Gini et al., 2018) to improve the accuracy of identification of tree species.

2.10 Future Directions

This review has evinced progress in UAS technology in various forest applications, though it is not yet fully embraced within the Miombo ecoregion as such data gaps still exist. There are several potential future directions for applying UAS technology in the Miombo woodlands, including, the choice of sensors and, data processing techniques which are available for the monitoring of Miombo woodlands. It is hoped that future research explores the utility of UAS technology to fill existing data gaps in (i) estimation of forest structural attributes, (ii) identification of tree species, (iii) monitoring forest health, (iv) monitoring forest fires, and (v) monitoring small scale degradation, which are critical to meeting the objectives of the REDD+ project. Challenges still exist in developing and operationalizing the UAS data collection and processing techniques in monitoring the Miombo woodlands. The existence of studies focusing on the use of UAS technology to estimate vegetation parameters within the Miombo ecoregion in the recent past (Kachamba et al., 2016b, 2017; Domingo et al., 2019), sets the tone for UAS based studies. With continuous improvement in UAS sensor and data processing technology coupled with the reduction in prices of specialized sensors (Colomina and Molina, 2014), it is

© University of Pretoria

envisaged that more studies focusing on the use of UAS technology for monitoring the Miombo woodlands. The focus should be towards developing best practices for data collection, data processing techniques and model validation, which can be achieved by testing the technology in different environments of the Miombo. Some of the initiatives that could be undertaken to enhance operationalization of the use of UAS technology in the Miombo woodlands are proposed in Table 2.7. It is anticipated the use of UAS based methods will complement the existing methods to fill the existing spatial gap between ground-based methods and wall to wall satellite imagery.

Table 2.7 Future directions.

Application	Sensors	Recommendation
Estimation biomass and other vegetation structural attributes	RGB, MS, HS, lidar	Comparing results from different algorithms in different environments and growth stages Comparing results of data collected in different seasons - Comparing results from different sensors and combination of sensors -testing the models for robustness and transferability to different environments Classification of tree species
Classification of tree species	RGB, MS, HS, lidar	Comparing the potential of data from different sensors and combination of sensors to classify tree species Comparing potential of using a combination of multi-temporal, and multi-spectral/hyperspectral data for classifying tree species Comparing results from different algorithms in different environments and growth stages
Forest health	MS, HS, lidar	Comparing results from different indices in assessing forest health Exploring the use of a combination UAS-lidar and Mult—spectral/hyperspectral imagery in monitoring forest health
Forest fires	RGB MS, Thermal, lidar	Use of UAS-lidar and UAS-SfM in quantifying combustible as early warning system for fire Use of UAS thermal infrared imagery to track active fires Use of UAS imagery to assess post fire damage and recovery

2.11 Conclusion

The Miombo woodlands ecoregion suffers from a lack of quantitative estimates of forest cover changes, species distributions and carbon stocks which is key information required for effective forest management and international carbon MRV requirements. UAS presents alternative and supplementary methods to rapidly collect forest data at high spatial and temporal resolution that is required for monitoring and management of the Miombo woodlands. The key attributes of the Miombo woodlands provide potential for application of UAS technology in undertaking

© University of Pretoria

forest inventory important for forest monitoring and management. It is a useful tool for estimating forest structure attributes, species identification, effects from fire and forest degradation, all of which are necessary for forest management. However, if the UAS technology is to be widely applied in the Miombo region, it is also important to comply with restrictive regulations and to obtain required flight permits.

© University of Pretoria

Chapter 3 : Use of multi-date and multi-spectral UAS imagery to classify dominant tree species in the wet Miombo woodlands of Zambia

This chapter was based on:

Shamaoma, H.; Chirwa, P.W.; Zekeng, J.C.; Ramoelo, A.; Hudak, A.T.; Handavu, F.; Syampungani, S. Use of Multi-Date and Multi-Spectral UAS Imagery to Classify Dominant Tree Species in the Wet Miombo Woodlands of Zambia. Sensors 2023, 23, 2241. https://doi.org/10.3390/s23042241

© University of Pretoria

Abstract

Accurate maps of tree species distributions are necessary for the sustainable management of forests with desired ecological functions. However, image classification methods to produce species distribution maps for supporting sustainable forest management are still lacking in Miombo woodland ecoregion. This study used multi-date multispectral Unmanned Aerial Systems (UAS) imagery collected at key phenological stages (leaf maturity, transition to senescence and leaf flushing) to classify five dominant canopy species of the wet Miombo woodlands of the Copperbelt province of Zambia. Object Based Image Analysis (OBIA) with a random forest algorithm was used on single date, multi-date and multi-feature UAS imagery for classifying the dominant canopy tree species of the wet Miombo woodlands. It was found that classification accuracy varies both with dates and features used. For example, the August image yielded the best single date Overall Accuracy (OA) (80.12% OA, 0.68 kappa), compared to October (73.25% OA, 0.59 kappa) and May (76.64% OA, 0.63 kappa). The use of a three-date image combination improved the classification accuracy to 84.25% OA and 0.72 kappa. After adding spectral indices to multi-date image combination, the accuracy was further improved to 87.07% and 0.83 Kappa . The results highlight the potential of using multispectral UAS imagery and phenology in mapping individual tree species in the Miombo ecoregion. It also provides guidance for future studies using multispectral UAS for sustainable management of Miombo tree species.

Keywords: Miombo woodlands; Multi-date; Multi-spectral; UAS; Object-based; Classification

© University of Pretoria

3.1 Introduction

The Miombo woodlands are the most extensive dry forest type in southern Africa, with an estimated area of about 2.7 million km2 covering Angola, Malawi, Mozambique, Tanzania, Zambia, Zimbabwe and most of the southern parts of the Democratic Republic of Congo (Frost, 1996). The woodlands have an estimated 8,500 plant species, more than 54 percent of which are endemic. They comprise one of the most important ecosystems in Africa because of their ecological, biological and socioeconomic significance (Syampungani et al., 2009; Chirwa et al., 2016; Kapinga et al., 2018). In addition, the Miombo woodlands contribute to the livelihoods of millions of rural and urban dwellers (Campbell, 1996). Some of the local ecosystem goods and services the woodland provides include fuelwood, charcoal, timber, fruit, beekeeping, mushrooms and medicines (Chirwa et al., 2016). These forest ecosystems provide valuable timber resources and support regional economic development, but their ecosystem services have been threatened by climate change and increasing disturbances from deforestation, fragmentation, degradation and other stressors (Luoga et al., 2002; Syampungani et al., 2009). Trees are the foundational component of the forest ecosystem, and their species composition has important influence on forest biodiversity (Madonsela et al., 2018). Furthermore, tree species composition and spatial distribution are critical information needed to address ecological problems in tropical ecosystems (He et al., 2022). As a result, accurate information on the spatial distribution of dominant tree species in tropical natural mixed forests, such as the Miombo woodlands, with complex distribution and structure, is critical for understanding the dynamics of forest ecosystems. Furthermore, precise mapping of dominant tree species is required for effective management of Miombo woodlands, as well as for characterizing ecosystem services and climate feedbacks on forests (Ribeiro et al., 2015). Researchers have mapped tree species composition and distributions to assess biodiversity in other African savanna ecosystems (Cho et al., 2012; Madonsela et al., 2018).

Up-to-date species distribution maps that may be attained from either the application of traditional surveys or remote sensing are critical for sustainable forest resource management (Turner et al., 2003). Traditional forest surveys could produce detailed and accurate maps of tree species distributions. However, they are time-consuming, labor-intensive, expensive, and prone to errors that may go undetected (Xie et al., 2008; Cho et al., 2012). Given the difficulties in conducting traditional species mapping surveys (Day

© University of Pretoria

et al., 2014), remote sensing has emerged as one of the tools for tree species mapping at scales ranging from landscape (Cao et al., 2018; Hologa et al., 2021) to regional (Fassnacht et al., 2016; Lim et al., 2019; Kollert et al., 2021). The understanding that species have unique spectral signatures associated with characteristic biochemical and biophysical properties can be exploited to map plant species mapping using remote sensing (Asner and Martin, 2009; Cho et al., 2010). Free multispectral imagery like Landsat and Sentinel has low spectral resolution (Nagendra and Rocchini, 2008), making them unsuitable for identifying plant species, especially in heterogeneous landscapes like the Miombo woodlands, but it can be used for regional species mapping in homogeneous landscapes dominated by planted forests (Naidoo et al., 2012). Hyperspectral imagery, on the other hand, has high spectral resolution with hundreds of contiguous bands across the electromagnetic spectrum, making it more suitable than multispectral imagery for capturing plant biochemical properties, which are closely linked to species identity (Asner and Martin, 2009; Cho et al., 2010), as has been demonstrated in many tree species classification studies across different vegetation formations at landscape scale (Cho et al., 2012; Naidoo et al., 2012; Cao et al., 2021; Mäyrä et al., 2021). However, hyperspectral data are not widely available and remain prohibitively expensive in most Sub-Saharan African countries (Madonsela et al., 2017).

To compensate for the low spectral resolution that is common to high resolution imagery (e.g. QuickBird, GeoEye, Rapideye, Pléiades, and WorldView), some studies investigated multi-seasonal imagery for tree species classification (Madonsela et al., 2017; Van Deventer et al., 2019). A study by Madonsela et al. (2017) used two–date WorldView-2 imagery (maximum leaf foliage and transition to senescence) to classify tree species in the South African savannas. Their study compensated for low spectral resolution in WorldView-2 imagery by using two-date Worldview imagery to achieve an overall accuracy (OA) of 80.4% compared to OA of 76.4% and 72% for maximum leaf foliage and transition to senescence imagery, respectively. Another study by Van Deventer et al. (2019) investigated the use of multi-season (winter, spring, summer, and autumn) RapidEye imagery for classifying wetland and dryland vegetation communities in Isimangaliso Wetland Park, South Africa's subtropical coastal region. According to their findings, the four-season imagery combination produced the highest overall classification accuracy (OA = 86 ± 2.8%), followed by the spring (80 ± 2.9%), summer (80 ± 3.1%), autumn (79 ±3.4%), and winter (66 ± 3.1%). Though the preceding studies

© University of Pretoria

demonstrated the ability of high spatial resolution, multi-date imagery to discriminate different tree species in the other African Savanna vegetation formations, none of these studies were conducted within the Miombo ecoregion, which has unique forest structure, species composition, and phenology (White, 1983). Furthermore, very high-resolution spaceborne imagery such as Rapid Eye and Worldview are not flexible enough to capture phenological events that are important for classifying tree species, as cloud cover can be a challenge in the tropics where these species are located. Additionally, the data sets used in these studies are expensive and out of reach for most African savanna researchers and forest managers.

Unmanned Aerial Systems (UAS) have the flexibility of acquiring data almost anytime, anywhere with limited logistics, making them an essential tool in gathering ultra-high spatial resolution imagery (under 10 cm) on forests for detailed characterization of canopies in contrast to manned airplane and satellite platforms having less flexible or fixed acquisition constraints. As a result, using multispectral UAS imagery to classify forest tree species is becoming a popular forestry application (Fassnacht et al., 2014b; Torresan et al., 2017).

The application of UAS imagery for tree species discrimination has shown promising results, as demonstrated in many studies (Feng et al., 2015; Lisein et al., 2015; Franklin and Ahmed, 2017; Gini et al., 2018; Feng and Li, 2019). However, all these studies were done in different ecosystems with different tree species, forest structure, and composition and therefore, the findings cannot be promulgated to the Miombo ecoregion. Furthermore, Franklin and Ahmed, (2017) observed that the application of UAS imagery for deciduous tree species classification is still at a rudimentary level and recommended that more tests are needed to ascertain its reliability and accuracy. As already stated, species distribution maps are still lacking in the Miombo ecoregion, and remote sensing methods for classifying tree species have not been explored. This study aims to evaluate the potential for mult-spectral and multi-date UAS imagery for classifying the dominant wet miombo species in Zambia. This study was designed to answer the following research questions:

(i). What is the optimal single season window for acquiring imagery to discriminate tree species in the Miombo ecoregion?

© University of Pretoria

(ii). Could multi-season imagery improve the discrimination of tree species in the Miombo ecoregion?

(iii). What other image features can improve Miombo species classification?

3.2 Materials and Methods

The workflow containing the methodological steps of this study is shown in Figure 3.1. Within the framework of this study, we acquired single-date and multi-spectral imagery from multi-rotor UAS combined with individual tree crown delineation algorithms and a machine-learning classifier to identify the dominant tree species in the Miombo woodland of Mwekera area in Zambia.

3.2.1 Study area

The study area is 22 hectares of wet Miombo woodland located (12.860977° S, 28.357049° E; Figure 3.2) in Mwekera national forest reserve number 6, about 15 Km south east of the central business district of the City of Kitwe, in the Copperbelt Province of Zambia. The average human population density in the Copperbelt province is 63.0 persons per km^2, with an average annual population growth rate of 2.2% (Central Statistical Office, 2012). Mwekera forest covers about 111 km^2 and the elevation ranges from 1210 to 1240 m above mean sea level. Annual rainfall ranges between 1000 and 1500 mm and temperature ranges between 25C° and 32C°. The Miombo woodlands, which cover approximately 45% of Zambia, is the predominant vegetation in Mwekera (Stringer et al., 2012). Mwekera forest was classified as a National Forest to protect the Mwekera stream catchment, which is part of the Kafue River system.

© University of Pretoria

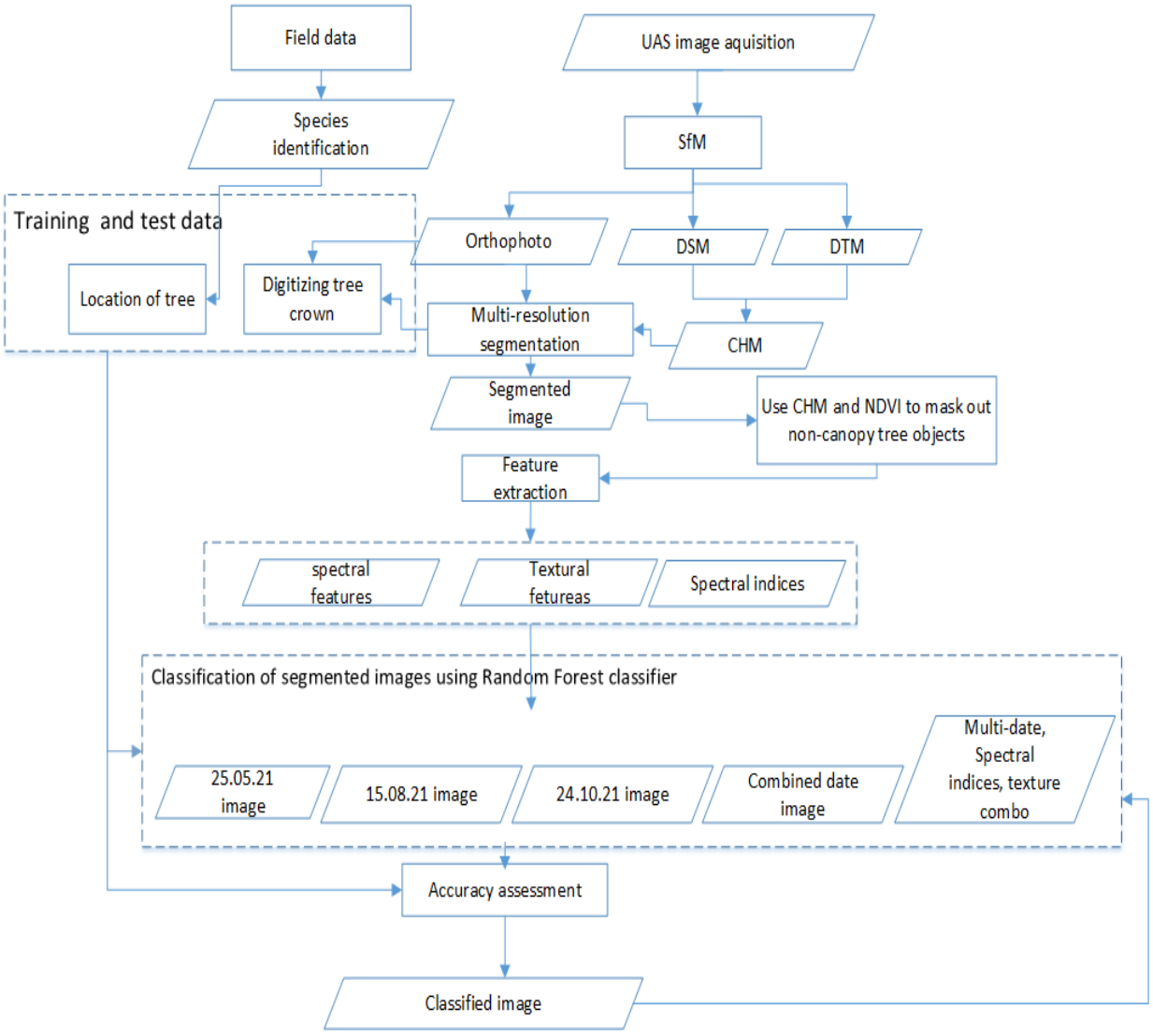

Figure 3.1 General UAS image acquisition, processing, and classification workflow

3.2.2 Field data collection

The fieldwork was conducted in May 2021, just before the first flight. Considering the accessibility of the field site and the heterogeneity of tree species, twenty plots of 20 m radius were set up at every 200 m and additional areas with sudden changes in tree cover in the study area. In each plot, all tree species (Appendix 3.1) with a diameter at breast height (DBH) greater than 5 cm were sampled (Number =688). The attributes of trees collected included individual tree positions, DBH, tree height and species name. The

© University of Pretoria

positions of all the sampled trees were measured using a CHC LT700H real-time kinematic (RTK) Global Navigation satellite system (GNSS) receiver. DBH was measured using a diameter tape and tree height was measured using a Nikon Forest Pro hypsometer. In this study, we conducted our classification experiments based on dominant tree species, which were *Julbernardia paniculata* (JP; 18.5%), *Isoberlinia angolensis* (IA; 16.6%), *Marquesia macroura* (MM; 15.7%), *Brachystegia longifolia* (BL; 9.3%) and *Brachystegia spiciformis* (BS; 7.4%) (Table 1; Appendix 3.1). The remaining species were recorded in less than 5% of the samples and were, therefore, not considered for classification. Furthermore, the dominant species found in Mwekera (Table 3.1), except for *Marquesia macroura*, were found to be preferred charcoal species (Syampungani et al., 2011), which makes the site vulnerable to over-exploitation.

Table 3.1 Sampled dominant tree species in the area

Species Code	Tree species	Common local uses	Trees sampled	Training samples	Validation samples
JP	*Julbernardia paniculata*	Charcoal, pole, timber	127	89	38
IA	*Isoberlinia anglolensis*	Charcoal, timber, pole	114	80	34
MM	*Marquesia macroura*	Poles, charcoal	108	76	32
BL	*Brachystegia longifolia*	Charcoal, bark rope	64	45	19
BS	*Brachystegia spiciformis*	Charcoal, bark rope	51	36	15

3.2.3 UAS image data acquisition

Three UAS images used to classify tree species were acquired on 25th May 2021 at full leaf maturity, 15th August 2021 at senescence for the majority of dominant canopy tree species and early flushing for *BL* and *BS* species, and 24th October 2021 at greening of flushed leaves for the majority of dominant species (Frost, 1996; Shamaoma et al., 2022). The DJI Phantom 4 RTK Multispectral multi-rotor UAS, equipped with one RGB camera and a multispectral camera array with five cameras covering blue (450 nm ±16 nm), green (560 nm ±16 nm), red (730 nm ±16 nm), red edge (450 nm ±16 nm) and near-infrared (840 nm ±26 nm), as well as a D-RTK 2 mobile Global Navigation Satellite System (GNSS) base

© University of Pretoria

station (DJI, 2019), was used to capture imagery for this study. This UAS was chosen for our study because of two capabilities: (i) Real Time Kinematic GNSS capability that enabled direct image georeferencing for easy processing and comparison of multi-date images and (ii) integrated sunlight sensor for consistency of images collected at different times of the day. All our flights were undertaken between 11:30 AM and 12:30 PM local time to minimize shadowing on the images. In order to ensure consistent comparisons between the multi-date UAS imagery, the same UAS flight parameters were applied on all dates (Table 3.2).

Table 3.2 Imagery acquisition parameters

UAS flight parameters	Value
Camera model	DJI P4 Multi-spectral
Flight height (m)	100
Flight speed (m/s)	5
Forward overlap (%)	85
Side Overlap (%)	75
Ground resolution (m)	0.05
Spectral bands	Blue, Green, Red, Red-Edge, Near Infra-Red
Time of flight	11: 30 AM – 12:30 PM

3.2.4 UAS data pre-processing

The UAS images from the three dates were processed using the Structure from Motion (SfM) approach (Snavely et al., 2007) based on the workflow in Agisoft metashape software version 1.7 (Agisoft LLC, 2019), summarized as follows: (i) added photos while selecting multi-camera system and arranged bands according to image metadata, (ii) calibrated the reflectance based on the sun sensor, (iii) aligned photos by estimating camera position of multi-camera system and generated sparse point clouds consisting of tie points and estimated interior orientation parameters for each sensor, (iv) generated a dense point cloud based on calculated exterior and interior orientation parameters using dense stereo matching to densify the point clouds, (v) generated a Digital Surface Model

© University of Pretoria

(DSM) based on the dense point cloud and resolution, (vi) generated an orthophoto mosaic based on the DSM, and (vii) exported the orthophoto mosaic in Geotiff format. The other process performed with Metashape software was to classify ground points and generate a digital terrain model (DTM), which was also exported together with the DSM for further processing in the calculation of the canopy height model (CHM). In order to optimize on storage space and processing time, the orthopho mosaic, DSM and DTM were exported at a degraded resolution of 0.30 m, which was tried and found suitable for segmenting tree crowns of mature deciduous trees (Effiom et al., 2019).

© University of Pretoria

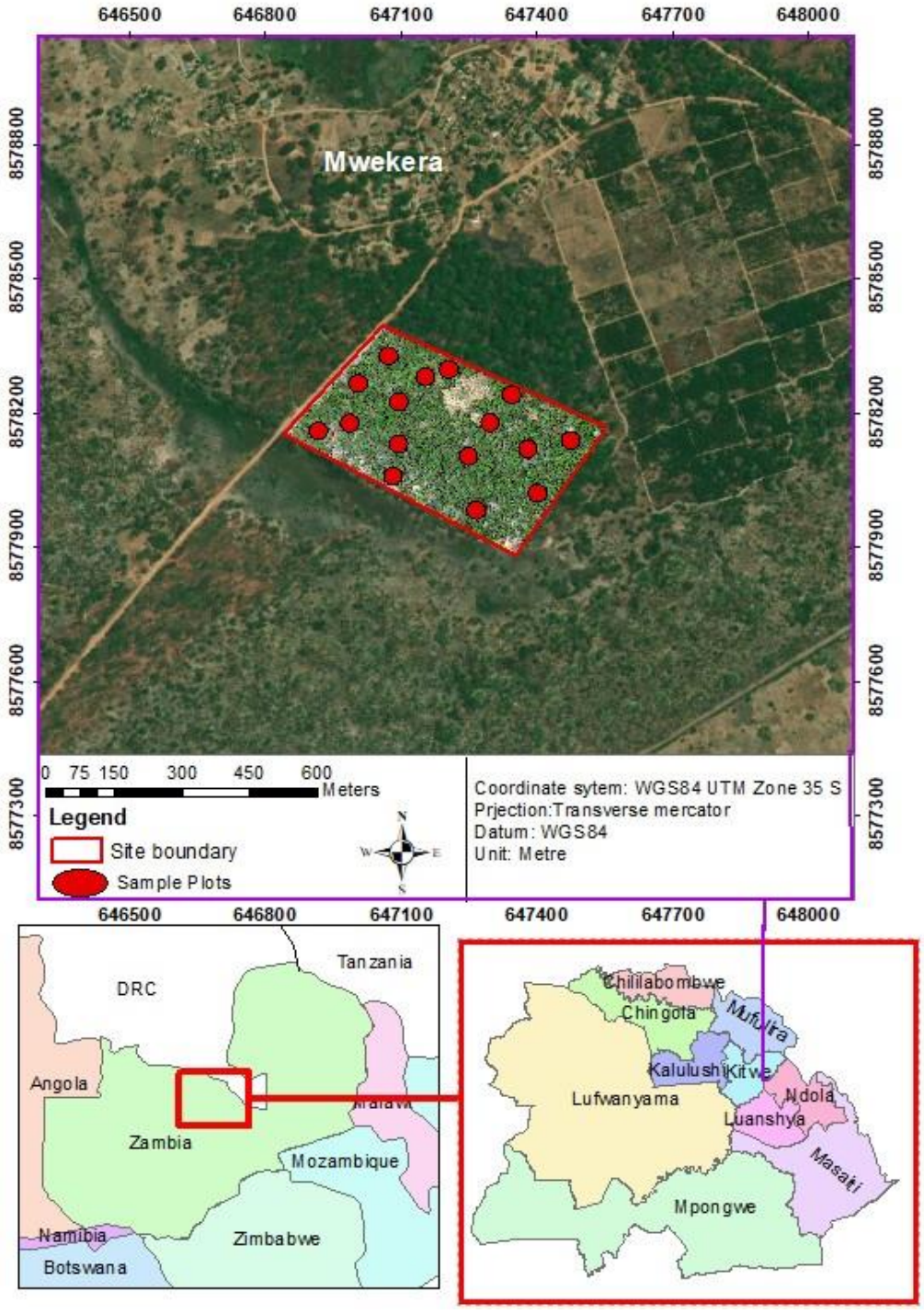

Figure 3.2 Study area location

© University of Pretoria

3.2.5 Computation of the CHM

The CHM was computed based on recommendations from Mlambo et al. (2017), who found combination of UASs with non-radiometric RGB sensors and SfM approach (UAS-SfM) to generate better DTMs in open woodlands compared to closed woodlands due to the inability of optical UAS imagery to capture the ground in closed canopy woodlands. Similar observations were made by (Aguilar et al., 2019), who used leaf-off UAS-SfM derived DTMs as ground reference for supporting teak plantations inventory in the dry forests of the coastal region of Ecuador. A study by Hentz and Strager, (2018) assessed tree damage in a West Virginia Research Forest using leaf-on generated UAS-SfM DSM and leaf-off DTM. Therefore, we took advantage of our multi-date data set to generate the best possible CHM from our available data sets by subtracting the leaf-off (15.08.21) DTM from leaf-on (25.0522) DSM. The computed CHM was resampled to 0.3 m resolution to match the orthopho and used an input in the tree species classification process.

3.2.6 Tree species classification

The tree species were classified using object-based image analysis (OBIA) (Shamaoma et al., 2006; Blaschke, 2010). This method outperforms pixel-based methods for classifying tree species from high-resolution imagery (Franklin, 2017). Therefore, OBIA was used in this study, and it was performed in three steps namely image segmentation, feature extraction and image classification.

Image segmentation

The orthophoto images were processed into homogeneous segments that closely correspond with individual tree crowns using the multi-resolution algorithm (Benz et al., 2004) implemented in eCognition Developer version 9.0 software (Trimble, 2018). This algorithm grows by merging one pixel with neighboring pixels based on spectral and/or shape similarity criteria. A combination of orthophoto and CHM was assessed in this study as CHM was found to improve individual tree segmentation in other studies (Jakubowski et al., 2013; Xu et al., 2020). The UAS imagery captured in May (leaf-maturity) was used for segmentation since all Miombo trees have a well-defined tree crown shapes at this stage of the year. Multiple iterations were performed via trial and error by varying the shape, compactness and scale parameters and comparing to the resulting tree crowns. Furthermore, the effect of combining the orthophoto and CHM to

© University of Pretoria

the segmentation result was also assessed. The result of the segmentation were polygons of homogeneous objects representing a tree crown or group of similar tree crowns. The image objects polygons generated were used as a basis for segmenting the August UAS orthophoto (senescence for most of the Miombo tree species) and October UAS orthophoto (leaf-flushing for Miombo tree species). This was done to make sure that we used the same tree objects when comparing the accuracy of the classification results from the three image dates.

Segmentation accuracy assessment

The accuracy of OBIA analysis is based on the accuracy of the segmentation process and it is therefore important to assess quality of the segmentation before proceeding to the subsequent processes of feature extraction and image segmentation. In this study, the area estimation technique described in Clinton et al. (2010) was used to assess the segmentation accuracy of tree crowns. The three measures were compared to assess the accuracy of the tree crown segmentation using the following equations:

$$Oversegmentation\ (OS) = \frac{area(ARP \cap ADP)}{area(ARP)} \quad (1)$$

$$Undersegmentation\ (US) = \frac{area(ARP \cap ADP)}{(ADP)} \quad (2)$$

$$Segmentation\ error\ (SE) = \sqrt{\left(\frac{(OS)^2 + (US)^2}{2}\right)} \quad (3)$$

Where ARP is a detected object area segmented by the multiresolution segmentation (MRS) algorithm that is one-to-one with reference polygony, ADP is area of the reference polygon (tree crown) which is manually digitized in ArcMap, ArcGIS Desktop Version 10.7.1 (ESRI, 2019) and Area (ARP∩ADP) is area of manually delineated polygon correctly identified by MRS algorithm. The ideal value of the over segmentation, under segmentation and total detection error is 0. The reference polygons (tree crowns) were manually digested in ArcGIS for two forest stands and then applied to quantify the segmentation error.

© University of Pretoria

Feature extraction

Before classification of tree species, it is essential to extract features of segmented tree objects that are used to discriminate different tree species in the subsequent classification process (Xu et al., 2020). The first step in our feature extraction process was to mask off non-canopy tree objects from canopy tree objects so that only features related to canopy tree objects are considered for subsequent tree species classification. This was done by applying a threshold height of greater than 3 m of CHM to represent canopy tree objects.

The non-canopy tree objects taller than 3 m were separated by using normalized difference vegetation index (NDVI) value of less than 0.1. We explored the use of a combination of spectral, texture and vegetation indices because use of multiple features have been found to improve tree species discrimination in other studies (Cao et al., 2018; Gini et al., 2018; Shen et al., 2019). All the canopy tree object features for the three dates were extracted in eCognition Developer software before exporting to ArcGIS for tree species classification. The extracted features built into eCognition Developer software (Trimble, 2018) included: spectral features (mean blue, mean green, mean red, mean red-edge, mean near infra-red (NIR), grey level co-occurrence matrix (GLCM) textural features (contrast, correlation, dissimilarity, and standard deviation) and band metrics (mean brightness and maximum difference). The vegetation indices included: green chromatic coordinate (GCC), red chromatic coordinate (RCC) and NDVI, which were computed and extracted within eCognition software using equations in Table 3.3.

Table 3.3. Equations of vegetation indices used

Vegetation index	Equation	Source
NDVI	*N*DVI= (nir-red)/(nir+red)	(Fuller and George, 1999)
GCC	GCC= green/(blue+green+red)	(Park et al., 2019)
RCC	(RCC= red/(blue+green+red)	(Park et al., 2019)

The tree objects were exported from eCognition as shape files with all the extracted features as attributes. The shape file attributes of the exported object features were rescaled by normalizing them to a common scale in order to prevent attributes with high range values from dominating those with low range values during the classification

© University of Pretoria

process (Hsu et al., 2016). All feature values were rescaled to a range of 0 to 1 in ArcMap using the attribute table field calculator (equation 1). The shape files were converted to raster in ArcMap with each feature been used to create a single band raster image.

$$rescaled\ value = \frac{(feature\ value - minmum\ value)}{(maximum\ value - minmum\ value} \qquad (4)$$

Species classification

The tree species classification was done using Random Forest (RF), a non-parametric machine learning classifier that has been used widely in tree species classification using very high resolution imagery (Immitzer et al., 2012; Lisein et al., 2015; Franklin and Ahmed, 2017; Van Deventer et al., 2019; Xu et al., 2020). RF uses training samples, validation samples, and the majority vote to classify an object into a specific class. In the current study, the RF was implemented in ArcMap. The training and validation sample image objects were collected using the training sample manager in ArcMap guided by field sample crowns, but only sunlit objects were collected to represent a pure sample for each tree species and a shadow class was added to classify shadowed areas. A total of 344 training samples were collected for the six classes divided as follows: JP (89), IA (80), MM (76), BL (45), BS (45) and shadow (19). The sample data were randomly split into training (70%) and validation (30%). The same training and validation samples were used to train and validate classification results for single-date imagery, multi-date and multi-feature image combination to find the optimal solution for discriminating different tree species within the Miombo woodland study area.

Class separability

The separability of the 6 classes was summarized by collecting mean statistics of training data for each class in ArcMap training manager and exporting to excel for plotting and visualization. The variability of spectral, vegetation indices and texture features across dates and image combinations were visualized to assess the separability of different species.

© University of Pretoria

Classification accuracy assessment

The effectiveness of the different image date combinations to discriminate different tree species was assessed using a confusion matrix. For each classification result, the producer's accuracy, user's accuracy, overall accuracy, and kappa statistics were computed to assess the ability to discriminate species.

3.2.7 Results

3.2.8 Identifying segmentation parameters

In this study, after a systematic trial and error process, the suitable segmentation parameter combinations for delineating tree crowns were scale (90) shape (0.8) and compactness (0.9). Scale was found to be the most sensitive parameter, and the effect of changing the scale while keeping the other parameters the same was evaluated by visual comparison. This showed that when scale factor was 50, tree crowns were over-segmented, when scale factor was 150, tree crowns were under-segmented, and when scale factor was 80, tree crowns were best segmented, as shown in Figure 3.3. We also compared the CHM's contribution to segmentation visually in Figure 3.4 and quantitatively in Table 3.4.

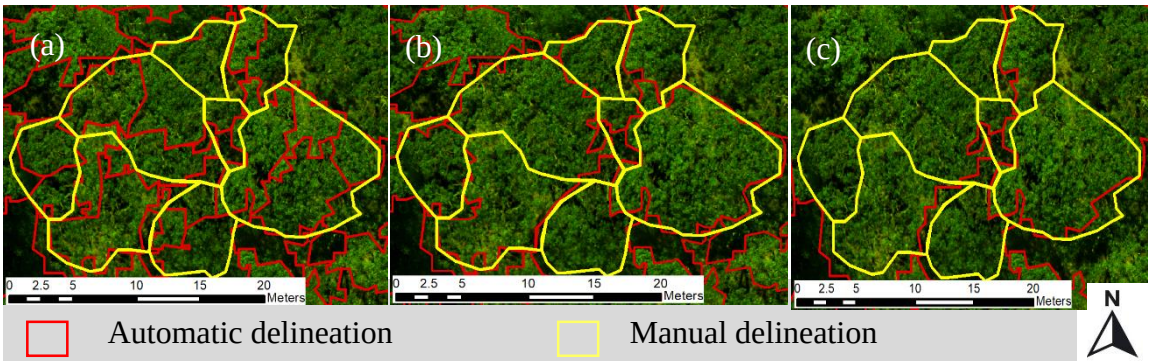

Figure 3.3 Visual comparison of segmentation using different scale parameter: (a) 50 (Oversegmentation), (b) 80 (correct segmentation), and (c) 150 (Undersegmentation)

© University of Pretoria

Table 3.4. Segmentation accuracy of using UAS orthopho and combination of UAS orthophoto and CHM

Image source	OS	US	SE	Accuracy (%)
Orthophoto	0.26	0.17	0.22	78
Orthophoto and CHM	0.17	0.14	0.16	84

OS = oversegmentation, US= undersegmentation, SE = segmentation error

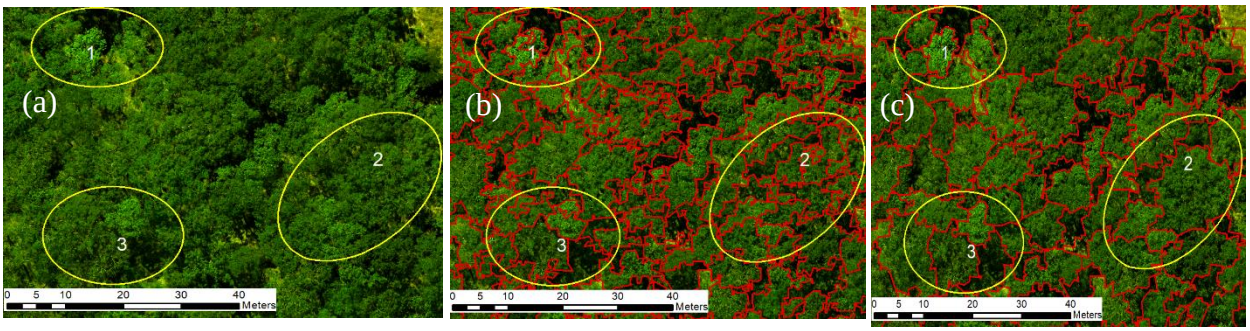

Figure 3.4. Visual comparison of segmentation using orthophoto alone vs orthophoto with CHM at highlighted sites 1-3: (a) Original orthophoto, (b) using only the orthophoto, over-segmentation with irregular outlines for tree crowns, (c) using orthophoto and CHM, tree crowns are well segmented with smoother outlines.

3.2.9 Discrimination of dominant tree species

The investigated image features (mean spectral bands, mean spectral indicies, and GLCM textural features) in discriminating tree species revealed that spectral indices performed better than other image features (Figure 3.5; Appendix 3.2). The performance of each image feature in discriminating the tree species for each of the image dates is indicated below.

Figure 3.5 shows the variability in the mean spectra across the three image dates. Figure 3.5a (May Image): in the blue band JP, BL and shadow were mixed, while IA, BS and MM were discriminable; in the green band, only JP stood out with relatively high reflectance and all the other species were mixed with shadow; in the red band, BL was discriminable, JP, IA, and Shadow were somewhat mixed, while BS and MM were mixed; and in the

© University of Pretoria

red-edge and NIR bands, only MM was discriminable, with all other species mixed with shadow. In Figure 5b (August image): the shadow was discriminable from all the species across the five bands; all the dominant species were clearly discriminable in the red and red-edge bands; in the blue band, JP and IA were discriminable while BS, BL and MM were somewhat mixed; in the green band, BS and BL were discriminable, while MM, IA and MM were somewhat mixed; and in the NIR band, JP, MM and BS were discriminable, while IA and BL were somewhat mixed. In Figure 3.5c (October image): the shadow was discriminable from all the tree species in all the bands except in the blue where it was somewhat mixed with BS; in the blue band, BL, JP, AI and MM were mixed; in the green band, all the species were mixed; in the red band, only MM was discriminable with the rest of the species somewhat mixed; and in the red-edge and NIR bands, MM, BL and BS were mixed, while IA and JP were discriminable (description summarised in Apendix 3.2).

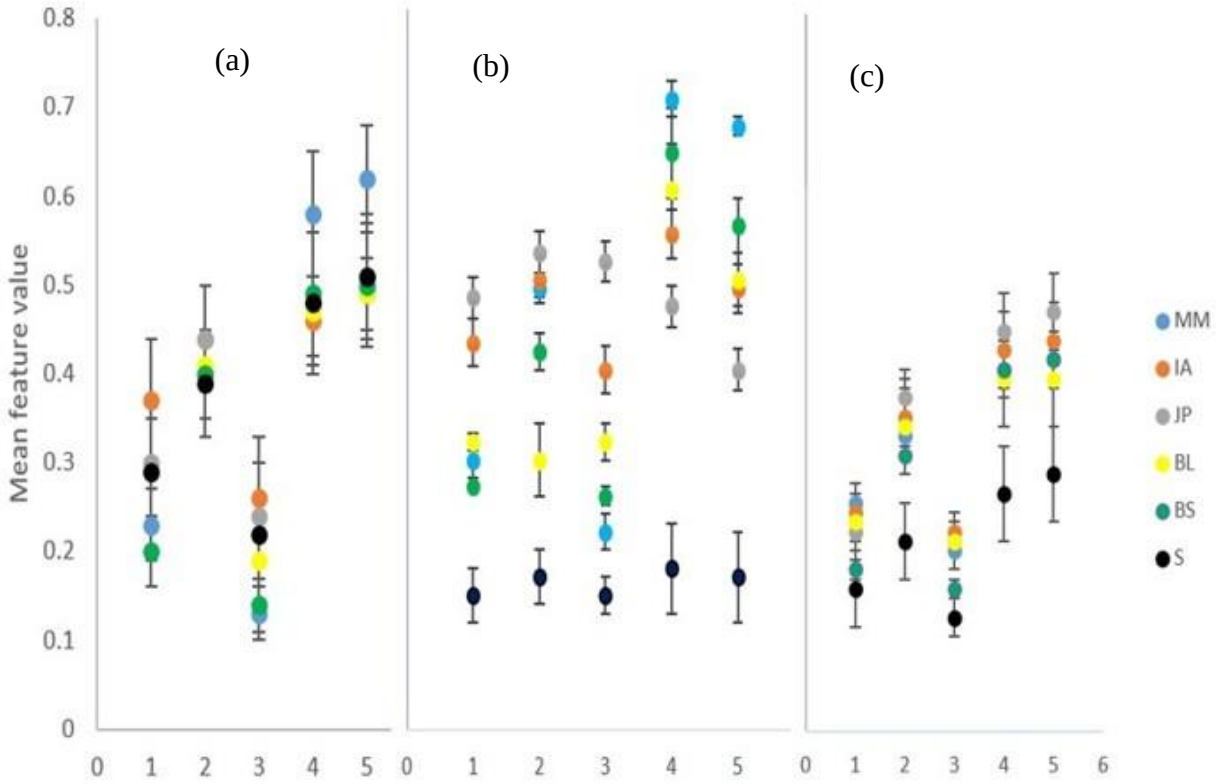

Figure 3.5. Species separability in different bands (1, blue; 2, green; 3, red, 4, red-edge; 5, near infrared): (a) 25.05.21 image, (b) 15.08.21 image, and (c) 24.10.21 image

© University of Pretoria

Figure 3.6 shows the variability in the extracted spectral indices features across the three image dates, which revealed improved species separability compared to raw spectral band data. Figure 3.6a (May Image): in the brightness band, only the shadow was discriminable, with all the species mixed due to uniform brightness in all species at leaf maturity; maximum difference band, all the species were mixed with shadow; BS was discriminable in the NDVI band, while all other species were mixed with shadow; in the GCC band, shadow, JP and BS were discriminable, while MM, IA, and BL were mixed; and in the RCC band, only BS was discriminable, while the rest of the species were mixed with shadow. In Figure 3.6b (August image): the shadow was discriminable from all the species across all spectral metrics bands except in GCC where it was mixed with IA; all the dominant tree species were discriminable in NDVI, RCC and maximum difference bands; and in the GCC band all species were discriminable except IA, which was mixed with shadow. In Figure 3.6c (November image): only MM was discriminable in the brightness band, with the rest of the species somewhat mixed with shadow; in the maximum difference band, IA, BS and MM were discriminable, while JP and BL were somewhat mixed with shadow; in the NDVI band, JP, IA, BS and MM were discriminable, while BL was somewhat mixed with shadow; in the GCC band, BL and IA were discriminable, while JP was mixed with shadow and BS was mixed with MM; and in the RCC band, BL, BS and MM were discriminable, while shadow, JP and IA were mixed (description summarised in appendix 3.3).

© University of Pretoria

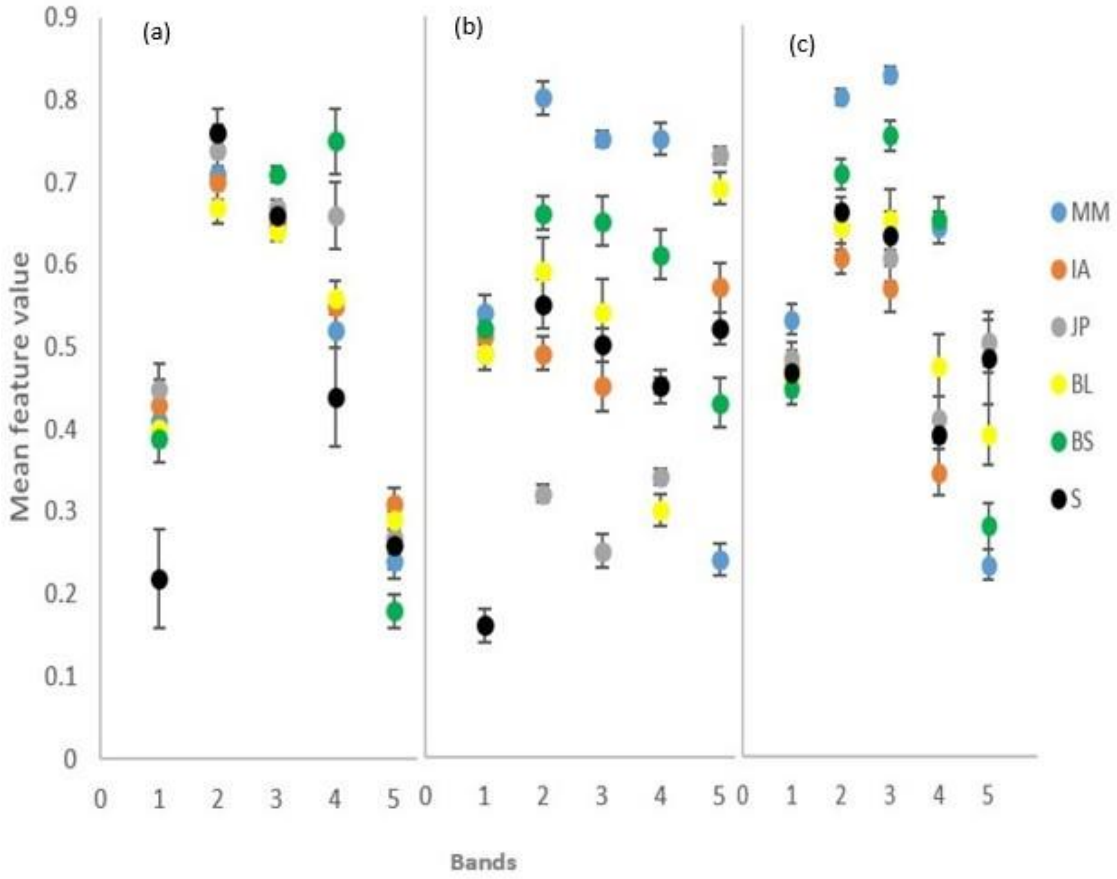

Figure 3.6. Species separability in band spectral metrics bands (1, Brightness; 2, Maximum difference; 3, NDVI; 4, GCC; 5 RCC): (a) 25.05.21 image, (b) 15.08.21 image, and (c) 24.10.21 image

© University of Pretoria

Figure 3.7 shows the variability in the extracted GLCM texture features across the three image dates, which exhibited more mixing among species compared to other considered features. Figure 3.7a (May Image): the shadow is discriminable in the contrast and standard deviation bands, BS was discriminable in the entropy band, and the rest of the species were mixed in the rest of the bands: In Figure 3.7b (August image): the shadow and JP were discriminable in the entropy band, while in the rest of the bands the classes were mixed. In Figure 3.7c (October image): shadow was discriminable in all bands except the standard deviation band, BS, BL and MM were discriminable in the entropy band; JP was discriminable in the correlation band; while in the rest of the bands the

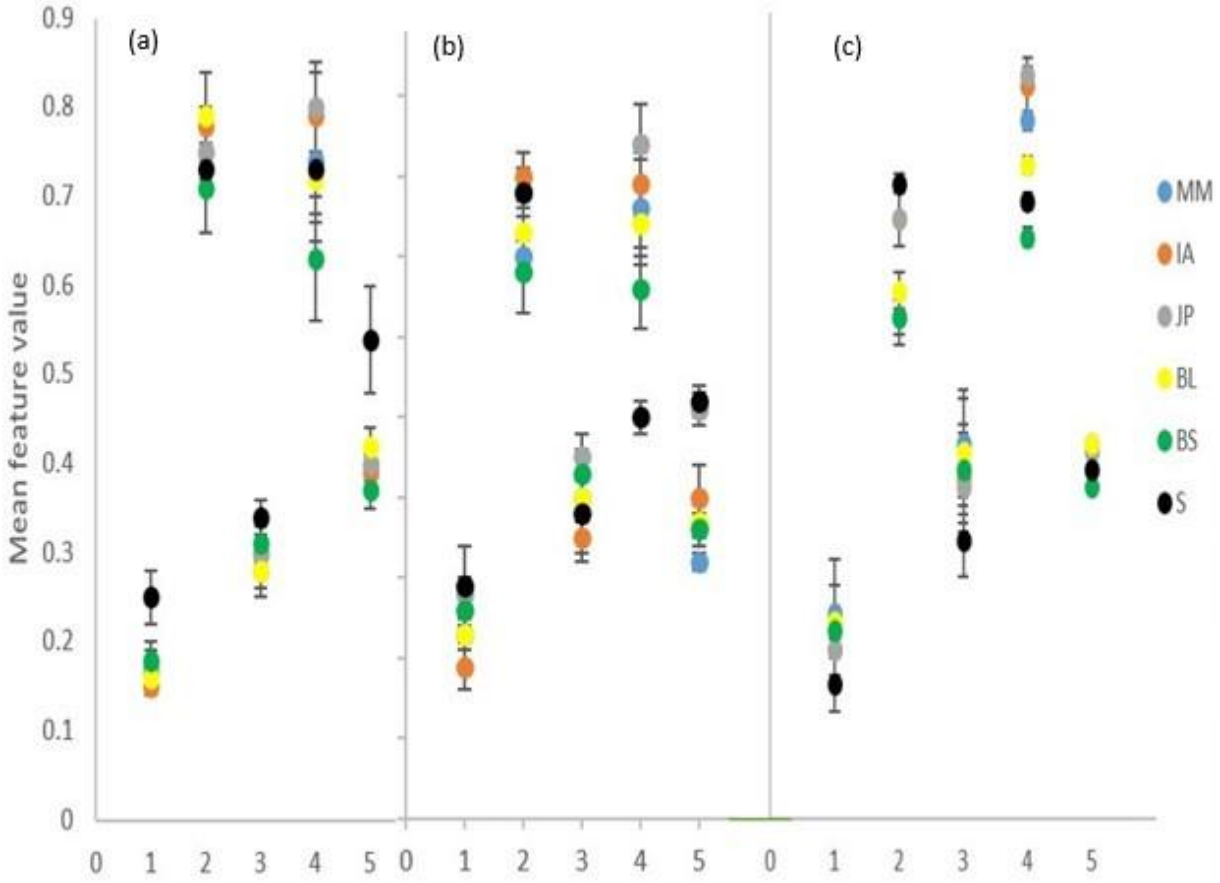

Figure 3.7. Species separability in GLCM texture bands (1, contrast; 2, correlation; 3, dissimilarity; 4, entropy; and 5, standard deviation): (a) 25.05.22 image, (b) 15.08.21 image, and (c) 24.10.21 image

classes were mixed (description summarised in Appendix 3.4).

© University of Pretoria

3.2.10 Tree species classification

Figure 3.8 presents the results of the tree species classification using the Random forest algorithm. The visual observation indicated that JP occupied the most significant distribution across the entire study area. Figure 3.8b depicts the results of canopy species and herbercous layer discrimination using data fusion of UAS CHM and multi-spectral orthophoto mosaic while Figure 3.8c-e show the classification results from the May, August and October images, respectively. Finally, Figure 3.8f shows the classification results of the best combination of multi-date and multi-feature images considered in the study.

The confusion matrix of the five dominant tree species using the three groups of metrics is shown in Table 3.5. In general, using single date data, the accuracy of the tree species classification, except for *Marquesia macroura*, is higher in the August image (Overall Accuracy: 80.12 %, Kappa Accuracy: 68%), followed by the May image with the October image being the least accurate. In addition, the average producer's accuracy (PA) and user's accuracy (UA) for all the dominant species were above 75%, which points to good spectral discrimination among species in the August image when JP is in senescence, while BS and BL are flushing and have a distinctive reddish colour. Furthermore, the species were poorly separable in the October image, with BS, BL and MM mixing across all bands and yielding an average PA and UA of less than 60%. Using multi-date images improved the tree species classification accuracy by about 4% to 84.25% OA and Kappa 0.72. Additionally, combining multi-date images, spectral indices and texture improved the classification accuracy to 87.07% OA and Kappa 0.83.

Table 3.5 Comparison of classification accuracies of tree species for single date, multi-date, and multi-feature imagery

Classes	*25.05.21 spectral*		*15.08.21 spectral*		*24.10.21 spectral*		*Multi-date spectral*		*Multi-date selection (spectral and indices)*	
	PA%	UA%	PA%	UA%	PA%	UA%	PA%	UA%	PA%	UA%
JP	61.42	53.56	93.21	84.74	79.61	72.00	95.11	93.17	96.50	96.03
IA	73.34	80.05	77.23	80.41	65.20	76.24	84.05	92.50	87.17	85.22

© University of Pretoria

MM	82.44	88.25	70.08	67.45	54.17	60.58	93.86	84.35	94.88	86.24
BL	58.22	67.45	86.08	79.44	57.28	44.56	86.75	72.04	92.15	85.36
BS	74.31	71.25	75.41	81.98	52.5	65.05	91.15	82.15	95.04	81.26
S	65.62	67.15	98.20	100	88.75	86.30	90.52	96.01	97.42	100
OA%	74.64		80.12		68.25		84.25		87.07	
Kappa	0.63		0.68		0.59		0.72		0.83	

Abbreviations: JP = *Julbernardia paniculate*, IA = *Isoberlinia anglosis*, MM = *Marquesia macroura*, BL = *Brachystegia longifolia*, BS = *Brachystegia speciformis*, S = *Shadow*

© University of Pretoria

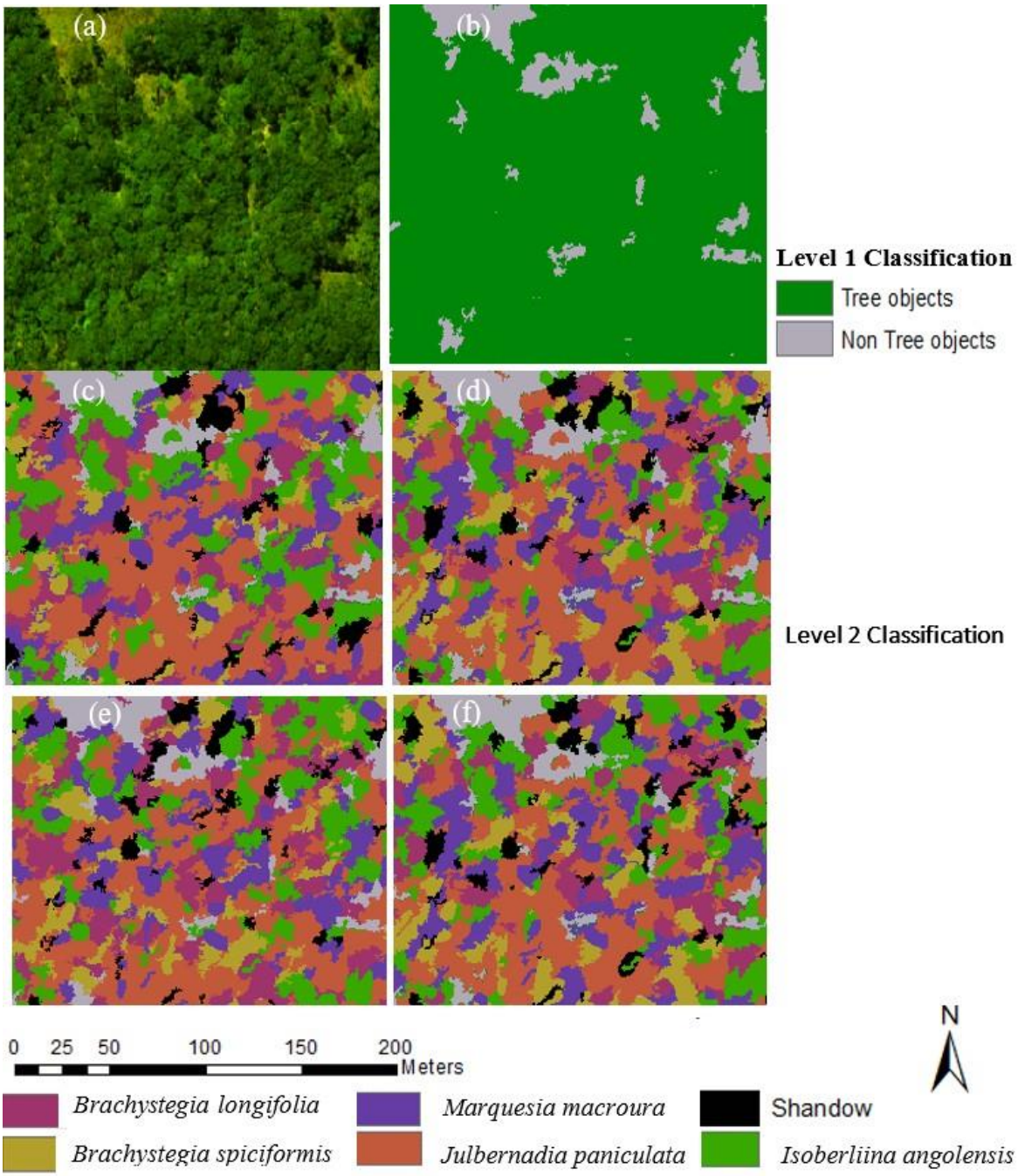

Figure 3.8. Classification of dominant tree species: (a) orthophoto mosaic at leaf maturity, (b) level 1 classification to separate trees from non-tree objects, (c) species classification at leaf maturity (May image), (d) species classification at transition to senescence (August image), (e) species classification at flushing of new leaves, and (f) species classification using multi-date and multi-feature image combination

© University of Pretoria

3.3 Discussion

3.3.1 Segmentation of tree crowns

The segmentation of tree crowns in this study was done by the MRS algorithm iteratively using trial and error method by varying the scale, shape and compactness parameters. The suitable parameters for delineating tree crowns in this study were 90, 0.8 and 0.9 for scale, shape and compactness, respectively. Among these parameters, the scale parameter was found to be the most sensitive and it substantially affected the segmentation results. This observation is consistent with the findings of studies by Effiom et al. (2019) in a mixed forest in Amstelveen, German and Xu et al. (2020) in a mixed forest in Xiagguqing, Diqing town, Yunna province China. The combination of multi-spectral orthophoto and CHM improved the segmentation accuracy by 6% compared with using only the multi-spectral orthophoto (Table 3.4). This improvement in segmentation accuracy can be attributed to the addition of the three-dimensional structural information of the trees contributed by the CHM. Such observations have also been seen in Arizona, United States of America (USA) (Sankey et al., 2017) and Qi'ao Island, China (Cao et al., 2018), both of which demonstrated the importance of tree height to improve the segmentation accuracy in natural forest stands.

The tree crown segmentation accuracy obtained in this study is within the range (60% to 95%) reported in other deciduous forests (Effiom et al., 2019; Xu et al., 2020). However, the accuracy of the tree crown segmentation may be dependent on many factors including image acquisition date and stand structure in different sites. For example Nevalainen et al. (2017) applied a local maxima method onto UAS-derived CHM to delineate individual tree crowns across a boreal forest, achieving accuracies between 40% -95%, depending on characteristics of the site. Another study by Yancho et al., (2019) used a combination of spectral and point cloud UAS data through sub-crown k-means clustering where 48% of the individual tree crown were correctly detected and segmented across a complex forest ecosystem. They also experimented using the same technique with CHM only and observed the accuracy degradation by 4.1%, thus confirming the observation elsewhere (Xu et al., 2020) that the synergy between CHM and spectral information gives superior results compared to a single data set approach.

© University of Pretoria

3.3.2 Optimal single date imagery

The August image (Figure 5b) was identified as the best single date image for discriminating tree species in the wet Miombo woodlands. August- September coincides with transition to senescence for most of dominant wet Miombo tree species and early flushing for some species in the *Brachystegia* genus (Frost, 1996). Moreover, interspecies phenological differences are more pronounced during this period, which maximizes interspecies spectral variability, a key feature for separating tree species (Hill et al., 2010). JP was strongly separable across all spectral bands in the August image resulting in high producer's and user's accuracies compared to other species and exhibited characteristics of a species in senescence, with high reflectance in the visible part of the spectrum and low reflectance in the red-edge and NIR part of the spectrum. In contrast, the MM and BS exhibited the characteristics of species at leaf flushing, with low reflectance in the pigment absorption bands (blue and red) and high reflectance in the red-edge and NIR bands. These results are consistent with findings in the study by (Madonsela et al., 2017), who also reported better classification accuracy in the image acquired during transition periods from full green canopy to senescence in the South African savannah. These findings corroborate earlier works in other regions by Key et al. (2001) in West Virginia, USA, (Hill et al., 2010) in Monks Wood, Cambridgeshire, eastern England and Somers and Asner, (2013) in Hawaii Volcanoes National Park, Hawai'i, USA. The October image, which coincided with the period when newly flushed leaves turn green in the wet Miombo woodlands (Frost, 1996; Ribeiro et al., 2020b), resulted in the lowest accuracy (Table 3.5) due to low interspecies spectral variability at this phenological stage. These results contrast with the findings by Lisein et al. (2015), who found early summer to be the optimal single date imagery for discriminating deciduous tree species in Grand-Leez municipality, Belguim. The differences in findings could be attributed to differences in species composition in the two regions.

3.3.3 Improved accuracy with multi-date image

The high accuracy achieved in the multi-date image compared to single date images (Figure 3.6 and Table 3.5) suggests that multi-date imagery takes advantage of interspecies differences in phenologies, exhibiting different spectral characteristics for tree species on different dates, which compensate for low spectral resolution (Key et al., 2001) for the UAS imagery used in this study. Furthermore, it demonstrates that using a single date image results in missing important information for tree species

© University of Pretoria

discrimination. The improvement in the classification results from multi-date image is in agreement with the observations in other studies elsewhere (Hill et al., 2010; Madonsela et al., 2017; Van Deventer et al., 2019), who found that utilizing multi-date image data improves the spectral variability among species because of differences in phenological developments of different species across the seasons. Lisein et al. (2015) captured multispectral UAS imagery at strategic dates of phenological development on 130 hectares of broadleaved forest in Grand-Leez, Belgium. They used the Random Forest (RF) classification approach to classify five deciduous species groups using single-date, two-date and three-date multispectral image combinations and observed that the three-date combination yielded superior results compared to the others.

3.3.4 Image indices improve classification accuracy

The addition of spectral indices increases separability of different classes as opposed to just using raw spectral information. For example, classes such as BS and shadow, which were difficult to separate using raw spectral information (Figure 5) in the May image become very separable using the spectral indices (Figure 6), thus demonstrating that a combination of raw spectral bands and spectral indices even for a single date image has potential to improve classification accuracy. These findings corroborate works by Xu et al. (2020) in China and (Ferreira et al., 2016) in Brazil, on how spectral indices improve classification accuracy of tree species. This highlights the importance of using a combination of raw spectral data and derived features such as texture and spectral indices when classifying tree species especially when using images of lower spectral resolution. This was in contrast to the findings of Van Deventer et al. (2019), who reported no improvements in vegetation community classification when spectral indices were used. Our study shows mixing of species when texture features are used in tree species classification (Figure 3.6), which result in low classification accuracies. This is in line with a study by Yang et al. (2019), who found that when combined with spectral features, GLCM textural features did not improve the classification accuracy of tree species in two observed sites in China (homogeneous park forest and heterogeneous management forest). However, our study contradicts studies by Gini et al. (2018), Ferreira et al. (2019), Xie et al.(2019) and Deur et al. (2020), who observed that texture features improve tree species discrimination. The difference in results could be attributed to the similar appearance of the Miombo woodlands species (Frost, 1996), which translates to a similar texture.

© University of Pretoria

The methods proposed add a new technique for mapping of Miombo woodland tree species targeted for various products at a local scale. For instance, all the dominant Miombo species identified in this study are targeted for fuelwood production because of their burning qualities (Campbell, 1996), *Isoberlinia anglolensis* is targeted for timber, and *Brachystwgia longifolia* is targeted for its bark rope, which qualifies them as candidates for conservation and sustainable utilization (Syampungani et al., 2011). The classification results attained using multi-date UAS imagery for the dominant Miombo species unlock the potential for mapping and monitoring their distribution as well as inform decision making for better management and conservation. Although the study was limited to a small site and a few species, site-specific studies confined to one or a small group of species are important for upgrading existing information, and thus help sustainable use and management of forest resources (Syampungani et al., 2009). Therefore, the approach used here can be a turnkey for species distribution mapping in the miombo to supplement already existing methods useful in conservation of tree species important for the desirable goods and ecosystem services provide.

3.4 Conclusion

This study investigated the potential for using multi-spectral UAS imagery in classifying the dominant tree species of the wet Miombo. Single dates, combination of dates, and combination of features used in the classification of tree species tend to influence the classification accuracy. The August image achieved the best single date accuracy (80.12% OA, 0.68 kappa), compared to (73.25% OA, 0.59 kappa) and (76.64% OA, 0.63 kappa) for the October and May images, respectively. Use of a multi-date image combination improved the classification accuracy to 84.25% OA and 0.72 kappa. After the addition of spectral indices, the accuracy was further improved to 87.07% and 0.83 kappa. The use of multi-date imagery was found to be very useful in capturing the interspecies phenological differences that are useful for separating different tree species in the Miombo woodlands. The study has demonstrated the applicability of multi-spectral UAS imagery and OBIA to classify tree species in the Miombo woodlands

The results have implications on the choice of dates for image acquisition for natural resources managers using multi-spectral UAS imagery to map tree species in the Miombo woodlands. Judging by the variation in species separability across different dates, it seems imperative to acquire imagery on seasonally separated dates that will enable

© University of Pretoria

capture of all important phenological traits that are important for separating the Miombo woodlands tree species using spectral information. However, denser image acquisition dates should be concentrated around July-September when most of the dominant Miombo tree species are in transition from mature leaves through senescence to flushing. Due to phenological variation of the Miombo woodland tree species, no single date imagery can outperform the broadly spread multi-date imagery combination in capturing the information required for separating different tree species.

© University of Pretoria

Chapter 4 : Exploring the potential of UAS-lidar for estimating forest structural attributes of the Miombo woodlands in Zambia

This chapter is based on:

Shamaoma, H.; Chirwa, P.W.; Zekeng, J.C.; Ramoelo, A.; Hudak, A.T.; Handavu, F.; Syampungani, S. Exploring the potential of UAS-lidar for estimating forest structural attributes of the Miombo woodlands in Zambia (Draft Manuscript)

© University of Pretoria

Abstract

The ability to collect precise three-dimensional (3D) forest structural information at a fraction of the cost of airborne light detection and ranging (lidar) makes unmanned aerial systems-lidar (UAS-lidar) a remote sensing tool with high potential for estimating forest structural attributes for enhanced forest management. The estimation of forest structural data in area-based forest inventories relies on the relationship between field-based estimates of forest structural attributes (FSA) and lidar-derived metrics at plot level, which can be modeled using either parametric or non-parametric regression techniques. In this study, the performance of UAS-lidar metrics was assessed and applied to estimate four FSA (above ground biomass (AGB), basal area (BA), diameter at breast height (DBH), and volume (Vol)) using multiple linear regression (MLR), a parametric technique, at two wet Miombo woodland sites in the Copperbelt province of Zambia. FSA were estimated using site-specific MLR models at the Mwekera and Miengwe sites and compared with FSA estimates from generic MLR models that employed combined data from the two sites. The results revealed that the model fit of site-specific MLR models was marginally better (Adj-R^2: AGB = 0.87–0.93; BA = 0.88–0.89; DBH = 0.86–0.96; and Vol = 0.87–0.98 than when using a generic combined data model (AGB = 0.80; BA = 0.81; DBH = 0.85; and Vol = 0.85). However, the rRMSE (2.01 – 20.89%) and rBias (0.01-1.03%) of site specific MLR models and combined data model rRMSE (3.40-16.71%) and rBias (0.55-1.16%) were within the same range, suggesting agreement between the site specific and combined data models. Furthermore, we assessed the applicability of a site-specific model to a different site without using local training data. The results obtained were inferior to both site-specific and combined data models (rRMSE: AGB = 36.29%–37.25%; BA = 52.98–54.52%; DBH = 55.57%–64.59%; and Vol = 26.10%–30.17%). The results obtained from this indicate potential for application in estimating FSA using UAS-lidar data in the Miombo woodlands and are a stepping stone towards sustainable local forest management and attaining international carbon reporting requirements. Further research into the performance of UAS-lidar data in the estimation of FSA under different Miombo vegetation characteristics, such as different age groups, hilly terrain, and dry Miombo, is recommended.

© University of Pretoria

Keywords: Keywords: Unmanned Aerial System, Lidar, Forest Structural Attributes, Miombo, Multiple Linear Regression

4.1 Introduction

About 10% of Africa's land area (c: a 2.5–4 million km^2) is covered by the Miombo ecoregion, an important biome (White, 1983; Kapinga et al., 2018), representing a sizeable component of the savanna biome, contributing substantially to the terrestrial carbon cycle and providing a variety of socioeconomic, ecological, and environmental services, such as climate regulation and carbon sequestration, as well as biodiversity conservation (Syampungani et al., 2009; Chirwa et al., 2016). Recent climate change, attributed to rising levels of greenhouse gas emissions, will likely have significant repercussions on intensified climate feedbacks (Law and Waring, 2015; Otu-Larbi et al., 2020), for example, droughts, extreme weather events. The impact of these effects on Miombo woodlands development, biomass production and carbon storage need to be adequately understood (Ribeiro et al., 2015). Concerns about global climate change in recent decades has underscored the necessity for effective techniques in assessing and reporting forest biomass and carbon stocks across various scales, including local, national, continental, and global (Goetz et al.,; Fawzy et al., 2020).

The Reduced Emissions from Deforestation and Forest Degradation (REDD+) program is a significant climate change mitigation initiative within the United Nations Framework Convention on Climate Change, focusing on promoting conservation and enhancing forest carbon stocks in developing nations (Goetz et al.,; Kachamba et al., 2016a), with a particular emphasis on forest-based solutions. Successful implementation of the REDD+ program entails precise data collections on forest biomass and carbon storage that are currently lacking in most African vegetation formations.

To achieve precise predictions regarding the interactive impacts of environmental changes, alterations in the distribution of forest species, and variations in the carbon storage capacity of forests, it is imperative to construct accurate models that take into account the current climatic conditions and the diverse uses of forests (Law and Waring, 2015). Accurate and reliable estimations of forest structural attributes (FSA) are

© University of Pretoria

paramount for forest managers to arrive at informed choices (Gibbs et al., 2007; Dash et al., 2015; Shen et al., 2019) regarding the sustainable use of forests.

Traditional field-based sample surveys, for instance, national forest inventories, are employed to assess FSA on a regional and national level (Naesset et al., 2004; White et al., 2016). However, field inventory is lengthy and laborious (Tomppo et al., 2008; Mitchell et al., 2017; Cao et al., 2018). Remote sensing can provide multifaceted, seamless, geographically precise observations in a quick and adaptable way for accurate FSA estimation (Wulder et al., 2013; White et al., 2016; Liu et al., 2018b; Shen et al., 2019). Light detection and ranging (lidar) is considered the most appropriate remote sensing technology for FSA estimation, as it has the ability to capture both the vertical and horizontal traits of vegetation (Lim et al., 2003a; Huang et al., 2011; Hudak et al., 2014; Maltamo et al., 2014a). Examples of application of lidar for estimating FSA include: diameter at breast height (DBH) (Huang et al., 2011), canopy cover (Korhonen and Morsdorf, 2014), stem density (Fekety et al., 2018), basal area (BA) (Hudak et al., 2006; Fekety et al., 2018), volume (Vol) (Naesset, 1997), and aboveground biomass (AGB) (Chen, 2013). However, the use of lidar for forest inventory in low-income countries, where the bulk of forests are located, is limited by high data collection costs and mission safety concerns associated with piloted aircraft, which are often used (Guo et al., 2017).

The advent of Unmanned Aerial Systems (UAS) and the advancement and downsizing of lidar sensors have made it possible to use UAS-mounted lidar systems (UAS-lidar) to assess FSA at a reduced price and with increased adaptability (Lin et al., 2011; Wallace et al., 2012b; Guo et al., 2017). In a groundbreaking study, Lin et al., (2011) developed a UAS-lidar and evaluated it for determining ground and tree heights in Vanttila, Espoo, Finland. A similar study by Wallace et al. (2012) utilized UAS-lidar to determine the position, height, and crown width of trees situated at the University of Tasmania farm in Australia. Another study by Guo et al. (2017) used a UAS-lidar system for estimating canopy height, canopy cover, leaf area index, and AGB in three distinct Chinese ecosystems, including a needleleaf-broadleaf mixed forest, an evergreen broadleaf forest, and a mangrove forest. Liu et al. (2018) used UAS-lidar generated point clouds to estimate six FSA: DBH (r^2 = 0.89), Lorey's mean height (r^2 =0.97), stem density (r^2 = 0.77), BA r^2 = 0.89), Vol (r^2 = 0.94) and AGB (r^2 = 0.95) in Pizhou Ginkgo plantations, China. Studies by Wallace et al., (2012), Guo et al., (2017) and Liu et al. (2018) have demonstrated

© University of Pretoria

the capability of UAS-lidar point clouds for estimating various forest attributes that are critical for forest management. However, none of the studies were carried out in African savannas or Miombo woodlands in particular.

Thus far only a few studies have employed remote sensing methods in estimating AGB in the Miombo ecoregion. For example, Kashindye et al., (2013) employed medium-resolution Landsat imagery and MLR to estimate FSA in the Miombo woodlands of Bereku and Duru Haitemba forests in Tanzania. Another study by Halperin et al., (2016) used Landsat imagery, a semiparametric generalized additive model (GAM), and two nonlinear models (sigmoidal and exponential) to predict AGB in the Miombo woodlands of Nyimba District in Zambia. However, the AGB estimates from imagery ulitised in studies by Kashindye et al., (2013) and Halperin et al., (2016) fall short of the precision required for international reporting mechanisms and sustainable forest management at a local level (Goetz et al., 2015; Jiang et al., 2019). Airborne lidar data, which overcome the shortcomings in imagery that were utilized by Kashindye et al., (2013) and Halperin et al., (2016), were used by Mauya et al., (2015) to estimate AGB in the Miombo woodlands of Tanzania with sufficient precision (rRMSE = 46.8%) for international reporting mechanisms and sustainable local forest management. They compared the parametric linear mixed effects (LMM) and non-parametric k-nearest neighbor (k-NN) models and revealed that both approaches are applicable for predicting AGB in the Miombo woodlands. However, the cost of acquiring airborne lidar is prohibitive for most forest managers in the Miombo ecoregion (Shamaoma et al., 2022), and this study only focused on the estimation of AGB, leaving out the other FSA that are also important for forest management (Gibbs et al., 2007; Dash et al., 2015).

A study by Kachamba et al., (2016b) utilized cheaper UAS imagery and Structure from Motion (SfM) (UAS-SfM) derived point clouds to estimate AGB using MLR models in the Miombo woodlands of Muyobe forest, Mzimba District, in northern Malawi, to levels of precision (rRMSE= 46.7%) sufficient for international reporting mechanisms and sustainable local forest management. Nevertheless, the UAS-SfM approach has been reported to perform poorly in denser forest environments (Mlambo et al., 2017), which would make it challenging to promulgate to denser parts of the Miombo woodlands. Furthermore, studies by Mauya et al. (2015) and Kachamba et al. (2016b) were based on models developed from data collected from a single site; the estimation of FSA using

© University of Pretoria

models developed using data from separate sites as demonstrated in earlier studies (Lefsky et al., 2002; Hudak et al., 2006; Naesset, 2007; Fekety et al., 2018) in other vegetation formations, is yet to be investigated in the Miombo woodlands.

Therefore, this study explored the use of UAS-lidar for supplementing and filling the gaps in other remote sensing imagery that have been used in predicting FSA (AGB, BA, and Vol) in Miombo woodlands. UAS-lidar from two sites, 95 km apart, and area-based methods were used to estimate FSA using multiple linear regression (MLR) models in the wet Miombo woodlands in the Copperbelt Province of Zambia. This modeling technique was chosen because it has been shown to perform well even on small sample data sets (Mountrakis et al., 2011; Morin et al., 2019), as was the case in this study. Furthermore, our choice was motivated by the recommendation by Næsset et al., (2005) that MLR is the method of choice for realistic forest inventories. To accomplish this, we attempted to answered the following questions:

i. How can UAS-lidar be used to improve FSA estimations in the Miombo ecoregion region?
ii. What are the suitable UAS-lidar metrics for estimating AGB in the Miombo woodlands of the Copperbelt province of Zambia?
iii. How does the regression model developed using data from a single site compare with that developed using combined data from two sites?
iv. Are the models developed on one site transferable to a different site where ground reference data are unavailable?

4.2 Materials and methods

4.2.1 Study area

The study was conducted at two test sites (Figure 4.1). The first one was undertaken in Mwekera national forest reserve number 6 (12.860977° S, 28.357049° E and mean altitude of 1225 m above mean sea level), in Kitwe district, about 15 km southeast of the central business district (CBD). Mwekera forest encompasses approximately 11,100 hectares. The other study site is located in Miengwe forest reserve number 36 (13.413889° S, 28.838889° E and mean altitude of 1328 m above mean sea level), in the Masaiti district, approximately 90 km, southwest of the city of Ndola CBD and about 17 km off the Ndola – Lusaka highway. Miengwe forest reserve covers an estimated area of 8,094 hectares. Both forests are located in the Copperbelt Province of Zambia, which experiences annual precipitation between 1000 and 1500 mm and temperatures between 25 and 32 degrees Celsius. The Miombo woodlands, which cover roughly 45 percent of Zambia's area, are

© University of Pretoria

the predominant vegetation in these forests (Zimba, 2007; Handavu et al., 2021). The woodlands are characterised by the dominance of three key deciduous genera (*Brachystegia, Julbernadia* and *Isoberlinia*) belonging to the family Fabaceae, subfamily Caesalpinioideae (Frost, 1996), though the dominant species vary (See Tables 4.1 and 4.2).

Table 4.1: Summary of collected data for 10 most dominant species at Mwekera site

Tree Species	N	% Abundance	DBH (cm) Mean	DBH (cm) Range	TH (m) Mean	TH (m) Range
Julbernardia paniculata	127	18.5	31.03	13.5 - 59.90	17.79	8.50 - 25.00
Isoberlinia angolensis	114	16.6	23.92	9.90 - 44.70	14.55	5.00 - 20.50
Marquesia macroura	108	15.7	29.21	5.30 - 70.00	15.10	3.25 - 25.00
Brachystegia longifolia	64	9.3	20.65	11.8 - 64.00	11.27	8.50 - 23.00
Brachystegia spiciformis	51	7.4	18.55	5.00 - 64.20	9.97	5.80 - 20.50
Parinari curatellifolia	18	2.6	23.48	6.00 - 53.50	13.67	6.00 - 24.00
Ochna pulchra	17	2.5	7.62	5.20 - 10.90	5.70	4.50 - 8.00
Baphia bequaertii	16	2.3	11.63	5.80 - 23.70	6.95	3.00 - 15.00
Pericopsis angolensis	16	2.3	24.42	10.3 - 70.00	14.01	5.00 - 25.10
Diplorhynchus condylocarpon	14	2.0	8.94	5.00 - 18.00	7.64	4.50 - 10.00

Table 4.2. Summary of diameter at breast height (DBH) and total height (TH) data collected for 10 most dominant species at Miengwe site

Tree Species	N	% Abundance	DBH (cm) Mean	DBH (cm) Range	TH (m) Mean	TH (m) Range
Brachystegia longifolia	112	22.1	22.6	7.7 - 81.0	13.68	5.0 - 27.1
Diplorynchus condylocarpon	68	11.4	9.4	5.0 - 30.9	8.26	5.6 – 15.0
Baphia bequaertii	56	9.3	12.8	5.2 - 25.1	7.78	5.7 – 11.0
Isoberlinia angolensis	48	8.1	17.9	6.4 - 59.2	25.50	7.1 – 22.0
Pseudolachnostylis maprouneifolia	36	6.0	13.6	5.2 - 24.7	8.33	5.2 - 11.2
Combretum zeyheri	32	5.3	9.2	5.1 - 15.3	9.05	6.2 – 12.0
Julbernadia paniculata	29	4.9	41.7	20.0 - 98.3	16.88	13.0 - 25.2
Pericopsis angolensis	23	3.9	20.8	6.4 - 47.0	11.33	5.1 - 19.8
Ochna schweinfurthiana	22	3.7	8.8	5.8 - 13.5	7.61	5.8 - 12.0
Combretum collinum	22	3.7	11.4	5.5 - 21.7	9.73	6.0 - 14.2

© University of Pretoria

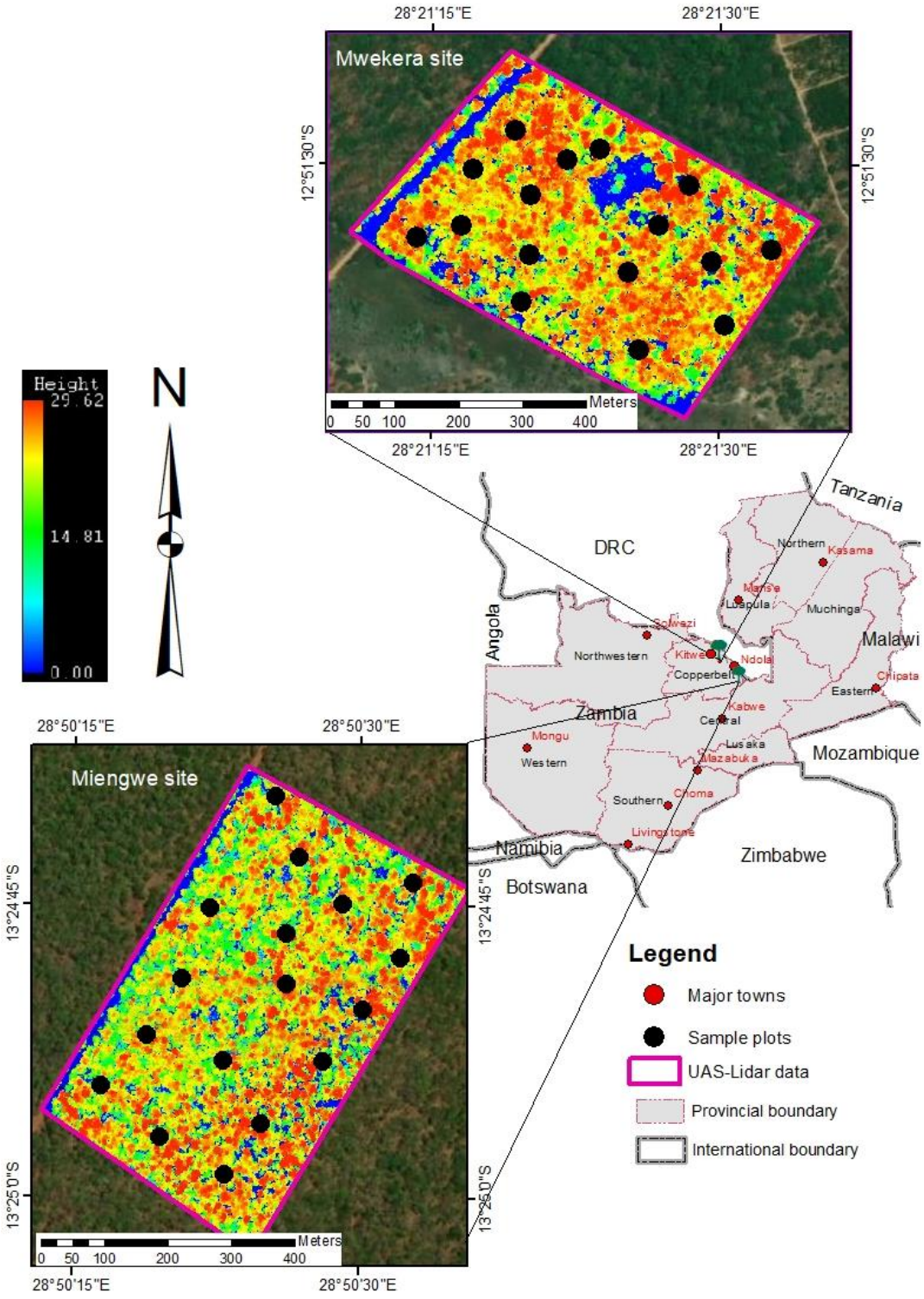

Figure 4.1. Location of study sites and distribution of sample plots

© University of Pretoria

4.2.2 Field data collection

Field work was conducted in November 2022 with sixteen (16) circular plots (radius = 20 m) established at a 200 metre grid spacing in areas with sudden changes in vegetation cover. The coordinates of each plot centre were located using a LT700H real-time kinematic (RTK) Global Navigation satellite system (GNSS) handheld tablet (Shanghai Heave Navigation Technology, China) receiving real-time differential signals from a Continuously Operating Reference Station. All trees in the marked plots with DBH greater than 5 cm were identified to the species level, and their DBH and total height (TH) were measured. The DBH was measured using a diameter tape and TH was measured using a Nikon Forest Pro hypsometer. The measurements of the ten most dominant species for the two sites are summarized in Table 4.1 and 4.2.

In this study, BA, Vol and AGB were calculated by aggregating the individual tree data to plot-level. Estimates of each of the FSA for the training data was calculated using following variables: DBH (basal area), DBH & TH (volume) and DBH, TH & wood density (AGB). The wood density (g/cm3) values were generated using species and genus wood density values from two data sources namely, Handavu et al. (2021) and the ICRAF database (www.worldagroforestry.org/wd/genus). For species that were not directly recoded in the above data sets, average wood density of the genus species was calculated. Standing tree volumes were calculated using three data parameters namely DBH, TH and tree form factor (0.74). Estimations of AGB were based on the best-fit models developed by Handavu et al., (2021).

© University of Pretoria

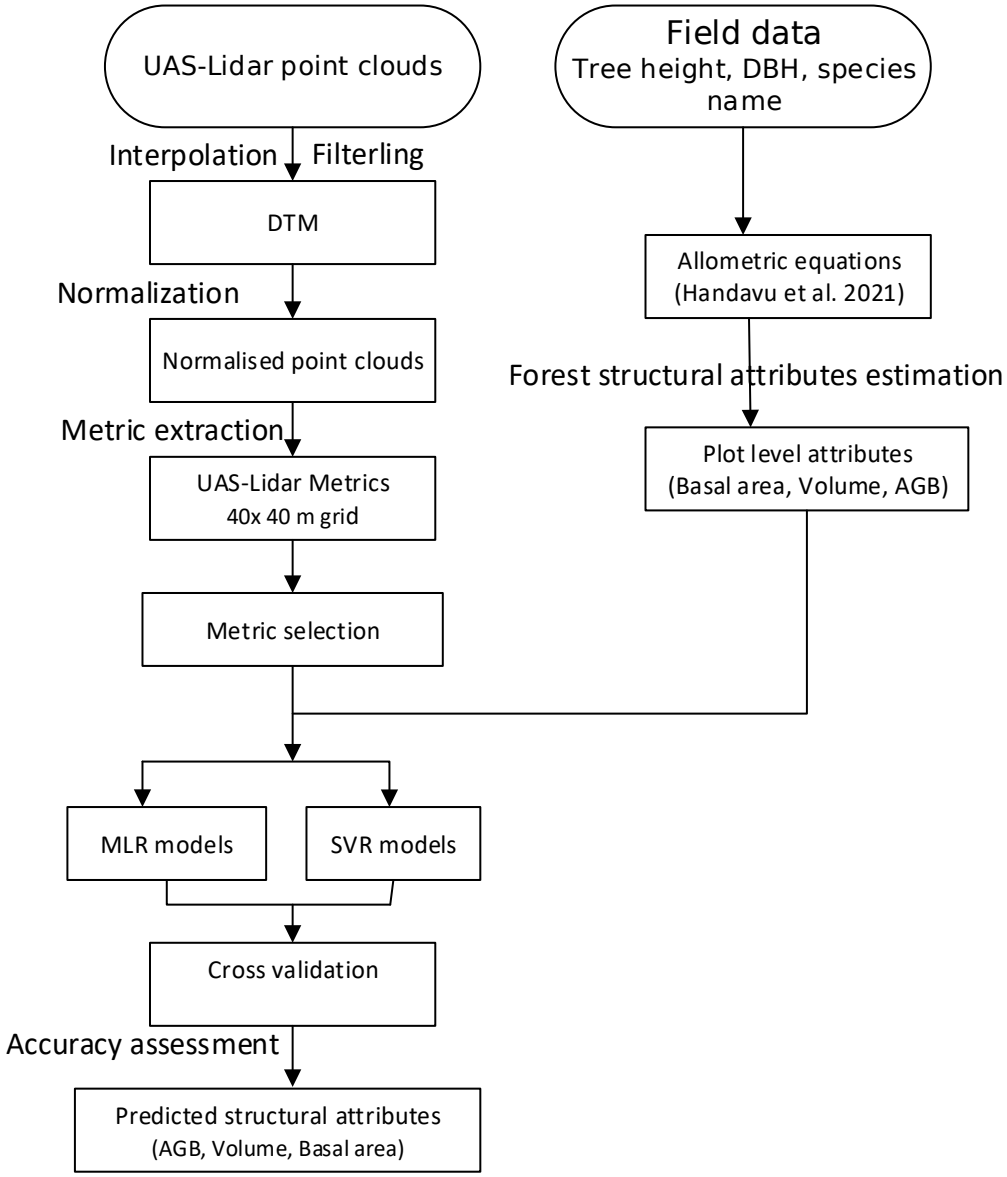

Figure 4.2. Forest structural estimation workflow

4.2.3 UAS Data collection

In this study, a T-Drone M1200 quadcopter with a gAirHawk GS-100C UAS-lidar scanning system (comprising an integrated Livox new generation laser scanner, GNSS and IMU positioning and attitude determination system, and a storage control unit) were used. Mission Planner open source software was used for flight planning and to continuously track the aircraft and monitor flight parameters of the system. In addition, a GNSS ground reference station was used to provide accurate reference measurements and other parameters for post processing the UAS-lidar data (Figure 4.3). The hardware

© University of Pretoria

setup for the for system is shown in Figure 4.3, while the specifications for T-Drone M1200 and GS-100C are shown in Table 4.3. The GS-100C lidar system is capable of recording up to three returns per pulse and uses a near-infrared wavelength of 905 nm (Table 4.3).

Table 4.3. T-Drone M1200 and GS-100C Sensor specifications

T-Drone M1200 Specifications		
Maximum (kg)	5	
Maximum flying weight (kg)	18.5	
Maximum flying time (min)	60	
Flying distance (km)	10	
Flying height (m)	1000	
Flying speed (ms^{-1})	10	
GS-100C Specifications		
Weight (Kg)	1.1	
lidar unit	lidar class	905 nm Class 1
	Range accuracy	1σ (@20 m) < 2 cm
	Data	Triple echo, 720000 points/sec
	FOV	70^0 the circular view
	Laser sensor	Livox Avia
POS Unit	Update frequency	200HZ
	Pitch accuracy	0.025^0
	Roll accuracy	0.025^0
	Heading accuracy	0.080^0
	Positional accuracy	0.02 ~0.05 m
Camera	Camera model	Sony a 6000 (Non standard)
	Effective pixel	24 Mega pixel
	Trigger event	Distance or time

© University of Pretoria

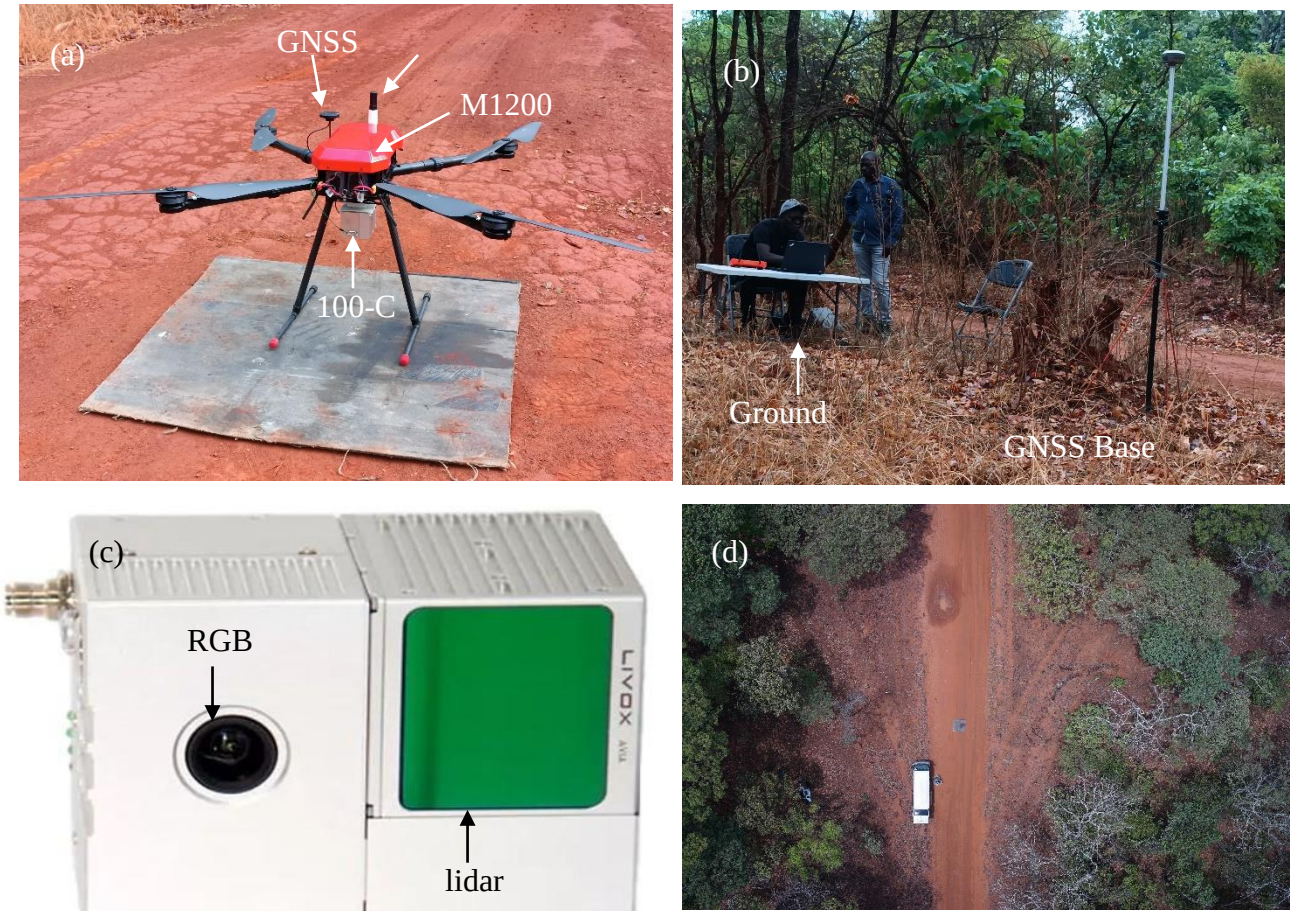

Figure 4.3. (a) T-Drone M1200 platform with 100-C sensor, (b) ground station and GNSS base station, (c) 100-sensor, and (d) aerial view of launch station

Flight planning and data acquisition

The raw UAS-lidar point clouds were acquired on 9th November 2021, after leaf-flushing of the dominant Miombo trees and before emergence of the herbaceous layer. This date was chosen to enable the capture of a well-defined canopy and bare ground for accurate normalized point cloud derivation, which is essential for the subsequent generation of lidar metrics and modeling. The lidar data were acquired at a flight altitude of 80 m above ground level, flight speed of 5 $m \cdot s^{-1}$ and swath width of 42 m.

lidar data pre-processing

The first stages of the pre-processing of the collected UAS-lidar data was done in gAirhawk 5.0 version software (Geosun Navigation Technology Limited, Wuhan,

© University of Pretoria

China), where lidar data, IMU data and GNSS base data were integrated to process the flight trajectory and generate georeferenced UAS-lidar point cloud data in las format. Additionally, the UAS-lidar point clouds were denoised using an outlier removal algorithm in Lidar360 software (GreenValley International, California, CA, USA). The algorithm utilizes adjacent data points and a multiple of the standard deviation to detect anomalous data points. The study utilized the enhanced progressive Triangulated Irregular Network (TIN) densification (IPTD) filter algorithm to differentiate between ground points and non-ground points (Zhao et al., 2016). Then the inverse distance weighting (IDW) interpolation algorithm was used to generate the Digital Terrain Model (DTM), which was subtracted from each point's elevation value to produce normalized point clouds (Kraus and Pfeifer, 1998).

4.2.4 Extraction of UAS-lidar Metrics

lidar metrics are commonly used to regress field plot data against lidar data (Korhonen and Morsdorf, 2014; Zhang et al., 2017; Liu et al., 2018b). In this study, a 40 x 40 grid was utilized to derive various UAS-lidar metrics (Table 4), detailed description of the metrics can be found in (GreenValley International, 2021). To ensure the exclusion of non-canopy returns, a height threshold of 2 m was implemented during the extraction of metrics (White et al., 2013a).

Table 4.4: Description of metrics derived from UAS-lidar data

lidar metrics	Description
Percentile heights (H1, H5, H10, H20, H25, H30, H40, H50, H60, H70, H75, H80, H90, H95, H99)	The percentile of the canopy height distributions (1st, 5th 10th, 20th, 25th, 30th 40th, 50th, 60th, 70th,75th, 80th 90th, 95th and 99th) of first returns
Canopy return density (D1, D2, D3, D4, D5, D6, D7, D8, D9)	The proportion of points above the quantiles (10th,20th, 30th, 40th, 50th and 60th, 70th, 80th and 90th) to total number of points
Variance of height (Hvar)	The variance of the heights of all points
Maximum height (Hmax)	Maximum of return heights above 2 m
Coefficient of variation of heights (Hcv)	Variation of heights of lidar returns above 2 m
MADMedian (Hmdm)	The median of median absolute deviation
Hmsq	Generalized means for the second power
Hskew	Skewness of height
Hkurtosis	The kurtosis of the heights of all points
Hstd	Standard deviation of height
Hmean	Mean height above ground of all first returns
Canopy relief ratio (CRR)	mean height returns minus the minimum height divided by the maximum height minus the minimum height

© University of Pretoria

Canopy cover (CC) above 2 m	Percentile of first returns above 2 m
Gap fraction (GF)	An indication how much of the sky is visible from beneath a plant canopy.
Leaf area index (LIA)	Half of the surface area of all leaves per unit ground area

4.2.5 Development of forest structural estimation models

As per the findings of previous studies (Brosofske et al., 2014; Fassnacht et al., 2014a), it has been observed that the utilization of distinct modeling methodologies can yield varying outcomes. This study developed and MLR models for estimating Miombo woodlands FSA based on extracted UAS-lidar metrics. Three key steps were followed in the modelling processes which included: (i) variable selection, (ii) model development/ fitting, and (iii) model validation. The details for each step are described below.

Variable selection

The area-based prediction of forest inventory properties is based on statistically significant relationships between the predictor variables, which are lidar metrics, and the response variables, which are plot-level FSA (Guyon and Elisseeff, 2003; Chandrashekar and Sahin, 2014; Prasetiyowati et al., 2020). The objective is to choose a superior subset of variables with the aim of maximizing the predictive efficacy of the model (Guyon and Elisseeff, 2003). The motivations for variable selection include enhancing universality, minimizing time, and simplifying comprehension (Prasetiyowati et al., 2020). The present study scrutinized the correlation between FSA and several UAS-lidar metrics using Pearson's correlation coefficient (r), and multi-collinear variables ($r > 0.85$) were excluded to facilitate model parsimony and minimize overfitting. The best subsets regression strategy was used to identify the most appropriate linear models for predicting the FSA based on selected variables (Hudak et al., 2006), which was implemented in Minitab Version 21.1.1 (Minitab, 2023) to select the best performing model and variables. The module explores different combinations of variables in order to create subsets for regression models. These subsets are then assessed and ranked using multiple scoring criteria, such as R^2, Akaike's Information Criterion corrected (AICc), Bayesian information criterion (BIC), and Mallow's Cp statistics (Brooks and Ruengvirayudh, 2016). In the present work, the AICc criterion, which has shown superior performance for smaller sample sizes (Sugiura, 1978; Brewer et al., 2016), was prioritized above other criteria in the determination of the best regression model. The selection of

© University of Pretoria

the optimum subset for model building included considering a combination of predictors that minimized AICc over each of the possible subsets.

MLR model

MLR method has been widely used in the estimation of FSA because of its ability to handle dependencies or correlations between the predictor variables (Hudak et al., 2006; Fassnacht et al., 2014a; Lu et al., 2020). MLR assumes a linear relationship between a dependent variable (e.g., AGB, BA and Vol) and a set of independent variables (lidar metrics). The natural logarithm data transformation was applied to the dependent variable to improve the model fitting in line with previous studies (Naesset et al., 2004; Hudak et al., 2006). The predictions obtained were subjected to a back-transformation process by exponentiation (Cao et al., 2019a). The log transformation introduces a systematic bias, which was corrected during the exponentiation using a bias correction factor based on half the mean squared error (Hudak et al. 2006). The MLR model with the lowest AICc for each FSA was implemented.

Model performance

The model performances were evaluated based on differences in the R^2 and RMSE.

$$RMSE = \sqrt{\sum_{i=1}^{n} \frac{(y_i - \hat{y}_i)^2}{n}} \quad (5)$$

$$rRMSE = \frac{RMSE}{\bar{y}} x100\% \quad (6)$$

$$Bias = \sum_{i=1}^{n} \frac{(\hat{y}_i - y_i)}{n} \quad (7)$$

$$rBias = \frac{Bias}{\bar{y}} x100\% \quad (4)$$

Where yi and ŷi denote field measured FSA and predicated FSA for plot i, respectively and n is the number of measured FSA. K-fold cross validation was used to compare the developed MLR and SVR models and understand their performance.

© University of Pretoria

This method entails randomly dividing the data into k approximately equivalent folds or groups. In k iterations, each of these folds is regarded as a validation set. We used a k-value of 10 because it has been widely used and empirically demonstrated to produce test error rate estimates with neither excessively high bias nor extremely high variance. The dataset was divided into 10 subsets for the 10-fold cross-validation. One subset was kept aside in each fold and used to evaluate the trained model (the validation set), while the remaining 9 subsets were used for training. Once a subset has been used for validation, the process is repeated until all subsets have been used. Finally, the predicted values from all the folds were compiled into a table, and the equations presented above were applied to the table to estimate cross validated RMSE.

4.3 Results

4.3.1 Variable selection

The selection of predictor variables (UAS-lidar metrics) was conducted separately for each dependent variable (AGB, BA, DBH, and Vol). The predictors that were selected comprised a combination of parameters relating to height, density, and canopy cover. Table 4.6 indicates that among the metrics associated with canopy, CC was the most often chosen in the majority of the models. In terms of metrics related to height, H25 and H80 were the most commonly picked. Additionally, for metrics related to density, D60 emerged as the most frequently chosen metric.

The selected models and variables are highlighted in Table 4.5. The models with a smaller number of predictors were prioritized over models with a larger number of predictors due to their demonstrated stability and ability to mitigate overfitting (Hudak et al., 2006; White et al., 2017). For example, when estimating the AGB, the model with four predictor variables was chosen based on lower AICc over the first model with five predictors, despite the latter exhibiting higher R^2 and adjusted R^2 values, as well as lower AICc values.

4.3.2 MLR forest structural attribute estimations

The modeling results are shown in Table 6. In general, the predictive performance of site-specific models for FSA was superior (Adj-R2: AGB = 0.87–0.93; BA = 0.88–0.89; DBH = 0.86–0.96; and Vol = 0.87–0.98) to that of the combined data model (AGB = 0.80;

© University of Pretoria

BA = 0.81; DBH = 0.85; and Vol = 0.85). In addition, this research evaluated the transferability of the site-specific models between Mwekera and Miengwe (as shown in Table 4.7) and found that these models exhibited lower levels of model fit (R2 = 0.41-0.54) compared to both the site-specific models (R2 = 0.94-0.99) and combined data models (R2 = 0.83-0.88).

© University of Pretoria

Table 4.5. Candidate Models for Field estimated forest structural attributes prediction using UAS-lidar metrics (see table 3 for UAS-lidar metrics description)

Vars	R^2	R^2 adj	R^2 -pred	Cp	AICc	BIC	CC	CRR	Haad	H25	H50	H80	H99	Hcv	Hstd	Hmdm	Hm	Hmd	D10	D30	D40	D60
Above ground biomass																						
1	0.52	0.50	0.36	21.2	255.824	258.508				X												
2	0.71	0.68	0.60	3.9	248.849	251.977					X										X	
3	0.75	0.72	0.60	3.0	247.057	250.347						X	X			X						
4	0.83	0.80	0.67	2.1	243.824	245.419	X					X	X			X						
5	0.84	0.80	0.68	2.2	243.351	245.936	X					X	X			X	X					
6	0.86	0.72	0.56	10.6	244.724	246.412	X					X	X	X		X			X			
7	0.91	0.77	0.62	12.0	247.354	247.423	X		X			X		X			X	X	X			
8	0.93	0.80	0.61	12.9	251.627	249.542	X		X			X		X			X	X	X	X		
9	0.93	0.80	0.60	13.6	256.438	251.420	X		X			X		X			X	X	X	X		X
10	0.94	0.70	0.42	18.405	263.081	254.178	X		X	X	X	X	X	X		X		X	X			
Basal area																						
1	0.50	0.48	0.38	175.26	177.77	32.4				X												
2	0.59	0.56	0.47	173.17	176.04	24.8						X									X	
3	0.65	0.61	0.56	172.17	175.11	20.1						X	X			X						

© University of Pretoria

4	0.73	0.67	0.61	169.71	172.36	14.2	X					X	X			X					
5	0.81	0.76	0.70	164.64	166.59	7.4					X		X		X	X				X	
6	0.85	0.80	0.73	163.16	163.91	5.1	X					X	X		X	X				X	
7	0.89	0.79	0.72	164.50	164.47	3.3	X		X			X	X		X	X				X	
8	0.90	0.78	0.68	164.39	160.86	4	X	X	X			X	X		X	X				X	
9	0.91	0.80	0.71	166.62	159.72	4.3	X	X	X			X	X		X	X				X	X
10	0.93	0.88	0.79	170.07	158.70	4.8	X	X	X			X	X		X	X		X		X	X
Diameter at breast height																					
1	0.66	0.65	0.58	143.39	145.90	21.4					X										
2	0.78	0.76	0.70	136.14	139.02	9.9							X	X							
3	0.86	0.84	0.79	128.03	130.96	2.2	X						X	X							
4	0.88	0.85	0.80	127.84	130.49	1.8	X						X	X							X
5	0.88	0.85	0.78	131.21	133.15	3.5	X						X	X				X			X
6	0.89	0.85	0.76	134.17	134.92	4.7	X			X		X	X	X							X
7	0.89	0.84	0.72	138.71	137.68	6.4	X			X	X		X	X				X			X
8	0.92	0.87	0.55	137.60	134.08	5.2	X			X	X	X	X		X		X	X			
9	0.93	0.88	0.75	140.72	133.82	5.9	X		X	X	X	X	X		X		X	X			
10	0.928	0.877	0.615	147.69	136.31	7.6	X		X	X	X	X	X		X		X	X			X

© University of Pretoria

Volume																				
1	0.72	0.70	0.59	171.84	174.35	8.1				X										
2	0.80	0.78	0.75	166.50	169.37	9.2				X									X	
3	0.85	0.83	0.78	162.19	165.12	7.4	X			X									X	
4	0.88	0.86	0.81	146.44	140.34	3.6	X			X				X					X	
5	0.91	0.78	0.74	148.01	140.64	6.9	X		X	X						X				X
6	0.93	0.71	0.69	147.24	148.74	7.7	X		X			X	X			X				X
7	0.95	0.73	0.67	152.60	151.57	9.4	X		X			X				X	X	X		X
8	0.97	0.75	0.69	159.63	162.28	12	X		X		X	X				X	X	X		X
9	0.97	0.76	0.62	156.91	158.85	15.4	X	X	X			X	X			X			X	X
10	0.98	0.86	0.68	154.89	155.64	21.8	X	X	X		X	X	X			X			X	X

Table 4.6. Summary of cross validation results of model for R^2, RSME and rRSME, Bias and rBias

Site	Response variable	Prediction equation	R^2	R^2_adj	RMSE	rRMSE (%)	Bias	rBias (%)
Mwekera	ln(AGB)	1.42CC + 0.02H25 + 1.27Hcv - 3.57D20 - 1.27D60 + 0.24	0.90	0.87	15.41	15.46	0.01	0.01
	ln(BA)	1.12LAI + 1.24CRR - 0.02H25 + 0.05H80 - 3.05Hcv + 9.16D10) + 1.96D60 -0.98	0.92	0.88	1.78	11.12	-0.01	-0.04
	ln(DBH)	0.25LAI – 0.05Haad + 1.12CRR + 0.01H25 + 0.08Hstd – 0.31D80 +0.32	0.90	0.86	1.51	6.37	0.05	0.19
	ln(Vol)	1.05LAI + 2.16CRR - 2.71Hcv + 0.13Hstd + 8.98D10 +1.94D60 - 0.21	0.94	0.87	28.29	14.08	2.06	1.03
Miengwe	ln(AGB)	2.52CC - 8.27Hcv + 0.85Hstd + 5.49D20 – 1.84D50 - 0.07	0.95	0.93	15.38	14.76	-0.73	-0.70

© University of Pretoria

	ln(BA)	2.19CC – 5.71Hcv + 1.83Hstd – 1.10Haad – 3.12D50 – 1.44	0.92	0.89	2.81	20.89	1.63	0.10
	ln(DBH)	0.62CC + 0.03H1 – 0.04H25 – 2.70Hcv + 0.20Hstd – 0.012D70+1.237	0.97	0.96	0.31	2.01	0.00	0.01
	ln(Vol)	1.81CC – 0.79Haad – 7.33Hcv +1.58Hstd + 3.16d20 -2.83D50 + 0.67D60 = 0.04	0.99	0.98	12.15	9.50	-0.73	-0.57
	ln(AGB)	0.87CC + 0.13H80 – 0.06H99 – 0.19Hmd + 0.73	0.83	0.80	18.39	16.05	1.26	1.10
Combined	ln(BA)	0.95CC + 0.17Haad + 0.07H80 + 0.07H99 +0.38Hstd -6.62D30 -0.04	0.85	0.81	2.69	16.71	0.19	1.16
	ln(DBH)	0.48CC + 0.03H99 -0.67Hcv + 0.26D60 +0.51	0.87	0.85	2.27	11.86	0.11	0.55
	ln(Vol)	1.21CC + 0.07H25 + 1.40Hcv -6.27D10 +0.37	0.88	0.85	5.94	3.40	1.38	0.79

© University of Pretoria

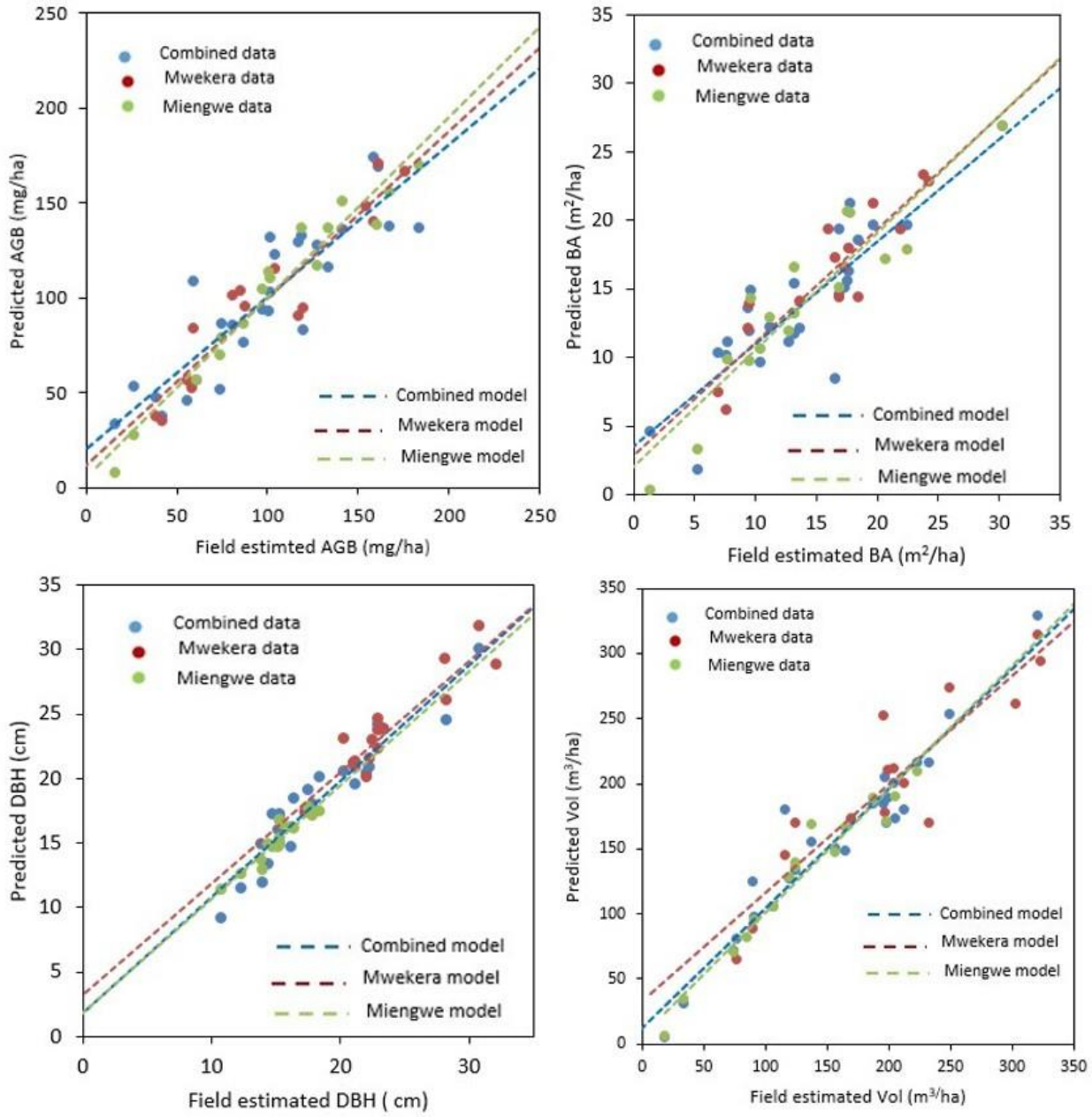

Figure 4.4. Shows a comparison of UAS-lidar estimated and field estimated FSA for Mwekera and Miengwe sites utilizing single site data models and combined data models. (a) above ground biomass, (b) basal area, (c) diameter at breast height and (d) Volume

© University of Pretoria

Table 4.7. Local model transferability R^2, RMSE and rRSME Bias, rBias

Site	Attributes	Model	R2	RMSE	rRMSE(%)	Bias	rBias (%)
Mwekera	AGB	Miengwe	0.55	23.25	23.33	6.20	6.22
	BA		0.52	8.02	50.33	3.71	23.29
	DBH		0.48	16.28	68.51	-4.32	-18.90
	Vol		0.48	37.07	18.45	13.33	6.63
Miengwe	AGB	Mwekera	0.53	20.02	19.21	2.50	2.40
	BA		0.42	3.58	26.02	0.90	6.50
	DBH		0.41	2.74	18.07	0.69	4.52
	Vol		0.50	29.76	23.26	-5.40	-4.22

4.4 Discussion

4.4.1 Selecting the best predictors for estimating FSA

We undertook variable selection to choose the best possible predictors (UAS-lidar metrics) to estimate the FSA of interest (AGB, BA, DBH or Vol). The best predictors for each forest structural attribute were a mix of height, density, and canopy cover-related metrics (Table 5). The height percentiles were the most selected lidar metrics across all FSA. This is consistent with earlier observations that demonstrated that height-related metrics (particularly high percentiles) are important in estimating FSA (Lefsky et al., 2005; Hudak et al., 2008; Bouvier et al., 2015; Liu et al., 2018b). However, there is a noticeable variation in the selected predictors for the two sites (site equations in Table 4.6) despite both being the wet Miombo woodlands. The observed differences may be ascribed to disparities in the structure and composition of the forests at the two locations, as seen in Tables 4.1 and 4.2. This finding is consistent with a previous investigation conducted by Bouvier et al. (2015).

4.4.2 Site specific vs combined data models

The results presented in Table 4.6 demonstrate that the Mwekera and Miengwe site-specific models exhibited superior model fit (adj-R2 = 0.86-0.98) compared to the combined site data model (adj-R2 = 0.80-0.85), confirming assertions by Foody et al. (2003). This agrees with claims by Bouvier et al. (2015) regarding the prominence of the dominant species in a forest stand, which significantly influences the correlation between lidar metrics and the FSA that is being estimated through area-based lidar techniques employed in this study. In relation to rBias the site-specific models (0.01-1.03%) exhibited a similar range to the combined data model (0.55-1.16%), indicating coherence between the site-specific and combined data models. This contradicts work by Bouvier et al. (2015), who found that site specific models yielded better estimates of FSA than large-areas combined data models.

© University of Pretoria

4.4.3 Site-specific model transferability

We assessed the efficacy of extrapolating single site models to estimate FSA in regions where UAS-lidar data is available, but field forest inventory measurements are assumed to be unavailable (Table 4.7). The obtained results (rRMSE = 26.10%-64.59%) fall within a similar range observed by Fekety et al., (2018). In their study, Fekety et al., (2018) evaluated the transferability of random forest regression models in estimating BA and Stem density (rRMSE = 32.3%-67.3%) across six lidar sites located in the Northern Rocky Mountains, Idaho, United States of America. In the present study, the performance of a transferred local model was found to be suboptimal when applied to a new site lacking field training data (Table 4.7) in comparison to the site where it was originally developed (Table 6). As such, this finding may serve as a starting step for forest managers wishing to incorporate UAS-lidar data gathered for non-forest applications into forest inventory processes. Nonetheless, the amalgamation of UAS-lidar collections from multiple sources presents challenges in terms of data quality. This is primarily due to the utilization of different flight settings and sensor characteristics (Goodwin et al., 2006; Hopkinson, 2007; Næsset, 2009). Consequently, forest managers wishing to combine USA-lidar from various sources are advised to employ a cautious, consistent approach to calculate reliable lidar metrics (Fekety et al., 2018).

4.4.4 UAS-lidar improved FSA estimates

This study used UAS-lidar to estimate more FSA (i.e. AGB, DBH, Vol and BA) compared to earlier studies that were carried out in the Miombo, which focused on AGB (Mauya et al., 2015; Kachamba et al., 2016b). We were able to achieve superior estimations of AGB: rRMSE = 14.76% - 16.05%, compared to rRMSE = 46.8% reached by Mauya et al. (2015) in Tanzania using airborne-lidar and rRMSE = 46.7% achieved by Kachamba et al. (2016b) in Malawi using UAS-SfM. The difference in AGB estimation accuracy from Mauya et al. (2015) was most likely caused by the differences in point cloud densities. The UAS-lidar used in this study had an average point density of about 300 pts m^{-2}, compared to the manned airborne lidar system used in Mauya et al. (2015) with an average point density of about 1.8 pts m^{-2}. An increased point density results in enhanced delineation of the canopy structure, consequently leading to more accurate estimations of AGB (Kato et al., 2009). The difference in results from Kachamba et al. (2016b) may be attributed to the superior DTM from UAS-lidar owing to its ability to penetrate the canopy and capture the vertical distribution of the canopy as opposed to UAS-SfM, used in (Kachamba et al., 2016b). This comforms with findings from studies by Wallace et al. (2016) and Cao et al. (2019), who compared UAS-lidar and UAS-SfM for estimating FSA in a dry sclerophy11 eucalypt forest in Australia and in a planted forest in China, respectively, and

© University of Pretoria

found that UAS-lidar yielded better estimates, due to the superior canopy penetration capability of active lidar technology versus the passive optical stereo imagery used in the UAS-SfM technique.

Although our study was confined to just two sites, site specific studies on a small number of species are critical to updating current knowledge and information thereby aiding in the sustainable use and management of forest resources (Syampungani et al., 2009). As a result, the techniques adopted here may be replicated in other parts of the Miombo with comparable vegetation formations. Further, considering the endurance and storage challenges that continue to plague UAS-lidar technology (Whitehead and Hugenholtz, 2014; Shamaoma et al., 2022), we believe that UAS-lidar should be used as a sampling tool to bridge the spatial gap between ground techniques and wall-to-wall satellite data. This may be accomplished by utilizing a two-phase sampling strategy in which regions to be covered by UAS-lidar data are sampled using ground techniques and areas to be covered by wall-to-wall satellite imagery are sampled using UAS-lidar (Shamaoma et al., 2022). As such, the relationship between UAS-lidar metrics and field estimated FSA at the local sample site is of prime importance for modelling generic wall-to-wall relationships.

4.5 Conclusion

In this study, we were able to extract and select suitable UAS-lidar metrics for estimating FSA at two wet Miombo woodlands sites. Four FSA (AGB, BA, DBH and Vol) were estimated using MLR (adj-R^2 > 0.79 and rRMSE < 21%). The results indicate that the UAS-lidar approach presented in this research provides a useful enhancement to the existing methodologies used for estimating aboveground biomass (AGB) in the Miombo woodlands. Also, the accuracy of FSA estimating models built using UAS-lidar data from a single site was compared to the accuracy of models built using data from two sites. The findings revealed that site-specific models exhibited superior performance compared to models using combined data. This phenomenon may be anticipated since the uniformity of forest structure and composition is expected to be stronger within a specific site compared to a broader geographical area. Nevertheless, a common data model exhibits more generality and is better suited for application over a broader geographic area.

The results obtained in this study provides alternative remote sensing based FSA estimation with precision required for sustainable forest management at a local level as well as for international reporting management requirements such as REDD+ and MVR.

© University of Pretoria

However, although this study demonstrated the utility of UAS-lidar in the estimation of FSA, we only considered mature wet Miombo woodlands in similar forest environments. Therefore, it is apparent that further work on this topic is required if the full potential of UAS-lidar as a source of forest inventory data in the Miombo woodlands is to be realized. Future works may be focused on estimation of FSA in the dry Miombo and hill Miombo, as well as different age groups of the regenerating Miombo woodlands, so as to have full understanding of the performance and limitations of UAS-lidar in estimating FSA across the entire spectrum of the Miombo woodlands. Furthermore, this study used area-based methods to estimate FSA from UAS-lidar. With continuous improvement of UAS-lidar sensors, increased point cloud densities per square meter, and advancement of processing technologies coupled with the open nature of the Miombo woodlands canopy, we expect future studies to focus on individual tree-based methods for estimating FSA, resulting in richer forest inventory data as would benefit sustainable management of the Miombo woodlands.

© University of Pretoria

Chapter 5 : Exploring UAS-lidar as a sampling tool for satellite-based AGB estimations in the Miombo woodland of Zambia

This chapter is based on:

Shamaoma, H.; Chirwa, P.W.; Zekeng, J.C.; Ramoelo, A.; Hudak, A.T.; Handavu, F.; Syampungani, S. Exploring UAS-lidar as a sampling tool for satellite-based AGB estimations in the Miombo woodland of Zambia (Draft manuscript)

© University of Pretoria

Abstract

To date, only a limited number of studies have utilized remote sensing imagery to estimate aboveground biomass (AGB) in the Miombo ecoregion using wall-to-wall medium resolution optical satellite imagery (Sentinel-2 and Landsat), localized airborne light detection and ranging (lidar), or localized unmanned aerial systems (UAS) images. On the one hand, the optical satellite imagery is suitable for wall-to-wall coverage, but the AGB estimates based on such imagery lack precision for local or stand-level sustainable forest management and international reporting mechanisms. On the other hand, the AGB estimates based on airborne lidar and UAS imagery have the precision required for sustainable forest management at a local level and international reporting requirements but lack capacity for wall-to-wall coverage. In order to bridge the spatial data gap, this study employed a two-phase sampling approach, utilizing Sentinel-2 imagery, partial-coverage UAS-lidar data, and field plot data to estimate AGB in the 8,094-hectare Miengwe Forest, Miombo Woodlands, Zambia, where UAS-lidar estimated AGB was used as reference data for estimating AGB using Sentinel-2 image metrics. The findings showed that utilizing UAS-lidar as reference data for predicting AGB using Sentinel-2 image metrics yielded superior results (Adj-R2 = 0.70, RMSE = 27.97) than using direct field estimated AGB and Sentinel-2 image metrics (R2 = 0.55, RMSE = 38.10). The quality of AGB estimates obtained from this approach, coupled with the ongoing advancement and cost-cutting of UAS-lidar technology as well as the continuous availability of wall-to-wall optical imagery such as Sentinel-2, provides much-needed direction for future forest structural attribute estimation for efficient management of the Miombo woodlands.

Key words: Above ground biomass, UAS-lidar, Two-phase, sampling tool

© University of Pretoria

5.1 Introduction

Sustainable management and carbon accounting of forests require accurate up-to-date vegetation structural data often covering extensive areas that are too huge to capture, process, and manage by manual methods (Kerr and Ostrovsky, 2003; Turner et al., 2003; Romijn et al., 2012; White et al., 2013b; Barquín et al., 2014; Day et al., 2014). Typically, above ground biomass (AGB) in the Miombo woodlands is determined using destructive harvesting procedures, for building allometric equations based on the observed data from these cut trees, such as diameter at breast height (DBH), tree height, and wood density (Mugasha et al., 2012; Kachamba et al., 2016a; Handavu et al., 2021). Nevertheless, the application of these allometric equations on extensive forest regions can pose challenges in terms of time, cost, and feasibility due to the difficulty in obtaining field measurement input parameters in remote terrains. Consequently, the AGB for most of vegetation formations in many parts of the African savannas, Miombo woodlands inclusive remains poorly understood.

Remote sensing has made it possible to measure vegetation structure across vast areas in an efficient and repetitive manner (Hosonuma et al., 2012; Weisberg et al., 2021). The application of remote sensing methods in estimating AGB in the Miombo woodlands (Samimi and Kraus, 2004; Kashindye et al., 2013; Mauya et al., 2015; Halperin et al., 2016a; Kachamba et al., 2016b; Næsset et al., 2016; Mareya et al., 2018) is becoming common. Most of these studies employ statistical models where field estimates of AGB are regressed against metrics generated from corresponding remote sensing data, followed by extrapolation of resulting models to the entire study area. The studies that have employed remote sensing imagery for estimation of AGB in the Miombo ecoregion so far have done it at two levels of abstraction, namely: (i) wall-to-wall estimation of AGB; and (ii) local or stand-level estimations. The wall-to-wall category includes, the use of atmospherically resistant vegetation indices (ARVI) and normalized difference vegetation indices (NDVI) derived from Landsat imagery to assess forest cover, stocking and above-ground tree biomass dynamics in the Miombo woodlands of Tanzania (Kashindye et al., 2013). In another study, Halperin et al. (2016a) estimated AGB in Nyimba district, Miombo woodlands, Zambia, using National Forest Inventory (NFI) data, estimated canopy cover, environmental data, disturbance data, and Landsat 8 OLI satellite imagery. The medium resolution imagery (Landsat) utilized in Kashindye et al. (2013) and Halperin et al. (2016a) are suitable for wall-to-wall coverage, but the AGB estimates based on such imagery lack precision for local or stand-level sustainable forest management, as well as international reporting mechanisms (Xie et al., 2008) such as reducing emissions from Deforestation and Forest Degradation, plus forest conservation, sustainable management of forests and enhancement of carbon stocks (REDD+) and Monitoring, Reporting and Verification (MRV), which offers monetary rewards to developing countries for forest conservation, and the execution of

© University of Pretoria

ecologically sound forest management based on national carbon stocks reported to the United Nations Framework Convention on Climate Change, UNFCCC (Day et al., 2014; Goetz et al., 2015).

At a local level, Mauya et al. (2015) employed airborne light detection and ranging (lidar) data to estimated AGB in the Miombo woodlands of Liwale district, Tanzania. Another study by Kachamba et al. (2016b), utilized unmanned aerial systems (UAS) image-based point clouds to estimate AGB in the Miombo woodlands, Muyobe forest, and Mzimba District in northern Malawi. The AGB data estimates by Mauya et al. (2015) and Kachamba et al. (2016b) have the precision required for sustainable forest management at a local level and international reporting requirements but lack capacity for wall-to-wall coverage. Furthermore, apart from the limited area coverage inherent in the UAS imagery approach employed in (Kachamba et al., 2016b), the imagery requires huge storage space and high processing speeds (Whitehead et al., 2014; Shamaoma et al., 2022) that are too demanding and still challenging for wall-to-wall estimations of AGB over a large area. As a result, the two levels of abstraction must be linked in order to get wall-to-wall AGB estimates with the accuracy necessary for local sustainable forest management and international carbon reporting requirements (Day et al., 2014; Goetz et al., 2015).

With regard to bridging the spatial gap between wall-to-wall satellite imagery and detailed airborne and UAS imagery, some studies have proposed a two-phase sampling design where areas covered by UAS or airborne imagery are sampled via field plots and areas covered by wall-to-wall satellite images are sampled using UAS or airborne imagery, for example, lidar sampling (Korhonen and Morsdorf, 2014; Su et al., 2016; Nelson et al., 2017; Matasci et al., 2018; Wang et al., 2019) and UAS imagery sampling (Puliti et al., 2017; Navarro et al., 2019). These strategies have demonstrated tremendous potential to reduce field plot installation costs and improve wall-to-wall AGB estimate accuracy, which could provide solutions for forest data collection in forest inventory-plagued regions such as the Miombo ecoregion. A study by Wulder et al. (2012) presented a complete review of employing lidar sampling to allow large-area forest characterizations, in which lidar samples were utilized in a way comparable to field samples. However, their review focused on airborne, which are still expensive to acquire in the Miombo region. UAS provide a more flexible and affordable sampling platform for use in conjunction with wall-to-wall satellite imagery, as demonstrated in recent studies (Puliti et al., 2017; Wang et al., 2019, 2020).

© University of Pretoria

In a pioneering study for UAS-based sampling, Puliti et al. (2017) used UAS photogrammetric point clouds as a sampling tool, together with a limited sample of field data and wall-to-wall Sentinel-2 images, to estimate growing stock volume in a 7330 hectare forest area in Norway using a hierarchical model-based inference and reported this approach to be cost-effective for large scale forest resource assessments. However, UAS photogrammetric point clouds have been reported to have challenges in capturing the vertical vegetation structure that are required for estimating AGB in denser forest environments (Mlambo et al., 2017; Shamaoma et al., 2022). In a related study, Wang et al. (2020) used a lidar sensor mounted on a UAS platform (UAS-lidar) partial coverage data as a link between field plot data and wall-to-wall Sentinel-2 imagery to estimate mangrove forests AGB in Hainan Island, China. Apart from lowering field sampling costs, their research observed that their method produced better AGB estimations (R^2 =0.62; rRMSE = 35.41%) than the usual method, which directly correlates field plots to Sentinel-2 data (R^2 = .0.52; rRMSE = 39.88%).

This paper proposes a two-phase sampling technique for low-cost, large-scale AGB estimate for the Miombo ecoregion by capitalizing on publicly-available Sentinel-2 satellite images and inexpensive UAS-lidar data. In order to achieve this, the specific objectives were: (i) identify suitable UAS-lidar metrics and Sentinel-2 metrics for estimating AGB in the Zambian Miombo, (ii) identify the optimal prediction model for mapping AGB (iii) assess if UAS-lidar-estimated AGB can replace field-estimated AGB as reference data. (iv) Compare the findings of direct field plots to Sentinel-2 AGB estimations from utilizing field plots to UAS-Lidar and UAS-lidar to Sentinel-2 in a two-phase sampling strategy.

5.2 Materials and method

5.2.1 Study area

The research was conducted in Miengwe Forest Reserve Number 36, Masaiti District, Copperbelt Province, Zambia (Figure 5.1). The forest reserve is situated approximately 17 kilometers from the Ndola-Lusaka highway and 90 kilometers southwest of the Ndola city center. The 8,094-hectare Miengwe Forest Reserve is located between 13°24′05″S and 28°49′00″E. The region receives an average of 1200 millimeters of rainfall annually and experiences three distinct seasons: hot dry (September-November), rainy (December-March), and cold dry (April-August) (Handavu et al., 2021). The most prevalent soil form is residual lateritic soil, which consists primarily of silty clays and sediments. The area is within the Wet Miombo region and is characterized by the dominance of the families of Papilionacae and Fabaceae. The dominant genera and species are Brachystegia (*Brachystegia spiciformis* and

© University of Pretoria

Brachystegia longifolia), Julbernardia (*Julbernadia globiflora* and *Julbernadia paniculata),* and Isoberlinia (*Isobernilia angolensis*).

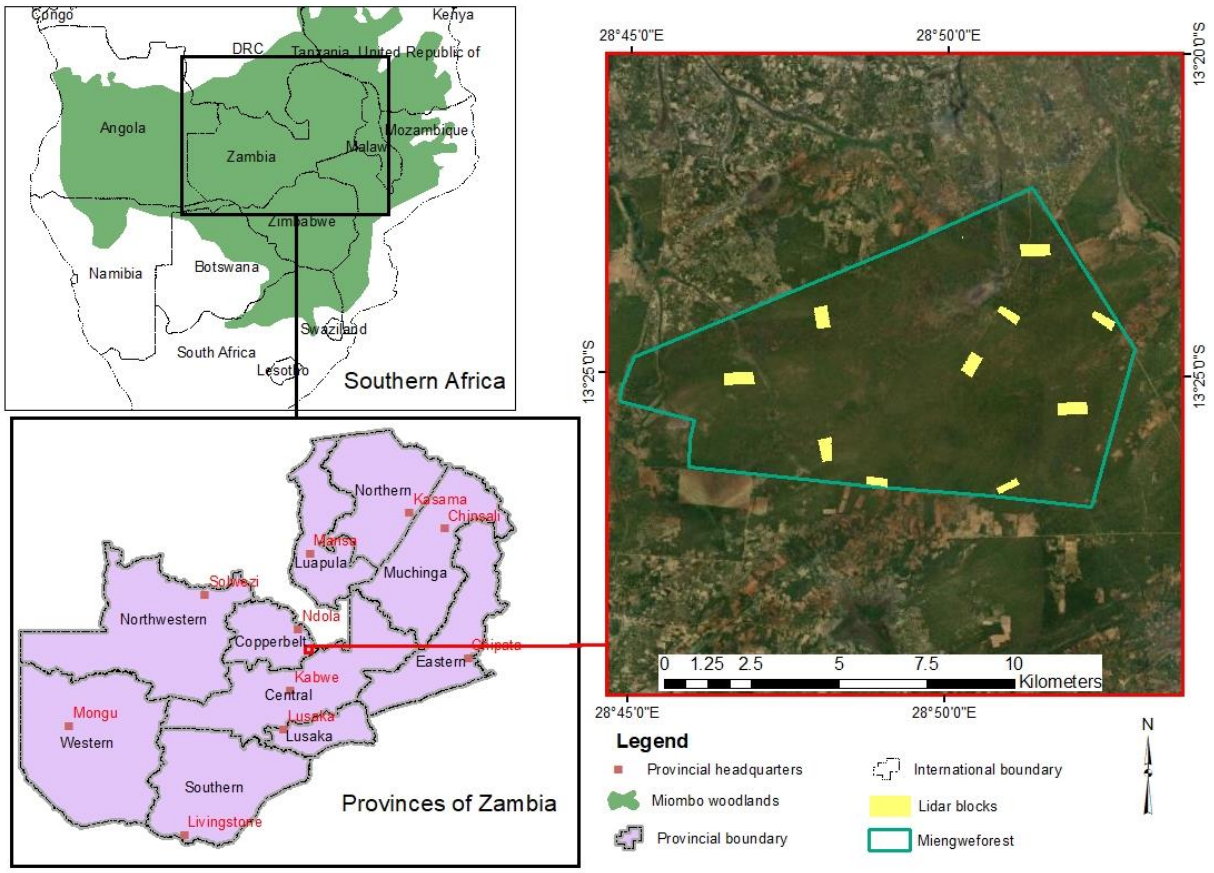

Figure 5.1. Location of study area

5.2.2 Field sample plots.

To ensure that field sample plots, UAS-lidar data, and Sentinel-2 data corresponded in the two-phase sampling approach (Nelson et al., 2009), the Sentinel-2 image covering the study area was resampled to 20 m spatial resolution and used to generate a 20 x 20 m grid framework that served as the foundation for both field and UAS-lidar sampling (Figure 5.2). The study area was divided into ten UAS lidar blocks ranging in size from 30 to 50 hectares, which were selected based on the vegetation coverage, accessibility, and availability of a UAS launch site as determined by visual interpretation of Google Earth images and field assessment. In each of the UAS-lidar blocks, ten to twelve circular sample plots of 10 m radius were established at 250 m spacing at the centre of the 20 x 20 m Sentinel-2 grid framework, at least 50 m distant from the block border. These plots were designed to align with the 20 x 20 m grids that were used for extracting UAS-lidar metrics. The LT700H real time kinematic RTK (Shanghai Huace Navigation Technology Limited, China) Global Navigation Satellite Systems (GNSS) receiver

© University of Pretoria

was used to precisely locate the centers of these plots on the ground to within a few centimeters. The DBH, tree height, and species names of trees with DBH more than 5 cm were recorded in each of the sample plots. Allometric equations proposed by (Handavu et al., 2021) were used to estimate AGB at the plot level.

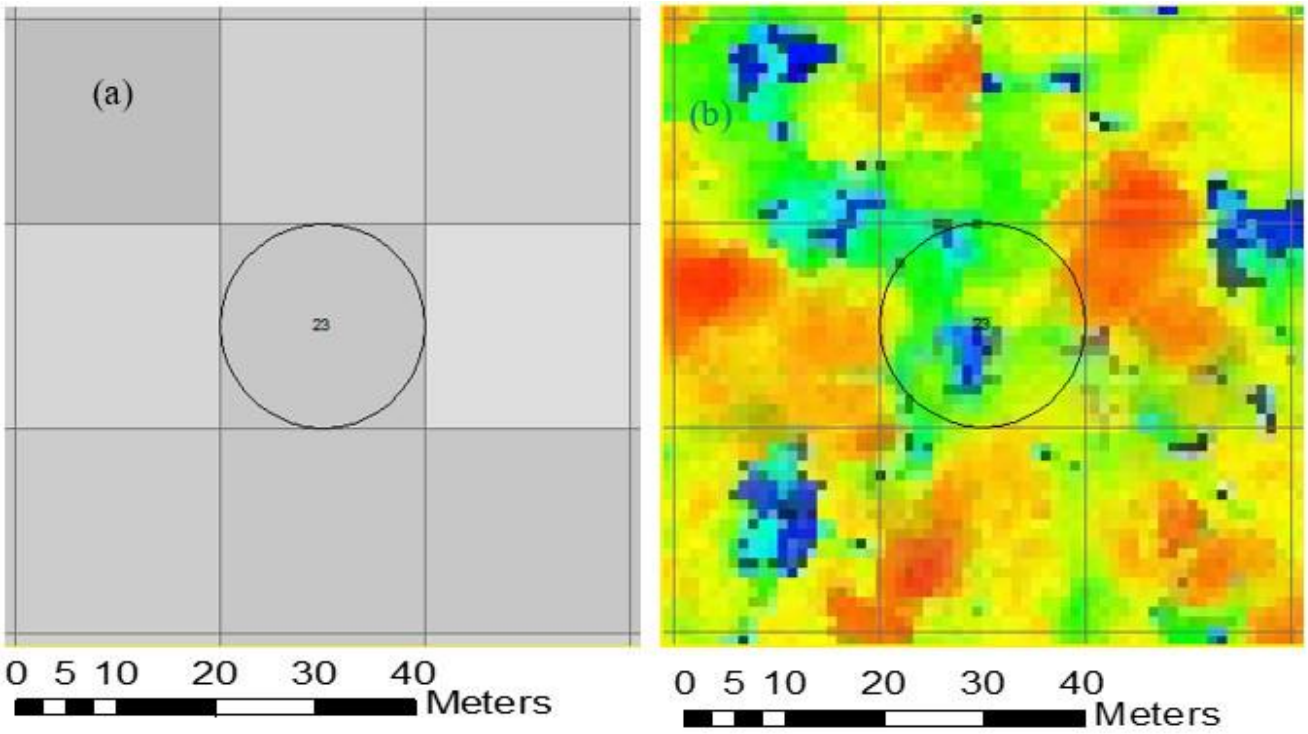

Figure 5.2. Sample plot and grid framework overlaid on: (a) Sentinel-2 image and (b) lidar point cloud

5.2.3 Collecting and pre-processing data from UAS-lidar

Using a T-Drone M1200 quadcopter equipped with a gAirHawk GS-100C UAS-lidar scanning system, we collected the raw UAV-lidar point clouds between November 10th and 12th, 2021. The Livox Avia sensor (Table 4.3) on the GS-100C UAS-lidar operates at 200 HZ and can provide up to 720000 points/sec in triple echo. The mission was planned using the open-source program Mission Planner, which was also used to track the aircraft in real-time and monitor its flight characteristics. UAS-lidar data were collected at an altitude of 80 meters, a speed of 5 meters per second, and a swath width of 42 meters. A GNSS ground base station was used as a reference for subsequent UAS-lidar data post-processing.

The unprocessed UAS-lidar data downloaded from the GS-100C comprised raw lidar points, UAS inertia measurement unit data, UAS GNSS data, and raw photogrammetry imagery (used for colourising the point cloud). The raw UAS-lidar data and raw GNSS data from the ground GNSS base station were first processed in gAirhawk 5.0 version software (Geosun Navigation

© University of Pretoria

Technology Limited, Wuhan, China), where lidar data, IMU data, and GNSS base data were integrated to process the flight trajectory and generate georeferenced UAS-lidar point cloud data in las format. The UAS-lidar point cloud data in las format underwent further processing in Lidar360 version 5.4.3.0 software (GreenValley International, California, CA, USA), which included: (i) denoising the lidar point cloud using an outlier reduction method; (ii) classification of point clouds into either ground or non-ground using an enhanced version of the progressive triangulated irregular network (TIN) densification filter method (Zhao et al., 2016) implemented in lidar 360 software and processing was carried out using the default settings (max cell size of 20 m, max terrain angle of 88°, iteration angle of 8°, and iteration distance of 1.4 m), with the lowest point in the grid serving as the seed; and (iii) normalizing point clouds by subtracting the elevation of each point from the DTM that was generated using the inverse distance weighting (IDW) interpolation technique. The normalized points were used as input for extracting UAS-lidar metrics which were used for the subsequent modelling.

5.2.4 Sentinel-2 data collection and pre-processing

The Sentinel-2 images with less than 5% cloud cover captured in November 2022 were downloaded from the open access European Space Agency (ESA, 2022). The Sentinel Application Platform (SNAP) and ArcGIS Desktop Version 10.7.1 (ESRI, 2019) software were used to pre-process the raw Sentinel-2 imagery. The Sen2Cor atmospheric correlation processor (version 2.5.5) was used to do atmospheric correction to create Level2A bottom-of-atmosphere reflectance data. Three visible bands (Blue (B2), Green (B3), and Red (B4)), three red edge bands (Red Edge 1 (B5), Red Edge 2 (B6), and Red Edge 3 (B7)), two near infrared bands (B8) and Narrow Near Infrared (B8a)), and two shortwave bands (Shortwave 2 (B12) and Shortwave 3 (B13)) were used in the Sentinel-2 image composite. Bands 1, 9, and 10 were removed because they were dedicated to atmospheric correction and had coarse resolution of 60 m. All adopted bands were resampled to 20 m resolution using the nearest neighbor approach in ArcGIS to match our sampling strategy (Wang et al., 2019; Mauya and Madundo, 2022; Muhe and Argaw, 2022). Finally, subsets of all generated sentinel-2 imagery products were clipped to the size of the study area.

5.2.5 Extraction of AGB predictors

The UAS-lidar metrics were extracted in Lidar360 software based on polygons generated from a 20 x 20 m resampled Sentinel-2 grid framework (Figure 2). We generated a total of 37 UAS-lidar metrics at the plot level (Table 5.1). The 20 x 20 m grid framework was generated based on the re-sampled Sentinel-2 using the “create fishnet tool’ in ArcToolbox, implemented in ArcGIS Desktop software, which includes an option for generating points inside each grid. The

© University of Pretoria

points inside each grid served as the basis for extracting Sentinel-2 image metrics for estimating the AGB for the study area.

Table 5.1. UAS-lidar metrics

lidar metrics	Description
Percentile heights (H1, H5, H10, H20, H25, H30, H40, H50, H60, H70, H75, H80, H90, H95, H99)	The percentile of the canopy height distributions (1st, 5th 10th, 20th, 25th, 30th 40th, 50th, 60th, 70th,75th, 80th 90th, 95th and 99th) of first returns
Canopy return density (D1, D2, D3, D4, D5, D6, D7, D8, D9)	The proportion of points above the quantiles (10th,20th, 30th, 40th, 50th and 60th, 70th, 80th and 90th) to total number of points
Variance of height (Hvar)	The variance of the heights of all points
Maximum height (Hmax)	Maximum of return heights above 2 m
Coefficient of variation of heights (Hcv)	Variation of heights of lidar returns above 2 m
Hskew	Skewness of height
Hmd	The median of absolute deviation of heights
Hkurtosis	The kurtosis of the heights of all points
Hstd	Standard deviation of height
Hmean	Mean height above ground of all first returns
Canopy relief ratio (CRR)	mean height returns minus the minimum height divided by the maximum height minus the minimum height
Canopy cover (CC) above 2 m	Percentile of first returns above 2 m
Gap fraction (GF)	An indication how much of the sky is visible from beneath a plant canopy.
Leaf area index (LAI)	Half of the surface area of all leaves per unit ground area

5.2.6 Acquiring Sentinel-2 Metrics

Prior experience (Mauya and Madundo, 2022; Muhe and Argaw, 2022) in estimating AGB using Sentinel-2 imagery influenced the choice of relevant bands as well as the derived vegetation

© University of Pretoria

indices (VI) and biophysical variables (BV) in this work (Table 5.2). In addition, normalized difference fraction index (NDFI), an index that has been widely used to monitor forest disturbances in the tropics (Souza et al., 2005, 2013; Bullock et al., 2018) was calculated. It is based on spectral unmixing, which is the breakdown of the spectral signature of a mixed pixel into proportions of endmembers (pure spectra) (Shi and Wang, 2014). Using this approach, (Souza et al., 2005) employed a linear mixture model to decompose field data on cleared, selectively logged, and undisturbed Amazon forests into proportions of soil, shade, green vegetation (GV), and non-photosynthetic vegetation (NPV). Dense forests revealed high GV and low soil, NPV, and shade percentages. Cleared and thinned forests exhibited greater canopy shade and GV than non-disturbed forests. The NDFI was adopted in this study because it emphasizes the difference between forest and non-forest pixels (Bullock et al., 2018), which is crucial for estimating AGB. The NDFI was calculated using equation 8 and GV_{shade} is the shade-normalised GV fraction given by equation 9 (Souza et al., 2005).

$$NDFI = \frac{GV_{shade} - (NPV + Soil)}{GV_{shade} + (NPV + Soil)} \quad (8)$$

$$GV_{shade} = \frac{GV}{1 + Shade} \quad (9)$$

NDFI is the ratio of the GV, NPV, soil, and shade endmember fractions, with the resulting NDFI values ranging from -1 to 1. In the present study, the calculation of the NDFI was implemented within the System for Earth Observation Data Access, Processing, and Analysis for Land Monitoring (SEPAL) cloud application (SEPAL,). Subsequently, the final suitable metrics for the study were arrived at after undergoing a variable section process.

Table 5.2 Selected multispectral bands, VI, and BF from Sentinel-2 images

Bands	***Description***	***Central wave length (nm)***
B2	*Blue*	*490*
B3	*Green*	*560*
B4	*Red*	*665*
B5	*Vegetation red edge*	*705*
B6	*Vegetation red edge*	*740*
B7	*Vegetation red edge*	*783*

© University of Pretoria

B8	*Near infrared (NIR)*	*842*
B11	*Short wave infrared (SWIR)*	*1.610*
B12	*Shortwave infrared (SWIR)*	*2.190*

Vegetation indices	*Description (reference)*	*Equation*
NDVI	*Normalized Difference Vegetation Index* (Xue and Su, 2017)	$\mathrm{NDVI} = \frac{\mathrm{B8} - \mathrm{B4}}{\mathrm{B8} + \mathrm{B4}}$
EVI	*Enhanced vegetation index* (Xue and Su, 2017)	$\mathrm{EVI} = 2.5 \times \frac{(\mathrm{B8} - \mathrm{B4})}{(\mathrm{B8} + 6 \times \mathrm{B4} - 7.5 \times \mathrm{B2} + 1)}$
SAVI	*Soil adjusted vegetation index* (Xue and Su, 2017)	$\mathrm{SAVI} = \frac{\mathrm{B8} - \mathrm{B4}}{\mathrm{B8} + \mathrm{B4} + \mathrm{L}} \times (1 + \mathrm{L})$
RENDVI_705	*Red-edge normalized difference vegetation index* (Xue and Su, 2017)	$\mathrm{RENDVI} = \frac{\mathrm{B8} - \mathrm{B5}}{\mathrm{B8} + \mathrm{B5}}$
NBRI	*Normalized Burn Ratio Index* (Miller and Thode, 2007)	$\mathrm{NBRI} = \frac{\mathrm{B8} - \mathrm{B12}}{\mathrm{B8} + \mathrm{B12}}$
GNDVI	*Green Normalized Difference Vegetation Index* (Askar et al., 2018)	$\mathrm{GNDVI} = \frac{\mathrm{B8} - \mathrm{B3}}{\mathrm{B8} + \mathrm{B3}}$

Biophysical variables	*Description (reference)*
LAI	*Leaf area index* (Muhe and Argaw, 2022)
FAPAR	*Fraction of absorbed photosynthetically active radiation* (Muhe and Argaw, 2022)
FCOVER	*Fraction of vegetation cover* (Muhe and Argaw, 2022)
CAB	*Chlorophyll content in the leaf* (Muhe and Argaw, 2022)

5.2.7 Predicting AGB

The multi-linear regression (MLR) approach was employed to predict AGB in this study because of its simplicity and ability to handle dependencies on or correlations between the

© University of Pretoria

predictor variables (Fassnacht et al., 2014a; Nelson et al., 2017). A two-phase sampling approach was utilized to estimate the AGB for the Miengwe forest. The first phase involved creating the ground plot to UAS-lidar relationship and estimating AGB in the blocks covered by UAS-lidar. The UAS-lidar blocks were selected based on accessibility and availability of a UAS launch site and did not follow a strict north-south orientation. Since the UAS-lidar blocks did not match the orientation of the Sentinel-2-generated grid framework, the grid cells in the UAS-lidar block's margins, covering less a fraction of the 400-meter square grid, were removed. We estimated the AGB for a total of 4248 grid cells covering all the 10 UAS-lidar blocks in the study area, representing about 2.5% of the total Miengwe forest area. The estimated AGB of the UAS-lidar blocks were used as reference points in the subsequent estimation of AGB in areas covered by Sentinel-2 imagery for the rest of the study area.

In the second phase, a relationship was established between the UAS-lidar predicted AGB (response variable) and wall-to-wall Sentinel-2 image metrics (Table 5.2) as predictor variables to estimate the AGB for the entire study area using MLR technique. Seven hundred random (700) points were generated within the 10 UAS-lidar blocks using the create random points tool implemented in ArcGIS Desktop Version 10.7.1. The 700 random samples of UAS-lidar estimated AGB grid cells served as training data for estimating AGB for the whole study area using Sentinel-2 image metrics.

We also predicted the AGB for the Miengwe forest using the direct relationship between ground plots and Sentinel-2 imagery metrics, which allowed us to assess whether or not the use of UAS-lidar as a bridging sampling tool between the two was beneficial. The UAS-lidar to Sentinel-2 estimated AGB was later compared with the one obtained directly the ground points to Sentinel-2 metrics estimated AGB.

5.2.8 The MLR modeling approach

The MLR modeling procedures included three main stages: (i) variable selection, (ii) model development and fitting, and (iii) model validation.

Variable selection and model development

The first stage of variable selection involved using Pearson's correlation coefficient (r) to evaluate the association between the dependent variable and the independent variables to ensure model parsimony and eliminate overfitting by removing predictor variables with high levels of correlation with each other ($r > 0.85$). The best subsets regression approach built in Minitab Version 21.1.1 (Minitab, 2023) was used to identify the best performing model and

© University of Pretoria

variables from a set of selected variables. As a model selection method, best subsets regression involves trying out every conceivable collection of predictor variables and picking the one that performs the best statistically (Hudak et al., 2006). The best model is chosen based different criteria including: highest adjusted-R^2 and predicted-R^2 as well as the lowest values for Mallows Cp, Akaike's Information Criterion corrected (AICc), and Bayesian information criterion (BIC). In our case the model with lowest AICc was considered to be the best as it has been proved to perform well for smaller samples in prior studies (Sugiura, 1978; Brewer et al., 2016). Finally, the best MLR model was used to predict the AGB.

Accuracy assessment

To compare the predicted values with the observed values (AGB values acquired from lidar), three accuracy assessment indicators employed in (Liu et al., 2018b) were utilized. The developed MLR models were tested using k-fold cross validation to determine their accuracy. The idea behind this method is to randomly divide the data into k groups or folds where each member is nearly the same size. When doing k-fold cross-validation, each fold is treated as its own validation set. We choose k=10 because this number has been widely used and empirically proved to provide non-biased and rather stable estimates of the test error rate. Ten subsets of the original dataset are created and used for 10-fold cross-validation. Each fold uses 9 of the 10 subsets for training and the remaining 1 for testing the accuracy of the learnt model on the validation set. Each subgroup will undergo the validation procedure many times. Finally, we utilized the aforementioned equations to calculate cross-validated RMSE from a table containing all of the folds' predicted values.

5.3 Results

5.3.1 Variables selection

Since the processes for models 1-3 are similar, we only show the variable selection process for model 1. The variable CC emerged as the primary predictor in all ten models identified in the best subsets approach, indicating its significant influence (Table 5.3). Hcv and H80 were also shown to be influential predictors, since they were picked in seven out of the ten models. Overall, height related metrics dominated the list of selected lidar metrics.

The model of four predictor variables was chosen to be the best model because it produced the highest predicted R^2 and lowest AICc (highlighted in Table 5.3), and was less complicated compared to the model of six predictor variables. After implementation of the chosen model, it resulted in model 1, equation 10. This selection procedure was repeated in phase two for

© University of Pretoria

estimating UAS-lidar-derived AGB using Sentinel-2 metrics. Vegetation indices NDFI and NBRI were the most influential predictors selected in 10 and 9, respectively, among the 10 models selected using the best subsets technique, highlighting their strong impact in estimating AGB using sentinel-2 imagery. The model with six predictor variables was selected as the best model since it gave the highest predicted R^2 and the lowest AICc (highlighted in Table 5.4) and resulted in model 2, equation 11. The same procedure was applied to directly estimate AGB using the relationship between field-estimated AGB and Sentinel-2 metrics, resulting in model 3, equation 12.

$$ln\ (\text{AGB}) = 1.68\text{CC} + 0.08\text{H80} + 5.32\text{D20} - 2.97\text{Hcv} + 0.20 \quad (10)$$

$$ln(AGB) = 4.53 + 7.25NDFI + 6.61NBRI + 0.60LAI + 6.89B12 + 0.2B7 - 7.09B6 \quad (11)$$

$$AGB = 2778B11 + 1084GNDVI + 59.1LAI - 1171 \quad (12)$$

© University of Pretoria

Table 5.3. Candidate MLR Models for Field estimated AGB prediction using UAS-lidar metrics

Vars	R^2	adj-R^2	pred-R^2	Cp	AICc	BIC	CC	Haad	Hmd	Hcv	Hstd	H1	H20	H80	D10	D20	D30	D40	D50	D60
1	0.46	0.35	0.26	8.7	978.46	980.79	X													
2	0.69	0.67	0.63	10	969.99	972.60	X			X										
3	0.76	0.74	0.71	4.9	962.31	964.87	X			X			X							
4	0.90	0.88	0.86	3.6	957.54	957.36	X			X			X	X						
5	0.91	0.85	0.62	7.3	958.32	959.56	X	X						X		X			X	
6	0.93	0.87	0.86	9.5	957.99	960.12	X	X		X				X		X			X	
7	0.95	0.77	0.75	13.2	958.35	958.10	X	X	X		X			X			X		X	
8	0.95	0.86	0.76	15.1	957.69	959.55	X	X	X	X	X			X		X			X	
9	0.96	0.85	0.67	11	959.303	959.262	X		X	X	X			X		X				X
10	0.97	0.84	0.54	10	964.606	959.379	X	X	X	X	X		X	X		X	X	X	X	

Table 5.4. Candidate MLR Models for UAS-lidar estimated AGB prediction using Sentinel-2 metrics

Vars	R^2	adj-R^2	pred-R^2	Cp	RMSE	AICc	BIC	NDFI	B02	NBRI	B06	B11	B07	B05	B12	B04	LAI
1	46.3	46.3	45.2	268.2	0.66021	1493.583	1507.379			X							
2	56.1	56.0	54.8	87.0	0.59750	1346.480	1364.864	X		X							
3	58.8	58.7	57.3	38.1	0.57911	1301.127	1324.092	X		X	X						
4	59.7	59.5	58.1	23.2	0.57311	1286.692	1314.234	X		X	X				X		
5	65.3	65.1	62.8	13.8	0.56914	1277.416	1309.529	X		X			X		X		X
6	78.7	70.4	63.9	9.5	0.56615	1273.136	1309.914	X		X	X		X		X		X
7	78.8	70.4	63.9	9.4	0.56671	1273.144	1314.382	X		X	X	X	X		X		X
8	78.9	70.5	63.8	9.4	0.56633	1273.184	1318.977	X	X	X	X		X	X	X		X
9	79.0	70.5	63.7	9.0	0.56579	1272.816	1323.157	X	X	X	X	X	X	X	X		X
10	79.0	70.5	63.3	11.0	0.56617	1274.856	1329.741	X	X	X	X	X	X	X	X	X	X

© University of Pretoria

5.3.2 AGB estimation at phase one

Estimation of AGB by applying the relationship between field estimated AGB and UAS-lidar metrics using model 1 explained 90% of the variance of AGB, RMSE of 17.70 Mg/ha and a bias of 3.79 Mg/ha (Table 5.5) and Figure 5.4a, indicating that the model successfully predicted the AGB.

Table 5.5 Summaries of used models

Model	R^2	adj-R^2	Pred-R^2	RMSE (Mg/ha)	rRMSE%	Bias (Mg/ha)
Ground - UAS-lidar	0.90	0.87	0.81	17.70	14.38	3.79
UAS-lidar – Sentinel-2	0.79	0.70	0.64	27.97	28.89	3.94
Ground - Sentinel-2	0.62	0.55	0.46	38.10	37.54	6.19

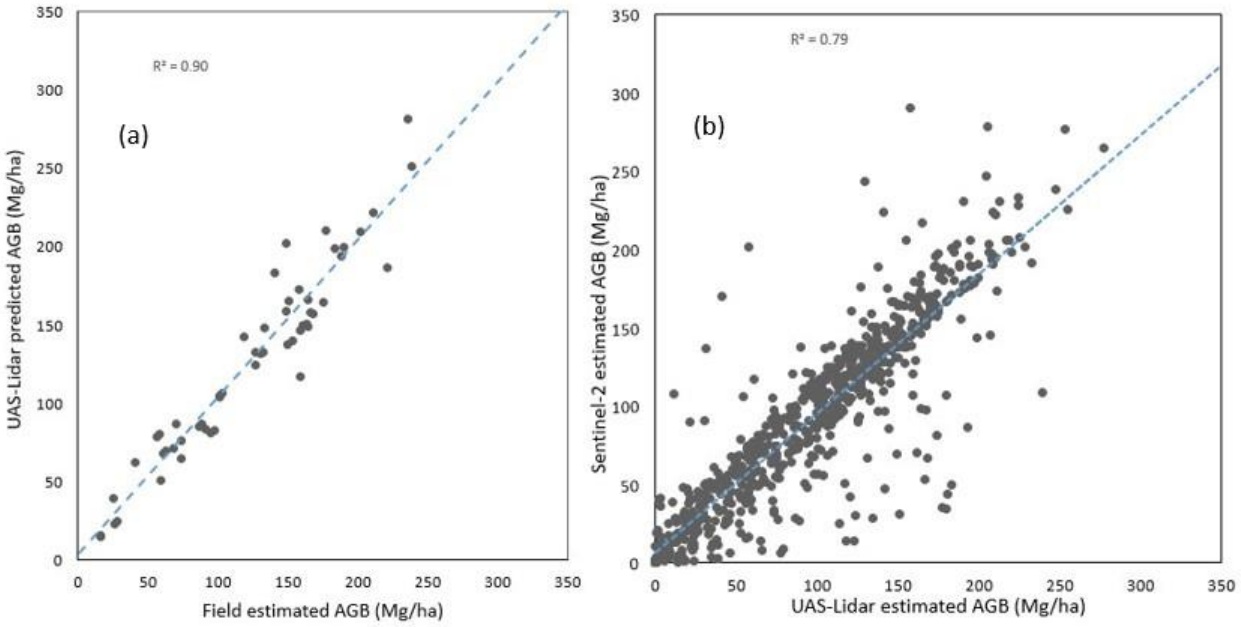

Figure 5.3.. Scatter plots showing estimation of above ground biomass: (a) Ground to UAS-lidar model and (b) UAS-lidar to Sentinel-2 model

5.3.3 AGB estimation at phase two

In phase 2, UAS-lidar prediction of AGB from phase one were used as sample data for predicting AGB using the relationship with Sentinel-2 variables (equation 11, model 2) and was

© University of Pretoria

able to explain 79% of the variance of AGB for the entire Miengwe forest. The RMSE of 27.97 Mg/ha and bias of 3.94 Mg/ha was achieved (Table 4) and Figure 5.4b. With a predicted R^2 = 0.64, this demonstrated potential for applying UAS-lidar sampling when estimating AGB using Sentinel-2 imagery, contrasting it with what was determined using usual direct ground sampling to Sentinel-2 metrics, explaining only 62% of the variance of AGB across the Miengwe forest and a cross-validated predicted R^2 = 0.46 Table 5.5 and Figure 5.5). The UAS-lidar-Sentinel-2 model has a bias of 3.94 Mg/ha, slightly higher than the bias of 3.79 Mg/ha in the Ground-UAS-lidar model, indicating a good match between Sentinel-2 data and UAS-lidar data, supporting usage for UAS-lidar sampling.

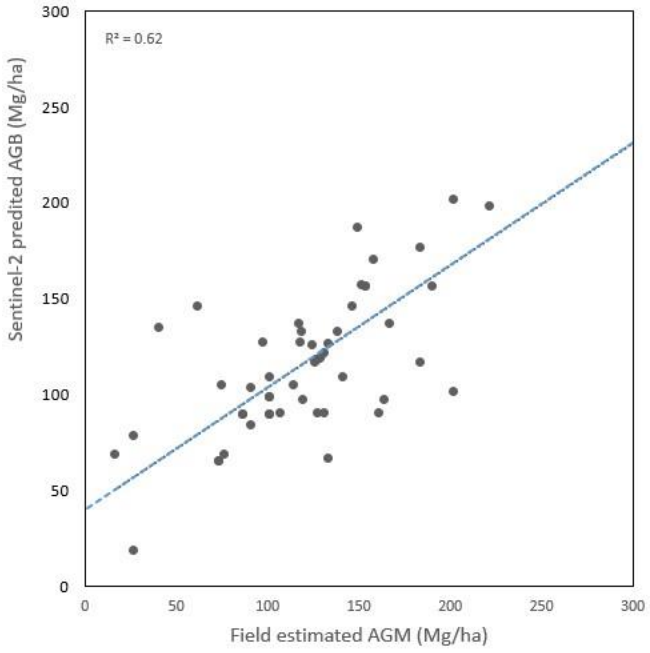

Figure 5.4. Scatter plots showing estimation of above ground biomass using ground to Sentinel-2 model

5.4 Discussion

Accurately estimating AGB across extensive forest areas presents a significant challenge. Currently, AGB estimates for the majority of the vegetation formations of the Miombo woodland remain unknown, and corresponding AGB maps for these areas are unavailable. The present study presents the approach for producing an AGB map (Figure 5.5) for Miombo woodland through utilization of a two-phase UAS-lidar sampling methodology that leverages the combined advantages of field plots, UAS-lidar technology, and Sentinel-2 imagery.

© University of Pretoria

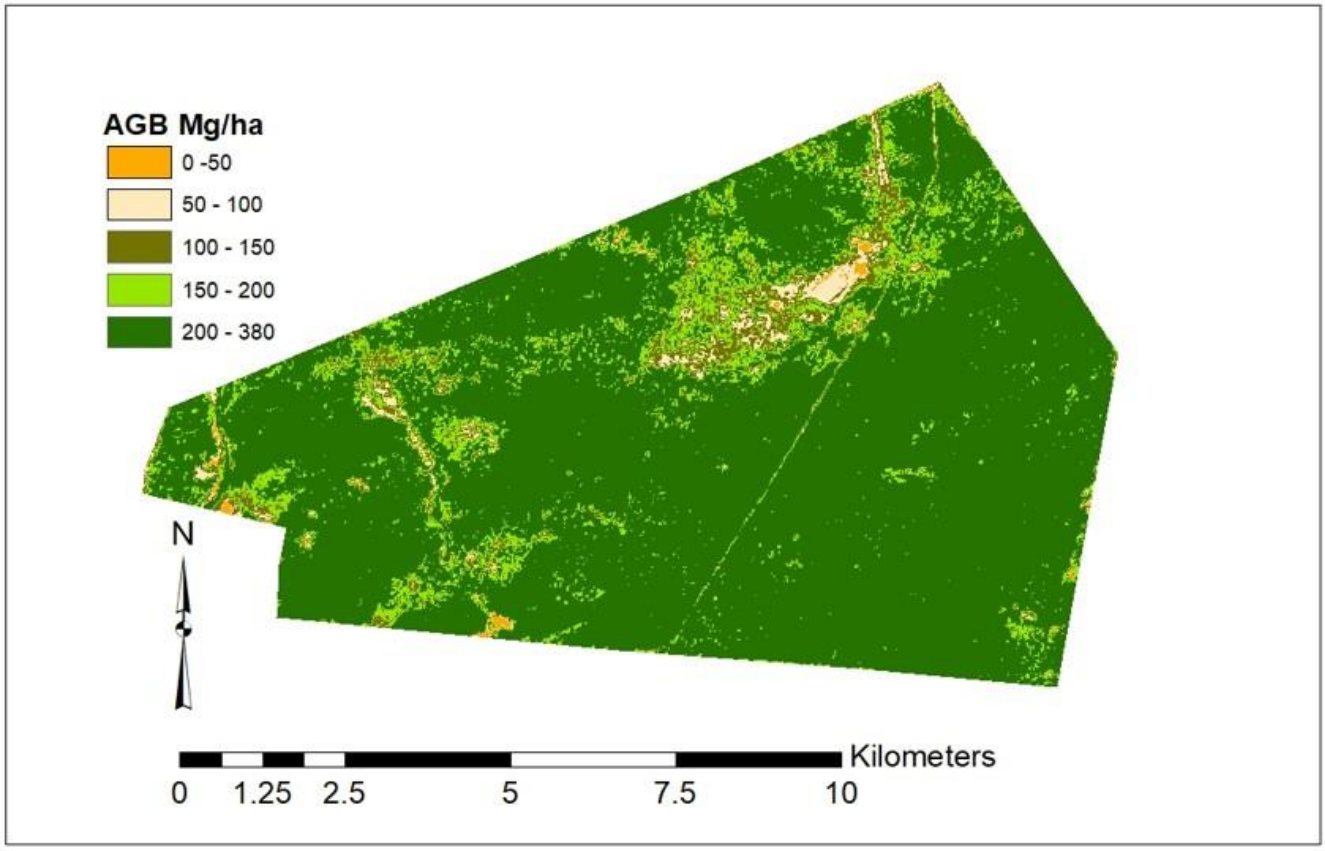

Figure 5.5. Biomass map for Miengwe forest at 20 m resolution

5.4.1 Choosing the optimal model and predictors for estimating the AGB

The process of variable selection was conducted in order to identify the optimal predictors for accurately estimating the AGB across all phases. The first phase involved selecting best predictors for estimating AGB using the relationship between field estimated AGB and UAS-lidar derived metrics. The second phase involved selecting best predictors for estimating AGB using the relationship between UAS-lidar metrics estimated AGB and metrics derived from Sentinel-2 imagery. The third and final phase was to select the best Sentinel-2 metrics for predicting AGB using the relationship between AGB estimated through field observations and Sentinel-2 image metrics.

In phase 1, the most important predicators for AGB were a set of metrics associated with height, density, and canopy cover. CC was the most important predictor selected in all the 10 models for predicting AGB, followed by Hcv and H80, which were selected in 7 of the 10 models (Table 5.3). This accords with UAS-lidar metrics selected in previous studies elsewhere, for example, height percentiles (Liu et al., 2018b; Cao et al., 2019a; Lu et al., 2020), canopy cover (Liu et al., 2018b; Lu et al., 2020), canopy density (Lu et al., 2020) and coefficient of variation for heights

© University of Pretoria

(Li et al., 2008; Bouvier et al., 2015; Liu et al., 2018b) for estimating AGB. Several previous studies (Cao et al., 2014, 2019b; Liu et al., 2018b) have demonstrated the utility of Hmean as a predictor for estimating aboveground biomass (AGB). However, in our study, it was seen that Hmean exhibited a strong correlation with other predictors, and as a result, it was excluded from further consideration. The differences in the selected predictors can be attributed to variation in metric selection algorithms, modelling approach and variation in forest structure and composition (Hopkinson, 2007; Næsset, 2009; Dube et al., 2016).

For phase 2, the best Sentinel-2 image metrics predictors for estimating AGB were vegetation indices (NDFI and NBRI), the red-edge band (B6 and B7), SWIR bands (B11 and B12) and the biophysical variable LAI. The vegetation indices (NDFI and NBRI) and red-edge bands (B7 and B6) were strong predictors for models with fewer predictor variables (models 1-3, Table 5.4) because they are known to be good for separating vegetated from non-vegetated areas (Souza et al., 2005; Miller and Thode, 2007; Bullock et al., 2018; Muhe and Argaw, 2022), which is critical for AGB estimation. The red edge band lies at a specific wavelength that fluctuates swiftly at the convergence of the near-infrared and red spectral bands (Dube et al., 2016). This band is highly responsive to subtle changes in both the structure of the plant canopy and the chlorophyll content. Consequently, it is regarded as having the capacity to mitigate saturation effects and improve estimation of AGB, supporting works by other researchers (e.g. Wallis et al., 2019). Furthermore, this supports an assertion by Adam et al. (2014) that vegetation indices possess the ability to mitigate the effects of shadows and environmental factors on reflectance, thereby enhancing their correlation with AGB. The addition of the SWIR bands and the biophysical variable LAI resulted in improved models (models 5-10, Table 5.4). This finding is consistent with previous studies conducted by Dang et al. (2019) in Yok Don National Park, Vietnam, Mauya and Madundo (2022) in tropical montane forests of Tanzania, and Moradi et al. (2022) in Zagros oak forests in Iran, who reported a high correlation between AGB and red, red-edge, NIR and SWIR bands and vegetation indices that are derived from them.

B11, NDFI, and LAI were the selected predictors (equation 12) for directly calculating AGB using field-estimated AGB and Sentinel-2 measurements. This was consistent with the results of Muhe and Argaw, (2022), who employed Sentinel-2 metrics to estimate AGB in a tropical afro-montane forest in Ethiopia. However, unlike Muhe and Argaw, (2022), Sentinel-2-derived biophysical variables were observed to be significantly correlated with each other, and just LAI was utilized to develop the model as opposed to the three biophysical variables used in Muhe and Argaw, (2022). Sentinel-2 derived products (indices and biophysical factors) were added instead of raw Sentinel-2 bands only since they were shown to enhance AGB estimates in

© University of Pretoria

previous research (Castillo et al., 2017; Muhe and Argaw, 2022). The NDFI was a strong predictor in both models 2 and 3. This is not surprising because this index has been observed to be good at discriminating vegetated from non-vegetated areas (Souza et al., 2005; Bullock et al., 2018). In addition to selecting a suitable regression model, the variable selection strategy approach was crucial to lowering the feature dimension, minimizing information redundancy, and enhancing modeling efficiency (Hudak et al., 2006).

5.4.2 Identify the optimal prediction model for mapping AGB

After choosing the most important predictors for estimating AGB at the two phases, best subsets regression (Hudak et al., 2006) was used to come up with the best models for predicting AGB at all phases (Tables 5.3 and 5.4). Our criteria were based on the model with the highest prediction accuracy (pred-R^2) as well as the lowest AICc, BIC and Mallows Cp, followed by the model with the fewest predictors, in that order. However, the most important consideration in selecting the optimal model was checking to see whether it contains variables that are consistent with ecological reasoning and have been shown to be strong AGB predictors in the literature (White et al., 2013a). The model included height metrics including the lower, middle, and upper percentiles, thereby offering data on the distribution of tree heights, as well as metrics for canopy cover and density, thereby yielding valuable insights into canopy cover. Previous studies have shown the efficacy of using the complement of selected metrics in estimating AGB (Bouvier et al., 2015; Liu et al., 2018b; Cao et al., 2019a). Our approach aligns with prior research that utilized the best subsets regression method, which was determined to be efficacious in identifying the optimal multiple linear regression (MLR) model (Hudak et al., 2006; Cao et al., 2019a).

5.4.3 Model comparison

Model 1 (equation 10), in which we estimated the AGB using the relationship between field AGB estimates and UAS-lidar metrics, yielded the best results overall (Adj-R^2 = 0.84, rRMSE= 14.7%). It outperformed models 2 and 3, which predicted AGB using Sentinel-2 metrics. This is not unexpected given that lidar data measures 3-dimensional vegetation structure (Lim et al., 2003b; Maltamo et al., 2014a) unlike optical images, which is essential for predicting AGB. Model 1 also performed better than (Mauya et al., 2015), who estimated AGB using airborne-lidar in the Miombo woodlands of Tanzania (rRMSE 46.8%). Point cloud densities may have caused the variation in AGB estimate accuracy from (Mauya et al., 2015). The airborne-lidar system utilized in (Mauya et al., 2015) had an average point density of 1.8 pts m^{-2}, whereas the UAS-lidar employed in this study had 300 pts m^{-2}. Since canopy height determination relies on

© University of Pretoria

the DTM, a greater point density will result in a better terrain surface model and more accurate canopy height determination (Kato et al., 2009; Cunliffe et al., 2020; Nandy et al., 2021). Model 2 (equation 11) used the relationship between UAS-lidar estimated AGB from model 1 with Sentinel-2 image metrics to estimate the AGB for the entire study area, achieving (Adj-R^2 = 0.7, rRMSE = 28.9%), which was obviously less precise than model 1, but achieved better results than model 3, which used direct relationship between field estimated AGB and Sentinel-2 metrics to estimate AGB. These findings corroborate works by (Wang et al., 2020), who employed UAS-lidar and Sentinel-2 imagery to estimate AGB in mangrove forests, northeastern Hainan island, China. The better performance of model 2 can be attributed to the large number of UAS-lidar estimated AGB reference points as well as the sampling strategy (Figure 2), which precisely linked the UAS-lidar data and Sentinel-2 data to a common location on the ground.

5.4.4 UAS-lidar as reference data

Previous research has shown that utilizing UAS imagery data to replace field data as reference data in a two-phase sampling approach is feasible (Puliti et al., 2017; Wang et al., 2020). This was demonstrated in this study when UAS-lidar estimated AGB was used as reference data to estimate AGB using Sentinel-2 imagery for the entire study area, achieving (Adj-R2 = 0.70), comparable to a study by Mauya et al., (2015) who used airborne-lidar to estimate AGB in the Miombo woodlands of Tanzania and achieved (Adj-R2 = 0.69). The positive relationship between UAS-lidar estimated AGB and Sentinel-2 image metrics exhibited in this study has benefits with synergistic potential to improve AGB estimation in the Miombo ecoregion. On the one hand, UAS-lidar offers the benefits of flexible deployment, affordability, and the capacity to capture precise vertical structure of vegetation, but it has drawbacks in terms of poor area coverage and massive processing and storage memory requirements (Guo et al., 2017; Shamaoma et al., 2022). On the other hand, we have multi-spectral Sentinel-2 imagery, which is suitable for wall-to-wall coverage at 10 m resolution with NIR, red-edge, and SWIR bands, and a short revisit period of five days that it is useful for AGB estimation but falls short of capturing the fine vertical vegetation structure details that are required for forest management at a local level (Day et al., 2014; Goetz et al., 2015). The findings of this study validate UAS data's capacity to deliver comprehensive training and validation information, which would have otherwise taken a significant amount of time and money utilizing field inventory processes. Furthermore, Sentinel-2-based AGB estimation offers a viable technique for broadening the scope of assessments beyond UAS-surveyed areas, boosting the efficiency of AGB estimation and monitoring operations. Previous research conducted on the estimation of

© University of Pretoria

AGB in the Miombo forests using direct ground to medium resolution Landsat data has shown suboptimal model fit. Kashindye et al. (2013) found R^2 values ranging from 0.47 to 0.65 in their research conducted in Babati district, Tanzania. Their finding falls within a similar range as the study conducted by Halperin et al. (2016b) in Nyimba district, Zambia, where the R^2 ranged from 0.35 to 0.59 and it agrees with what was found utilizing direct ground to Sentinel-2 estimation in this study (R^2 = 0.62). These were all lower than the estimations derived in this work by ground-UAS-Lidar-Sentinel-2 two-phase sampling (R^2 = 0.79). Hence, the integration of the two remote sensing data sources, as exemplified in this research, in conjunction with field techniques, enables the estimation of AGB in the Miombo woodlands with comprehensive accuracy that surpasses the individual capabilities of either data source, as evinced in prior studies (Riihimäki et al., 2019; Wang et al., 2020; Mao et al., 2022).

5.4.5 Benefits of two phase-sampling

Estimation of AGB across vast Miombo woodlands is often restricted by the difficulty in obtaining sufficient field measurements owing to a variety of reasons such as limited labour, limited financial resources, remoteness, and poor access to their location. Most Miombo woodlands AGB estimation studies are undertaken over small regions or at a local scale using either destructive sampling (Mugasha et al., 2013; Kachamba et al., 2016a; Handavu et al., 2021) or remote sensing methods (Mauya et al., 2015; Kachamba et al., 2016b) and a modest number of field samples. The two-phase sampling approach has demonstrated how UAS-lidar could be used to upscale the field sampling to cover extensive areas, even with few field sample plots. From a modest 54 field points in phase 1, we were able to upscale to 700 UAS-lidar sample points in phase 2 to cover extensive areas and easily relate between UAS-lidar estimated AGB and Sentinel-2 metrics to estimate AGB over an expanded area covered by the Sentinel-2 image. The benefits of using the upscaling UAS-Lidar-Sentinel-2 imagery model (adj-R^2 = 0.70) as opposed to the direct field Plots-Sentinel-2 imagery model (adj-R^2 = 0.55) to estimate AGB have been demonstrated. The reason for an improved result from the UAS-lidar sampling technique could be because UAS-lidar covers a larger area with more points representing a wide range of vertical and horizontal vegetation structural changes and accurately measures terrain morphology. Then, using the UAS-lidar estimated AGB as training samples, the model can fit AGB variations over the entire study area and generate high prediction accuracy. This assertion is supported by earlier studies that employed lidar as a sampling tool for biomass estimation (Nelson et al., 2017; Matasci et al., 2018; Wang et al., 2020). Though not investigated in this study, earlier studies have demonstrated that UAS-lidar sampling reduces the required number of field samples and the overall sampling cost (Puliti et al., 2017; Wang et al., 2020).

© University of Pretoria

Previous research, however, has shown that optical Sentinel-2 images may become saturated in densely forested regions. This saturation problem may negatively impact AGB estimations. Nonetheless, Wang et al. (2023) showed that adding Sentinel-1 synthetic aperture radar (SAR) data might assist reduce saturation and improve AGB estimates over wide regions. They did so by using data from UAS-Lidar, Sentinel-1, and Sentinel-2 satellites to estimate AGB for regional coniferous forests in China. Similarly, Novarro et al. (2018) estimated AGB in Senegalese mangrove plantations using UAS-SfM point clouds, Sentinel-1, and Sentinel-2 data. The outcomes of this research and other related studies suggest that this technique can be used for improved AGB estimation for the entire Miombo ecoregion.

Arguably, the best approach could have been using most accurate UAS-lidar to estimate the AGB for estimating the AGB for the whole study area. But UAS-lidar has limitations in terms of area covered per flight, storage space and processing speed (Whitehead et al., 2014; Shamaoma et al., 2022), which makes it cumbersome to cover extensive areas. In the present study, for example, the coverage area achieved during each flight utilizing our UAS was limited to 30-40 hectares. Moreover, the point clouds from flight (one UAS-lidar block) required 30 – 40 Giga Bites (GB) of storage space for processing. These factors provided a substantial challenge for our field laptop, which had just 150 GB of free space, restricting us to processing three blocks at a time and backing them up to an external drive before moving on to the next batch. With all of the aforementioned problems and what the literature has adequately stated (Whitehead et al., 2014; Shamaoma et al., 2022), it can be concluded that the utilization of UAS-lidar technology is currently limited to small sites and can only serve as a sampling tool for larger sites.

5.5 Conclusion

A two-phase sampling approach was used to estimate total AGB in the Miengwe forest reserve in the Miombo woodlands of Zambia. The findings of this study show the potential of using UAS-lidar as a sampling tool for estimating and monitoring AGB and other forest structural attributes across vast regions using wall-to-wall Sentinel-2 imagery when field data are limited. The AGB estimates are of a precision that is suitable for local forest management and international reporting mechanisms such as REDD+ and MRV. The approach used in this study could be up-scaled to provide spatially consistent, low cost and precise AGB estimates over extensive regions for supporting the long-term sustainability of carbon monitoring and reporting initiatives in Miombo woodlands. The continuous improvement and reduction in cost of UAS-lidar technology and the continuous availability of wall-to-wall optical imagery

© University of Pretoria

such as Sentinel-2 assure viability and warrant further investigation and refinement of this approach for future wall-to-wall carbon monitoring and reporting programs in the Miombo ecoregion.

© University of Pretoria

Chapter 6 : Synthesis

© University of Pretoria

6.1 Introduction

The main objective of this study was to explore the use of UAS imagery and associated processing tools in the management of the Miombo woodlands of Zambia. In order to achieve this objective, four different studies were undertaken namely: (i) to review of the application of UAS in forest management and monitoring with a focus on challenges and opportunities for use in the Miombo woodlands; (ii) to explore the use of multi-date and multispectral UAS imagery in classification of dominant tree species in the wet Miombo woodlands of Zambia; (iii) to explore the use of UAS-lidar in estimating the forest structural attributes in the wet Miombo woodlands of Zambia; and (iv) to explore the use of a two phase sampling approach in estimating the forest structural attributes in the Miombo woodlands of Zambia by coupling UAS-lidar and Sentinel-2 imagery.

6.1.1 Why UAS for managing the Miombo woodlands?

In order to establish connections on how UAS technology may be implemented in the Miombo woodlands, we reviewed the key attributes of the Miombo woodlands (structure, composition and phenology) and the existing application of UAS technology in forestry, focusing on sensors employed, data processing methodologies, challenges and limitations (Chapter 2). The primary characteristic of the Miombo woodlands is their deciduous nature (Frost, 1996), characterized by open woodlands as indicated in Table 2.4. This attribute makes the use of low cost UAS-SfM a suitable method for estimating forest structural attributes, especially in the dry Miombo region. In the wet Miombo, where there is denser vegetation coverage, it may be difficult to use UAS-SfM because it may not be able to adequately capture the ground, which is needed to make accurate DTMs (Mlambo et al., 2017). However, an alternative approach involving the use of UAS-lidar can be employed to estimate forest structure attributes and generate precise DTMs. These DTMs can then be utilized repeatedly to monitor FSA within the UAS-SfM framework. The UAS technology provides the scarce detailed forest inventory data that is essential for the implementation of sustainable forest management practices at the local level, as well as for international reporting initiatives such REDD+ and MRV. Additionally, it plays a crucial role in supporting forest conservation efforts, promoting sustainable forest management, and enhancing carbon stocks. The MRV system further incentivizes developing countries to engage in forest conservation and sustainable forest management by providing financial rewards based on the national carbon stocks reported to the United UNFCCC (Day et al., 2014; Goetz et al., 2015).

The utilization of ultra-high-resolution UAS imagery offers the necessary spatial precision for studying leaf and flowering phenology in Miombo tree species, which is another important attribute for the successful application of UAS. Moreover, the use of UAS offers a significant

© University of Pretoria

advantage in terms of data acquisition flexibility. This allows for the precise timing for capturing crucial phenological events, which may prove challenging for other remote sensing platforms like satellites and manned airplanes. These challenges include issues such as cloud cover or the lack of synchronization between data capture and the actual occurrence of the event. Understanding the phenology of Miombo woodlands is important for identifying tree species using UAS imagery and for the timing of UAS data acquisition for the estimation of FSA. For example, the temporal patterns of leaf flushing, leaf maturity, and senescence among different species can be utilized to identify tree species, as demonstrated in Chapter 3. Additionally, the collection of UAS data during the period of late October to early November, when trees have fully flushed leaves but before the emergency of herbaceous layer, allows for the extraction of accurate DTM and well-defined tree crowns.

This, in turn, facilitates the precise estimation of FSA. Previous research (Anderson and Gaston, 2013; Tang and Shao, 2015; Guimarães et al., 2020), as discussed in Chapter 2, has demonstrated that UAS provide a high spatial resolution and flexible temporal resolution. This makes them well-suited for monitoring disturbances that are challenging to detect using readily available satellite images (such as Landsat and Sentinel-2) (Hosonuma et al., 2012; Romijn et al., 2012; Mitchell et al., 2017). Additionally, UAS can effectively capture disturbances occurring at spatial and temporal scales that are impractical and expensive to cover using traditional field methods.

6.1.2 Challenges of using UAS imageries in the Miombo woodlands

Although UAS technology has presented a multitude of opportunities for improving the management of forest resources in the Miombo woodland region, it is imperative to comprehend the associated challenges that might impinge on its successful implementation (Whitehead et al., 2014), which were discussed in Chapter 2. The challenges stem from the limitations of UAS technology, site conditions, as well as local and global operational guidelines and regulations. Weather conditions, like high wind speed, precipitation, and extreme temperatures, can affect UAS operations by hindering data collection during crucial events and potentially causing damage to UAS components (ClimaCell, 2018). The major limitation of UAS imagery compared to freely available medium resolution in forest applications is its limited endurance, which means that only a small area can be covered per site. Furthermore, the low flying height results in a high number of ultra-high-resolution images for a small area, which require huge storage space and high-speed processing computers that are relatively expensive for most forest managers in the Miombo ecoregion (Shamaoma et al., 2022). Although there are anticipated implementation challenges, UAS provides an alternate and supplemental technique for speedily collecting forest data with high spatial and temporal resolution, which is necessary for Miombo woodland monitoring and

© University of Pretoria

management. It is a valuable tool for evaluating forest structure attributes, species identification, fire and forest degradation impacts, and other tasks required for forest management and international carbon MRV requirements. This study's relevance in directing future uses of UAS technology in the Miombo woodlands ecoregion was shown by the successful demonstration of UAS applicability in the Miombo woodlands (Chapters 3-5) following the recommendations from Chapter 2.

6.1.3 Tree species phenology and identification of tree species

Understanding the local species phenology is important for successful identification of tree species using remote UAS imagery in complex natural tropical forest environments as demonstrated in other studies (Key et al., 2001; Lisein et al., 2015; Madonsela et al., 2017). In Chapter 3 we demonstrated that even with low spectral resolution, understanding species phenology can guide the choice of appropriate UAS image acquisition dates to accurately identify dominant tree species in the Miombo woodlands. This research used OBIA (Lang, 2008), because it has been observed to outperform pixel-based approaches for classifying tree species from high-resolution imagery (Franklin, 2017). The OBIA procedure included three stages: image segmentation, feature extraction, and image classification. Each of these stages is important for successful tree species classification (Franklin, 2017; Xu et al., 2020). In this study multi-resolution segmentation algorithm implemented in eCognition Developer version 9.1 was used to delineate tree crown objects (chapter 3). We found that data fusion of multi-spectral orthophoto and CHM, increased the segmentation accuracy by 6% compared to only utilizing the multi-spectral orthophoto alone. These results were consistent with findings of other studies in different vegetation formations (Sankey et al., 2017; Xu et al., 2020). Other factors that have been found to affect image segmentation include image acquisition date and stand structure (Nevalainen et al., 2017). In our study area, the May image (leaf maturity) yielded the best image segmentation results because all Miombo trees have well-defined tree crown shapes at this phenological stage, as opposed to August image (transition to senescence), when Miombo trees drop their leaves and shapes are more difficult to define (chapter 2 and 3). Difficulties were encountered in delineating different tree species in overlapping canopies but this might be mitigated by adopting improvements in image segmentation tools proposed by (Torres et al., 2020; Gu and Congalton, 2022).

The study has demonstrated that several image features (raw spectral values, spectral indices, and textural features) must be examined before reaching the acceptable accuracy in tree species classification (Chapter 3). As compared to utilizing just raw spectral bands, the inclusion of spectral indices improves the separability of different species. Even for a single-date image, combining raw spectral bands and spectral indices has the potential to improve classification

© University of Pretoria

accuracy; for instance, *Brachystegia speciformis* and shadow classes, were difficult to separate using raw spectral information in the May image but become very separable using the spectral indices. These results are consistent with those found in Xu et al. (2020) in China and Ferreira et al. (2016) in Brazil, which demonstrate how spectral indices enhance the accuracy of tree species classification even though the spectral indices they used were different from what were used in this study. Nevertheless, our findings contradict previous research (Gini et al., 2018; Ferreira et al., 2019; Xie et al., 2019; Deur et al., 2020), that found that textural features improve tree species classification. The differences in results could be attributed to the similar appearance of the Miombo woodlands species (Frost, 1996), which translates to a similar texture.

In line with findings from previous studies (Key et al., 2001; Madonsela et al., 2017; Van Deventer et al., 2019), this study demonstrated that the use of multi-date imagery is important for identification of tree species in complex forest environments because it takes advantage of interspecies differences in phonologies, exhibiting different spectral characteristics for tree species on different dates, which compensate for the low spectral resolution. Furthermore, this study revealed that a combination of multi-feature (spectral bands, spectral indices and texture) and multi-date images improves tree species classification for Miombo tree species. The proposed approach adds a novel tool for mapping Miombo forest tree species that are targeted for diverse products at a local scale. For example, because of their high heat output and burning properties, all of the major Miombo species found in this research are preferred for fuelwood production (Syampungani et al., 2011). *Isoberlinia angolensis* is targeted for its timber, while *Brachystegia longifolia* is sought after for its bark rope, making them suitable candidates for conservation and sustainable usage. The precise mapping of dominant tree species is required for effective management of Miombo woodlands as well as for characterizing ecosystem services and climate feedbacks on forests. Moreover, the methodology employed in this research can be effectively applied to detect and control the proliferation of invasive species in the Miombo woodlands, akin to the methodology employed in other studies (Müllerová et al., 2017; Weisberg et al., 2021). Another potential application of the findings from the identification of individual tree species in Chapter 3 is their utilization as inputs for estimating the aboveground biomass (AGB) of individual species, as demonstrated in previous research (Alonzo et al., 2018; Dalponte et al., 2018; Brede et al., 2022). Nevertheless, it is important to exercise caution when utilizing classification results to obtain accurate estimates of AGB for individual trees. This is due to the potential for misclassification errors, which can lead to the assignment of incorrect species-specific equations and subsequently impact the estimation of AGB.

© University of Pretoria

6.1.4 Using UAS-lidar to estimate forest structural attributes in the Miombo woodlands

The achievement of efficient forest management and the successful execution of REDD+ programs necessitate accurate data pertaining to forest biomass and carbon storage, which are presently insufficient in the majority of African vegetation formations. In Chapter 4 we demonstrated the capability of UAS-lidar data in precisely estimating four forest structural attributes (FSA): AGB (rRMSE: 12.67-21.57%), BA (rRMSE:18.36-26.09%), DBH (rRMSE:3.08-8.33%), and Vol (rRMSE:15.42-51.53%) using area-based methods and MLR technique. The findings suggest that the UAS-lidar method proposed in this study offers a valuable addition to the current techniques used for estimating AGB in the Miombo woodlands. Furthermore, the precision of this approach meets the standards necessary for international carbon reporting mechanisms and sustainable forest management at the local level. Our AGB estimations outperformed those obtained by Mauya et al. (2015) using airborne lidar (rRMSE = 46.8%) and Kachamba et al. (2016b) utilizing UAS photographic image point clouds (rRMSE = 46.7) in Tanzania and Malawi, respectively, in similar vegetation formations.

We also investigated the performance of FSA estimation models developed using UAS-lidar data collected from a single site compared to combined data from two sites 95 Km apart within the Miombo woodlands and found that site-specific models outperformed combined data models. This is expected, as vegetation structure and composition are likely to be more homogenous at a local site than over an extended geographical region. However, a combined data model is more generic and suitable for application over the broader geographical region. This fact was confirmed when we assessed the transferability of site-specific models to a different site and found that they performed poorly (rRMSE% = 16.8-72.1) compared to both site-specific (rRMSE% = 4.31–26.09) and combined (rRMSE% = 3.08–51.23) data models but were within the range (rRMSE% = 32.3–67.3) reported by Fekety et al. (2018) in mixed conifer and Douglas-fir forests, Idaho, United States of America. While the transferability approach may have exhibited inferior performance when compared to site-specific and combined site data models, its significance lies in its potential to assist forest managers in Miombo woodlands. Specifically, it can serve as an initial step for integrating UAS-lidar data, obtained for non-forest purposes, into forest inventory procedures in the absence of field forest inventory data.

6.1.5 UAS connects ground- and satellite-based forest inventory approaches

Despite success stories of UAS use in forestry, as demonstrated in Chapters 2-4, it is nevertheless plagued by problems such as restricted area coverage and storage (Whitehead et

© University of Pretoria

al., 2014), which hamper effective application in forestry. Currently, UAS are more suitable for filling the spatial data gap between precise field inventory techniques and satellite-based remote sensing techniques needed for wall-to-wall mapping of the Miombo woodlands. Prior studies have demonstrated the feasibility of employing UAS imagery data as a substitute for field data in a two-phase sampling approach (Puliti et al., 2017; Wang et al., 2020). This phenomenon was exemplified in Chapter 5, wherein UAS-lidar estimated AGB data was employed as the reference to estimate AGB for the entirety of the study area utilizing Sentinel-2 imagery. The achieved results (Adj-R^2 = 0.70) were found to be comparable to a previous study conducted by Mauya et al. (2015), which utilized airborne lidar to estimate AGB (Adj-R^2 = 0.69) in the Miombo woodlands of Tanzania. The correlation between UAS-lidar estimated AGB and Sentinel-2 derived image metrics exhibited in this study has significant implications for enhancing AGB estimation in the Miombo ecoregion, as it offers synergistic advantages. UAS-lidar presents several advantages, including its adaptable deployment, cost-effectiveness, and ability to accurately capture the vertical structure of vegetation. However, it also has limitations in terms of limited area coverage and significant processing and storage memory demands as highlighted in Chapter 2.

In contrast, the utilization of multi-spectral Sentinel-2 imagery presents a viable option for achieving comprehensive coverage at a resolution of 10 meters, incorporating near-infrared (NIR), red-edge, and shortwave infrared (SWIR) bands. This imagery possesses a short revisit interval of five days, rendering it valuable for estimating and monitoring AGB in the Miombo region. However, it does not fully capture the intricate vertical structure of vegetation necessary for localized forest management. Hence, the integration of both remote sensing data sources, as exemplified in Chapter 5 in conjunction with field measurements, enables the estimation of FSA in the Miombo woodlands with comprehensive accuracy that surpasses the individual capabilities of either method. The findings of this study validate the efficacy of using UAS data for generating reliable training and validation data. This approach offers a significant advantage over traditional field inventory methods, which often demand extensive time and resources. In addition, the use of Sentinel-2 data for estimating AGB offers a reliable method to expand the range of assessment beyond regions examined by UAS. This, in turn, enhances the effectiveness of AGB estimate and monitoring initiatives in the Miombo ecoregion. Earlier works by Puliti et al. (2017) in southern Norway and Wang et al. (2019) in mangrove forests on Hainan Island, China, explored the usefulness of the UAS sampling technique to extensive area estimation of FSA and found that it decreases the number of necessary field samples, hence lowering operating costs. However, previous studies have indicated that optical Sentinel-2 imagery may become saturated in denser vegetation environments. This saturation issue can

© University of Pretoria

potentially impact the accuracy of AGB estimates. Nevertheless, Wang et al. (2023) demonstrated that incorporating Sentinel-1 synthetic aperture radar (SAR) data can help alleviate the saturation problem and enhance AGB estimation across large areas. They achieved this by combining UAS-Lidar, Sentinel-1, and Sentinel-2 data to estimate AGB for regional coniferous forests in China. Similarly, Novarro et al. (2018) combined UAS-SfM point clouds, Sentinel-1, and Sentinel-2 imagery to estimate AGB in mangrove plantations in Senegal.

This research demonstrated the effectiveness of estimating AGB in the Miombo forests utilizing UAS-lidar as a link between precise field inventory techniques and wall-to-wall Sentinel-2 data. The findings demonstrate the promising future for upscaling limited coverage UAS image-generated maps to wall-to-wall satellite image-generated maps, presenting a robust tool to aid in the management of the Miombo woodlands in applications such as tree species identification, biodiversity assessments, and habitant mapping (Immitzer et al., 2017; Sprott and Piwowar, 2021), as well as mapping extent of invasive species, controlling and managing them (Rivas-Torres et al., 2018; Kattenborn et al., 2019; Bergamo et al., 2023). The synergistic benefit of utilizing UAS imagery and Sentinel-2 imagery is a powerful, low-cost mapping and monitoring tool for budget-constrained forest management agencies in the Miombo ecoregion.

6.2 Management implications

Results from objectives 1, 2, 3, and 4 show that UAS technology is an effective addition to current methods for managing the Miombo woodland. The precision of FSA estimation demonstrated that using UAS-SfM (Kachamba et al., 2016b) and using USA-lidar in Chapter 4 adds significant value in the context of mapping and monitoring forest biomass. Additionally, it contributes to a deeper comprehension of forest carbon dynamics within the broader framework of the global carbon cycle, as the study results have the potential to make a valuable contribution to the field of carbon trading in Zambia, which has been identified as a measure for preventing deforestation and forest degradation. The precision of carbon estimates is a crucial determinant for sellers and buyers to reach a consensus. The high spatial resolution 3D forest structure data generated from UAS has great potential for detecting small scale degradation resulting from selective harvesting of trees for timber and charcoal production, which are very important for local forest management. Particularly, the study results will be valuable for enhancing local forest management and the effective implementation of REDD+ and MRV mechanisms.

In addition, the method presented in Chapter 3 for classifying tree species has considerable promise for mapping tree species distributions, which are essential for effective management

© University of Pretoria

of Miombo woodlands, as well as for characterizing ecosystem services and climate feedbacks on forests. Species distribution maps, in particular, might be utilized for biodiversity evaluations as well as habitat and species conservation strategies, identifying and prioritizing the conservation of species with multiple uses and assisting in the overall successful management of the Miombo forests. The classification approach used could also be extended to identifying and managing the invasive species that are currently threatening parts of the Miombo woodlands (Witt et al., 2019). Colomina and Molina (2014), Eugenio et al. (2020), and Guimares et al. (2020) have all shown additional UAS applications in other vegetation formations that are amenable to the Miombo woodlands and have the potential to enhance Miombo woodland management. These include forest health monitoring and management, forest fire management and forest degradation monitoring.

6.3 General Conclusions

The primary goal of this study was to investigate the application of UAS technology and associated processing tools in inventory data acquisition for use in the sustainable management of the Miombo woodlands of Zambia. Reviewing the current use of UAS technology in forestry and comparing it to the key characteristics of the Miombo woodlands showed that the technology was well-suited to this ecosystem. UAS has been found to provide a complementary and alternative way to swiftly collect forest inventory data at high spatial and temporal resolution that facilitates monitoring and management of the Miombo woodlands.

The developed methods for dominant Miombo tree species identification, utilizing multi-date, multi-spectral UAS imagery, have proven to be highly valuable in capturing interspecies phenological variations. These variations were exploited to discriminate between different tree species within the Miombo woodlands. The use of multi-date UAS images has yielded classification results for the dominant Miombo species, which has the potential to facilitate the mapping and monitoring of their distribution. Furthermore, these results may provide valuable insights for decision-making processes aimed at enhancing management and conservation efforts.

As a demonstration of the utility of UAS-lidar for estimating FSA, UAS-lidar technology was employed to estimate four FSA (AGB, BA, DBH, and Vol). The findings demonstrate that the UAS-lidar estimates meet the necessary level of accuracy for international carbon reporting obligations and local forest management purposes. Moreover, the utilization of UAS-lidar presents a valuable improvement to the existing methodologies employed for estimating FSA in the Miombo woodlands.

© University of Pretoria

Despite claimed accomplishments in a variety of forest applications, UAS technology remains constrained in terms of geographical coverage and large data storage and processing requirements. As a consequence, existing uses are more appropriate for small sites or as a sampling tool for wall-to-wall satellite imagery. This research effectively established the applicability of UAS-lidar as a sampling tool for estimating AGB using Sentinel-2 imagery, yielding better findings than using direct field sampling and Sentinel-2 data.

6.4 Future research avenues

The ongoing advancements in UAS sensor and data processing technology, together with the decreasing costs of specialized sensors, suggest that there will be an increase in research endeavors centered on the use of UAS technology to fill the gaps that were not explored in this research for managing the Miombo woodlands. The primary objective should be the establishment of optimal methodologies for data gathering, data processing approaches, and model validation. This may be accomplished by conducting rigorous testing of the UAS technology in various forest applications across various Miombo environments.

Some of the pressing issues to be considered for future research include: (i) the use of UAS multispectral and hyperspectral imagery for identifying and managing invasive species in the Miombo woodlands; (ii) employing UAS-lidar and UAS-SfM to estimate FSA using different algorithms in different environments and at different growth stages of the Miombo woodlands; (iii) comparing results from UAS data collected in different seasons for estimating FSA in the Miombo woodlands; and comparing the performance of classification algorithms in identifying dominant tree species at different growth stages in the Miombo woodlands.

References

Adam, E., O. Mutanga, E. M. Abdel-Rahman, and R. Ismail. 2014. Estimating standing biomass in papyrus (Cyperus papyrus L.) swamp: Exploratory of in situ hyperspectral indices and random forest regression. Int. J. Remote Sens. 35:693–714 Available at http://dx.doi.org/10.1080/01431161.2013.870676.

Adão, T., J. Hruška, L. Pádua, J. Bessa, E. Peres, R. Morais, and J. J. Sousa. 2017. Hyperspectral Imaging : A Review on UAV-Based Sensors , Data Processing and Applications for Agriculture and Forestry. Remote Sens. 9:1–30.

Agapiou, A. 2020. Vegetation Extraction Using Visible-Bands from Openly Licensed Unmanned Aerial Vehicle Imagery. Drones 4:1–15.

Agisoft LLC. 2019. Agisoft Metashape User Manual. St. Petersburg, Russia, Russia.

© University of Pretoria

Aguilar, F. J., J. R. Rivas, A. Nemmaoui, A. Peñalver, and M. A. Aguilar. 2019. UAV-Based Digital Terrain Model Generation under Leaf-O ff Conditions to Support Teak Plantations Inventories in Tropical Dry Forests . A Case of the Coastal Region of Ecuador. Sensors 19:1–21.

Ahmed, O. S., A. Shemrock, D. Chabot, C. Dillon, R. Wasson, S. E. Franklin, O. S. Ahmed, A. Shemrock, D. Chabot, C. Dillon, R. Wasson, and S. E. Franklin. 2017. Hierarchical land cover and vegetation classification using multispectral data acquired from an unmanned aerial vehicle. Int. J. Remote Sens. Available at http://dx.doi.org/10.1080/01431161.2017.1294781.

Alonzo, M., H. E. Andersen, D. C. Morton, and B. D. Cook. 2018. Quantifying boreal forest structure and composition using UAV structure from motion. Forests 9.

Anderson, K., and K. J. Gaston. 2013. Lightweight unmanned aerial vehicles will revolutionize spatial ecology. Front. Ecol. Environ.

Askar, N. Nuthammachot, W. Phairuang, P. Wicaksono, and T. Sayektiningsih. 2018. Estimating aboveground biomass on private forest using sentinel-2 imagery. J. Sensors 2018.

Asner, G. P., and R. E. Martin. 2009. Airborne spectranomics: Mapping canopy chemical and taxonomic diversity in tropical forests. Front. Ecol. Environ. 7:269–276.

Aubry, P., and D. Debouzie. 2001. Estimation of the mean from a two-dimensional sample: The geostatistical model-based approach. Ecology 82:1484–1494.

Bannari, A., D. Morin, F. Bonn, and A. R. Huete. 1995. A review of vegetation indices. A Rev. Veg. indices 13:95–120.

Banu, T. P., and G. F. Borlea. 2016. The Use of Drones in Forestry. J. Environ. Sci. Eng. B5:557–562.

Barber, N., E. Alvarado, V. R. Kane, W. E. Mell, and L. M. Moskal. 2021. Estimating Fuel Moisture in Grasslands Using UAV-Mounted Infrared and Visible Light Sensors. Sensors:1–16.

Barquín, L., M. Chacón, S. Panfil, A. Adeleke, E. Florian, and R. Triraganon. 2014. The Knowledge and Skills Needed to Engage in REDD+: A Competencies Framework. Conservation International. Arlington, Virginia, USA.

Benz, U. C., P. Hofmann, G. Willhauck, I. Lingenfelder, and M. Heynen. 2004. Multi-resolution , object-oriented fuzzy analysis of remote sensing data for GIS-ready information. ISPRS J. Photogramm. Remote Sens. 58:239–258.

© University of Pretoria

Bergamo, T. F., R. S. de Lima, T. Kull, R. D. Ward, K. Sepp, and M. Villoslada. 2023. From UAV to PlanetScope: Upscaling fractional cover of an invasive species Rosa rugosa. J. Environ. Manage. 336:117693 Available at https://doi.org/10.1016/j.jenvman.2023.117693.

Blaschke, T. 2010. Object based image analysis for remote sensing. ISPRS J. Photogramm. Remote Sens. 65:2–16 Available at http://dx.doi.org/10.1016/j.isprsjprs.2009.06.004.

Bossoukpe, M., E. Faye, O. Ndiaye, S. Diatta, O. Diatta, A. A. Diouf, M. Dendoncker, M. H. Assouma, and S. Taugourdeau. 2021a. Low-cost drones help measure tree characteristics in the Sahelian savanna. J. Arid Environ. 187:104449 Available at https://doi.org/10.1016/j.jaridenv.2021.104449.

Bossoukpe, M., O. Ndiaye, O. Diatta, S. Diatta, A. Audebert, P. Couteron, L. Leroux, A. A. Diouf, M. Dendoncker, E. Faye, and S. Taugourdeau. 2021b. Unmanned aerial vehicle for the assessment of woody and herbaceous phytomass in Sahelian savanna. Rev. d'Elevage Med. Vet. des Pays Trop. 74:199–205.

Bouvier, M., S. Durrieu, R. A. Fournier, and J. P. Renaud. 2015. Generalizing predictive models of forest inventory attributes using an area-based approach with airborne LiDAR data. Remote Sens. Environ. 156:322–334 Available at http://dx.doi.org/10.1016/j.rse.2014.10.004.

Brede, B., L. Terryn, N. Barbier, H. M. Bartholomeus, R. Bartolo, K. Calders, G. Derroire, S. M. Krishna Moorthy, A. Lau, S. R. Levick, P. Raumonen, H. Verbeeck, D. Wang, T. Whiteside, J. van der Zee, and M. Herold. 2022. Non-destructive estimation of individual tree biomass: Allometric models, terrestrial and UAV laser scanning. Remote Sens. Environ. 280.

Brewer, M. J., A. Butler, and S. L. Cooksley. 2016. The relative performance of AIC, AICC and BIC in the presence of unobserved heterogeneity. Methods Ecol. Evol. 7:679–692.

Brooks, G. P., and P. Ruengvirayudh. 2016. Best-Subset Selection Criteria for Multiple Linear Regression. Gen. Linear Model J. 42:14–25.

Brosofske, K. D., R. E. Froese, M. J. Falkowski, and A. Banskota. 2014. A review of methods for mapping and prediction of inventory attributes for operational forest management. For. Sci. 60:733–756.

Bullock, E. L., C. E. Woodcock, and P. Olofsson. 2018. Remote Sensing of Environment Monitoring tropical forest degradation using spectral unmixing and Landsat time series analysis. Remote Sens. Environ.:0–1 Available at https://doi.org/10.1016/j.rse.2018.11.011.

Cabral, A. I. R., M. J. Vasconcelos, D. Oom, and R. Sardinha. 2010. Spatial dynamics and quanti fi cation of deforestation in the central-plateau woodlands of Angola (1990 - 2009

© University of Pretoria

). Appl. Geogr. 31:1185–1193 Available at http://dx.doi.org/10.1016/j.apgeog.2010.09.003.

Campbell, B. 1996. The Miombo in Transition : Woodlands and Welfare in Africa (B Campbell, Ed.). Center for International Forestry Research, Bogor, Indonesia.

Cao, L., N. C. Coops, T. Hermosilla, J. Innes, J. Dai, and G. She. 2014. Using small-footprint discrete and full-waveform airborne LiDAR metrics to estimate total biomass and biomass components in subtropical forests. Remote Sens. 6:7110–7135.

Cao, J., W. Leng, K. Liu, L. Liu, and Z. He. 2018. Object-Based Mangrove Species Classification Using Unmanned Aerial Vehicle Hyperspectral Images and Digital Surface Models. Remote Sens. 10:1–20.

Cao, L., H. Liu, X. Fu, Z. Zhang, X. Shen, and H. Ruan. 2019a. Comparison of UAV LiDAR and Digital Aerial Photogrammetry Point Clouds for Estimating Forest Structural Attributes in Subtropical Planted Forests. :1–26.

Cao, L., K. Liu, X. Shen, X. Wu, and H. Liu. 2019b. Estimation of Forest Structural Parameters Using UAV-LiDAR Data and a Process-Based Model in Ginkgo Planted Forests. IEEE J. Sel. Top. Appl. Earth Obs. Remote Sens. 12:4175–4190.

Cao, J., K. Liu, L. Zhuo, L. Liu, Y. Zhu, and L. Peng. 2021. Combining UAV-based hyperspectral and LiDAR data for mangrove species classification using the rotation forest algorithm. Int. J. Appl. Earth Obs. Geoinf. 102:102414 Available at https://doi.org/10.1016/j.jag.2021.102414.

Cao, L., Z. Zhang, T. Yun, G. Wang, H. Ruan, and G. She. 2019c. Estimating Tree Volume Distributions in Subtropical Forests Using Airborne LiDAR Data. Remote Sens. 11:97.

Castillo, J. A. A., A. A. Apan, T. N. Maraseni, and S. G. Salmo. 2017. Estimation and mapping of above-ground biomass of mangrove forests and their replacement land uses in the Philippines using Sentinel imagery. ISPRS J. Photogramm. Remote Sens. 134:70–85 Available at https://doi.org/10.1016/j.isprsjprs.2017.10.016.

Cessna, J., M. G. Alonzo, A. C. Foster, and B. D. Cook. 2021. Mapping boreal forest spruce beetle health status at the individual crown scale using fused spectral and structural data. Forests 12.

Chamuya, N., and J. Mgoo. 2014. Tanzania National Forest Resources Monitoring and Assessment . NAFORMA. Brief report. Tanzania Forest Services Agency. :1–14.

Chandrashekar, G., and F. Sahin. 2014. A survey on feature selection methods. Comput. Electr. Eng. 40:16–28 Available at http://dx.doi.org/10.1016/j.compeleceng.2013.11.024.

Chen, Q. 2013. LiDAR remote sensing of vegetation biomass (Q Weng, Ed.). Remote Sens.

© University of Pretoria

Nat. Resour.:399–420.

Chidumayo, E. N. 2013. Forest degradation and recovery in a miombo woodland landscape in Zambia : 22 years of observations on permanent sample plots. For. Ecol. Manage. 291:154–161 Available at http://dx.doi.org/10.1016/j.foreco.2012.11.031.

Chidumayo, E. N., and D. J. Gumbo. 2013. The environmental impacts of charcoal production in tropical ecosystems of the world: A synthesis. Energy Sustain. Dev. 17:86–94 Available at http://dx.doi.org/10.1016/j.esd.2012.07.004.

Chirwa, P. W., M. Larwanou, S. Syampungani, and B. D. Folaranmi. 2015. Management and restoration practices in degraded landscapes of Eastern Africa and requirements for up-scaling. Int. For. Rev. 17:20–30.

Chirwa, P. W., S. Syampungani, and C. J. Geldenhuys. 2016. The ecology and management of the Miombo woodlands for sustainable livelihoods in southern Africa : the case for non-timber forest products. South. For. 70:237–245.

Chisholm, R. A., J. Cui, S. K. Y. Lum, and B. M. Chen. 2013. UAV LiDAR for below-canopy forest surveys. J. Unmmaned Veh. Syst. 68:61–68.

Cho, M. A., P. Debba, R. Mathieu, L. Naidoo, J. Van Aardt, and G. P. Asner. 2010. Improving Discrimination of Savanna Tree Species Through a Multiple-Endmember Spectral Angle Mapper Approach : Canopy-Level Analysis. IEEE Trans. Geosci. Remote Sens. 48:4133–4142.

Cho, A. M., R. Mathieu, G. P. Asner, L. Naidoo, J. Van Aardt, A. Ramoelo, P. Debba, K. Wessels, R. Main, I. P. J. Smit, and B. Erasmus. 2012. Remote Sensing of Environment Mapping tree species composition in South African savannas using an integrated airborne spectral and LiDAR system. Remote Sens. Environ. 125:214–226 Available at http://dx.doi.org/10.1016/j.rse.2012.07.010.

ClimaCell. 2018. Why Drone Can’t Use Regular Weather ForecastsNo Title. Available at https://www.tomorrow.io/blog/why-%0Adrones-cant-use-regular-weather-forecasts (verified 12 August 2022).

Clinton, N., A. Holt, J. Scarborough, L. Yan, and P. Gong. 2010. Accuracy assessment measures for object-based image segmentation goodness. Photogramm. Eng. Remote Sens. 76:289–299.

Colomina, I., and P. Molina. 2014. Unmanned aerial systems for photogrammetry and remote sensing: A review. ISPRS J. Photogramm. Remote Sens. 92:79–97 Available at http://dx.doi.org/10.1016/j.isprsjprs.2014.02.013.

© University of Pretoria

Costa, H., G. M. Foody, and D. S. Boyd. 2017. Supervised methods of image segmentation accuracy assessment in land cover mapping. Remote Sens. Environ. xxx:https://10.1016/j.rse.2017.11.024.

Cromwell, C., J. Giampaolo, J. Hupy, Z. Miller, and A. Chandrasekaran. 2021. A systematic review of best practices for uas data collection in forestry-related applications. Forests 12.

Cunliffe, A. M., J. J Assmann, G. N Daskalova, J. T. Kerby, and I. H. Myers-Smith. 2020. Aboveground biomass corresponds strongly with drone-derived canopy height but weakly with greenness (NDVI) in a shrub tundra landscape. Environ. Res. Lett. 15.

Czapski, P., M. Kacprzak, J. Kotlarz, K. Mrowiec, K. Kubiak, and M. Tkaczyk. 2015. Preliminary analysis of the forest health state based on multispectral images acquired by Unmanned Aerial Vehicle. Folia For. Pol. Ser. A 57:138–144.

Dalponte, M., L. Frizzera, H. O. Ørka, T. Gobakken, E. Næsset, and D. Gianelle. 2018. Predicting stem diameters and aboveground biomass of individual trees using remote sensing data. Ecol. Indic. 85:367–376 Available at http://dx.doi.org/10.1016/j.ecolind.2017.10.066.

Dandois, J. P., and E. C. Ellis. 2010. Remote Sensing of Vegetation Structure Using Computer Vision. :1157–1176.

Dandois, J. P., M. Olano, and E. C. Ellis. 2015. Optimal altitude, overlap, and weather conditions for computer vision uav estimates of forest structure. Remote Sens. 7:13895–13920.

Dash, J. P., H. M. Marshall, and B. Rawley. 2015. Methods for estimating multivariate stand yields and errors using k-NN and aerial laser scanning. Forestry 88:237–247.

Dash, J. P., G. D. Pearse, and M. S. Watt. 2018. UAV Multispectral Imagery Can Complement Satellite Data for Monitoring Forest Health. Remote Sens. 10:1–22.

Dash, J. P., M. S. Watt, G. D. Pearse, M. Heaphy, and H. S. Dungey. 2017. ISPRS Journal of Photogrammetry and Remote Sensing Assessing very high resolution UAV imagery for monitoring forest health during a simulated disease outbreak. ISPRS J. Photogramm. Remote Sens. 131:1–14 Available at http://dx.doi.org/10.1016/j.isprsjprs.2017.07.007.

Day, M., D. Gumbo, K. B. Moombe, A. Wijaya, and T. Sunderland. 2014. Zambia country profile Monitoring , reporting and verification for REDD +. Occas. Pap. 113.

Deur, M., M. Gašparović, and I. Balenović. 2020. Tree species classification in mixed deciduous forests using very high spatial resolution satellite imagery and machine learning methods. Remote Sens. 12:1–18.

© University of Pretoria

Van Deventer, H., M. Azong, and O. Mutanga. 2019. Multi-season RapidEye imagery improves the classification of wetland and dryland communities in a subtropical coastal region. ISPRS J. Photogramm. Remote Sens. 157:171–187 Available at https://doi.org/10.1016/j.isprsjprs.2019.09.007.

DJI. 2019. P4 MULTISPECTRAL User Manual v1.0 2019.12.

Domingo, D., H. O. Ørka, E. Næsset, D. Kachamba, and T. Gobakken. 2019. Effects of UAV Image Resolution , Camera Type , and Image Overlap on Accuracy of Biomass Predictions in a Tropical Woodland. Remote Sens. 11:1–17.

Doughty, C. L., and K. C. Cavanaugh. 2019. Mapping coastal wetland biomass from high resolution unmanned aerial vehicle (UAV) imagery. Remote Sens. 11.

Dube, T., O. Mutanga, S. Cletah, S. Adelabu, and B. Tsitsi. 2016. Remote sensing of aboveground forest biomass: A review. Trop. Ecol. 57:125–132.

Dublin, H. T., A. R. E. Sinclair, and J. McGlade. 1990. Elephants and Fire as Causes of Multiple Stable States in the Serengeti-Mara Woodlands. J. Anim. Ecol. 59:1147.

Duffy, J. P., A. M. Cunliffe, L. Debell, C. Sandbrook, S. A. Wich, J. D. Shutler, I. H. Myers-smith, M. R. Varela, and K. Anderson. 2017. Location , location , location : considerations when using lightweight drones in challenging environments. Remote Sens. Ecol. Conserv. 4:7–19.

Eames, T., J. Russell-Smith, C. Yates, A. Edwards, R. Vernooij, N. Ribeiro, F. Steinbruch, and G. R. van der Werf. 2021. Instantaneous pre-fire biomass and fuel load measurements from multi-spectral UAS mapping in southern African Savannas. Fire 4.

Effiom, A. E., L. M. Van Leeuwen, P. Nyktas, J. A. Okojie, and J. Erdbrügger. 2019. Combining unmanned aerial vehicle and multispectral Pleiades data for tree species identification , a prerequisite for accurate carbon estimation. J. AppliedRemote Sens. 13.

ESA. 2022. European Space Agency. Sentinel online. Available at https://sentinel.esa.int/web/sentinel/user-guides/sentinel-1-sar/acquisition-modes/interferometric-wide-swath (verified 6 December 2022).

ESRI. 2019. ArcGIS Desktop: Release 10.7.1 Redlands, CA: Environmental Systems Research Institute.

Eugenio, F. C., C. T. Schons, C. L. Mallmann, M. S. Schuh, P. Fernandes, and T. L. Badin. 2020. Remotely piloted aircraft systems and forests : a global state of the art and future challenges 1. Can. J. For. Res. 50:705–716.

Fassnacht, F. E., F. Hartig, H. Latifi, C. Berger, J. Hernández, P. Corvalán, and B. Koch. 2014a.

© University of Pretoria

Importance of sample size, data type and prediction method for remote sensing-based estimations of aboveground forest biomass. Remote Sens. Environ. 154:102–114.

Fassnacht, F. E., H. Latifi, K. Stereńczak, A. Modzelewska, M. Lefsky, L. T. Waser, C. Straub, and A. Ghosh. 2016. Review of studies on tree species classification from remotely sensed data. Remote Sens. Environ. 186:64–87.

Fassnacht, F. E., C. Neumann, M. Förster, H. Buddenbaum, A. Ghosh, A. Clasen, P. K. Joshi, and B. Koch. 2014b. Comparison of Feature Reduction Algorithms for Classifying Tree Species With Hyperspectral Data on Three Central European Test Sites. IEEE J. Sel. Top. Appl. EARTH Obs. Remote Sens. 7:2547–2561.

Fawzy, S., A. I. Osman, J. Doran, and D. W. Rooney. 2020. Strategies for mitigation of climate change: a review. Environ. Chem. Lett. 18:2069–2094 Available at https://doi.org/10.1007/s10311-020-01059-w.

Fekety, P. A., M. J. Falkowski, A. T. Hudak, T. B. Jain, and J. S. Evans. 2018. Transferability of Lidar-derived Basal Area and Stem Density Models within a Northern Idaho Ecoregion. Can. J. Remote Sens. 44:131–143 Available at https://doi.org/10.1080/07038992.2018.1461557.

Feng, X., and P. Li. 2019. A Tree Species Mapping Method from UAV Images over Urban Area Using Similarity in Tree-Crown Object Histograms. Remote Sens. 11:1–19.

Feng, Q., J. Liu, and J. Gong. 2015. UAV Remote Sensing for Urban Vegetation Mapping Using Random Forest and Texture Analysis. Remote Sens. 7:1074–1094.

Fernández-Álvarez, M., J. Armesto, and J. Picos. 2019. LiDAR-Based Wildfire Prevention in WUI : The Automatic Detection , Measurement and Evaluation of Forest Fuels. Forests 10.

Ferreira, M. P., F. H. Wagner, L. E. O. C. Aragão, Y. E. Shimabukuro, and C. R. de Souza Filho. 2019. Tree species classification in tropical forests using visible to shortwave infrared WorldView-3 images and texture analysis. ISPRS J. Photogramm. Remote Sens. 149:119–131 Available at https://doi.org/10.1016/j.isprsjprs.2019.01.019.

Ferreira, M. P., M. Zortea, D. C. Zanotta, Y. E. Shimabukuro, and C. R. de Souza Filho. 2016. Mapping tree species in tropical seasonal semi-deciduous forests with hyperspectral and multispectral data. Remote Sens. Environ. 179:66–78 Available at http://dx.doi.org/10.1016/j.rse.2016.03.021.

Franklin, S. E. 2017. Pixel- and object-based multispectral classification of forest tree species from small unmanned aerial vehicles. J. Unmmaned Veh. Syst. 6:195–211.

© University of Pretoria

Franklin, S. E., and O. S. Ahmed. 2017. Deciduous tree species classification using object-based analysis and machine learning with unmanned aerial vehicle multispectral data multispectral data. Int. J. Remote Sens.:1–10 Available at https://doi.org/10.1080/01431161.2017.1363442.

Fraser, R. H., J. Van Der Sluijs, and R. J. Hall. 2017. Calibrating Satellite-Based Indices of Burn Severity from UAV-Derived Metrics of a Burned Boreal Forest. Remote Sens. 9:1–17.

Frost, P. 1996. The Ecology of Miombo Woodlands.Pages 11–57 in The Miombo in Transition: Woodlands and Welfare in Africa. Campbell, B., ed. Center for International Forestry Research (CIFOR), Jakarta, Indonesia.

Fuller, D. O., and T. George. 1999. Canopy phenology of some mopane and miombo woodlands in eastern Zambia. Golobal Ecol. Biogeogr.:199–209.

Fung, T., H. Fung, Y. Ma, and W. L. Siu. 2008. Band Selection Using Hyperspectral Data of Subtropical Tree Species Band Selection Using Hyperspectral Data of Subtropical Tree Species. Geocarto Int. 18:3–11.

Gibbs, H. K., S. Brown, J. O. Niles, and J. A. Foley. 2007. Monitoring and estimating tropical forest carbon stocks: Making REDD a reality. Environ. Res. Lett. 2.

Gini, R., D. Passoni, L. Pinto, and G. Sona. 2014. Use of Unmanned Aerial Systems for multispectral survey and tree classification : a test in a park area of northern Italy multispectral survey and tree classification : Eur. J. Remote Sens. 47:251–269.

Gini, R., G. Sona, G. Ronchetti, D. Passoni, and L. Pinto. 2018. Improving Tree Species Classification Using UAS Multispectral Images and Texture Measures. Int. J. Geo-Information 7:1–18.

Gizachew, B., and L. A. Duguma. 2016. Forest Carbon Monitoring and Reporting for REDD + : What Future for Africa ? Environ. Manage.:0–1 Available at http://dx.doi.org/10.1007/s00267-016-0762-7.

Global Drone Regulations Database. 2014. Available at https://droneregulations.info/index.html (verified 11 December 2020).

Goetz, S. J., M. Hansen, R. A. Houghton, W. Walker, N. Laporte, and J. Busch. Measurement and monitoring needs , capabilities and potential for addressing reduced emissions from deforestation and forest degradation under REDD +. Environ. Res. Lett. 10:123001 Available at http://dx.doi.org/10.1088/1748-9326/10/12/123001.

Goetz, S. J., M. Hansen, R. A. Houghton, W. Walker, N. Laporte, and J. Busch. 2015. Measurement and monitoring needs , capabilities and potential for addressing reduced

© University of Pretoria

emissions from deforestation and forest degradation under Measurement and monitoring needs , capabilities and potential for addressing reduced emissions from deforestatio. Environ. Res. Lett. 10.

GOFC-GOLD. 2016. A SOURCEBOOK OF METHODS AND PROCEDURES FOR MONITORING AND REPORTING ANTHROPOGENIC GREENHOUSE GAS EMISSIONS AND REMOVALS ASSOCIATED WITH DEFORESTATION , GAINS AND LOSSES OF CARBON STOCKS IN FORESTS REMAINING FORESTS , AND FORESTATION.

Gomes, M. F., and P. Maillard. 2016. Detection of Tree Crowns in Very High Spatial Resolution Images. Environ. Appl. Remote Sens.:41–71.

Goodwin, N. R., N. C. Coops, and D. S. Culvenor. 2006. Assessment of forest structure with airborne LiDAR and the effects of platform altitude. Remote Sens. Environ. 103:140–152.

Government of Malawi. 2018. REPUBLIC OF MALAWI NATIONAL FOREST INVENTORY 2018 Analysis Report.

GreenValley International. 2021. LiDAR360 User Guide. Available at https://eur-lex.europa.eu/legal-content/PT/TXT/PDF/?uri=CELEX:32016R0679&from=PT%0Ahttp://eur-lex.europa.eu/LexUriServ/LexUriServ.do?uri=CELEX:52012PC0011:pt:NOT (verified 23 January 2023).

GRZ. 2016. ZAMBIA ' S FOREST REFERENCE EMISSIONS LEVEL SUBMISSION TOTHE UNFCCC.

Gu, J., and R. G. Congalton. 2022. Individual Tree Crown Delineation from UAS Imagery Based on Region Growing by Over-Segments with a Competitive Mechanism. IEEE Trans. Geosci. Remote Sens. 60.

Guerra-hernández, J., D. N. Cosenza, L. Carlos, E. Rodriguez, M. Silva, M. Tomé, R. A. Díaz-varela, D. N. Cosenza, L. Carlos, E. Rodriguez, M. Silva, M. Tomé, R. A. Díaz-varela, and E. González-ferreiro. 2018. Comparison of ALS- and UAV (SfM) -derived high- density point clouds for individual tree detection in Eucalyptus plantations. Int. J. Remote Sens.:DOI: 10.1080/01431161.2018.1486519 To Available at https://doi.org/10.1080/01431161.2018.1486519.

Guimarães, N., L. Pádua, P. Marques, N. Silva, E. Peres, and J. J. Sousa. 2020. Forestry Remote Sensing from Unmanned Aerial Vehicles : A Review Focusing on the Data , Processing and Potentialities. Remote Sens. 12:1–35.

Guo, Q., Y. Su, T. Hu, X. Zhao, F. Wu, Y. Li, J. Liu, L. Chen, G. Xu, G. Lin, Y. Zheng, Y. Lin, X.

© University of Pretoria

Mi, L. Fei, and X. Wang. 2017. An integrated UAV-borne lidar system for 3D habitat mapping in three forest ecosystems across China An integrated UAV-borne lidar system for 3D habitat mapping in three forest ecosystems across China. Available at http://dx.doi.org/10.1080/01431161.2017.1285083.

Guy, P. R. 1981. Changes in the Biomass and Productivity of Woodlands in the Sengwa Wildlife Research Area, Zimbabwe. J. Appl. Ecol. 18:507–519.

Guyon, I., and A. Elisseeff. 2003. An Introduction to Variable and Feature Selection. J. ofMachine Learn. Res. 3:1157–1182.

Hadush, T., A. Girma, and A. Zenebe. 2022. Tree Height Estimation from Unmanned Aerial Vehicle Imagery and Its Sensitivity on Above Ground Biomass Estimation in Dry Afromontane Forest, Northern Ethiopia. Momona Ethiop. J. Sci. 13:256–280.

Halperin, J., V. LeMay, E. Chidumayo, L. Verchot, and P. Marshall. 2016a. Model-based estimation of above-ground biomass in the miombo ecoregion of Zambia. For. Ecosyst. 3 Available at http://dx.doi.org/10.1186/s40663-016-0077-4.

Halperin, J., V. LeMay, N. Coops, L. Verchot, P. Marshall, and K. Lochhead. 2016b. Remote Sensing of Environment Canopy cover estimation in miombo woodlands of Zambia : Comparison of Landsat 8 OLI versus RapidEye imagery using parametric , nonparametric , and semiparametric methods. Remote Sens. Environ. 179:170–182 Available at http://dx.doi.org/10.1016/j.rse.2016.03.028.

Handavu, F., S. Syampungani, G. W. Sileshi, and P. W. C. Chirwa. 2021. Aboveground and belowground tree biomass and carbon stocks in the miombo woodlands of the Copperbelt in Zambia. Carbon Manag. 12:307–321 Available at https://doi.org/10.1080/17583004.2021.1926330.

Hardin, P. J., V. Lulla, and R. R. Jensen. 2018. Small Unmanned Aerial Systems (sUAS) for environmental remote sensing : challenges and opportunities revisited. GIScience Remote Sens.:1–14 Available at https://doi.org/10.1080/15481603.2018.1510088.

He, C., S. Jia, Y. Luo, Z. Hao, and Q. Yin. 2022. Spatial Distribution and Species Association of Dominant Tree Species in Huangguan Plot of Qinling Mountains, China. Forests 13.

Hempson, G. P., S. Archibald, and W. J. Bond. 2015. A continent-wide assessment of the form and intensity of large mammal herbivory in Africa. Science (80-.). 350:1056–1061.

Hentz, K. M. Â., and M. P. Strager. 2018. Cicada (Magicicada) Tree Damage Detection Based on UAV Spectral and 3D Data. Nat. Sci. 10:31–44.

Herold, M., and F. Schiller. 2009. An assessment of national forest monitoring capabilities in

© University of Pretoria

tropical non-Annex I countries : Recommendations for capacity building Prepared by.

Hill, R. A., A. K. Wilson, M. George, and S. A. Hinsley. 2010. Mapping tree species in temperate deciduous woodland using time-series multi-spectral data. Appl. Veg. Sci. 13:86–99.

Hologa, R., K. Scheffczyk, C. Dreiser, and S. Gärtner. 2021. Tree species classification in a temperate mixed mountain forest landscape using random forest and multiple datasets. Remote Sens. 13:1–21.

Hopkinson, C. 2007. The influence of flying altitude, beam divergence, and pulse repetition frequency on laser pulse return intensity and canopy frequency distribution. Can. J. Remote Sens. 33:312–324.

Hosonuma, N., M. Herold, V. De Sy, R. S. De Fries, M. Brockhaus, L. Verchot, A. Angelsen, and E. Romijn. 2012. An assessment of deforestation and forest degradation drivers in developing countries. Environ. Res. Lett. 7:1–12.

Hossain, M. D., and D. Chen. 2019. Segmentation for Object-Based Image Analysis (OBIA): A review of algorithms and challenges from remote sensing perspective. ISPRS J. Photogramm. Remote Sens. 150:115–134 Available at https://doi.org/10.1016/j.isprsjprs.2019.02.009.

Hristov, G., J. Raychev, D. Kinaneva, and P. Zahariev. 2018. Emerging Methods for Early Detection of Forest Fires Using Unmanned Aerial Vehicles and Lorawan Sensor Networks.Pages 1–9 in 2018 28th EAEEIE Annual Conference, EAEEIE 2018. IEEE, Reykjavik, Iceland.

Hsu, C.-W., C.-C. Chang, and C.-J. Lin. 2016. A Practical Guide to Support Vector Classification. Tech. Rep. Available at https://www.csie.ntu.edu.tw/~cjlin/ (verified 19 January 2023).

Huang, H., Z. Li, P. Gong, X. Cheng, N. Clinton, C. Cao, W. Ni, and L. Wang. 2011. Automated methods for measuring DBH and tree heights with a commercial scanning lidar. Photogramm. Eng. Remote Sensing 77:219–227.

Hudak, A. T., N. L. Crookston, J. S. Evans, M. J. Falkowski, A. M. S. Smith, P. E. Gessler, and P. Morgan. 2006. Regression modeling and mapping of coniferous forest basal area and tree density from discrete-return lidar and multispectral satellite data. Can. J. Remote Sens. 32:126–138.

Hudak, A. T., N. L. Crookston, J. S. Evans, D. E. Hall, and M. J. Falkowski. 2008. Nearest neighbor imputation of species-level , plot-scale forest structure attributes from LiDAR data. Remote Sens. Environ. 112:2232–2245.

© University of Pretoria

Hudak, A. T., A. T. Haren, N. L. Crookston, R. J. Liebermann, and J. L. Ohmann. 2014. Imputing Forest Structure Attributes from Stand Inventory and Remotely Sensed Data in Western Oregon, USA. Fores Sci. 60:253–269.

Iglhaut, J., C. Cabo, S. Puliti, L. Piermattei, J. O'Connor, and J. Rosette. 2019. Structure from Motion Photogrammetry in Forestry : a Review. Curr. For. Reports.

Immitzer, M., C. Atzberger, and T. Koukal. 2012. Tree Species Classification with Random Forest Using Very High Spatial Resolution 8-Band WorldView-2 Satellite Data. Remote Sens. 4:2661–2693.

Immitzer, M., S. Böck, K. Einzmann, F. Vuolo, N. Pinnel, A. Wallner, and C. Atzberger. 2017. Remote Sensing of Environment Fractional cover mapping of spruce and pine at 1 ha resolution combining very high and medium spatial resolution satellite imagery. Remote Sens. Environ.:0–1 Available at http://dx.doi.org/10.1016/j.rse.2017.09.031.

Jakubowski, M. K., W. Li, Q. Guo, and M. Kelly. 2013. Delineating individual trees from lidar data: A comparison of vector- and raster-based segmentation approaches. Remote Sens. 5:4163–4186.

Jia, Y., Z. Su, Q. Zhang, Y. Zhang, Y. Gu, and Z. Chen. 2015. Research on UAV Remote Sensing Image Mosaic Method Based on SIFT. Int. J. Signal Process. Image Process. Pattern Recognit. 8:365–374.

Jiang, Q., S. Fang, Y. Peng, Y. Gong, R. Zhu, and X. Wu. 2019. UAV-Based Biomass Estimation for Rice-Combining Spectral , TIN-Based Structural and Meteorological Features.

Kachamba, D. J., T. Eid, and T. Gobakken. 2016a. Above- and Belowground Biomass Models for Trees in the Miombo Woodlands of Malawi. Forests.

Kachamba, D. J., T. Eid, and T. Gobakken. 2017. Influence of Plot Size on Efficiency of Biomass Estimates in Inventories of Dry Tropical Forests Assisted by Photogrammetric Data from an Unmanned Aircraft System. Remote Sens. 9:1–15.

Kachamba, D. J., H. O. Ørka, T. Gobakken, T. Eid, and W. Mwase. 2016b. Biomass estimation using 3D data from unmanned aerial vehicle imagery in a tropical woodland. Remote Sens. 8.

Kapinga, K., S. Syampungani, R. Kasubika, A. M. Yambayamba, and H. Shamaoma. 2018. Forest Ecology and Management Species-speci fi c allometric models for estimation of the above-ground carbon stock in miombo woodlands of Copperbelt Province of Zambia. For. Ecol. Manage. 417:184–196 Available at https://doi.org/10.1016/j.foreco.2018.02.044.

Kashindye, A., E. Mtalo, M. M. Mpanda, E. Liwa, and R. Giliba. 2013. Multi-temporal

© University of Pretoria

assessment of forest cover, stocking parameters and above-ground tree biomass dynamics in Miombo Woodlands of Tanzania. African J. Environ. Sci. Technol. 7:611–623.

Kato, A., L. M. Moskal, P. Schiess, M. E. Swanson, D. Calhoun, and W. Stuetzle. 2009. Capturing tree crown formation through implicit surface reconstruction using airborne lidar data. Remote Sens. Environ. 113:1148–1162 Available at http://dx.doi.org/10.1016/j.rse.2009.02.010.

Kattenborn, T., J. Lopatin, M. Förster, A. C. Braun, and F. E. Fassnacht. 2019. UAV data as alternative to field sampling to map woody invasive species based on combined Sentinel-1 and Sentinel-2 data. Remote Sens. Environ. 227:61–73 Available at https://doi.org/10.1016/j.rse.2019.03.025.

Kelcey, J., and A. Lucieer. 2013. IEEE International Geoscience and Remote Sensing Symposium (IGARSS).Pages 3884–3886 in AN ADAPTIVE TEXTURE SELECTION FRAMEWORK FOR ULTRA-HIGH RESOLUTION UAV IMAGERY. Melbourne, Australia 21–26 July 2013.

Kerr, J. T., and M. Ostrovsky. 2003. From space to species: Ecological applications for remote sensing. Trends Ecol. Evol. 18:299–305.

Key, T., T. A. Warner, J. B. Mcgraw, and M. A. Fajvan. 2001. A Comparison of Multispectral and Multitemporal Information in High Spatial Resolution Imagery for Classification of Individual Tree Species in a Temperate Hardwood Forest. Remote Sens. Environ. 75:100–112.

Kolarik, N. E., A. E. Gaughan, F. R. Stevens, N. G. Pricope, K. Woodward, L. Cassidy, J. Salerno, and J. Hartter. 2020. A multi-plot assessment of vegetation structure using a micro-unmanned aerial system (UAS) in a semi-arid savanna environment. ISPRS J. Photogramm. Remote Sens. 164:84–96 Available at https://doi.org/10.1016/j.isprsjprs.2020.04.011.

Kollert, A., M. Bremer, M. Löw, and M. Rutzinger. 2021. Exploring the potential of land surface phenology and seasonal cloud free composites of one year of Sentinel-2 imagery for tree species mapping in a mountainous region. Int. J. Appl. Earth Obs. Geoinf. 94:102208 Available at https://doi.org/10.1016/j.jag.2020.102208.

Korhonen, L., and F. Morsdorf. 2014. Estimation of Canopy Cover, Gap Fraction and Leaf Area Index with Airborne Laser.Pages 397–417 in Forest Applications of Airborne Laser Scanning: Concepts and Case Studies. Maltamo, M., Naesset, E., Vauhkonen, J., eds. Springer, Dordrecht.

Kraus, K., and N. Pfeifer. 1998. Determination of terrain models in wooded areas with airborne laser scanner data. ISPRS J. Photogramm. Remote Sens. 53:193–203.

© University of Pretoria

Kuželka, K., M. Slavík, and P. Surový. 2020. Very High Density Point Clouds from UAV Laser Scanning for Automatic Tree Stem Detection and Direct Diameter Measurement. Remote Sens. 12:doi:10.3390/rs12081236 Available at 10.3390/rs12081236.

Lang, S. 2008. Object-based image analysis for remote sensing applications : modeling reality – dealing with complexity.Pages 3–27 in Lecture Notes in Geoinformation and Cartography. Blaschke, T., Lang, S., J., H.G., eds. Springer.

Law, B. E., and R. H. Waring. 2015. Carbon implications of current and future effects of drought, fire and management on Pacific Northwest forests. For. Ecol. Manage. 355:4–14 Available at http://dx.doi.org/10.1016/j.foreco.2014.11.023.

Lefsky, M. A., W. B. Cohen, D. J. Harding, G. G. Parker, S. A. Acker, and S. T. Gower. 2002. Lidar remote sensing of above-ground biomass in three biomes. Glob. Ecol. Biogeogr. 11:393–399.

Lefsky, M. A., A. T. Hudak, W. B. Cohen, and S. A. Acker. 2005. Patterns of covariance between forest stand and canopy structure in the Pacific Northwest. Remote Sens. Environ. 95:517–531.

Levick, S. R., G. P. Asner, T. Kennedy-Bowdoin, and D. E. Knapp. 2009. The relative influence of fire and herbivory on savanna three-dimensional vegetation structure. Biol. Conserv. 142:1693–1700 Available at http://dx.doi.org/10.1016/j.biocon.2009.03.004.

Li, Y., H.-E. Andersen, and R. McGaughey. 2008. A Comparison of Statistical Methods for Estimating Data. West. J. Appl. For. For. 23:223–231.

Lillesand, T. M., R. W. Kiefer, and J. W. Chipma. 2015. Remote Sensing and Image Interpretation. 7th Editio. Wiley.

Lim, J., K. M. Kim, and R. Jin. 2019. Tree species classification using hyperion and sentinel-2 data with machine learning in South Korea and China. ISPRS Int. J. Geo-Information 8.

Lim, K., P. Treitz, K. Baldwin, I. Morrison, and J. Green. 2003a. Lidar remote sensing of biophysical properties of tolerant northern hardwood forests. Can. J. Remote Sens. 29:658–678.

Lim, K., P. Treitz, M. Wulder, and M. Flood. 2003b. LiDAR remote sensing of forest structure. Prog. Phys. Geogr. 27:88–106.

Lin, Y., J. Hyyppä, and A. Jaakkola. 2011. Mini-UAV-borne LIDAR for fine-scale mapping. IEEE Geosci. Remote Sens. Lett. 8:426–430.

Lisein, J., A. Michez, H. Claessens, and P. Lejeune. 2015. Discrimination of Deciduous Tree Species from Time Series of Unmanned Aerial System Imagery. PLoS One 10:1–20.

© University of Pretoria

Lisein, J., M. Pierrot-deseilligny, P. Lejeune, and N. Management. 2013. A Photogrammetric Workflow for the Creation of a Forest Canopy Height Model from Small Unmanned Aerial System Imagery. :922–944.

Liu, T., A. Abd-Elrahman, J. Morton, and V. L. Wilhelm. 2018a. Comparing fully convolutional networks, random forest, support vector machine, and patch-based deep convolutional neural networks for object-based wetland mapping using images from small unmanned aircraft system. GIScience Remote Sens. 55:243–264 Available at https://doi.org/10.1080/15481603.2018.1426091.

Liu, K., X. Shen, L. Cao, G. Wang, and F. Cao. 2018b. Estimating forest structural attributes using UAV-LiDAR data in Ginkgo plantations. ISPRS J. Photogramm. Remote Sens. 146:465–482 Available at https://doi.org/10.1016/j.isprsjprs.2018.11.001.

Lu, J., H. Wang, S. Qin, L. Cao, R. Pu, G. Li, and J. Sun. 2020. Estimation of aboveground biomass of Robinia pseudoacacia forest in the Yellow River Delta based on UAV and Backpack LiDAR point clouds. Int. J. Appl. Earth Obs. Geoinf. 86.

Luoga, E. J., E. T. F. Witkowski, and K. Balkwill. 2002. Harvested and standing wood stocks in protected and communal miombo woodlands of eastern Tanzania. For. Ecol. Manage. 164:15–30.

Macave, O. A., N. S. Ribeiro, A. I. Ribeiro, A. Chaúque, R. Bandeira, C. Branquinho, and R. Washington-Allen. 2022. Modelling Aboveground Biomass of Miombo Woodlands in Niassa Special Reserve, Northern Mozambique. Forests 13:1–16.

Madonsela, S., M. Azong, R. Mathieu, O. Mutanga, A. Ramoelo, R. Van De Kerchove, and E. Wolff. 2017. International Journal of Applied Earth Observation and Geoinformation Multi-phenology WorldView-2 imagery improves remote sensing of savannah tree species. Int. J. Appl. Earth Obs. Geoinf. 58:65–73.

Madonsela, S., M. Azong, A. Ramoelo, and O. Mutanga. 2018. Estimating tree species diversity in the savannah using NDVI and woody canopy cover. Int J Appl Earth Obs Geoinf. 66:106–115 Available at https://doi.org/10.1016/j.jag.2017.11.005.

Magnussen, S., and P. Boudewyn. 1998. Derivations of stand heights from airborne laser scanner data with canopy-based quantile estimators. Can. J. For. Res. 28:1016–1031.

Maltamo, M., E. Naesset, and J. Vauhkonen. 2014a. Forestry Applications of Airborne Laser Scanning (M Maltamo, E Næsset, and J Vauhkonen, Eds.). Springer Netherlands, Dordrecht.

Maltamo, M., E. Naesset, and J. Vauhkonen. 2014b. Forestry Applications of Airborne Laser Scanning: Concepts and Case Studies (K von Gadow, T Pukkala, and Margarida Tomé,

© University of Pretoria

Eds.). Springer, Newyork.

Mao, P., J. Ding, B. Jiang, L. Qin, and G. Y. Qiu. 2022. How can UAV bridge the gap between ground and satellite observations for quantifying the biomass of desert shrub community? ISPRS J. Photogramm. Remote Sens. 192:361–376 Available at https://doi.org/10.1016/j.isprsjprs.2022.08.021.

Mareya, H. T., P. Tagwireyi, H. Ndaimani, T. W. Gara, and D. Gwenzi. 2018. Estimating Tree Crown Area and Aboveground Biomass in Miombo Woodlands from High-Resolution RGB-Only Imagery. IEEE J. Sel. Top. Appl. Earth Obs. Remote Sens. 11:868–875.

Matasci, G., T. Hermosilla, M. A. Wulder, J. C. White, N. C. Coops, G. W. Hobart, and H. S. J. Zald. 2018. Large-area mapping of Canadian boreal forest cover, height, biomass and other structural attributes using Landsat composites and lidar plots. Remote Sens. Environ. 209:90–106 Available at https://doi.org/10.1016/j.rse.2017.12.020.

Mauya, E. W., L. T. Ene, O. M. Bollandsås, T. Gobakken, E. Næsset, R. E. Malimbwi, and E. Zahabu. 2015. Modelling aboveground forest biomass using airborne laser scanner data in the miombo woodlands of Tanzania. Carbon Balance Manag. 10:1–16.

Mauya, E. W., and S. Madundo. 2022. Modelling Above Ground Biomass Using Sentinel 2 and Planet Scope Data in Dense Tropical Montane Forests of Tanzania. Tanzania J. For. Nat. Conserv. 91:132–153.

Mayes, M. T., J. F. Mustard, and J. M. Melillo. 2015. Remote Sensing of Environment Forest cover change in Miombo Woodlands : modeling land cover of African dry tropical forests with linear spectral mixture analysis. Remote Sens. Environ. 165:203–215 Available at http://dx.doi.org/10.1016/j.rse.2015.05.006.

Mayr, M. J., S. Malß, E. Ofner, and C. Samimi. 2018. Disturbance feedbacks on the height of woody vegetation in a savannah: a multi-plot assessment using an unmanned aerial vehicle (UAV). Int. J. Remote Sens. 39:4761–4785 Available at https://doi.org/10.1080/01431161.2017.1362132.

Mäyrä, J., S. Keski-Saari, S. Kivinen, T. Tanhuanpää, P. Hurskainen, P. Kullberg, L. Poikolainen, A. Viinikka, S. Tuominen, T. Kumpula, and P. Vihervaara. 2021. Tree species classification from airborne hyperspectral and LiDAR data using 3D convolutional neural networks. Remote Sens. Environ. 256.

Mckenna, P., P. D. Erskine, A. M. Lechner, and S. Phinn. 2017. Measuring fire severity using UAV imagery in semi- arid central Queensland , Australia. Int. J. Remote Sens. 38:4244–4264 Available at https://doi.org/10.1080/01431161.2017.1317942.

Means, J. E., S. A. Acker, B. J. Fitt, M. Renslow, L. Emerson, and C. J. Hendrix. 2000.

© University of Pretoria

Predicting Forest Stand Characteristics with Airborne Scanning Lidar. Photogramm. Eng. Remote Sens. 66:1367–1371.

Merino, L., F. Caballero, J. R. Martínez-De-Dios, I. Maza, and A. Ollero. 2012. An unmanned aircraft system for automatic forest fire monitoring and measurement. J. Intell. Robot. Syst. Theory Appl. 65:533–548.

Miller, J. D., and A. E. Thode. 2007. Quantifying burn severity in a heterogeneous landscape with a relative version of the delta Normalized Burn Ratio (dNBR). Remote Sens. Environ. 109:66–80.

Minarik, R., and J. Langhammer. 2016. USE OF A MULTISPECTRAL UAV PHOTOGRAMMETRY FOR DETECTION AND TRACKING OF FOREST DISTURBANCE DYNAMICS.in The International Archives of the Photogrammetry , Remote Sensing and Spatial Information Sciences, Voluma XLI-B8, 2016 XXIII ISPRS Congress, 12-19 July 2016. Prague, Czech Republic.

Mishra, N. B., K. P. Mainali, B. B. Shrestha, J. Radenz, and D. Karki. 2018. Species-level Vegetation Mapping in a Himalayan Treeline Ecotone using Species-Level Vegetation Mapping in a Himalayan Treeline Ecotone Using Unmanned Aerial System (UAS) Imagery. 7:1–16.

Mitchell, A. L., A. Rosenqvist, and B. Mora. 2017. Current remote sensing approaches to monitoring forest degradation in support of countries measurement , reporting and verification (MRV) systems for REDD +. Carbon Balance Manag. 12:1–22.

Mlambo, R., I. H. Woodhouse, F. Gerard, and K. Anderson. 2017. Structure from Motion (SfM) Photogrammetry with Drone Data : A Low Cost Structure from Motion (SfM) Photogrammetry with Drone Data : A Low Cost Method for Monitoring Greenhouse Gas Emissions from Forests in Developing Countries. Forests 8.

Mohan, M., C. A. Silva, C. Klauberg, P. Jat, G. Catts, A. T. Hudak, and M. Dia. 2017. Individual Tree Detection from Unmanned Aerial Vehicle (UAV) Derived Canopy Height Model in an Open Canopy Mixed Conifer Forest. Forestry 8:340.

Morin, D., M. Planells, D. Guyon, L. Villard, S. Mermoz, A. Bouvet, H. Thevenon, J. F. Dejoux, T. Le Toan, and G. Dedieu. 2019. Estimation and mapping of forest structure parameters from open access satellite images: Development of a generic method with a study case on coniferous plantation. Remote Sens. 11.

Mountrakis, G., J. Im, and C. Ogole. 2011. Support vector machines in remote sensing: A review. ISPRS J. Photogramm. Remote Sens. 66:247–259 Available at http://dx.doi.org/10.1016/j.isprsjprs.2010.11.001.

© University of Pretoria

Mugasha, W. ., T. Eid, O. M. Bollandsås, R. E. Malimbwi, S. A. . Chamshama, E. Zahabu, and J. Z. Katani. 2012. Allometric models for prediction of aboveground biomass of single trees in miombo woodlands in Tanzania.Pages 8–17 in Proceedings of the first Climate Change Impacts, Mitigation and Adaptation Programme Scientific Conference.

Mugasha, W. A., T. Eid, O. M. Bollandsås, R. E. Malimbwi, S. A. O. Chamshama, E. Zahabu, and J. Z. Katani. 2013. Allometric models for prediction of above- and belowground biomass of trees in the miombo woodlands of Tanzania. For. Ecol. Manage. 310:87–101 Available at http://dx.doi.org/10.1016/j.foreco.2013.08.003.

Muhe, S., and M. Argaw. 2022. Estimation of above-ground biomass in tropical afro-montane forest using Sentinel-2 derived indices. Environ. Syst. Res. 11 Available at https://doi.org/10.1186/s40068-022-00250-y.

Müllerová, J., J. Bruna, T. Bartaloš, P. Dvorák, M. Vítková, and P. Pyšek. 2017. Timing Is Important_ Unmanned Aircraft vs. Satellite Imagery in Plant Invasion Monitoring. Front. Plant Sci. 8.

Naesset, E. 1997. Estimating timber volume of forests stands using laser scanner data. Remote Sens. Environ. 67:246–253.

Naesset, E. 2007. Airborne laser scanning as a method in operational forest inventory: Status of accuracy assessments accomplished in Scandinavia. Scand. J. For. Res. 22:433–442.

Næsset, E. 2009. Effects of different sensors, flying altitudes, and pulse repetition frequencies on forest canopy metrics and biophysical stand properties derived from small-footprint airborne laser data. Remote Sens. Environ. 113:148–159 Available at http://dx.doi.org/10.1016/j.rse.2008.09.001.

Næsset, E., O. M. Bollandsås, and T. Gobakken. 2005. Comparing regression methods in estimation of biophysical properties of forest stands from two different inventories using laser scanner data. Remote Sens. Environ. 94:541–553.

Naesset, E., T. Gobakken, J. Holmgren, and M. Maltamo. 2004. Laser scanning of forest resources : The Nordic experience Laser Scanning of Forest Resources : The Nordic Experience.

Næsset, E., H. O. Ørka, S. Solberg, O. M. Bollandsås, E. H. Hansen, E. Mauya, E. Zahabu, R. Malimbwi, N. Chamuya, H. Olsson, and T. Gobakken. 2016. Mapping and estimating forest area and aboveground biomass in miombo woodlands in Tanzania using data from airborne laser scanning, TanDEM-X, RapidEye, and global forest maps: A comparison of estimated precision. Remote Sens. Environ. 175:282–300 Available at http://dx.doi.org/10.1016/j.rse.2016.01.006.

© University of Pretoria

Nagendra, H., and D. Rocchini. 2008. High resolution satellite imagery for tropical biodiversity studies: The devil is in the detail. Biodivers. Conserv. 17:3431–3442.

Naidoo, L., M. A. Cho, R. Mathieu, and G. Asner. 2012. Classification of savanna tree species , in the Greater Kruger National Park region , by integrating hyperspectral and LiDAR data in a Random Forest data mining environment. ISPRS J. Photogramm. Remote Sens. 69:167–179 Available at http://dx.doi.org/10.1016/j.isprsjprs.2012.03.005.

Nandy, S., R. Srinet, and H. Padalia. 2021. Mapping Forest Height and Aboveground Biomass by Integrating ICESat-2, Sentinel-1 and Sentinel-2 Data Using Random Forest Algorithm in Northwest Himalayan Foothills of India. Geophys. Res. Lett. 48:1–10.

Navarro, J. A., N. Algeet, A. Fernández-Landa, J. Esteban, P. Rodríguez-Noriega, and M. L. Guillén-Climent. 2019. Integration of UAV, Sentinel-1, and Sentinel-2 data for mangrove plantation aboveground biomass monitoring in Senegal. Remote Sens. 11:1–23.

Nebikera, S., A. Annena, M. Scherrerb, and D. Oeschc. 2008. Multispectral Sensor for Micro UAV – Opportunities for Very High Resolution Airborne Remote Sensing.Pages 1193–1200 in The International Archives of the Photogrammetry, Remote Sensing and Spatial Information Sciences. Vol. XXXVII. Part B1. Beijing 2008.

Nelson, R., J. Boudreau, T. G. Gregoire, H. Margolis, E. Næsset, T. Gobakken, and G. Ståhl. 2009. Estimating Quebec provincial forest resources using ICESat/GLAS. Can. J. For. Res. 39:862–881.

Nelson, R., H. Margolis, P. Montesano, G. Sun, B. Cook, L. Corp, H. E. Andersen, B. deJong, F. P. Pellat, T. Fickel, J. Kauffman, and S. Prisley. 2017. Lidar-based estimates of aboveground biomass in the continental US and Mexico using ground, airborne, and satellite observations. Remote Sens. Environ. 188:127–140 Available at http://dx.doi.org/10.1016/j.rse.2016.10.038.

Nevalainen, O., E. Honkavaara, S. Tuominen, N. Viljanen, T. Hakala, X. Yu, J. Hyyppä, H. Saari, I. Pölönen, N. N. Imai, and A. M. G. Tommaselli. 2017. Individual tree detection and classification with UAV-Based photogrammetric point clouds and hyperspectral imaging. Remote Sens. 9.

Ota, T., O. S. Ahmed, S. Thu, T. Cin, and N. Mizoue. 2019. Forest Ecology and Management Estimating selective logging impacts on aboveground biomass in tropical forests using digital aerial photography obtained before and after a logging event from an unmanned aerial vehicle. For. Ecol. Manage. 433:162–169 Available at https://doi.org/10.1016/j.foreco.2018.10.058.

Otu-Larbi, F., A. Conte, S. Fares, O. Wild, and K. Ashworth. 2020. Current and future impacts of drought and ozone stress on Northern Hemisphere forests. Glob. Chang. Biol. 26:6218–

© University of Pretoria

6234.

Pádua, L., J. Vanko, J. Hruška, T. Adão, J. J. Sousa, E. Peres, and R. Morais. 2017. UAS , sensors , and data processing in agroforestry : a review towards practical applications. Int. J. Remote Sens.:1–43 Available at http://dx.doi.org/10.1080/01431161.2017.1297548.

Pal, N. R., and S. K. Pal. 1993. A review on image segmentation techniques. Parttern Recognit. 26:1277–1294.

Park, J. Y., H. C. Muller-landau, J. W. Lichstein, S. W. Rifai, J. P. Dandois, and S. A. Bohlman. 2019. Quantifying Leaf Phenology of Individual Trees and Species in a Tropical Forest Using Unmanned Aerial Vehicle (UAV) Images. Remote Sens. 11.

Poley, L. G., and G. J. McDermid. 2020. A Systematic Review of the Factors Influencing the Estimation of Vegetation Aboveground Biomass Using Unmanned Aerial Systems. Remote Sens. 12:1–46.

Popescu, S. c., and M. Hauglin. 2014. Estimation of Biomass Components by Airborne Laser Scanning.Pages 157–175 in Forest Application of Airborne Laser Scanning: Concepts and Case Studies, Managing Forest Ecosystems. Maltamo, M., Naesset, E., Vauhkonen, J., eds.

Prasetiyowati, M. I., N. U. Maulidevi, and K. Surendro. 2020. Feature selection to increase the random forest method performance on high dimensional data. Int. J. Adv. Intell. Informatics 6:303–312.

Pu, R. 2014. Tree species Classifcation.Pages 1–529 in Remote Sensing of Natural Resources. Wang, G., Weng, Q., eds. CRC Press, Taylor & Francis Group.

Puliti, S. 2018. Tree-Stump Detection , Segmentation , Classification , and Measurement Using Unmanned Aerial Vehicle (UAV) Imagery.

Puliti, S., L. T. Ene, T. Gobakken, and E. Næsset. 2017. Use of partial-coverage UAV data in sampling for large scale forest inventories. Remote Sens. Environ. 194:115–126 Available at http://dx.doi.org/10.1016/j.rse.2017.03.019.

Rango, A., and A. S. Laliberte. 2010. Impact of flight regulations on effective use of unmanned aircraft systems for natural resources applications. J. Appl. Remote Sens. 4:1–12.

Reutebuch, S. E., R. J. Mcgaughey, H. Andersen, and W. W. Carson. 2003. Accuracy of a high-resolution lidar terrain model under a conifer forest canopy. Can. J. Remote Sens. 29:527–535.

Ribeiro, N., M. Cumbana, F. Mamugy, and A. Chaúque. 2012. Remote Sensing of Biomass in the Miombo Woodlands of Southern Africa : Opportunities and Limitations for Research.Pages 77–98 in Remote Sensing of Biomass – Principles and Applications.

© University of Pretoria

Fatoyinbo, T., ed. InTech., Rijeka, Croatia.

Ribeiro, N. S., P. L. S. de Miranda, and J. Timberlake. 2020a. Biogeography and Ecology of Miombo Woodlands.Pages 9–53 in Miombo Woodlands in a Changing Environment : Securing the Resilience and Sustainability of People and Woodlands. Ribeiro, N.S., Yemi, K., Chirwa, P.W., Grundy, I.M., eds.

Ribeiro, N. S., P. L. S. de Miranda, and J. Timberlake. 2020b. Miombo Woodlands in a Changing Environment: Securing the Resilience and Sustainability of People and Woodlands.Pages 188–189 in Miombo Woodlands in a Changing Sustainability of People the Resilience and Environment: Securing and Woodlands. Ribeiro, N.S., Katerere, Y., Chirwa, P.W., Grundy, I.M., eds. Springer Nature Switzerland.

Ribeiro, N. S., H. H. Shugart, and R. Washington-Allen. 2008. The effects of fire and elephants on species composition and structure of the Niassa Reserve, northern Mozambique. For. Ecol. Manage. 255:1626–1636.

Ribeiro, N. S., S. Syampungani, N. M. Matakala, D. Nangoma, and R. A. Isabel. 2015. Miombo Woodlands Research Towards the Sustainable Use of Ecosystem Services in Southern Africa.in Miombo Woodlands Research Towards the Sustainable Use of Ecosystem Services in Southern Africa.

Riihimäki, H., M. Luoto, and J. Heiskanen. 2019. Estimating fractional cover of tundra vegetation at multiple scales using unmanned aerial systems and optical satellite data. Remote Sens. Environ. 224:119–132 Available at https://doi.org/10.1016/j.rse.2019.01.030.

Rivas-Torres, G. F., F. L. Benítez, D. Rueda, C. Sevilla, and C. F. Mena. 2018. A methodology for mapping native and invasive vegetation coverage in archipelagos: An example from the Galápagos Islands. Prog. Phys. Geogr. 42:83–111.

Romijn, E., M. Herold, L. Kooistra, D. Murdiyarso, and L. Verchot. 2012. Assessing capacities of non-Annex I countries for national forest monitoring in the context of REDD +. Environ. Sci. Policy 19–20:33–48 Available at http://dx.doi.org/10.1016/j.envsci.2012.01.005.

Ryan, C. M., M. Williams, and J. Grace. 2011a. Above- and Belowground Carbon Stocks in a Miombo Woodland Landscape of Mozambique. Biotropica 43:423–432.

Ryan, C. M., M. Williams, and J. Grace. 2011b. Above - and Belowground Carbon Stocks in a Miombo Woodland Landscape of Above- and Belowground Carbon Stocks in a Miombo Woodland.

Samiappan, S., G. Turnage, C. Mccraine, J. Skidmore, L. Hathcock, and R. Moorhead. 2017. Post-Logging Estimation of Loblolly Pine (Pinus taeda) Stump Size , Area and

© University of Pretoria

Population Using Imagery from a Small Unmanned Aerial System.

Samimi, C., and T. Kraus. 2004. Biomass estimation using Landsat-TM and -ETM+. Towards a regional model for Southern Africa? GeoJournal 59:177–187.

Sankey, T., J. Donager, J. McVay, and J. B. Sankey. 2017. UAV lidar and hyperspectral fusion for forest monitoring in the southwestern USA. Remote Sens. Environ. 195:30–43 Available at http://dx.doi.org/10.1016/j.rse.2017.04.007.

Sedano, F., P. Gong, and M. Ferra. 2005. Land cover assessment with MODIS imagery in southern African Miombo ecosystems. 98:429–441.

Sedano, F., S. N. Lisboa, L. Duncanson, N. Ribeiro, A. Sitoe, R. Sahajpal, and G. Hurtt. 2020a. Monitoring forest degradation from charcoal production with historical Landsat imagery . A case study in southern Mozambique Monitoring forest degradation from charcoal production with historical Landsat imagery . A case study in southern Mozambique.

Sedano, F., S. Lisboa, L. Duncanson, N. Ribeiro, A. Sitoe, R. Sahajpal, G. Hurtt, and C. Tucker. 2020b. Int J Appl Earth Obs Geoinformation Monitoring intra and inter annual dynamics of forest degradation from charcoal production in Southern Africa with Sentinel – 2 imagery. Int J Appl Earth Obs Geoinf. 92:102184 Available at https://doi.org/10.1016/j.jag.2020.102184.

SEPAL. System for Earth Observation Data Access, Processing and Analysis for Land Monitoring. Available at https://sepal.io (verified 13 April 2023).

Shamaoma, H., P. W. Chirwa, A. Ramoelo, A. T. Hudak, and S. Syampungani. 2022. The Application of UASs in Forest Management and Monitoring : Challenges and Opportunities for Use in the Miombo Woodland. Forests 13.

Shamaoma, H., N. Kerle, and D. Alkema. 2006. Extraction of Flood-Modelling Related Base-Data From Multi- Source Remote Sensing Imagery.in Commission VII, WG/7: Problem Solving Methodologies for Less Developed Countries. Kerle, N., Skidmore, A., eds. The International Society for Photogrammetry and Remote Sensing, Enschede, The Netherlands.

Shen, X., L. Cao, B. Yang, Z. Xu, and G. Wang. 2019. Estimation of Forest Structural Attributes Using Spectral Indices and Point Clouds from UAS-Based. Remote Sens. 11:1–24.

Shi, C., and L. Wang. 2014. Incorporating spatial information in spectral unmixing: A review. Remote Sens. Environ. 149:70–87 Available at http://dx.doi.org/10.1016/j.rse.2014.03.034.

Shin, P., T. Sankey, M. M. Moore, and A. E. Thode. 2018. Evaluating Unmanned Aerial Vehicle Images for Estimating Forest Canopy Fuels in a Ponderosa Pine Stand. Remote

© University of Pretoria

Sens.:2–22.

Shin, J., W. Seo, T. Kim, J. Park, and C. Woo. 2019. Using UAV Multispectral Images for Classification of Forest Burn Severity — A Case Study of the 2019 Gangneung Forest Fire. Forests 10.

Siewert, M. B., and J. Olofsson. 2021. UAV reveals substantial but heterogeneous effects of herbivores on Arctic vegetation. Sci. Rep. 11 Available at https://doi.org/10.1038/s41598-021-98497-5.

Singh, M., D. Evans, B. S. Tan, and C. S. Nin. 2015. Mapping and Characterizing Selected Canopy Tree Species at the Angkor World Heritage Site in Cambodia Using Aerial Data. PLoS One 10:1–26.

Smigaj, M., R. Gaulton, S. L. Barr, J. C. Suárez, C. Vi, and W. G. Vi. 2015. The International Archives of the Photogrammetry, Remote Sensing and Spatial Information Sciences, Volume XL-3/W3, 2015 ISPRS Geospatial Week 2015, 28 Sep – 03 Oct 2015, La Grande Motte, France.Pages 349–354 in UAV-BORNE THERMAL IMAGING FOR FOREST HEALTH MONITORING: DETECTION OF DISEASE-INDUCED CANOPY TEMPERATURE INCREASE M. G. Rabatel and M. Pierrot-Deseilligny, ed. La Grande Motte, France.

Snavely, N., S. M. Seitz, and R. Szeliski. 2007. Modeling the World from Internet Photo Collections. Int. J. Comput. Vis. 6:245–255.

Somers, B., and G. P. Asner. 2013. Multi-temporal hyperspectral mixture analysis and feature selection for invasive species mapping in rainforests. Remote Sens. Environ. 136:14–27 Available at http://dx.doi.org/10.1016/j.rse.2013.04.006.

Souza, C. M., D. A. Roberts, and M. A. Cochrane. 2005. Combining spectral and spatial information to map canopy damage from selective logging and forest fires. Remote Sens. Environ. 98:329–343.

Souza, C. M., J. V Siqueira, M. H. Sales, A. V Fonseca, J. G. Ribeiro, I. Numata, M. A. Cochrane, C. P. Barber, D. A. Roberts, and J. Barlow. 2013. Ten-Year Landsat Classification of Deforestation and Forest Degradation in the Brazilian Amazon. Remote Sens. 5:5493–5513.

Sprott, A. H., and J. M. Piwowar. 2021. How to recognize different types of trees from quite a long way away: combining UAV and spaceborne imagery for stand-level tree species identification. J. Unmanned Veh. Syst. 9:166–181.

Stöcker, C., R. Bennett, F. Nex, M. Gerke, and J. Zevenbergen. 2017. Review of the Current State of UAV Regulations. Remote Sens. 9:1–26.

© University of Pretoria

Stringer, L. C., A. J. Dougill, D. D. Mkwambisi, J. C. Dyer, F. K. Kalaba, and M. Mngoli. 2012. Challenges and opportunities for carbon management in Malawi and Zambia. Carbon Manag. 3:159–173.

Su, Y., Q. Guo, B. Xue, T. Hu, O. Alvarez, S. Tao, and J. Fang. 2016. Spatial distribution of forest aboveground biomass in China: Estimation through combination of spaceborne lidar, optical imagery, and forest inventory data. Remote Sens. Environ. 173:187–199 Available at http://dx.doi.org/10.1016/j.rse.2015.12.002.

Sugiura, N. 1978. Further Analysis of the Data by Anaike' S Information Criterion and the Finite Corrections. Commun. Stat. - Theory Methods 7:13–26.

Syampungani, S., P. W. Chirwa, F. K. Akinnifesi, G. Sileshi, and O. C. Ajayi. 2009. The miombo woodlands at the cross roads : Potential threats , sustainable livelihoods , policy gaps and challenges. 33:150–159.

Syampungani, S., C. J. Geldenhuys, and P. W. Chirwa. 2011. Journal of Natural Resources Policy Miombo Woodland Utilization and Management , and Impact Perception among Stakeholders in Zambia : A Call for Policy Change in Southern Africa. :37–41.

Tang, L., and G. Shao. 2015. Drone remote sensing for forestry research and practices. J. For. Res. 26:791–797.

Thiel, C., M. M. Müller, C. Berger, F. Cremer, S. Hese, J. Baade, F. Klan, and C. Pathe. 2020. Monitoring Selective Logging in a Pine-Dominated Forest in Central Germany with Repeated Drone Flights Utilizing A Low Cost RTK Quadcopter.

Thomson, P. J. 1975. The role of elephants, fire and other agents in the decline of a Brachystegia boehmii woodland. J. South. African Wildl. Manag. Assoc. 5:11–18 Available at http://scholar.google.com/scholar?hl=en&btnG=Search&q=intitle:The+role+of+elephants,+fire+and+other+agents+in+the+decline+of+a+Brachystegia+boehmii+woodland#0.

Tomaštík, J., M. Mokroš, P. Surový 2, A. Grznárová, and J. Merganič. 2019. UAV RTK / PPK Method — An Optimal Solution for Mapping Inaccessible Forested Areas ? Remote Sens. 11:1–19.

Tomppo, E., H. Olsson, G. Ståhl, M. Nilsson, O. Hagner, and M. Katila. 2008. Combining national forest inventory field plots and remote sensing data for forest databases. Remote Sens. Environ. 112:1982–1999.

Torres, D. L., R. Q. Feitosa, P. N. Happ, L. E. C. La Rosa, J. M. Junior, J. Martins, P. O. Bressan, W. N. Gonçalves, and V. Liesenberg. 2020. Applying fully convolutional architectures for semantic segmentation of a single tree species in urban environment on high resolution

© University of Pretoria

UAV optical imagery. Sensors 20.

Torresan, C., A. Berton, F. Carotenuto, S. F. Di, B. Gioli, A. Matese, F. Miglietta, A. Zaldei, L. Wallace, C. Torresan, A. Berton, F. Carotenuto, and S. F. Di. 2017. Forestry applications of UAVs in Europe : a review. Int. J. Remote Sens. 38:2427–2447 Available at http://dx.doi.org/10.1080/01431161.2016.1252477.

Trimble. 2018. eCognition Developer User Guide. Version 9. Trimble Germany GmbH, Munic, Germany.

Turner, W., S. Spector, N. Gardiner, M. Fladeland, E. Sterling, and M. Steininger. 2003. Remote sensing for biodiversity science and conservation. Trends Ecol. Evol. 18:306–314.

UNFCCC. 2015. ADOPTION OF THE PARIS AGREEMENT Proposal by the President. 21930 Available at http://unfccc.int/resource/docs/2015/cop21/eng/109.pdf (verified 21 November 2019).

Valero, M. M., O. Rios, C. Mata, E. Pastor, and E. Planas. 2017. An integrated approach for tactical monitoring and data-driven spread forecasting of wild fires. Fire Saf. J. 91:835–844 Available at http://dx.doi.org/10.1016/j.firesaf.2017.03.085.

Vastaranta, M., M. Holopainen, X. Yu, R. Haapanen, T. Melkas, J. Hyyppä, and H. Hyyppä. 2011. INDIVIDUAL TREE DETECTION AND AREA-BASED APPROACH IN RETRIEVAL OF FOREST INVENTORY CHARACTERISTICS FROM LOW-PULSE AIRBORNE LASER SCANNING DATA. 22:1–13.

Wallace, L., A. Lucieer, Z. Malenovskỳ, D. Turner, and P. Vopěnka. 2016. Assessment of forest structure using two UAV techniques: A comparison of airborne laser scanning and structure from motion (SfM) point clouds. Forests 7:1–16.

Wallace, L. O., A. Lucieer, and C. S. Watson. 2012a. International Archives of the Photogrammetry, Remote Sensing and Spatial Information Sciences.Pages 499–504 in ASSESSING THE FEASIBILITY OF UAV-BASED LIDAR FOR HIGH RESOLUTION FOREST CHANGE DETECTION. XXII ISPRS Congress, Melbourne, Australia.

Wallace, L., A. Lucieer, and C. S. Watson. 2014. Evaluating Tree Detection and Segmentation Routines on Very High Resolution UAV LiDAR Data. IEEE Trans. Geosci. Remote Sens. 52:7619–7628.

Wallace, L., A. Lucieer, C. Watson, and D. Turner. 2012b. Development of a UAV-LiDAR system with application to forest inventory. Remote Sens. 4:1519–1543.

Wallis, C. I. B., J. Homeier, J. Peña, R. Brandl, N. Farwig, and J. Bendix. 2019. Modeling tropical montane forest biomass, productivity and canopy traits with multispectral

© University of Pretoria

remote sensing data. Remote Sens. Environ. 225:77–92 Available at https://doi.org/10.1016/j.rse.2019.02.021.

Wang, D., B. Wan, J. Liu, Y. Su, Q. Guo, P. Qiu, and X. Wu. 2020. Estimating aboveground biomass of the mangrove forests on northeast Hainan Island in China using an upscaling method from field plots, UAV-LiDAR data and Sentinel-2 imagery. Int. J. Appl. Earth Obs. Geoinf. 85:101986 Available at http://dx.doi.org/10.1016/j.jag.2019.101986.

Wang, D., B. Wan, P. Qiu, Z. Zuo, R. Wang, and X. Wu. 2019. Mapping height and aboveground biomass of mangrove forests on Hainan Island using UAV-LiDAR sampling. Remote Sens. 11:1–25.

Wang, K., T. Wang, and X. Liu. 2018. A review: Individual tree species classification using integrated airborne LiDAR and optical imagery with a focus on the urban environment. Forests 10:1–18.

Weatheronline. 2022. Historical wether data. Available at https://www.woeurope.eu/ (verified 18 August 2022).

Weisberg, P. J., T. E. Dilts, J. A. Greenberg, K. N. Johnson, H. Pai, C. Sladek, C. Kratt, S. W. Tyler, and A. Ready. 2021. Phenology-based classification of invasive annual grasses to the species level. Remote Sens. Environ. 263:112568 Available at https://doi.org/10.1016/j.rse.2021.112568.

Westoby, M. J., J. Brasington, N. F. Glasser, M. J. Hambrey, and J. M. Reynolds. 2012. “Structure-from-Motion” photogrammetry: A low-cost, effective tool for geoscience applications. Geomorphology 179:300–314 Available at http://dx.doi.org/10.1016/j.geomorph.2012.08.021.

White, F. 1983. The vegetaion of frica. Natural Resources Reasearch. UNESCO, Paris.

White, J. C., N. C. Coops, M. A. Wulder, M. Vastaranta, T. Hilker, and P. Tompalski. 2016. Remote Sensing Technologies for Enhancing Forest Inventories : A Review Remote Sensing Technologies for Enhancing Forest Inventories : A Review.

White, J. C., P. Tompalski, M. Vastaranta, M. A. Wulder, N. Saarinen, C. Stepper, and N. C. Coops. 2017. A model development and application guide for generating an enhanced forest inventory using airborne laser scanning data and an area-based approach. Information Report FI-X-18. Victoria, B.C.

White, J. C., M. A. Wulder, A. Varhola, M. Vastaranta, N. C. Coops, B. D. Cook, D. Pitt, and M. Woods. 2013a. A best practices guide for generating forest inventory attributes from airborne laser scanning data using an area-based approach.

© University of Pretoria

White, J. C., M. A. Wulder, M. Vastaranta, N. C. Coops, D. Pitt, and M. Woods. 2013b. The Utility of Image-Based Point Clouds for Forest Inventory: A Comparison with Airborne Laser Scanning. :518–536.

Whitehead, K., and C. H. Hugenholtz. 2014. Remote Sensing of the Environment with Small Unmanned Aircraft Systems (UASs), Part 1 : A review of progress and challenges. J. Unmmaned Veh. Syst. 2:69–85.

Whitehead, K., C. H. Hugenholtz, S. Myshak, O. Brown, A. Leclair, A. Tamminga, T. E. Barchyn, B. Moorman, and B. Eaton. 2014. Remote sensing of the environment with small unmanned aircraft systems (UASs), part 2 : scientific and commercial applications 1. J. Unmmaned Veh. Syst. 102:86–102.

Witczuk, J., S. Pagacz, A. Zmarz, M. Cypel, and J. Witczuk. 2017. Exploring the feasibility of unmanned aerial vehicles and thermal imaging for ungulate surveys in forests - preliminary results results. Int. J. Remote Sens.:1–18 Available at https://doi.org/10.1080/01431161.2017.1390621.

Witt, A. B. R., R. T. Shackleton, T. Beale, W. Nunda, and B. W. van Wilgen. 2019. Distribution of invasive alien Tithonia (Asteraceae) species in eastern and southern Africa and the socio-ecological impacts of T. Diversifolia in Zambia. Bothalia 49:1–11.

Wulder, M. A., N. C. Coops, A. T. Hudak, F. Morsdorf, R. Nelson, G. Newnham, and M. Vastaranta. 2013. Status and prospects for LiDAR remote sensing of forested ecosystems. Can. J. Remote Sens. 39:1–5 Available at http://dx.doi.org/130051.

Wulder, M. A., J. C. White, R. F. Nelson, E. Næsset, H. O. Ørka, N. C. Coops, T. Hilker, C. W. Bater, and T. Gobakken. 2012. Lidar sampling for large-area forest characterization: A review. Remote Sens. Environ. 121:196–209 Available at http://dx.doi.org/10.1016/j.rse.2012.02.001.

Xie, Z., Y. Chen, D. Lu, G. Li, and E. Chen. 2019. Classification of land cover, forest, and tree species classes with Ziyuan-3 multispectral and stereo data. Remote Sens. 11:1–27.

Xie, Y., Z. Sha, and M. Yu. 2008. Remote sensing imagery in vegetation mapping : a review. J. Plant Ecol. 1:9–23.

Xu, Z., and H. Ruan. 2020. Estimation of secondary forest parameters by integrating image and point cloud-based metrics acquired from unmanned aerial vehicle. 14.

Xu, Z., X. Shen, L. Cao, N. C. Coops, T. R. H. Goodbody, T. Zhong, W. Zhao, Q. Sun, S. Ba, Z. Zhang, and X. Wu. 2020. Int J Appl Earth Obs Geoinformation Tree species classi fi cation using UAS-based digital aerial photogrammetry point clouds and multispectral imageries in subtropical natural forests. Int J Appl Earth Obs Geoinf. 92:1–14 Available at

© University of Pretoria

https://doi.org/10.1016/j.jag.2020.102173.

Xue, J., and B. Su. 2017. Significant Remote Sensing Vegetation Indices : A Review of Developments and Applications. J. Sensors 2017:1–17.

Yancho, J. M. M., N. C. Coops, P. Tompalski, T. R. H. Goodbody, and A. Plowright. 2019. Fine-Scale Spatial and Spectral Clustering of UAV-Acquired Digital Aerial Photogrammetric (DAP) Point Clouds for Individual Tree Crown Detection and Segmentation. IEEE J. Sel. Top. Appl. Earth Obs. Remote Sens. 12:4131–4148.

Yang, G., Y. Zhao, B. Li, Y. Ma, R. Li, J. Jing, and Y. Dian. 2019. Tree species classification by employing multiple features acquired from integrated sensors. J. Sensors.

Yao, H., R. Qin, and X. Chen. 2019. Unmanned Aerial Vehicle for Remote Sensing Applications — A Review. Remote Sens. 11:1–22.

Yu, X., J. Hyyppä, M. Holopainen, and M. Vastaranta. 2010. Comparison of Area-Based and Individual Tree-Based Methods for Predicting Plot-Level Forest Attributes. :1481–1495.

Zahawi, R. A., J. P. Dandois, K. D. Holl, D. Nadwodny, J. L. Reid, and E. C. Ellis. 2015. Using lightweight unmanned aerial vehicles to monitor tropical forest recovery. Biol. Conserv. 186:287–295 Available at http://dx.doi.org/10.1016/j.biocon.2015.03.031.

Zhang, Z., L. Cao, and G. She. 2017. Estimating Forest Structural Parameters Using Canopy Metrics Derived from Airborne LiDAR Data in Subtropical Forests. Remote Sens. 9:1–26.

Zhang, X., F. Zhang, Y. Qi, L. Deng, and X. Wang. 2019. Int J Appl Earth Obs Geoinformation New research methods for vegetation information extraction based on visible light remote sensing images from an unmanned aerial vehicle (UAV). Int J Appl Earth Obs Geoinf. 78:215–226 Available at https://doi.org/10.1016/j.jag.2019.01.001.

Zhao, X., Q. Guo, Y. Su, and B. Xue. 2016. Improved progressive TIN densification filtering algorithm for airborne LiDAR data in forested areas. ISPRS J. Photogramm. Remote Sens. 117:79–91 Available at http://dx.doi.org/10.1016/j.isprsjprs.2016.03.016.

Zimba, S. . 2007. The fate of forest reserves in Zambia, a case study of Mwekera national forest No. 6. Ndola, Zambia.

© University of Pretoria

References

Adam, E., O. Mutanga, E. M. Abdel-Rahman, and R. Ismail. 2014. Estimating standing biomass in papyrus (Cyperus papyrus L.) swamp: Exploratory of in situ hyperspectral indices and random forest regression. Int. J. Remote Sens. 35:693–714 Available at http://dx.doi.org/10.1080/01431161.2013.870676.

Adão, T., J. Hruška, L. Pádua, J. Bessa, E. Peres, R. Morais, and J. J. Sousa. 2017. Hyperspectral Imaging : A Review on UAV-Based Sensors , Data Processing and Applications for Agriculture and Forestry. Remote Sens. 9:1–30.

Agapiou, A. 2020. Vegetation Extraction Using Visible-Bands from Openly Licensed Unmanned Aerial Vehicle Imagery. Drones 4:1–15.

Agisoft LLC. 2019. Agisoft Metashape User Manual. St. Petersburg, Russia, Russia.

Aguilar, F. J., J. R. Rivas, A. Nemmaoui, A. Peñalver, and M. A. Aguilar. 2019. UAV-Based Digital Terrain Model Generation under Leaf-O ff Conditions to Support Teak Plantations Inventories in Tropical Dry Forests . A Case of the Coastal Region of Ecuador. Sensors 19:1–21.

Ahmed, O. S., A. Shemrock, D. Chabot, C. Dillon, R. Wasson, S. E. Franklin, O. S. Ahmed, A. Shemrock, D. Chabot, C. Dillon, R. Wasson, and S. E. Franklin. 2017. Hierarchical land cover and vegetation classification using multispectral data acquired from an unmanned aerial vehicle. Int. J. Remote Sens. Available at http://dx.doi.org/10.1080/01431161.2017.1294781.

Alonzo, M., H. E. Andersen, D. C. Morton, and B. D. Cook. 2018. Quantifying boreal forest structure and composition using UAV structure from motion. Forests 9.

Anderson, K., and K. J. Gaston. 2013. Lightweight unmanned aerial vehicles will revolutionize spatial ecology. Front. Ecol. Environ.

© University of Pretoria

Askar, N. Nuthammachot, W. Phairuang, P. Wicaksono, and T. Sayektiningsih. 2018. Estimating aboveground biomass on private forest using sentinel-2 imagery. J. Sensors 2018.

Asner, G. P., and R. E. Martin. 2009. Airborne spectranomics: Mapping canopy chemical and taxonomic diversity in tropical forests. Front. Ecol. Environ. 7:269–276.

Aubry, P., and D. Debouzie. 2001. Estimation of the mean from a two-dimensional sample: The geostatistical model-based approach. Ecology 82:1484–1494.

Bannari, A., D. Morin, F. Bonn, and A. R. Huete. 1995. A review of vegetation indices. A Rev. Veg. indices 13:95–120.

Banu, T. P., and G. F. Borlea. 2016. The Use of Drones in Forestry. J. Environ. Sci. Eng. B5:557–562.

Barber, N., E. Alvarado, V. R. Kane, W. E. Mell, and L. M. Moskal. 2021. Estimating Fuel Moisture in Grasslands Using UAV-Mounted Infrared and Visible Light Sensors. Sensors:1–16.

Barquín, L., M. Chacón, S. Panfil, A. Adeleke, E. Florian, and R. Triraganon. 2014. The Knowledge and Skills Needed to Engage in REDD+: A Competencies Framework. Conservation International. Arlington, Virginia, USA.

Benz, U. C., P. Hofmann, G. Willhauck, I. Lingenfelder, and M. Heynen. 2004. Multi-resolution , object-oriented fuzzy analysis of remote sensing data for GIS-ready information. ISPRS J. Photogramm. Remote Sens. 58:239–258.

Bergamo, T. F., R. S. de Lima, T. Kull, R. D. Ward, K. Sepp, and M. Villoslada. 2023. From UAV to PlanetScope: Upscaling fractional cover of an invasive species Rosa rugosa. J. Environ. Manage. 336:117693 Available at https://doi.org/10.1016/j.jenvman.2023.117693.

© University of Pretoria

Blaschke, T. 2010. Object based image analysis for remote sensing. ISPRS J. Photogramm. Remote Sens. 65:2–16 Available at http://dx.doi.org/10.1016/j.isprsjprs.2009.06.004.

Bossoukpe, M., E. Faye, O. Ndiaye, S. Diatta, O. Diatta, A. A. Diouf, M. Dendoncker, M. H. Assouma, and S. Taugourdeau. 2021a. Low-cost drones help measure tree characteristics in the Sahelian savanna. J. Arid Environ. 187:104449 Available at https://doi.org/10.1016/j.jaridenv.2021.104449.

Bossoukpe, M., O. Ndiaye, O. Diatta, S. Diatta, A. Audebert, P. Couteron, L. Leroux, A. A. Diouf, M. Dendoncker, E. Faye, and S. Taugourdeau. 2021b. Unmanned aerial vehicle for the assessment of woody and herbaceous phytomass in Sahelian savanna. Rev. d'Elevage Med. Vet. des Pays Trop. 74:199–205.

Bouvier, M., S. Durrieu, R. A. Fournier, and J. P. Renaud. 2015. Generalizing predictive models of forest inventory attributes using an area-based approach with airborne LiDAR data. Remote Sens. Environ. 156:322–334 Available at http://dx.doi.org/10.1016/j.rse.2014.10.004.

Brede, B., L. Terryn, N. Barbier, H. M. Bartholomeus, R. Bartolo, K. Calders, G. Derroire, S. M. Krishna Moorthy, A. Lau, S. R. Levick, P. Raumonen, H. Verbeeck, D. Wang, T. Whiteside, J. van der Zee, and M. Herold. 2022. Non-destructive estimation of individual tree biomass: Allometric models, terrestrial and UAV laser scanning. Remote Sens. Environ. 280.

Brewer, M. J., A. Butler, and S. L. Cooksley. 2016. The relative performance of AIC, AICC and BIC in the presence of unobserved heterogeneity. Methods Ecol. Evol. 7:679–692.

Brooks, G. P., and P. Ruengvirayudh. 2016. Best-Subset Selection Criteria for Multiple Linear Regression. Gen. Linear Model J. 42:14–25.

Brosofske, K. D., R. E. Froese, M. J. Falkowski, and A. Banskota. 2014. A review of methods

© University of Pretoria

for mapping and prediction of inventory attributes for operational forest management. For. Sci. 60:733–756.

Bullock, E. L., C. E. Woodcock, and P. Olofsson. 2018. Remote Sensing of Environment Monitoring tropical forest degradation using spectral unmixing and Landsat time series analysis. Remote Sens. Environ.:0–1 Available at https://doi.org/10.1016/j.rse.2018.11.011.

Cabral, A. I. R., M. J. Vasconcelos, D. Oom, and R. Sardinha. 2010. Spatial dynamics and quanti fi cation of deforestation in the central-plateau woodlands of Angola (1990 - 2009). Appl. Geogr. 31:1185–1193 Available at http://dx.doi.org/10.1016/j.apgeog.2010.09.003.

Campbell, B. 1996. The Miombo in Transition : Woodlands and Welfare in Africa (B Campbell, Ed.). Center for International Forestry Research, Bogor, Indonesia.

Cao, L., N. C. Coops, T. Hermosilla, J. Innes, J. Dai, and G. She. 2014. Using small-footprint discrete and full-waveform airborne LiDAR metrics to estimate total biomass and biomass components in subtropical forests. Remote Sens. 6:7110–7135.

Cao, J., W. Leng, K. Liu, L. Liu, and Z. He. 2018. Object-Based Mangrove Species Classification Using Unmanned Aerial Vehicle Hyperspectral Images and Digital Surface Models. Remote Sens. 10:1–20.

Cao, L., H. Liu, X. Fu, Z. Zhang, X. Shen, and H. Ruan. 2019a. Comparison of UAV LiDAR and Digital Aerial Photogrammetry Point Clouds for Estimating Forest Structural Attributes in Subtropical Planted Forests. :1–26.

Cao, L., K. Liu, X. Shen, X. Wu, and H. Liu. 2019b. Estimation of Forest Structural Parameters Using UAV-LiDAR Data and a Process-Based Model in Ginkgo Planted Forests. IEEE J. Sel. Top. Appl. Earth Obs. Remote Sens. 12:4175–4190.

Cao, J., K. Liu, L. Zhuo, L. Liu, Y. Zhu, and L. Peng. 2021. Combining UAV-based hyperspectral and LiDAR data for mangrove species classification using the rotation

© University of Pretoria

forest algorithm. Int. J. Appl. Earth Obs. Geoinf. 102:102414 Available at https://doi.org/10.1016/j.jag.2021.102414.

Cao, L., Z. Zhang, T. Yun, G. Wang, H. Ruan, and G. She. 2019c. Estimating Tree Volume Distributions in Subtropical Forests Using Airborne LiDAR Data. Remote Sens. 11:97.

Castillo, J. A. A., A. A. Apan, T. N. Maraseni, and S. G. Salmo. 2017. Estimation and mapping of above-ground biomass of mangrove forests and their replacement land uses in the Philippines using Sentinel imagery. ISPRS J. Photogramm. Remote Sens. 134:70–85 Available at https://doi.org/10.1016/j.isprsjprs.2017.10.016.

Cessna, J., M. G. Alonzo, A. C. Foster, and B. D. Cook. 2021. Mapping boreal forest spruce beetle health status at the individual crown scale using fused spectral and structural data. Forests 12.

Chamuya, N., and J. Mgoo. 2014. Tanzania National Forest Resources Monitoring and Assessment . NAFORMA. Brief report. Tanzania Forest Services Agency. :1–14.

Chandrashekar, G., and F. Sahin. 2014. A survey on feature selection methods. Comput. Electr. Eng. 40:16–28 Available at http://dx.doi.org/10.1016/j.compeleceng.2013.11.024.

Chen, Q. 2013. LiDAR remote sensing of vegetation biomass (Q Weng, Ed.). Remote Sens. Nat. Resour.:399–420.

Chidumayo, E. N. 2013. Forest degradation and recovery in a miombo woodland landscape in Zambia : 22 years of observations on permanent sample plots. For. Ecol. Manage. 291:154–161 Available at http://dx.doi.org/10.1016/j.foreco.2012.11.031.

Chidumayo, E. N., and D. J. Gumbo. 2013. The environmental impacts of charcoal production in tropical ecosystems of the world: A synthesis. Energy Sustain. Dev. 17:86–94 Available at http://dx.doi.org/10.1016/j.esd.2012.07.004.

© University of Pretoria

Chirwa, P. W., M. Larwanou, S. Syampungani, and B. D. Folaranmi. 2015. Management and restoration practices in degraded landscapes of Eastern Africa and requirements for up-scaling. Int. For. Rev. 17:20–30.

Chirwa, P. W., S. Syampungani, and C. J. Geldenhuys. 2016. The ecology and management of the Miombo woodlands for sustainable livelihoods in southern Africa : the case for non-timber forest products. South. For. 70:237–245.

Chisholm, R. A., J. Cui, S. K. Y. Lum, and B. M. Chen. 2013. UAV LiDAR for below-canopy forest surveys. J. Unmmaned Veh. Syst. 68:61–68.

Cho, M. A., P. Debba, R. Mathieu, L. Naidoo, J. Van Aardt, and G. P. Asner. 2010. Improving Discrimination of Savanna Tree Species Through a Multiple-Endmember Spectral Angle Mapper Approach : Canopy-Level Analysis. IEEE Trans. Geosci. Remote Sens. 48:4133–4142.

Cho, A. M., R. Mathieu, G. P. Asner, L. Naidoo, J. Van Aardt, A. Ramoelo, P. Debba, K. Wessels, R. Main, I. P. J. Smit, and B. Erasmus. 2012. Remote Sensing of Environment Mapping tree species composition in South African savannas using an integrated airborne spectral and LiDAR system. Remote Sens. Environ. 125:214–226 Available at http://dx.doi.org/10.1016/j.rse.2012.07.010.

ClimaCell. 2018. Why Drone Can’t Use Regular Weather ForecastsNo Title. Available at https://www.tomorrow.io/blog/why-%0Adrones-cant-use-regular-weather-forecasts (verified 12 August 2022).

Clinton, N., A. Holt, J. Scarborough, L. Yan, and P. Gong. 2010. Accuracy assessment measures for object-based image segmentation goodness. Photogramm. Eng. Remote Sens. 76:289–299.

Colomina, I., and P. Molina. 2014. Unmanned aerial systems for photogrammetry and remote

© University of Pretoria

sensing: A review. ISPRS J. Photogramm. Remote Sens. 92:79–97 Available at http://dx.doi.org/10.1016/j.isprsjprs.2014.02.013.

Costa, H., G. M. Foody, and D. S. Boyd. 2017. Supervised methods of image segmentation accuracy assessment in land cover mapping. Remote Sens. Environ. xxx:https://10.1016/j.rse.2017.11.024.

Cromwell, C., J. Giampaolo, J. Hupy, Z. Miller, and A. Chandrasekaran. 2021. A systematic review of best practices for uas data collection in forestry-related applications. Forests 12.

Cunliffe, A. M., J. J Assmann, G. N Daskalova, J. T. Kerby, and I. H. Myers-Smith. 2020. Aboveground biomass corresponds strongly with drone-derived canopy height but weakly with greenness (NDVI) in a shrub tundra landscape. Environ. Res. Lett. 15.

Czapski, P., M. Kacprzak, J. Kotlarz, K. Mrowiec, K. Kubiak, and M. Tkaczyk. 2015. Preliminary analysis of the forest health state based on multispectral images acquired by Unmanned Aerial Vehicle. Folia For. Pol. Ser. A 57:138–144.

Dalponte, M., L. Frizzera, H. O. Ørka, T. Gobakken, E. Næsset, and D. Gianelle. 2018. Predicting stem diameters and aboveground biomass of individual trees using remote sensing data. Ecol. Indic. 85:367–376 Available at http://dx.doi.org/10.1016/j.ecolind.2017.10.066.

Dandois, J. P., and E. C. Ellis. 2010. Remote Sensing of Vegetation Structure Using Computer Vision. :1157–1176.

Dandois, J. P., M. Olano, and E. C. Ellis. 2015. Optimal altitude, overlap, and weather conditions for computer vision uav estimates of forest structure. Remote Sens. 7:13895–13920.

Dash, J. P., H. M. Marshall, and B. Rawley. 2015. Methods for estimating multivariate stand yields and errors using k-NN and aerial laser scanning. Forestry 88:237–247.

© University of Pretoria

Dash, J. P., G. D. Pearse, and M. S. Watt. 2018. UAV Multispectral Imagery Can Complement Satellite Data for Monitoring Forest Health. Remote Sens. 10:1–22.

Dash, J. P., M. S. Watt, G. D. Pearse, M. Heaphy, and H. S. Dungey. 2017. ISPRS Journal of Photogrammetry and Remote Sensing Assessing very high resolution UAV imagery for monitoring forest health during a simulated disease outbreak. ISPRS J. Photogramm. Remote Sens. 131:1–14 Available at http://dx.doi.org/10.1016/j.isprsjprs.2017.07.007.

Day, M., D. Gumbo, K. B. Moombe, A. Wijaya, and T. Sunderland. 2014. Zambia country profile Monitoring , reporting and verification for REDD +. Occas. Pap. 113.

Deur, M., M. Gašparović, and I. Balenović. 2020. Tree species classification in mixed deciduous forests using very high spatial resolution satellite imagery and machine learning methods. Remote Sens. 12:1–18.

Van Deventer, H., M. Azong, and O. Mutanga. 2019. Multi-season RapidEye imagery improves the classification of wetland and dryland communities in a subtropical coastal region. ISPRS J. Photogramm. Remote Sens. 157:171–187 Available at https://doi.org/10.1016/j.isprsjprs.2019.09.007.

DJI. 2019. P4 MULTISPECTRAL User Manual v1.0 2019.12.

Domingo, D., H. O. Ørka, E. Næsset, D. Kachamba, and T. Gobakken. 2019. Effects of UAV Image Resolution , Camera Type , and Image Overlap on Accuracy of Biomass Predictions in a Tropical Woodland. Remote Sens. 11:1–17.

Doughty, C. L., and K. C. Cavanaugh. 2019. Mapping coastal wetland biomass from high resolution unmanned aerial vehicle (UAV) imagery. Remote Sens. 11.

Dube, T., O. Mutanga, S. Cletah, S. Adelabu, and B. Tsitsi. 2016. Remote sensing of aboveground forest biomass: A review. Trop. Ecol. 57:125–132.

© University of Pretoria

Dublin, H. T., A. R. E. Sinclair, and J. McGlade. 1990. Elephants and Fire as Causes of Multiple Stable States in the Serengeti-Mara Woodlands. J. Anim. Ecol. 59:1147.

Duffy, J. P., A. M. Cunliffe, L. Debell, C. Sandbrook, S. A. Wich, J. D. Shutler, I. H. Myers-smith, M. R. Varela, and K. Anderson. 2017. Location , location , location : considerations when using lightweight drones in challenging environments. Remote Sens. Ecol. Conserv. 4:7–19.

Eames, T., J. Russell-Smith, C. Yates, A. Edwards, R. Vernooij, N. Ribeiro, F. Steinbruch, and G. R. van der Werf. 2021. Instantaneous pre-fire biomass and fuel load measurements from multi-spectral UAS mapping in southern African Savannas. Fire 4.

Effiom, A. E., L. M. Van Leeuwen, P. Nyktas, J. A. Okojie, and J. Erdbrügger. 2019. Combining unmanned aerial vehicle and multispectral Pleiades data for tree species identification , a prerequisite for accurate carbon estimation. J. AppliedRemote Sens. 13.

ESA. 2022. European Space Agency. Sentinel online. Available at https://sentinel.esa.int/web/sentinel/user-guides/sentinel-1-sar/acquisition-modes/interferometric-wide-swath (verified 6 December 2022).

ESRI. 2019. ArcGIS Desktop: Release 10.7.1 Redlands, CA: Environmental Systems Research Institute.

Eugenio, F. C., C. T. Schons, C. L. Mallmann, M. S. Schuh, P. Fernandes, and T. L. Badin. 2020. Remotely piloted aircraft systems and forests : a global state of the art and future challenges 1. Can. J. For. Res. 50:705–716.

Fassnacht, F. E., F. Hartig, H. Latifi, C. Berger, J. Hernández, P. Corvalán, and B. Koch. 2014a. Importance of sample size, data type and prediction method for remote sensing-based estimations of aboveground forest biomass. Remote Sens. Environ. 154:102–114.

Fassnacht, F. E., H. Latifi, K. Stereńczak, A. Modzelewska, M. Lefsky, L. T. Waser, C. Straub,

© University of Pretoria

and A. Ghosh. 2016. Review of studies on tree species classification from remotely sensed data. Remote Sens. Environ. 186:64–87.

Fassnacht, F. E., C. Neumann, M. Förster, H. Buddenbaum, A. Ghosh, A. Clasen, P. K. Joshi, and B. Koch. 2014b. Comparison of Feature Reduction Algorithms for Classifying Tree Species With Hyperspectral Data on Three Central European Test Sites. IEEE J. Sel. Top. Appl. EARTH Obs. Remote Sens. 7:2547–2561.

Fawzy, S., A. I. Osman, J. Doran, and D. W. Rooney. 2020. Strategies for mitigation of climate change: a review. Environ. Chem. Lett. 18:2069–2094 Available at https://doi.org/10.1007/s10311-020-01059-w.

Fekety, P. A., M. J. Falkowski, A. T. Hudak, T. B. Jain, and J. S. Evans. 2018. Transferability of Lidar-derived Basal Area and Stem Density Models within a Northern Idaho Ecoregion. Can. J. Remote Sens. 44:131–143 Available at https://doi.org/10.1080/07038992.2018.1461557.

Feng, X., and P. Li. 2019. A Tree Species Mapping Method from UAV Images over Urban Area Using Similarity in Tree-Crown Object Histograms. Remote Sens. 11:1–19.

Feng, Q., J. Liu, and J. Gong. 2015. UAV Remote Sensing for Urban Vegetation Mapping Using Random Forest and Texture Analysis. Remote Sens. 7:1074–1094.

Fernández-Álvarez, M., J. Armesto, and J. Picos. 2019. LiDAR-Based Wildfire Prevention in WUI : The Automatic Detection , Measurement and Evaluation of Forest Fuels. Forests 10.

Ferreira, M. P., F. H. Wagner, L. E. O. C. Aragão, Y. E. Shimabukuro, and C. R. de Souza Filho. 2019. Tree species classification in tropical forests using visible to shortwave infrared WorldView-3 images and texture analysis. ISPRS J. Photogramm. Remote Sens. 149:119–131 Available at https://doi.org/10.1016/j.isprsjprs.2019.01.019.

© University of Pretoria

Ferreira, M. P., M. Zortea, D. C. Zanotta, Y. E. Shimabukuro, and C. R. de Souza Filho. 2016. Mapping tree species in tropical seasonal semi-deciduous forests with hyperspectral and multispectral data. Remote Sens. Environ. 179:66–78 Available at http://dx.doi.org/10.1016/j.rse.2016.03.021.

Franklin, S. E. 2017. Pixel- and object-based multispectral classification of forest tree species from small unmanned aerial vehicles. J. Unmmaned Veh. Syst. 6:195–211.

Franklin, S. E., and O. S. Ahmed. 2017. Deciduous tree species classification using object-based analysis and machine learning with unmanned aerial vehicle multispectral data multispectral data. Int. J. Remote Sens.:1–10 Available at https://doi.org/10.1080/01431161.2017.1363442.

Fraser, R. H., J. Van Der Sluijs, and R. J. Hall. 2017. Calibrating Satellite-Based Indices of Burn Severity from UAV-Derived Metrics of a Burned Boreal Forest. Remote Sens. 9:1–17.

Frost, P. 1996. The Ecology of Miombo Woodlands.Pages 11–57 in The Miombo in Transition: Woodlands and Welfare in Africa. Campbell, B., ed. Center for International Forestry Research (CIFOR), Jakarta, Indonesia.

Fuller, D. O., and T. George. 1999. Canopy phenology of some mopane and miombo woodlands in eastern Zambia. Golobal Ecol. Biogeogr.:199–209.

Fung, T., H. Fung, Y. Ma, and W. L. Siu. 2008. Band Selection Using Hyperspectral Data of Subtropical Tree Species Band Selection Using Hyperspectral Data of Subtropical Tree Species. Geocarto Int. 18:3–11.

Gibbs, H. K., S. Brown, J. O. Niles, and J. A. Foley. 2007. Monitoring and estimating tropical forest carbon stocks: Making REDD a reality. Environ. Res. Lett. 2.

Gini, R., D. Passoni, L. Pinto, and G. Sona. 2014. Use of Unmanned Aerial Systems for multispectral survey and tree classification : a test in a park area of northern Italy

© University of Pretoria

multispectral survey and tree classification : Eur. J. Remote Sens. 47:251–269.

Gini, R., G. Sona, G. Ronchetti, D. Passoni, and L. Pinto. 2018. Improving Tree Species Classification Using UAS Multispectral Images and Texture Measures. Int. J. Geo-Information 7:1–18.

Gizachew, B., and L. A. Duguma. 2016. Forest Carbon Monitoring and Reporting for REDD + : What Future for Africa ? Environ. Manage.:0–1 Available at http://dx.doi.org/10.1007/s00267-016-0762-7.

Global Drone Regulations Database. 2014. Available at https://droneregulations.info/index.html (verified 11 December 2020).

Goetz, S. J., M. Hansen, R. A. Houghton, W. Walker, N. Laporte, and J. Busch. Measurement and monitoring needs , capabilities and potential for addressing reduced emissions from deforestation and forest degradation under REDD +. Environ. Res. Lett. 10:123001 Available at http://dx.doi.org/10.1088/1748-9326/10/12/123001.

Goetz, S. J., M. Hansen, R. A. Houghton, W. Walker, N. Laporte, and J. Busch. 2015. Measurement and monitoring needs , capabilities and potential for addressing reduced emissions from deforestation and forest degradation under Measurement and monitoring needs , capabilities and potential for addressing reduced emissions from deforestatio. Environ. Res. Lett. 10.

GOFC-GOLD. 2016. A SOURCEBOOK OF METHODS AND PROCEDURES FOR MONITORING AND REPORTING ANTHROPOGENIC GREENHOUSE GAS EMISSIONS AND REMOVALS ASSOCIATED WITH DEFORESTATION , GAINS AND LOSSES OF CARBON STOCKS IN FORESTS REMAINING FORESTS , AND FORESTATION.

Gomes, M. F., and P. Maillard. 2016. Detection of Tree Crowns in Very High Spatial

© University of Pretoria

Resolution Images. Environ. Appl. Remote Sens.:41–71.

Goodwin, N. R., N. C. Coops, and D. S. Culvenor. 2006. Assessment of forest structure with airborne LiDAR and the effects of platform altitude. Remote Sens. Environ. 103:140–152.

Government of Malawi. 2018. REPUBLIC OF MALAWI NATIONAL FOREST INVENTORY 2018 Analysis Report.

GreenValley International. 2021. LiDAR360 User Guide. Available at https://eur-lex.europa.eu/legal-content/PT/TXT/PDF/?uri=CELEX:32016R0679&from=PT%0Ahttp://eur-lex.europa.eu/LexUriServ/LexUriServ.do?uri=CELEX:52012PC0011:pt:NOT (verified 23 January 2023).

GRZ. 2016. ZAMBIA ' S FOREST REFERENCE EMISSIONS LEVEL SUBMISSION TOTHE UNFCCC.

Gu, J., and R. G. Congalton. 2022. Individual Tree Crown Delineation from UAS Imagery Based on Region Growing by Over-Segments with a Competitive Mechanism. IEEE Trans. Geosci. Remote Sens. 60.

Guerra-hernández, J., D. N. Cosenza, L. Carlos, E. Rodriguez, M. Silva, M. Tomé, R. A. Díaz-varela, D. N. Cosenza, L. Carlos, E. Rodriguez, M. Silva, M. Tomé, R. A. Díaz-varela, and E. González-ferreiro. 2018. Comparison of ALS- and UAV (SfM) -derived high- density point clouds for individual tree detection in Eucalyptus plantations. Int. J. Remote Sens.:DOI: 10.1080/01431161.2018.1486519 To Available at https://doi.org/10.1080/01431161.2018.1486519.

Guimarães, N., L. Pádua, P. Marques, N. Silva, E. Peres, and J. J. Sousa. 2020. Forestry Remote Sensing from Unmanned Aerial Vehicles : A Review Focusing on the Data , Processing and Potentialities. Remote Sens. 12:1–35.

© University of Pretoria

Guo, Q., Y. Su, T. Hu, X. Zhao, F. Wu, Y. Li, J. Liu, L. Chen, G. Xu, G. Lin, Y. Zheng, Y. Lin, X. Mi, L. Fei, and X. Wang. 2017. An integrated UAV-borne lidar system for 3D habitat mapping in three forest ecosystems across China An integrated UAV-borne lidar system for 3D habitat mapping in three forest ecosystems across China. Available at http://dx.doi.org/10.1080/01431161.2017.1285083.

Guy, P. R. 1981. Changes in the Biomass and Productivity of Woodlands in the Sengwa Wildlife Research Area, Zimbabwe. J. Appl. Ecol. 18:507–519.

Guyon, I., and A. Elisseeff. 2003. An Introduction to Variable and Feature Selection. J. ofMachine Learn. Res. 3:1157–1182.

Hadush, T., A. Girma, and A. Zenebe. 2022. Tree Height Estimation from Unmanned Aerial Vehicle Imagery and Its Sensitivity on Above Ground Biomass Estimation in Dry Afromontane Forest, Northern Ethiopia. Momona Ethiop. J. Sci. 13:256–280.

Halperin, J., V. LeMay, E. Chidumayo, L. Verchot, and P. Marshall. 2016a. Model-based estimation of above-ground biomass in the miombo ecoregion of Zambia. For. Ecosyst. 3 Available at http://dx.doi.org/10.1186/s40663-016-0077-4.

Halperin, J., V. LeMay, N. Coops, L. Verchot, P. Marshall, and K. Lochhead. 2016b. Remote Sensing of Environment Canopy cover estimation in miombo woodlands of Zambia : Comparison of Landsat 8 OLI versus RapidEye imagery using parametric , nonparametric , and semiparametric methods. Remote Sens. Environ. 179:170–182 Available at http://dx.doi.org/10.1016/j.rse.2016.03.028.

Handavu, F., S. Syampungani, G. W. Sileshi, and P. W. C. Chirwa. 2021. Aboveground and belowground tree biomass and carbon stocks in the miombo woodlands of the Copperbelt in Zambia. Carbon Manag. 12:307–321 Available at https://doi.org/10.1080/17583004.2021.1926330.

© University of Pretoria

Hardin, P. J., V. Lulla, and R. R. Jensen. 2018. Small Unmanned Aerial Systems (sUAS) for environmental remote sensing : challenges and opportunities revisited. GIScience Remote Sens.:1–14 Available at https://doi.org/10.1080/15481603.2018.1510088.

He, C., S. Jia, Y. Luo, Z. Hao, and Q. Yin. 2022. Spatial Distribution and Species Association of Dominant Tree Species in Huangguan Plot of Qinling Mountains, China. Forests 13.

Hempson, G. P., S. Archibald, and W. J. Bond. 2015. A continent-wide assessment of the form and intensity of large mammal herbivory in Africa. Science (80-.). 350:1056–1061.

Hentz, K. M. Â., and M. P. Strager. 2018. Cicada (Magicicada) Tree Damage Detection Based on UAV Spectral and 3D Data. Nat. Sci. 10:31–44.

Herold, M., and F. Schiller. 2009. An assessment of national forest monitoring capabilities in tropical non-Annex I countries : Recommendations for capacity building Prepared by.

Hill, R. A., A. K. Wilson, M. George, and S. A. Hinsley. 2010. Mapping tree species in temperate deciduous woodland using time-series multi-spectral data. Appl. Veg. Sci. 13:86–99.

Hologa, R., K. Scheffczyk, C. Dreiser, and S. Gärtner. 2021. Tree species classification in a temperate mixed mountain forest landscape using random forest and multiple datasets. Remote Sens. 13:1–21.

Hopkinson, C. 2007. The influence of flying altitude, beam divergence, and pulse repetition frequency on laser pulse return intensity and canopy frequency distribution. Can. J. Remote Sens. 33:312–324.

Hosonuma, N., M. Herold, V. De Sy, R. S. De Fries, M. Brockhaus, L. Verchot, A. Angelsen, and E. Romijn. 2012. An assessment of deforestation and forest degradation drivers in developing countries. Environ. Res. Lett. 7:1–12.

© University of Pretoria

Hossain, M. D., and D. Chen. 2019. Segmentation for Object-Based Image Analysis (OBIA): A review of algorithms and challenges from remote sensing perspective. ISPRS J. Photogramm. Remote Sens. 150:115–134 Available at https://doi.org/10.1016/j.isprsjprs.2019.02.009.

Hristov, G., J. Raychev, D. Kinaneva, and P. Zahariev. 2018. Emerging Methods for Early Detection of Forest Fires Using Unmanned Aerial Vehicles and Lorawan Sensor Networks.Pages 1–9 in 2018 28th EAEEIE Annual Conference, EAEEIE 2018. IEEE, Reykjavik, Iceland.

Hsu, C.-W., C.-C. Chang, and C.-J. Lin. 2016. A Practical Guide to Support Vector Classification. Tech. Rep. Available at https://www.csie.ntu.edu.tw/~cjlin/ (verified 19 January 2023).

Huang, H., Z. Li, P. Gong, X. Cheng, N. Clinton, C. Cao, W. Ni, and L. Wang. 2011. Automated methods for measuring DBH and tree heights with a commercial scanning lidar. Photogramm. Eng. Remote Sensing 77:219–227.

Hudak, A. T., N. L. Crookston, J. S. Evans, M. J. Falkowski, A. M. S. Smith, P. E. Gessler, and P. Morgan. 2006. Regression modeling and mapping of coniferous forest basal area and tree density from discrete-return lidar and multispectral satellite data. Can. J. Remote Sens. 32:126–138.

Hudak, A. T., N. L. Crookston, J. S. Evans, D. E. Hall, and M. J. Falkowski. 2008. Nearest neighbor imputation of species-level , plot-scale forest structure attributes from LiDAR data. Remote Sens. Environ. 112:2232–2245.

Hudak, A. T., A. T. Haren, N. L. Crookston, R. J. Liebermann, and J. L. Ohmann. 2014. Imputing Forest Structure Attributes from Stand Inventory and Remotely Sensed Data in Western Oregon, USA. Fores Sci. 60:253–269.

© University of Pretoria

Iglhaut, J., C. Cabo, S. Puliti, L. Piermattei, J. O'Connor, and J. Rosette. 2019. Structure from Motion Photogrammetry in Forestry : a Review. Curr. For. Reports.

Immitzer, M., C. Atzberger, and T. Koukal. 2012. Tree Species Classification with Random Forest Using Very High Spatial Resolution 8-Band WorldView-2 Satellite Data. Remote Sens. 4:2661–2693.

Immitzer, M., S. Böck, K. Einzmann, F. Vuolo, N. Pinnel, A. Wallner, and C. Atzberger. 2017. Remote Sensing of Environment Fractional cover mapping of spruce and pine at 1 ha resolution combining very high and medium spatial resolution satellite imagery. Remote Sens. Environ.:0–1 Available at http://dx.doi.org/10.1016/j.rse.2017.09.031.

Jakubowski, M. K., W. Li, Q. Guo, and M. Kelly. 2013. Delineating individual trees from lidar data: A comparison of vector- and raster-based segmentation approaches. Remote Sens. 5:4163–4186.

Jia, Y., Z. Su, Q. Zhang, Y. Zhang, Y. Gu, and Z. Chen. 2015. Research on UAV Remote Sensing Image Mosaic Method Based on SIFT. Int. J. Signal Process. Image Process. Pattern Recognit. 8:365–374.

Jiang, Q., S. Fang, Y. Peng, Y. Gong, R. Zhu, and X. Wu. 2019. UAV-Based Biomass Estimation for Rice-Combining Spectral , TIN-Based Structural and Meteorological Features.

Kachamba, D. J., T. Eid, and T. Gobakken. 2016a. Above- and Belowground Biomass Models for Trees in the Miombo Woodlands of Malawi. Forests.

Kachamba, D. J., T. Eid, and T. Gobakken. 2017. Influence of Plot Size on Efficiency of Biomass Estimates in Inventories of Dry Tropical Forests Assisted by Photogrammetric Data from an Unmanned Aircraft System. Remote Sens. 9:1–15.

Kachamba, D. J., H. O. Ørka, T. Gobakken, T. Eid, and W. Mwase. 2016b. Biomass estimation using 3D data from unmanned aerial vehicle imagery in a tropical woodland. Remote

© University of Pretoria

Sens. 8.

Kapinga, K., S. Syampungani, R. Kasubika, A. M. Yambayamba, and H. Shamaoma. 2018. Forest Ecology and Management Species-speci fi c allometric models for estimation of the above-ground carbon stock in miombo woodlands of Copperbelt Province of Zambia. For. Ecol. Manage. 417:184–196 Available at https://doi.org/10.1016/j.foreco.2018.02.044.

Kashindye, A., E. Mtalo, M. M. Mpanda, E. Liwa, and R. Giliba. 2013. Multi-temporal assessment of forest cover, stocking parameters and above-ground tree biomass dynamics in Miombo Woodlands of Tanzania. African J. Environ. Sci. Technol. 7:611–623.

Kato, A., L. M. Moskal, P. Schiess, M. E. Swanson, D. Calhoun, and W. Stuetzle. 2009. Capturing tree crown formation through implicit surface reconstruction using airborne lidar data. Remote Sens. Environ. 113:1148–1162 Available at http://dx.doi.org/10.1016/j.rse.2009.02.010.

Kattenborn, T., J. Lopatin, M. Förster, A. C. Braun, and F. E. Fassnacht. 2019. UAV data as alternative to field sampling to map woody invasive species based on combined Sentinel-1 and Sentinel-2 data. Remote Sens. Environ. 227:61–73 Available at https://doi.org/10.1016/j.rse.2019.03.025.

Kelcey, J., and A. Lucieer. 2013. IEEE International Geoscience and Remote Sensing Symposium (IGARSS).Pages 3884–3886 in AN ADAPTIVE TEXTURE SELECTION FRAMEWORK FOR ULTRA-HIGH RESOLUTION UAV IMAGERY. Melbourne, Australia 21–26 July 2013.

Kerr, J. T., and M. Ostrovsky. 2003. From space to species: Ecological applications for remote sensing. Trends Ecol. Evol. 18:299–305.

Key, T., T. A. Warner, J. B. Mcgraw, and M. A. Fajvan. 2001. A Comparison of Multispectral and Multitemporal Information in High Spatial Resolution Imagery for Classification of

© University of Pretoria

Individual Tree Species in a Temperate Hardwood Forest. Remote Sens. Environ. 75:100–112.

Kolarik, N. E., A. E. Gaughan, F. R. Stevens, N. G. Pricope, K. Woodward, L. Cassidy, J. Salerno, and J. Hartter. 2020. A multi-plot assessment of vegetation structure using a micro-unmanned aerial system (UAS) in a semi-arid savanna environment. ISPRS J. Photogramm. Remote Sens. 164:84–96 Available at https://doi.org/10.1016/j.isprsjprs.2020.04.011.

Kollert, A., M. Bremer, M. Löw, and M. Rutzinger. 2021. Exploring the potential of land surface phenology and seasonal cloud free composites of one year of Sentinel-2 imagery for tree species mapping in a mountainous region. Int. J. Appl. Earth Obs. Geoinf. 94:102208 Available at https://doi.org/10.1016/j.jag.2020.102208.

Korhonen, L., and F. Morsdorf. 2014. Estimation of Canopy Cover, Gap Fraction and Leaf Area Index with Airborne Laser.Pages 397–417 in Forest Applications of Airborne Laser Scanning: Concepts and Case Studies. Maltamo, M., Naesset, E., Vauhkonen, J., eds. Springer, Dordrecht.

Kraus, K., and N. Pfeifer. 1998. Determination of terrain models in wooded areas with airborne laser scanner data. ISPRS J. Photogramm. Remote Sens. 53:193–203.

Kuželka, K., M. Slavík, and P. Surový. 2020. Very High Density Point Clouds from UAV Laser Scanning for Automatic Tree Stem Detection and Direct Diameter Measurement. Remote Sens. 12:doi:10.3390/rs12081236 Available at 10.3390/rs12081236.

Lang, S. 2008. Object-based image analysis for remote sensing applications : modeling reality – dealing with complexity.Pages 3–27 in Lecture Notes in Geoinformation and Cartography. Blaschke, T., Lang, S., J., H.G., eds. Springer.

Law, B. E., and R. H. Waring. 2015. Carbon implications of current and future effects of

© University of Pretoria

drought, fire and management on Pacific Northwest forests. For. Ecol. Manage. 355:4–14 Available at http://dx.doi.org/10.1016/j.foreco.2014.11.023.

Lefsky, M. A., W. B. Cohen, D. J. Harding, G. G. Parker, S. A. Acker, and S. T. Gower. 2002. Lidar remote sensing of above-ground biomass in three biomes. Glob. Ecol. Biogeogr. 11:393–399.

Lefsky, M. A., A. T. Hudak, W. B. Cohen, and S. A. Acker. 2005. Patterns of covariance between forest stand and canopy structure in the Pacific Northwest. Remote Sens. Environ. 95:517–531.

Levick, S. R., G. P. Asner, T. Kennedy-Bowdoin, and D. E. Knapp. 2009. The relative influence of fire and herbivory on savanna three-dimensional vegetation structure. Biol. Conserv. 142:1693–1700 Available at http://dx.doi.org/10.1016/j.biocon.2009.03.004.

Li, Y., H.-E. Andersen, and R. McGaughey. 2008. A Comparison of Statistical Methods for Estimating Data. West. J. Appl. For. For. 23:223–231.

Lillesand, T. M., R. W. Kiefer, and J. W. Chipma. 2015. Remote Sensing and Image Interpretation. 7th Editio. Wiley.

Lim, J., K. M. Kim, and R. Jin. 2019. Tree species classification using hyperion and sentinel-2 data with machine learning in South Korea and China. ISPRS Int. J. Geo-Information 8.

Lim, K., P. Treitz, K. Baldwin, I. Morrison, and J. Green. 2003a. Lidar remote sensing of biophysical properties of tolerant northern hardwood forests. Can. J. Remote Sens. 29:658–678.

Lim, K., P. Treitz, M. Wulder, and M. Flood. 2003b. LiDAR remote sensing of forest structure. Prog. Phys. Geogr. 27:88–106.

Lin, Y., J. Hyyppä, and A. Jaakkola. 2011. Mini-UAV-borne LIDAR for fine-scale mapping.

© University of Pretoria

IEEE Geosci. Remote Sens. Lett. 8:426–430.

Lisein, J., A. Michez, H. Claessens, and P. Lejeune. 2015. Discrimination of Deciduous Tree Species from Time Series of Unmanned Aerial System Imagery. PLoS One 10:1–20.

Lisein, J., M. Pierrot-deseilligny, P. Lejeune, and N. Management. 2013. A Photogrammetric Workflow for the Creation of a Forest Canopy Height Model from Small Unmanned Aerial System Imagery. :922–944.

Liu, T., A. Abd-Elrahman, J. Morton, and V. L. Wilhelm. 2018a. Comparing fully convolutional networks, random forest, support vector machine, and patch-based deep convolutional neural networks for object-based wetland mapping using images from small unmanned aircraft system. GIScience Remote Sens. 55:243–264 Available at https://doi.org/10.1080/15481603.2018.1426091.

Liu, K., X. Shen, L. Cao, G. Wang, and F. Cao. 2018b. Estimating forest structural attributes using UAV-LiDAR data in Ginkgo plantations. ISPRS J. Photogramm. Remote Sens. 146:465–482 Available at https://doi.org/10.1016/j.isprsjprs.2018.11.001.

Lu, J., H. Wang, S. Qin, L. Cao, R. Pu, G. Li, and J. Sun. 2020. Estimation of aboveground biomass of Robinia pseudoacacia forest in the Yellow River Delta based on UAV and Backpack LiDAR point clouds. Int. J. Appl. Earth Obs. Geoinf. 86.

Luoga, E. J., E. T. F. Witkowski, and K. Balkwill. 2002. Harvested and standing wood stocks in protected and communal miombo woodlands of eastern Tanzania. For. Ecol. Manage. 164:15–30.

Macave, O. A., N. S. Ribeiro, A. I. Ribeiro, A. Chaúque, R. Bandeira, C. Branquinho, and R. Washington-Allen. 2022. Modelling Aboveground Biomass of Miombo Woodlands in Niassa Special Reserve, Northern Mozambique. Forests 13:1–16.

Madonsela, S., M. Azong, R. Mathieu, O. Mutanga, A. Ramoelo, R. Van De Kerchove, and E.

© University of Pretoria

Wolff. 2017. International Journal of Applied Earth Observation and Geoinformation Multi-phenology WorldView-2 imagery improves remote sensing of savannah tree species. Int. J. Appl. Earth Obs. Geoinf. 58:65–73.

Madonsela, S., M. Azong, A. Ramoelo, and O. Mutanga. 2018. Estimating tree species diversity in the savannah using NDVI and woody canopy cover. Int J Appl Earth Obs Geoinf. 66:106–115 Available at https://doi.org/10.1016/j.jag.2017.11.005.

Magnussen, S., and P. Boudewyn. 1998. Derivations of stand heights from airborne laser scanner data with canopy-based quantile estimators. Can. J. For. Res. 28:1016–1031.

Maltamo, M., E. Naesset, and J. Vauhkonen. 2014a. Forestry Applications of Airborne Laser Scanning (M Maltamo, E Næsset, and J Vauhkonen, Eds.). Springer Netherlands, Dordrecht.

Maltamo, M., E. Naesset, and J. Vauhkonen. 2014b. Forestry Applications of Airborne Laser Scanning: Concepts and Case Studies (K von Gadow, T Pukkala, and Margarida Tomé, Eds.). Springer, Newyork.

Mao, P., J. Ding, B. Jiang, L. Qin, and G. Y. Qiu. 2022. How can UAV bridge the gap between ground and satellite observations for quantifying the biomass of desert shrub community? ISPRS J. Photogramm. Remote Sens. 192:361–376 Available at https://doi.org/10.1016/j.isprsjprs.2022.08.021.

Mareya, H. T., P. Tagwireyi, H. Ndaimani, T. W. Gara, and D. Gwenzi. 2018. Estimating Tree Crown Area and Aboveground Biomass in Miombo Woodlands from High-Resolution RGB-Only Imagery. IEEE J. Sel. Top. Appl. Earth Obs. Remote Sens. 11:868–875.

Matasci, G., T. Hermosilla, M. A. Wulder, J. C. White, N. C. Coops, G. W. Hobart, and H. S. J. Zald. 2018. Large-area mapping of Canadian boreal forest cover, height, biomass and other structural attributes using Landsat composites and lidar plots. Remote Sens.

© University of Pretoria

Environ. 209:90–106 Available at https://doi.org/10.1016/j.rse.2017.12.020.

Mauya, E. W., L. T. Ene, O. M. Bollandsås, T. Gobakken, E. Næsset, R. E. Malimbwi, and E. Zahabu. 2015. Modelling aboveground forest biomass using airborne laser scanner data in the miombo woodlands of Tanzania. Carbon Balance Manag. 10:1–16.

Mauya, E. W., and S. Madundo. 2022. Modelling Above Ground Biomass Using Sentinel 2 and Planet Scope Data in Dense Tropical Montane Forests of Tanzania. Tanzania J. For. Nat. Conserv. 91:132–153.

Mayes, M. T., J. F. Mustard, and J. M. Melillo. 2015. Remote Sensing of Environment Forest cover change in Miombo Woodlands : modeling land cover of African dry tropical forests with linear spectral mixture analysis. Remote Sens. Environ. 165:203–215 Available at http://dx.doi.org/10.1016/j.rse.2015.05.006.

Mayr, M. J., S. Malß, E. Ofner, and C. Samimi. 2018. Disturbance feedbacks on the height of woody vegetation in a savannah: a multi-plot assessment using an unmanned aerial vehicle (UAV). Int. J. Remote Sens. 39:4761–4785 Available at https://doi.org/10.1080/01431161.2017.1362132.

Mäyrä, J., S. Keski-Saari, S. Kivinen, T. Tanhuanpää, P. Hurskainen, P. Kullberg, L. Poikolainen, A. Viinikka, S. Tuominen, T. Kumpula, and P. Vihervaara. 2021. Tree species classification from airborne hyperspectral and LiDAR data using 3D convolutional neural networks. Remote Sens. Environ. 256.

Mckenna, P., P. D. Erskine, A. M. Lechner, and S. Phinn. 2017. Measuring fire severity using UAV imagery in semi- arid central Queensland , Australia. Int. J. Remote Sens. 38:4244–4264 Available at https://doi.org/10.1080/01431161.2017.1317942.

Means, J. E., S. A. Acker, B. J. Fitt, M. Renslow, L. Emerson, and C. J. Hendrix. 2000. Predicting Forest Stand Characteristics with Airborne Scanning Lidar. Photogramm. Eng.

© University of Pretoria

Remote Sens. 66:1367–1371.

Merino, L., F. Caballero, J. R. Martínez-De-Dios, I. Maza, and A. Ollero. 2012. An unmanned aircraft system for automatic forest fire monitoring and measurement. J. Intell. Robot. Syst. Theory Appl. 65:533–548.

Miller, J. D., and A. E. Thode. 2007. Quantifying burn severity in a heterogeneous landscape with a relative version of the delta Normalized Burn Ratio (dNBR). Remote Sens. Environ. 109:66–80.

Minarik, R., and J. Langhammer. 2016. USE OF A MULTISPECTRAL UAV PHOTOGRAMMETRY FOR DETECTION AND TRACKING OF FOREST DISTURBANCE DYNAMICS.in The International Archives of the Photogrammetry , Remote Sensing and Spatial Information Sciences, Voluma XLI-B8, 2016 XXIII ISPRS Congress, 12-19 July 2016. Prague, Czech Republic.

Mishra, N. B., K. P. Mainali, B. B. Shrestha, J. Radenz, and D. Karki. 2018. Species-level Vegetation Mapping in a Himalayan Treeline Ecotone using Species-Level Vegetation Mapping in a Himalayan Treeline Ecotone Using Unmanned Aerial System (UAS) Imagery. 7:1–16.

Mitchell, A. L., A. Rosenqvist, and B. Mora. 2017. Current remote sensing approaches to monitoring forest degradation in support of countries measurement , reporting and verification (MRV) systems for REDD +. Carbon Balance Manag. 12:1–22.

Mlambo, R., I. H. Woodhouse, F. Gerard, and K. Anderson. 2017. Structure from Motion (SfM) Photogrammetry with Drone Data : A Low Cost Structure from Motion (SfM) Photogrammetry with Drone Data : A Low Cost Method for Monitoring Greenhouse Gas Emissions from Forests in Developing Countries. Forests 8.

Mohan, M., C. A. Silva, C. Klauberg, P. Jat, G. Catts, A. T. Hudak, and M. Dia. 2017.

© University of Pretoria

Individual Tree Detection from Unmanned Aerial Vehicle (UAV) Derived Canopy Height Model in an Open Canopy Mixed Conifer Forest. Forestry 8:340.

Morin, D., M. Planells, D. Guyon, L. Villard, S. Mermoz, A. Bouvet, H. Thevenon, J. F. Dejoux, T. Le Toan, and G. Dedieu. 2019. Estimation and mapping of forest structure parameters from open access satellite images: Development of a generic method with a study case on coniferous plantation. Remote Sens. 11.

Mountrakis, G., J. Im, and C. Ogole. 2011. Support vector machines in remote sensing: A review. ISPRS J. Photogramm. Remote Sens. 66:247–259 Available at http://dx.doi.org/10.1016/j.isprsjprs.2010.11.001.

Mugasha, W. ., T. Eid, O. M. Bollandsås, R. E. Malimbwi, S. A. . Chamshama, E. Zahabu, and J. Z. Katani. 2012. Allometric models for prediction of aboveground biomass of single trees in miombo woodlands in Tanzania.Pages 8–17 in Proceedings of the first Climate Change Impacts, Mitigation and Adaptation Programme Scientific Conference.

Mugasha, W. A., T. Eid, O. M. Bollandsås, R. E. Malimbwi, S. A. O. Chamshama, E. Zahabu, and J. Z. Katani. 2013. Allometric models for prediction of above- and belowground biomass of trees in the miombo woodlands of Tanzania. For. Ecol. Manage. 310:87–101 Available at http://dx.doi.org/10.1016/j.foreco.2013.08.003.

Muhe, S., and M. Argaw. 2022. Estimation of above-ground biomass in tropical afro-montane forest using Sentinel-2 derived indices. Environ. Syst. Res. 11 Available at https://doi.org/10.1186/s40068-022-00250-y.

Müllerová, J., J. Bruna, T. Bartaloš, P. Dvorák, M. Vítková, and P. Pyšek. 2017. Timing Is Important_ Unmanned Aircraft vs. Satellite Imagery in Plant Invasion Monitoring. Front. Plant Sci. 8.

Naesset, E. 1997. Estimating timber volume of forests stands using laser scanner data. Remote

© University of Pretoria

Sens. Environ. 67:246–253.

Naesset, E. 2007. Airborne laser scanning as a method in operational forest inventory: Status of accuracy assessments accomplished in Scandinavia. Scand. J. For. Res. 22:433–442.

Næsset, E. 2009. Effects of different sensors, flying altitudes, and pulse repetition frequencies on forest canopy metrics and biophysical stand properties derived from small-footprint airborne laser data. Remote Sens. Environ. 113:148–159 Available at http://dx.doi.org/10.1016/j.rse.2008.09.001.

Næsset, E., O. M. Bollandsås, and T. Gobakken. 2005. Comparing regression methods in estimation of biophysical properties of forest stands from two different inventories using laser scanner data. Remote Sens. Environ. 94:541–553.

Naesset, E., T. Gobakken, J. Holmgren, and M. Maltamo. 2004. Laser scanning of forest resources : The Nordic experience Laser Scanning of Forest Resources : The Nordic Experience.

Næsset, E., H. O. Ørka, S. Solberg, O. M. Bollandsås, E. H. Hansen, E. Mauya, E. Zahabu, R. Malimbwi, N. Chamuya, H. Olsson, and T. Gobakken. 2016. Mapping and estimating forest area and aboveground biomass in miombo woodlands in Tanzania using data from airborne laser scanning, TanDEM-X, RapidEye, and global forest maps: A comparison of estimated precision. Remote Sens. Environ. 175:282–300 Available at http://dx.doi.org/10.1016/j.rse.2016.01.006.

Nagendra, H., and D. Rocchini. 2008. High resolution satellite imagery for tropical biodiversity studies: The devil is in the detail. Biodivers. Conserv. 17:3431–3442.

Naidoo, L., M. A. Cho, R. Mathieu, and G. Asner. 2012. Classification of savanna tree species , in the Greater Kruger National Park region , by integrating hyperspectral and LiDAR data in a Random Forest data mining environment. ISPRS J. Photogramm. Remote Sens.

© University of Pretoria

69:167–179 Available at http://dx.doi.org/10.1016/j.isprsjprs.2012.03.005.

Nandy, S., R. Srinet, and H. Padalia. 2021. Mapping Forest Height and Aboveground Biomass by Integrating ICESat-2, Sentinel-1 and Sentinel-2 Data Using Random Forest Algorithm in Northwest Himalayan Foothills of India. Geophys. Res. Lett. 48:1–10.

Navarro, J. A., N. Algeet, A. Fernández-Landa, J. Esteban, P. Rodríguez-Noriega, and M. L. Guillén-Climent. 2019. Integration of UAV, Sentinel-1, and Sentinel-2 data for mangrove plantation aboveground biomass monitoring in Senegal. Remote Sens. 11:1–23.

Nebikera, S., A. Annena, M. Scherrerb, and D. Oeschc. 2008. Multispectral Sensor for Micro UAV – Opportunities for Very High Resolution Airborne Remote Sensing.Pages 1193–1200 in The International Archives of the Photogrammetry, Remote Sensing and Spatial Information Sciences. Vol. XXXVII. Part B1. Beijing 2008.

Nelson, R., J. Boudreau, T. G. Gregoire, H. Margolis, E. Næsset, T. Gobakken, and G. Ståhl. 2009. Estimating Quebec provincial forest resources using ICESat/GLAS. Can. J. For. Res. 39:862–881.

Nelson, R., H. Margolis, P. Montesano, G. Sun, B. Cook, L. Corp, H. E. Andersen, B. deJong, F. P. Pellat, T. Fickel, J. Kauffman, and S. Prisley. 2017. Lidar-based estimates of aboveground biomass in the continental US and Mexico using ground, airborne, and satellite observations. Remote Sens. Environ. 188:127–140 Available at http://dx.doi.org/10.1016/j.rse.2016.10.038.

Nevalainen, O., E. Honkavaara, S. Tuominen, N. Viljanen, T. Hakala, X. Yu, J. Hyyppä, H. Saari, I. Pölönen, N. N. Imai, and A. M. G. Tommaselli. 2017. Individual tree detection and classification with UAV-Based photogrammetric point clouds and hyperspectral imaging. Remote Sens. 9.

Ota, T., O. S. Ahmed, S. Thu, T. Cin, and N. Mizoue. 2019. Forest Ecology and Management

© University of Pretoria

Estimating selective logging impacts on aboveground biomass in tropical forests using digital aerial photography obtained before and after a logging event from an unmanned aerial vehicle. For. Ecol. Manage. 433:162–169 Available at https://doi.org/10.1016/j.foreco.2018.10.058.

Otu-Larbi, F., A. Conte, S. Fares, O. Wild, and K. Ashworth. 2020. Current and future impacts of drought and ozone stress on Northern Hemisphere forests. Glob. Chang. Biol. 26:6218–6234.

Pádua, L., J. Vanko, J. Hruška, T. Adão, J. J. Sousa, E. Peres, and R. Morais. 2017. UAS , sensors , and data processing in agroforestry : a review towards practical applications. Int. J. Remote Sens.:1–43 Available at http://dx.doi.org/10.1080/01431161.2017.1297548.

Pal, N. R., and S. K. Pal. 1993. A review on image segmentation techniques. Parttern Recognit. 26:1277–1294.

Park, J. Y., H. C. Muller-landau, J. W. Lichstein, S. W. Rifai, J. P. Dandois, and S. A. Bohlman. 2019. Quantifying Leaf Phenology of Individual Trees and Species in a Tropical Forest Using Unmanned Aerial Vehicle (UAV) Images. Remote Sens. 11.

Poley, L. G., and G. J. McDermid. 2020. A Systematic Review of the Factors Influencing the Estimation of Vegetation Aboveground Biomass Using Unmanned Aerial Systems. Remote Sens. 12:1–46.

Popescu, S. c., and M. Hauglin. 2014. Estimation of Biomass Components by Airborne Laser Scanning.Pages 157–175 in Forest Application of Airborne Laser Scanning: Concepts and Case Studies, Managing Forest Ecosystems. Maltamo, M., Naesset, E., Vauhkonen, J., eds.

Prasetiyowati, M. I., N. U. Maulidevi, and K. Surendro. 2020. Feature selection to increase the random forest method performance on high dimensional data. Int. J. Adv. Intell. Informatics 6:303–312.

© University of Pretoria

Pu, R. 2014. Tree species Classifcation.Pages 1–529 in Remote Sensing of Natural Resources. Wang, G., Weng, Q., eds. CRC Press, Taylor & Francis Group.

Puliti, S. 2018. Tree-Stump Detection , Segmentation , Classification , and Measurement Using Unmanned Aerial Vehicle (UAV) Imagery.

Puliti, S., L. T. Ene, T. Gobakken, and E. Næsset. 2017. Use of partial-coverage UAV data in sampling for large scale forest inventories. Remote Sens. Environ. 194:115–126 Available at http://dx.doi.org/10.1016/j.rse.2017.03.019.

Rango, A., and A. S. Laliberte. 2010. Impact of flight regulations on effective use of unmanned aircraft systems for natural resources applications. J. Appl. Remote Sens. 4:1–12.

Reutebuch, S. E., R. J. Mcgaughey, H. Andersen, and W. W. Carson. 2003. Accuracy of a high-resolution lidar terrain model under a conifer forest canopy. Can. J. Remote Sens. 29:527–535.

Ribeiro, N., M. Cumbana, F. Mamugy, and A. Chaúque. 2012. Remote Sensing of Biomass in the Miombo Woodlands of Southern Africa : Opportunities and Limitations for Research.Pages 77–98 in Remote Sensing of Biomass – Principles and Applications. Fatoyinbo, T., ed. InTech., Rijeka, Croatia.

Ribeiro, N. S., P. L. S. de Miranda, and J. Timberlake. 2020a. Biogeography and Ecology of Miombo Woodlands.Pages 9–53 in Miombo Woodlands in a Changing Environment : Securing the Resilience and Sustainability of People and Woodlands. Ribeiro, N.S., Yemi, K., Chirwa, P.W., Grundy, I.M., eds.

Ribeiro, N. S., P. L. S. de Miranda, and J. Timberlake. 2020b. Miombo Woodlands in a Changing Environment: Securing the Resilience and Sustainability of People and Woodlands.Pages 188–189 in Miombo Woodlands in a Changing Sustainability of People the Resilience and Environment: Securing and Woodlands. Ribeiro, N.S., Katerere, Y.,

© University of Pretoria

Chirwa, P.W., Grundy, I.M., eds. Springer Nature Switzerland.

Ribeiro, N. S., H. H. Shugart, and R. Washington-Allen. 2008. The effects of fire and elephants on species composition and structure of the Niassa Reserve, northern Mozambique. For. Ecol. Manage. 255:1626–1636.

Ribeiro, N. S., S. Syampungani, N. M. Matakala, D. Nangoma, and R. A. Isabel. 2015. Miombo Woodlands Research Towards the Sustainable Use of Ecosystem Services in Southern Africa.in Miombo Woodlands Research Towards the Sustainable Use of Ecosystem Services in Southern Africa.

Riihimäki, H., M. Luoto, and J. Heiskanen. 2019. Estimating fractional cover of tundra vegetation at multiple scales using unmanned aerial systems and optical satellite data. Remote Sens. Environ. 224:119–132 Available at https://doi.org/10.1016/j.rse.2019.01.030.

Rivas-Torres, G. F., F. L. Benítez, D. Rueda, C. Sevilla, and C. F. Mena. 2018. A methodology for mapping native and invasive vegetation coverage in archipelagos: An example from the Galápagos Islands. Prog. Phys. Geogr. 42:83–111.

Romijn, E., M. Herold, L. Kooistra, D. Murdiyarso, and L. Verchot. 2012. Assessing capacities of non-Annex I countries for national forest monitoring in the context of REDD +. Environ. Sci. Policy 19–20:33–48 Available at http://dx.doi.org/10.1016/j.envsci.2012.01.005.

Ryan, C. M., M. Williams, and J. Grace. 2011a. Above- and Belowground Carbon Stocks in a Miombo Woodland Landscape of Mozambique. Biotropica 43:423–432.

Ryan, C. M., M. Williams, and J. Grace. 2011b. Above - and Belowground Carbon Stocks in a Miombo Woodland Landscape of Above- and Belowground Carbon Stocks in a Miombo Woodland.

Samiappan, S., G. Turnage, C. Mccraine, J. Skidmore, L. Hathcock, and R. Moorhead. 2017.

© University of Pretoria

Post-Logging Estimation of Loblolly Pine (Pinus taeda) Stump Size , Area and Population Using Imagery from a Small Unmanned Aerial System.

Samimi, C., and T. Kraus. 2004. Biomass estimation using Landsat-TM and -ETM+. Towards a regional model for Southern Africa? GeoJournal 59:177–187.

Sankey, T., J. Donager, J. McVay, and J. B. Sankey. 2017. UAV lidar and hyperspectral fusion for forest monitoring in the southwestern USA. Remote Sens. Environ. 195:30–43 Available at http://dx.doi.org/10.1016/j.rse.2017.04.007.

Sedano, F., P. Gong, and M. Ferra. 2005. Land cover assessment with MODIS imagery in southern African Miombo ecosystems. 98:429–441.

Sedano, F., S. N. Lisboa, L. Duncanson, N. Ribeiro, A. Sitoe, R. Sahajpal, and G. Hurtt. 2020a. Monitoring forest degradation from charcoal production with historical Landsat imagery . A case study in southern Mozambique Monitoring forest degradation from charcoal production with historical Landsat imagery . A case study in southern Mozambique.

Sedano, F., S. Lisboa, L. Duncanson, N. Ribeiro, A. Sitoe, R. Sahajpal, G. Hurtt, and C. Tucker. 2020b. Int J Appl Earth Obs Geoinformation Monitoring intra and inter annual dynamics of forest degradation from charcoal production in Southern Africa with Sentinel – 2 imagery. Int J Appl Earth Obs Geoinf. 92:102184 Available at https://doi.org/10.1016/j.jag.2020.102184.

SEPAL. System for Earth Observation Data Access, Processing and Analysis for Land Monitoring. Available at https://sepal.io (verified 13 April 2023).

Shamaoma, H., P. W. Chirwa, A. Ramoelo, A. T. Hudak, and S. Syampungani. 2022. The Application of UASs in Forest Management and Monitoring : Challenges and Opportunities for Use in the Miombo Woodland. Forests 13.

Shamaoma, H., N. Kerle, and D. Alkema. 2006. Extraction of Flood-Modelling Related Base-

© University of Pretoria

Data From Multi- Source Remote Sensing Imagery.in Commission VII, WG/7: Problem Solving Methodologies for Less Developed Countries. Kerle, N., Skidmore, A., eds. The International Society for Photogrammetry and Remote Sensing, Enschede, The Netherlands.

Shen, X., L. Cao, B. Yang, Z. Xu, and G. Wang. 2019. Estimation of Forest Structural Attributes Using Spectral Indices and Point Clouds from UAS-Based. Remote Sens. 11:1–24.

Shi, C., and L. Wang. 2014. Incorporating spatial information in spectral unmixing: A review. Remote Sens. Environ. 149:70–87 Available at http://dx.doi.org/10.1016/j.rse.2014.03.034.

Shin, P., T. Sankey, M. M. Moore, and A. E. Thode. 2018. Evaluating Unmanned Aerial Vehicle Images for Estimating Forest Canopy Fuels in a Ponderosa Pine Stand. Remote Sens.:2–22.

Shin, J., W. Seo, T. Kim, J. Park, and C. Woo. 2019. Using UAV Multispectral Images for Classification of Forest Burn Severity — A Case Study of the 2019 Gangneung Forest Fire. Forests 10.

Siewert, M. B., and J. Olofsson. 2021. UAV reveals substantial but heterogeneous effects of herbivores on Arctic vegetation. Sci. Rep. 11 Available at https://doi.org/10.1038/s41598-021-98497-5.

Singh, M., D. Evans, B. S. Tan, and C. S. Nin. 2015. Mapping and Characterizing Selected Canopy Tree Species at the Angkor World Heritage Site in Cambodia Using Aerial Data. PLoS One 10:1–26.

Smigaj, M., R. Gaulton, S. L. Barr, J. C. Suárez, C. Vi, and W. G. Vi. 2015. The International Archives of the Photogrammetry, Remote Sensing and Spatial Information Sciences, Volume XL-3/W3, 2015 ISPRS Geospatial Week 2015, 28 Sep – 03 Oct 2015, La Grande Motte, France.Pages 349–354 in UAV-BORNE THERMAL IMAGING FOR FOREST

© University of Pretoria

HEALTH MONITORING: DETECTION OF DISEASE-INDUCED CANOPY TEMPERATURE INCREASE M. G. Rabatel and M. Pierrot-Deseilligny, ed. La Grande Motte, France.

Snavely, N., S. M. Seitz, and R. Szeliski. 2007. Modeling the World from Internet Photo Collections. Int. J. Comput. Vis. 6:245–255.

Somers, B., and G. P. Asner. 2013. Multi-temporal hyperspectral mixture analysis and feature selection for invasive species mapping in rainforests. Remote Sens. Environ. 136:14–27 Available at http://dx.doi.org/10.1016/j.rse.2013.04.006.

Souza, C. M., D. A. Roberts, and M. A. Cochrane. 2005. Combining spectral and spatial information to map canopy damage from selective logging and forest fires. Remote Sens. Environ. 98:329–343.

Souza, C. M., J. V Siqueira, M. H. Sales, A. V Fonseca, J. G. Ribeiro, I. Numata, M. A. Cochrane, C. P. Barber, D. A. Roberts, and J. Barlow. 2013. Ten-Year Landsat Classification of Deforestation and Forest Degradation in the Brazilian Amazon. Remote Sens. 5:5493–5513.

Sprott, A. H., and J. M. Piwowar. 2021. How to recognize different types of trees from quite a long way away: combining UAV and spaceborne imagery for stand-level tree species identification. J. Unmanned Veh. Syst. 9:166–181.

Stöcker, C., R. Bennett, F. Nex, M. Gerke, and J. Zevenbergen. 2017. Review of the Current State of UAV Regulations. Remote Sens. 9:1–26.

Stringer, L. C., A. J. Dougill, D. D. Mkwambisi, J. C. Dyer, F. K. Kalaba, and M. Mngoli. 2012. Challenges and opportunities for carbon management in Malawi and Zambia. Carbon Manag. 3:159–173.

Su, Y., Q. Guo, B. Xue, T. Hu, O. Alvarez, S. Tao, and J. Fang. 2016. Spatial distribution of

© University of Pretoria

forest aboveground biomass in China: Estimation through combination of spaceborne lidar, optical imagery, and forest inventory data. Remote Sens. Environ. 173:187–199 Available at http://dx.doi.org/10.1016/j.rse.2015.12.002.

Sugiura, N. 1978. Further Analysis of the Data by Anaike' S Information Criterion and the Finite Corrections. Commun. Stat. - Theory Methods 7:13–26.

Syampungani, S., P. W. Chirwa, F. K. Akinnifesi, G. Sileshi, and O. C. Ajayi. 2009. The miombo woodlands at the cross roads : Potential threats , sustainable livelihoods , policy gaps and challenges. 33:150–159.

Syampungani, S., C. J. Geldenhuys, and P. W. Chirwa. 2011. Journal of Natural Resources Policy Miombo Woodland Utilization and Management , and Impact Perception among Stakeholders in Zambia : A Call for Policy Change in Southern Africa. :37–41.

Tang, L., and G. Shao. 2015. Drone remote sensing for forestry research and practices. J. For. Res. 26:791–797.

Thiel, C., M. M. Müller, C. Berger, F. Cremer, S. Hese, J. Baade, F. Klan, and C. Pathe. 2020. Monitoring Selective Logging in a Pine-Dominated Forest in Central Germany with Repeated Drone Flights Utilizing A Low Cost RTK Quadcopter.

Thomson, P. J. 1975. The role of elephants, fire and other agents in the decline of a Brachystegia boehmii woodland. J. South. African Wildl. Manag. Assoc. 5:11–18 Available at http://scholar.google.com/scholar?hl=en&btnG=Search&q=intitle:The+role+of+elephants,+fire+and+other+agents+in+the+decline+of+a+Brachystegia+boehmii+woodland#0.

Tomaštík, J., M. Mokroš, P. Surový 2, A. Grznárová, and J. Merganič. 2019. UAV RTK / PPK Method — An Optimal Solution for Mapping Inaccessible Forested Areas ? Remote Sens. 11:1–19.

© University of Pretoria

Tomppo, E., H. Olsson, G. Ståhl, M. Nilsson, O. Hagner, and M. Katila. 2008. Combining national forest inventory field plots and remote sensing data for forest databases. Remote Sens. Environ. 112:1982–1999.

Torres, D. L., R. Q. Feitosa, P. N. Happ, L. E. C. La Rosa, J. M. Junior, J. Martins, P. O. Bressan, W. N. Gonçalves, and V. Liesenberg. 2020. Applying fully convolutional architectures for semantic segmentation of a single tree species in urban environment on high resolution UAV optical imagery. Sensors 20.

Torresan, C., A. Berton, F. Carotenuto, S. F. Di, B. Gioli, A. Matese, F. Miglietta, A. Zaldei, L. Wallace, C. Torresan, A. Berton, F. Carotenuto, and S. F. Di. 2017. Forestry applications of UAVs in Europe : a review. Int. J. Remote Sens. 38:2427–2447 Available at http://dx.doi.org/10.1080/01431161.2016.1252477.

Trimble. 2018. eCognition Developer User Guide. Version 9. Trimble Germany GmbH, Munic, Germany.

Turner, W., S. Spector, N. Gardiner, M. Fladeland, E. Sterling, and M. Steininger. 2003. Remote sensing for biodiversity science and conservation. Trends Ecol. Evol. 18:306–314.

UNFCCC. 2015. ADOPTION OF THE PARIS AGREEMENT Proposal by the President. 21930 Available at http://unfccc.int/resource/docs/2015/cop21/eng/109.pdf (verified 21 November 2019).

Valero, M. M., O. Rios, C. Mata, E. Pastor, and E. Planas. 2017. An integrated approach for tactical monitoring and data-driven spread forecasting of wild fires. Fire Saf. J. 91:835–844 Available at http://dx.doi.org/10.1016/j.firesaf.2017.03.085.

Vastaranta, M., M. Holopainen, X. Yu, R. Haapanen, T. Melkas, J. Hyyppä, and H. Hyyppä. 2011. INDIVIDUAL TREE DETECTION AND AREA-BASED APPROACH IN RETRIEVAL OF FOREST INVENTORY CHARACTERISTICS FROM LOW-PULSE

© University of Pretoria

AIRBORNE LASER SCANNING DATA. 22:1–13.

Wallace, L., A. Lucieer, Z. Malenovskỳ, D. Turner, and P. Vopěnka. 2016. Assessment of forest structure using two UAV techniques: A comparison of airborne laser scanning and structure from motion (SfM) point clouds. Forests 7:1–16.

Wallace, L. O., A. Lucieer, and C. S. Watson. 2012a. International Archives of the Photogrammetry, Remote Sensing and Spatial Information Sciences.Pages 499–504 in ASSESSING THE FEASIBILITY OF UAV-BASED LIDAR FOR HIGH RESOLUTION FOREST CHANGE DETECTION. XXII ISPRS Congress, Melbourne, Australia.

Wallace, L., A. Lucieer, and C. S. Watson. 2014. Evaluating Tree Detection and Segmentation Routines on Very High Resolution UAV LiDAR Data. IEEE Trans. Geosci. Remote Sens. 52:7619–7628.

Wallace, L., A. Lucieer, C. Watson, and D. Turner. 2012b. Development of a UAV-LiDAR system with application to forest inventory. Remote Sens. 4:1519–1543.

Wallis, C. I. B., J. Homeier, J. Peña, R. Brandl, N. Farwig, and J. Bendix. 2019. Modeling tropical montane forest biomass, productivity and canopy traits with multispectral remote sensing data. Remote Sens. Environ. 225:77–92 Available at https://doi.org/10.1016/j.rse.2019.02.021.

Wang, D., B. Wan, J. Liu, Y. Su, Q. Guo, P. Qiu, and X. Wu. 2020. Estimating aboveground biomass of the mangrove forests on northeast Hainan Island in China using an upscaling method from field plots, UAV-LiDAR data and Sentinel-2 imagery. Int. J. Appl. Earth Obs. Geoinf. 85:101986 Available at http://dx.doi.org/10.1016/j.jag.2019.101986.

Wang, D., B. Wan, P. Qiu, Z. Zuo, R. Wang, and X. Wu. 2019. Mapping height and aboveground biomass of mangrove forests on Hainan Island using UAV-LiDAR sampling. Remote Sens. 11:1–25.

© University of Pretoria

Wang, K., T. Wang, and X. Liu. 2018. A review: Individual tree species classification using integrated airborne LiDAR and optical imagery with a focus on the urban environment. Forests 10:1–18.

Weatheronline. 2022. Historical wether data. Available at https://www.woeurope.eu/ (verified 18 August 2022).

Weisberg, P. J., T. E. Dilts, J. A. Greenberg, K. N. Johnson, H. Pai, C. Sladek, C. Kratt, S. W. Tyler, and A. Ready. 2021. Phenology-based classification of invasive annual grasses to the species level. Remote Sens. Environ. 263:112568 Available at https://doi.org/10.1016/j.rse.2021.112568.

Westoby, M. J., J. Brasington, N. F. Glasser, M. J. Hambrey, and J. M. Reynolds. 2012. "Structure-from-Motion" photogrammetry: A low-cost, effective tool for geoscience applications. Geomorphology 179:300–314 Available at http://dx.doi.org/10.1016/j.geomorph.2012.08.021.

White, F. 1983. The vegetaion of frica. Natural Resources Reasearch. UNESCO, Paris.

White, J. C., N. C. Coops, M. A. Wulder, M. Vastaranta, T. Hilker, and P. Tompalski. 2016. Remote Sensing Technologies for Enhancing Forest Inventories : A Review Remote Sensing Technologies for Enhancing Forest Inventories : A Review.

White, J. C., P. Tompalski, M. Vastaranta, M. A. Wulder, N. Saarinen, C. Stepper, and N. C. Coops. 2017. A model development and application guide for generating an enhanced forest inventory using airborne laser scanning data and an area-based approach. Information Report FI-X-18. Victoria, B.C.

White, J. C., M. A. Wulder, A. Varhola, M. Vastaranta, N. C. Coops, B. D. Cook, D. Pitt, and M. Woods. 2013a. A best practices guide for generating forest inventory attributes from airborne laser scanning data using an area-based approach.

© University of Pretoria

White, J. C., M. A. Wulder, M. Vastaranta, N. C. Coops, D. Pitt, and M. Woods. 2013b. The Utility of Image-Based Point Clouds for Forest Inventory: A Comparison with Airborne Laser Scanning. :518–536.

Whitehead, K., and C. H. Hugenholtz. 2014. Remote Sensing of the Environment with Small Unmanned Aircraft Systems (UASs), Part 1 : A review of progress and challenges. J. Unmmaned Veh. Syst. 2:69–85.

Whitehead, K., C. H. Hugenholtz, S. Myshak, O. Brown, A. Leclair, A. Tamminga, T. E. Barchyn, B. Moorman, and B. Eaton. 2014. Remote sensing of the environment with small unmanned aircraft systems (UASs), part 2 : scientific and commercial applications 1. J. Unmmaned Veh. Syst. 102:86–102.

Witczuk, J., S. Pagacz, A. Zmarz, M. Cypel, and J. Witczuk. 2017. Exploring the feasibility of unmanned aerial vehicles and thermal imaging for ungulate surveys in forests - preliminary results results. Int. J. Remote Sens.:1–18 Available at https://doi.org/10.1080/01431161.2017.1390621.

Witt, A. B. R., R. T. Shackleton, T. Beale, W. Nunda, and B. W. van Wilgen. 2019. Distribution of invasive alien Tithonia (Asteraceae) species in eastern and southern Africa and the socio-ecological impacts of T. Diversifolia in Zambia. Bothalia 49:1–11.

Wulder, M. A., N. C. Coops, A. T. Hudak, F. Morsdorf, R. Nelson, G. Newnham, and M. Vastaranta. 2013. Status and prospects for LiDAR remote sensing of forested ecosystems. Can. J. Remote Sens. 39:1–5 Available at http://dx.doi.org/130051.

Wulder, M. A., J. C. White, R. F. Nelson, E. Næsset, H. O. Ørka, N. C. Coops, T. Hilker, C. W. Bater, and T. Gobakken. 2012. Lidar sampling for large-area forest characterization: A review. Remote Sens. Environ. 121:196–209 Available at http://dx.doi.org/10.1016/j.rse.2012.02.001.

© University of Pretoria

Xie, Z., Y. Chen, D. Lu, G. Li, and E. Chen. 2019. Classification of land cover, forest, and tree species classes with Ziyuan-3 multispectral and stereo data. Remote Sens. 11:1–27.

Xie, Y., Z. Sha, and M. Yu. 2008. Remote sensing imagery in vegetation mapping : a review. J. Plant Ecol. 1:9–23.

Xu, Z., and H. Ruan. 2020. Estimation of secondary forest parameters by integrating image and point cloud-based metrics acquired from unmanned aerial vehicle. 14.

Xu, Z., X. Shen, L. Cao, N. C. Coops, T. R. H. Goodbody, T. Zhong, W. Zhao, Q. Sun, S. Ba, Z. Zhang, and X. Wu. 2020. Int J Appl Earth Obs Geoinformation Tree species classi fi cation using UAS-based digital aerial photogrammetry point clouds and multispectral imageries in subtropical natural forests. Int J Appl Earth Obs Geoinf. 92:1–14 Available at https://doi.org/10.1016/j.jag.2020.102173.

Xue, J., and B. Su. 2017. Significant Remote Sensing Vegetation Indices : A Review of Developments and Applications. J. Sensors 2017:1–17.

Yancho, J. M. M., N. C. Coops, P. Tompalski, T. R. H. Goodbody, and A. Plowright. 2019. Fine-Scale Spatial and Spectral Clustering of UAV-Acquired Digital Aerial Photogrammetric (DAP) Point Clouds for Individual Tree Crown Detection and Segmentation. IEEE J. Sel. Top. Appl. Earth Obs. Remote Sens. 12:4131–4148.

Yang, G., Y. Zhao, B. Li, Y. Ma, R. Li, J. Jing, and Y. Dian. 2019. Tree species classification by employing multiple features acquired from integrated sensors. J. Sensors.

Yao, H., R. Qin, and X. Chen. 2019. Unmanned Aerial Vehicle for Remote Sensing Applications — A Review. Remote Sens. 11:1–22.

Yu, X., J. Hyyppä, M. Holopainen, and M. Vastaranta. 2010. Comparison of Area-Based and Individual Tree-Based Methods for Predicting Plot-Level Forest Attributes. :1481–1495.

© University of Pretoria

Zahawi, R. A., J. P. Dandois, K. D. Holl, D. Nadwodny, J. L. Reid, and E. C. Ellis. 2015. Using lightweight unmanned aerial vehicles to monitor tropical forest recovery. Biol. Conserv. 186:287–295 Available at http://dx.doi.org/10.1016/j.biocon.2015.03.031.

Zhang, Z., L. Cao, and G. She. 2017. Estimating Forest Structural Parameters Using Canopy Metrics Derived from Airborne LiDAR Data in Subtropical Forests. Remote Sens. 9:1–26.

Zhang, X., F. Zhang, Y. Qi, L. Deng, and X. Wang. 2019. Int J Appl Earth Obs Geoinformation New research methods for vegetation information extraction based on visible light remote sensing images from an unmanned aerial vehicle (UAV). Int J Appl Earth Obs Geoinf. 78:215–226 Available at https://doi.org/10.1016/j.jag.2019.01.001.

Zhao, X., Q. Guo, Y. Su, and B. Xue. 2016. Improved progressive TIN densification filtering algorithm for airborne LiDAR data in forested areas. ISPRS J. Photogramm. Remote Sens. 117:79–91 Available at http://dx.doi.org/10.1016/j.isprsjprs.2016.03.016.

Zimba, S. . 2007. The fate of forest reserves in Zambia, a case study of Mwekera national forest No. 6. Ndola, Zambia.

© University of Pretoria

Appendices

Appendix 3.1. Sampled Tree Species in the Study Area

Tree Species	N	%	DBH (cm)		TH(m)	
			Mean	Range	Mean	Range
Julbernardia paniculata	127	18.5	31.03	13.5 - 59.90	17.79	8.50 - 25.00
Isoberlinia angolensis	114	16.6	23.92	9.90 - 44.70	14.55	5.00 - 20.50
Marquesia macroura	108	15.7	29.21	5.30 - 70.00	15.10	3.25 - 25.00
Brachystegia longifolia	64	9.3	20.65	11.8 - 64.00	11.27	8.50 - 23.00
Brachystegia spiciformis	51	7.4	18.55	5.00 - 64.20	9.97	5.80 - 20.50
Parinari curatellifolia	18	2.6	23.48	6.00 - 53.50	13.67	6.00 - 24.00
Ochna pulchra	17	2.5	7.62	5.20 - 10.90	5.70	4.50 - 8.00
Baphia bequaertii	16	2.3	11.63	5.80 - 23.70	6.95	3.00 - 15.00
Pericopsis angolensis	16	2.3	24.42	10.3 - 70.00	14.01	5.00 - 25.10
Diplorhynchus condylocarpon	14	2.0	8.94	5.00 - 18.00	7.64	4.50 - 10.00
Anisophyllea boehmii	11	1.6	18.77	5.10 - 44.90	11.74	3.75 - 19.50
Erythrina abyssinica	11	1.6	18.05	8.60 - 33.30	10.21	5.30 - 20.50
Hymenocardia ulmoides	8	1.2	24.05	5.40 - 9.90	19.94	4.50 - 7.00
Pseudolachnostylis maprouneifolia	7	1.0	22.04	7.00 - 20.80	11.64	5.00 - 10.00
Syzygium cordatum	7	1.0	21.20	9.10 - 19.20	11.21	5.25 - 10.00
Hexalobus monopetalus	7	1.0	14.13	5.80 - 57.30	7.94	4.75 - 22.00
Pterocarpus angolensis	7	1.0	12.29	5.30 - 28.10	8.22	5.30 - 15.00
Swartzia madagascariensis	7	1.0	8.16	5.50 - 10.80	5.34	3.30 - 8.75
Diospyros batocana	4	0.6	10.75	9.00 - 11.60	10.13	7.00 - 17.50
Burkia africana	4	0.6	8.55	7.80 - 9.30	6.38	6.25 - 6.50

© University of Pretoria

Albizia adianthifolia	4	0.6	14.15	12.3 - 18.00	13.00	10.75 - 16.50
Uapaca sansibarica	4	0.6	15.23	8.90 - 22.00	10.44	6.00 - 15.75
Lannea discolor	4	0.6	13.73	5.50 - 23.50	9.58	5.00 - 14.50
Diospyros mespiliformis	4	0.6	19.73	19.1 - 20.90	12.30	12.30 - 12.30
Brachystegia floribunda	4	0.6	34.45	25.7 - 44.50	19.00	17.50 - 20.00
Mapraunea africana	3	0.4	8.90	6.80 - 10.60	5.83	4.25 - 6.75
Bobgunnia madagascariensis	3	0.4	7.90	7.50 - 8.70	4.50	4.25 - 5.00
Dalbergia nitidula	3	0.4	27.93	22.0 - 30.90	13.17	13.00 - 13.25
Strychnos innocua	3	0.4	7.27	6.40 - 7.70	6.78	5.35 - 7.50
Pseudochnostylis maprouneifolia	3	0.4	7.77	5.80 - 11.60	5.87	5.30 - 7.00
Maprounea africana	3	0.4	8.90	6.80 - 10.60	5.83	4.25 - 6.75
Rhus longipes	3	0.4	9.43	8.80 - 9.90	5.50	5.00 - 6.00
Albizya adiansfolia	3	0.4	18.43	7.80 - 26.70	13.08	6.75 - 17.50
Combretum zeyheri	2	0.3	23.65	17.7 - 29.60	12.00	9.00 - 15.00
Faurea speciosa	2	0.3	8.90	8.90 - 8.90	5.75	5.75 - 5.75
Magnistipula butayei	2	0.3	15.90	15.9 - 15.90	8.00	8.00 - 8.00
Erythropeleum africanum	2	0.3	30.10	30.1 - 30.10	17.75	17.75 - 17.75
Ochna schweinfurthiana	2	0.3	6.80	6.60 - 7.00	5.95	5.00 - 6.90
Albizia antunesiana	2	0.3	32.40	21.6 - 43.20	17.90	17.50 - 18.30
Albizia versicolor	2	0.3	33.50	33.5 - 33.50	11.25	11.25 - 11.25
Phyllocosmos lemaireanus	2	0.3	5.75	5.70 - 5.80	6.13	5.75 - 6.50
Uapaca kirkiana	2	0.3	14.35	8.90 - 19.80	9.50	5.50 - 13.50
Harungana madagascariensis	1	0.1	5.70	5.70 - 5.70	4.50	4.50 - 4.50

© University of Pretoria

Canthium crassum	1	0.1	37.00	37.0 - 37.00	22.00	22.00 - 22.00
Oxtenanthera abyssinica	1	0.1	9.20	9.20 - 9.20	11.00	11.00 - 11.00
Dallbegiella nyasae	1	0.1	33.30	33.3 - 33.30	17.25	17.25 - 17.25
Monotes africanus	1	0.1	7.20	7.20 - 7.20	10.75	10.75 - 10.75
Syzygium guineense	1	0.1	5.90	5.90 - 5.90	6.70	6.70 - 6.70
Uapaca nitida	1	0.1	14.60	14.6 - 14.60	6.00	6.00 - 6.00
Albizya atunizyana	1	0.1	7.50	7.50 - 7.50	7.75	7.75 - 7.75
Total	688	100				

Appendix 3.2. Summary of class separability using mean spectral features across the 3 sampled dates

Bands	Separable classes	Mixed classes	Date
Blue	IA. BS. MM	BL. JP and shadow	25.05.21
Green	JP	IA, BS, BL, MM, Shadow	
Red	BL	JP. IA and shadow/ BS. MM	
Red-edge	MM	IA, BS, BL, JP, shadow	
Near infrared	MM	IA, BS, BL, JP, shadow	
Blue	shadow. JP. IA	BL. BS. MM	15.08.21
Green	shadow. BS. BL	IA. MM. JP	
Red	shadow and all		
Red-edge	shadow and all		
Near infrared	shadow, JP, MM, BS	IA and BL	
Blue	shadow. BS	BL. BS. MM	24.10.21
Green	shadow	All species	
Red	shadow, BS	JP, BL, MM, IA	
Red-edge	shadow, JP IA	BS, BL, MM	
Near infrared	shadow, JP, IA, BL	BS, BL, MM	

© University of Pretoria

Appendix 3.3. Summary of class separability using mean spectral indices features across the 3 sampled dates

Bands	Separable classes	Mixed classes	Date
Brightness	shadow	All species	25.05.21
Maximum		All species, shadow	
NDVI	BS	JP, IA, BL, MM,	
GCC	Shadow, MM, JP, BS	IA, BL	
RCC	BS	IA, MM, BL, JP,	
Brightness	shadow, JP, IA	BL, BS and MM	15.08.21
Maximum	All species and shadow		
NDVI	All species and shadow		
GCC	BL, BS, JP, MM	Shadow, IA	
RCC	All species and shadow		
Brightness	MM	BL, BS, IA, JP,	24.10.21
Maximum	IA, BS, MM	shadow, BL, JP	
NDVI	BS, MM, JP, IA	BL, shadow	
GCC	BL, IA	JP, shadow/ BS, MM	
RCC	BS, MM, BL	shadow, JP, IA	

Appendix 3.4. Summary of class separability using mean textural features across the 3 sampled dates

Bands	Separable classes	Mixed classes	Date
Contrast	shadow	All species	25.05.21
Correlation		JP, shadow, BS,	
Dissimilarity		All classes	
entropy	BS	IA, BL, MM, JP, shadow	
Standard deviation	shadow	All species	
Contrast	IA	BS, BL, MM, JP,	15.08.21
Correlation		All classes	
Dissimilarity		All classes	
entropy	Shadow, JP, BS	IA, MM, BL	
Standard deviation		JP, shadow/ MM, BS,	
Contrast	shadow	All species	24.10.21
Correlation	Shadow, JP	MM, IA, BS, BL	
Dissimilarity	shadow	All species	
entropy	Shadow, BS, BL, MM	JP, IA	
Standard deviation		All classes	

© University of Pretoria